Structural Studies On Purple Non-Sulphur Bacterial Pigment-Protein Complexes

Iain Andrew Mitchell

Submitted in fulfilment for the Degree of M.Sc.

University of Glasgow

Department of Chemistry

August 2003

Declaration

I declare that this thesis has been written in accordance with University regulations and is less than 50,000 words in length. All work contained herein was performed by the author unless otherwise stated.

Iain Andrew Mitchell

August 2003

Abstract

The B800-820 light harvesting complexes from the purple non-sulphur bacteria *Rhodopseudomonas acidophila* strains 7050 and 7750 are integral membrane pigment-protein complexes. They have been studied using protein crystallography and mass spectrometry in an attempt to determine the high-resolution structure and to characterise the polypeptides.

The growth of the bacteria and the subsequent purification of the B800-820 complex from each of the strains of bacteria are described. Also described is the growth of crystals of both complexes, which were then exposed to x-rays in order to test their diffraction quality. No crystals were observed to diffract x-rays beyond the 3.0Å resolution currently available for the LH3 complex from strain 7050 (McLuskey, 1999) and none were observed to diffract to high resolution for the LH3 complex from strain 7750.

MALDI-TOF mass spectrometry was employed to identify any contaminating polypeptides in the purified complexes. The polypeptides and contaminants were proposed to be identifiable by comparison of theoretical masses. Fragmentation studies were carried out by the enzymatic digest of the whole complex by different proteinases. The differences in masses of the fragments produced were then used in an attempt to assign partial sequences to the polypeptides. The results from the mass spectrometry are described, showing that several polypeptides are present in sample previously thought to contain only one pair.

X-ray crystallography was used to determine the structure of a reaction centre mutant from *Rhodobacter sphaeroides* R26-1 at 2.8Å resolution. This mutant is carotenoidless, and this work was carried out in order to prove, crystallographically, the presence of a reconstituted carotenoid. The carotenoid was reconstituted chemically, with one purified from another strain of bacteria. The structure was solved using molecular replacement, with the search model being a high-resolution reaction centre structure containing a carotenoid. Several rounds of refinement were carried out with the carotenoid omitted from the search model in order to minimise model bias. The carotenoid, spheroidene, is found in the same binding pocket, and in the 15-cis confirmation as in the wild type structure (within resolution limits). A comparison of the solved reaction centre with the structure used as the search model is given.

Acknowledgements

I am grateful to many people who have given their assistance over the course of this thesis. I have been on the receiving end of a great deal of generosity of two of the most valuable commodities- time and knowledge and I would like to thank everybody who has helped me throughout.

Firstly I must thank my supervisors, Profs. Neil Isaacs and Richard Cogdell. They have given me the opportunity to attend various conferences and schools at which I have expanded my knowledge and met some truly great people in the fields of crystallography and photosynthesis. Between them, they were able to guide me in new directions when all I could see was a brick wall.

This work would not have been possible, or at least would have been immeasurably harder, were it not for the patience, help, cajoling and beer from Tina Howard, "my" post-doc. She was always on hand to offer advice, help mount crystals, take me to the synchrotron, and provide help in a wide range of tasks.

On the crystallographic side of this project, I was fortunate to have Aleks Rosak to call on and he managed to somehow help me through the Reaction Centre structure. He gave up many hours to guide me through the programmes; what they were doing, how to get them to do what I wanted, and how to find out what they had actually done (these things were so often not the same when I was involved).

Many thanks also must go to Dr. Sharon Kelly for the help with the MALDI-TOF. Despite a busy schedule, she made time to show me how to use the mass spec and didn't (seem to) mind phone calls when her trouble-shooting skills were required.

A special thanks to Bernhard, not so much for scientific input, although there was some of that too, but for the beers, and listening and keeping me on the rails. Sort of! Thanks also to the rather mixed group of Friday footie players for the (sometimes) weekly kickabout.

And then there are all the people who have helped me day in, day out in the lab, even if it was just helping me to retain some semblance of sanity! My heartfelt thanks to Alastair, the champion teamaker, and provider of references, life will be quiet without his wit; to Niall, who will, one of these days be in need of a cup of tea, his devotion and hard work was an inspiration; to June for the practical help around the lab and a cheery smile; to Stuart, Kim, Katherine and Paul and everyone else in

the "MP lab." And thanks also to the people in PX: to Pixie, Adrian, Comedy, Dina, Lewis, Claire, and Andy and to many other people I have probably forgotten. I'm sorry.

Last, but by no means least, thanks to my family: my sisters, Morag and Lorna, for dinners and listening and so much more; and my parents who encouraged me, cajoled me, bullied me and nagged me, but above all supported me throughout my time doing this MSc . I wouldn't have made it without you!

Abbreviations

Å	Angstrom 10^{-10}m
Abs.	Absorbance
Acid.	*acidophila*
AML	Artificial mother liquor
AMS	Ammonium sulphate
ATP	Adenosine triphosphate
BA	Benzamidine hydrochlorate
Bchl *a*	Bacteriochlorophyll *a*
β-OG	n-octyl-β-D-glucopyranoside
Bphe	Bacteriopheophytin
CCP4	Collaborative computational project number 4
CHCA	α-cyano-4-hydroxycinnamic acid
CMC	Critical Micelle Concentration
cp	cryoprotectant
cyt	cytochrome
Da	Daltons
ENDOR	Electron Nuclear Double Resonance
EPR	Electron Paramegnetic Resonance
ESRF	European Synchrotron Radiation Facility
FPLC	Fast Protein Liquid Chromatography
HL	High Light
HPT	Heptane-1,2,3-triol
ICM	Intracytoplasmic Membrane
I_r	Integrity ratio
KP_i	Di-potassium hydrogen orthophosphate
LDAO	N,N-dimethyldodecylamine-N-oxide
LH	Light Harvesting
LH1	Core light harvesting complex
LH2	Peripheral light harvesting complex
LH3	Low light peripheral light harvesting complex
LL	Low Light

MALDI	Matrix Assisted Laser Desorption Ionisation
MR	Molecular Replacement
MWCO	Molecular Weight Cut Off
OD	Optical Density
PDB	Protein data bank
P_r	Peak ratio
PSU	Photosynthetic unit
Q	Quinone
Rb.	*Rhodobacter*
RC	Reaction Centre
Rps.	*Rhodopseudomonas*
Rsp.	*Rhodospirillum*
sph.	*sphaeroides*
TFA	Trifluoroacetic acid
TOF	time-of-flight
Tris	Tris-hydroxymethyl-aminomethane
UDAO	N,N-dimethylundecylamine-N-oxide
WT	Wild Type

Contents

Table of Figures

1. Chapter 1 Introduction

1.1.Photosynthesis

Photosynthesis is the basis of almost all life on earth. It provides energy either directly, as in plants, or indirectly, by using those plants as a food source. Light is a difficult form of energy to be used practically, as it cannot be stored, eaten, or used to drive mechanical processes. Photosynthesis is carried out in order to convert light energy from the sun into chemical energy.

Photosynthesis is actually a two-part process. The first part, the absorption of light energy and its conversion to chemical energy, is collectively known as the light reactions. The light reactions produce the energy rich molecule adenosine triphosphate (ATP) and the reducing molecule NADPH. The second part of photosynthesis, known as the Calvin cycle or the dark reactions, uses the ATP and NADPH from the light reactions to produce sugars from CO_2.

Photosynthesis can be thought of as the photochemical reduction of CO_2 to organic substrates. In higher plants, the formation of glucose by photosynthesis can be represented by the equation:

$$6CO_2 + 12H_2O \xrightarrow{h\nu} 6O_2 + C_6H_{12}O_6 + 6H_2O.$$

However, plants are not the only species to use photosynthesis in order to capture the energy required for life.

1.2.Photosynthetic Bacteria

Some species of bacteria survive solely by respiration, however others have the ability to also survive by photosynthesis. In fact the first photosynthetic organisms were bacteria which had evolved to use sunlight as an energy source over 3 billion years ago. In some bacterial photosynthesis, no oxygen is evolved, hence the bacteria must have access to a reducing substrate to provide hydrogen for the reduction of CO_2 according to the general equation (van Neil, 1941)

$$CO_2 + 2H_2A \xrightarrow{h\nu} (CH_2O) + H_2O + 2A$$

where H_2A may be H_2, H_2S or a variety of simple organic molecules. When H_2A is an organic compound, it may serve as a source of carbon instead of CO_2.

Anaerobic photosynthetic bacteria can be classified as purple bacteria, heliobacteria and green bacteria. Only cyanobacteria have the ability to evolve oxygen, and are hence termed photoautotrophs. The other three groups use light energy to make ATP whilst using atmospheric CO_2 as a carbon source, but use an organic material or H_2S as the reductant. They are termed photoheterotrophs. During this project, work was carried out on purple bacteria which can be made to use an organic compound e.g. succinate or pyruvate, as the carbon source as well as the reductant.

1.2.1. Purple Bacteria

Purple bacteria can be classified as sulphur and non-sulphur according to their ability to utilise sulphur as the reducing substrate. There are two families of sulphur bacteria: *Chromatiaceae* and *Ectothiorhodospiraceae*. Bacteria belonging to the *Chromatiaceae* family deposit globules of elemental sulfur inside the cells, given the proper growth conditions (Imhoff, 1984a). *Ectothiorhodospiraceae* differ in that they deposit sulphur outside the cells during oxidation of sulphide (Imhoff, 1984a). This project was concerned with non-sulphur bacteria and therefore they shall be discussed in more depth.

The family of non-sulphur purple bacteria, *Rhodospirillaceae*, are the most diverse of the phototrophic purple bacteria groups (Imhoff and Truper, 1989). They are split into 7 genera: *Rhodopseudomonas, Rhodospirillum, Rhodobacter, Rhodocyclus, Rhodopila, Rubrivivax,* and *Rhodomicrobium* (Willems et al., 1991; Imhoff, 1995). A schematic diagram of the classification of purple bacteria can be found in figure 1.

Many of these bacteria can survive by respiration under aerobic and dark conditions when they have an unpigmented appearance, as there is no need for the cells to produce the pigment molecules used in photosynthesis. However, when grown anaerobically and in the presence of light a different way of growing is required by the cells and they switch to a photosynthetic mode (see figure 2).

In the photosynthetic mode, the cytoplasmic membranes become invaginated and extended in area, creating intracytoplasmic membranes (ICM) in which the cells produce the necessary complexes to harvest light energy. This apparatus is known as

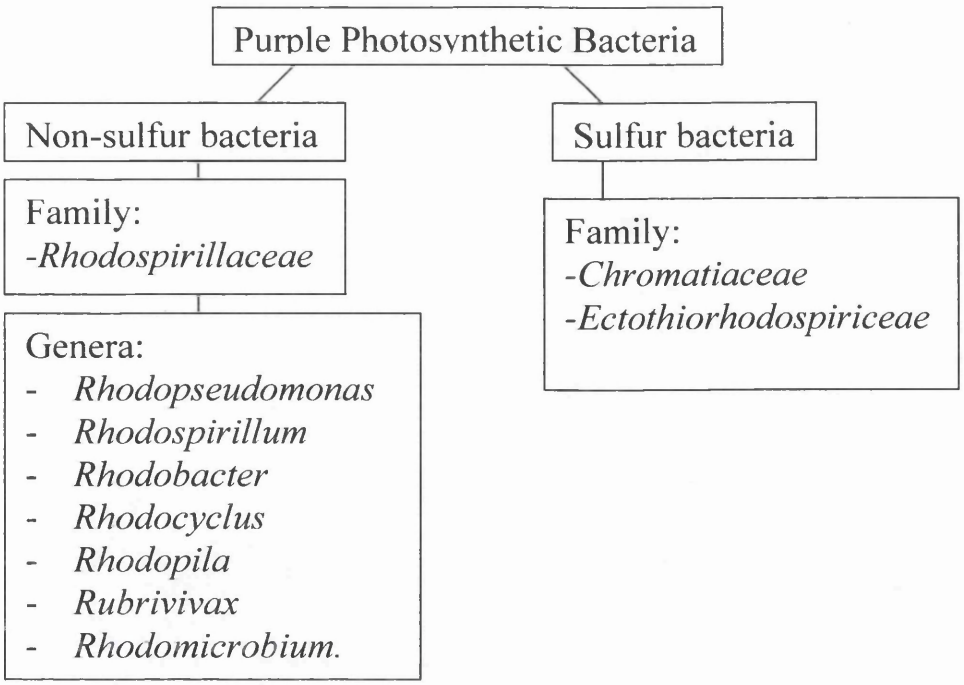

Figure 1. Schematic representation of the classification of purple photosynthetic bacteria.

Figure 2. Photograph of bottles containing *Rps. acidophila* strain 7050 aerobically grown on the left (showing unpigmented appearance) and photosynthetically grown bacteria on the right.

the photosynthetic unit (PSU) and contains the necessary pigment and protein molecules required to harvest light energy. The extended membranes give a greater surface area over which the PSU can be produced and therefore over which the cell can absorb light. Different arrangements of these membranes are formed within the cytoplasm. There are of four main types of membrane arrangement as shown in figure

3- these are; vesicles, tubuli, thylakoid-like (in regular stacks), and large thylakoids (which are partially stacked and irregularly arranged) (Oelze and Drews, 1972; Collins and Rensen, 1991). These different arrangements of the intracytoplasmic membrane have been used to classify the different genera of bacteria.

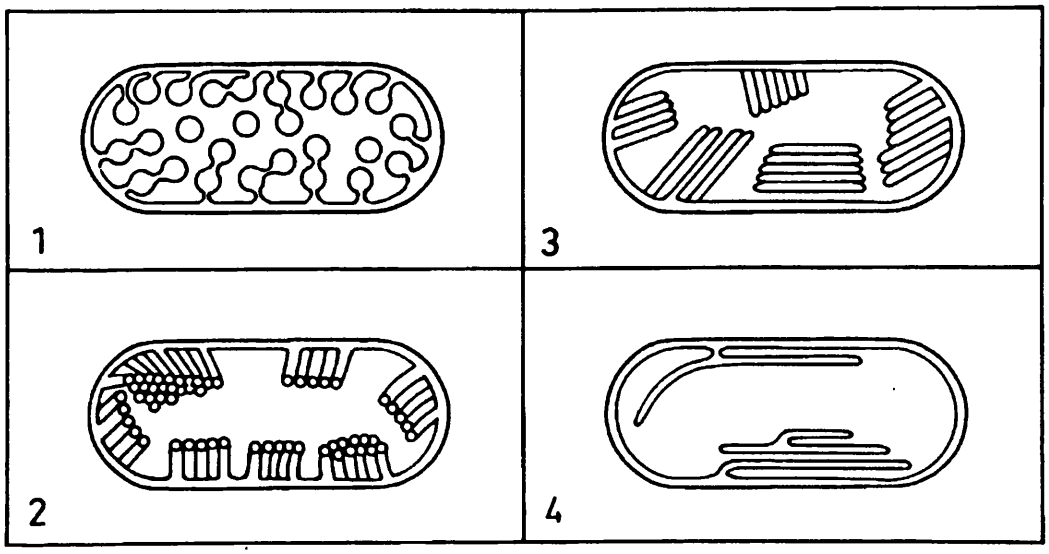

Figure 3. Schematic representation of different types of intracytoplasmic membranes (ICM) that contain the photosynthetic unit (PSU). 1. Vesicle type (as seen in *Rsp. rubrum*). 2. Tubuli type (as seen in *Thiocapsa pfennigii*). 3. Thylakoid-like, arranged in regular stacks (as seen in *Rsp. molischianum*). 4. Large thylakoid, partially stacked and irregularly arranged (as seen in *Rps. acidophila*). (Reproduced from Drews and Imhoff, 1991)

1.3. The Photosynthetic Unit (PSU)

The PSU is the collection of components required by the bacteria to collect light energy and convert it to a proton gradient across the membrane. The PSU consists of several different complexes, which each contain apoproteins and associated pigment molecules. In purple bacteria, the main pigments are bacteriochlorophyll (Bchl) and carotenoids although there are also bacteriopheophytin and ubiquinone molecules present.

Bacteriochlorophyll *a*, the main light harvesting pigment found in purple bacteria, is a large macrocyclic molecule analogous to the chlorophyll molecule found in green plants. It has a bacteriochlorin conjugated head group with a magnesium ion in the centre and an unsaturated hydrocarbon phytyl tail (see figure 4).

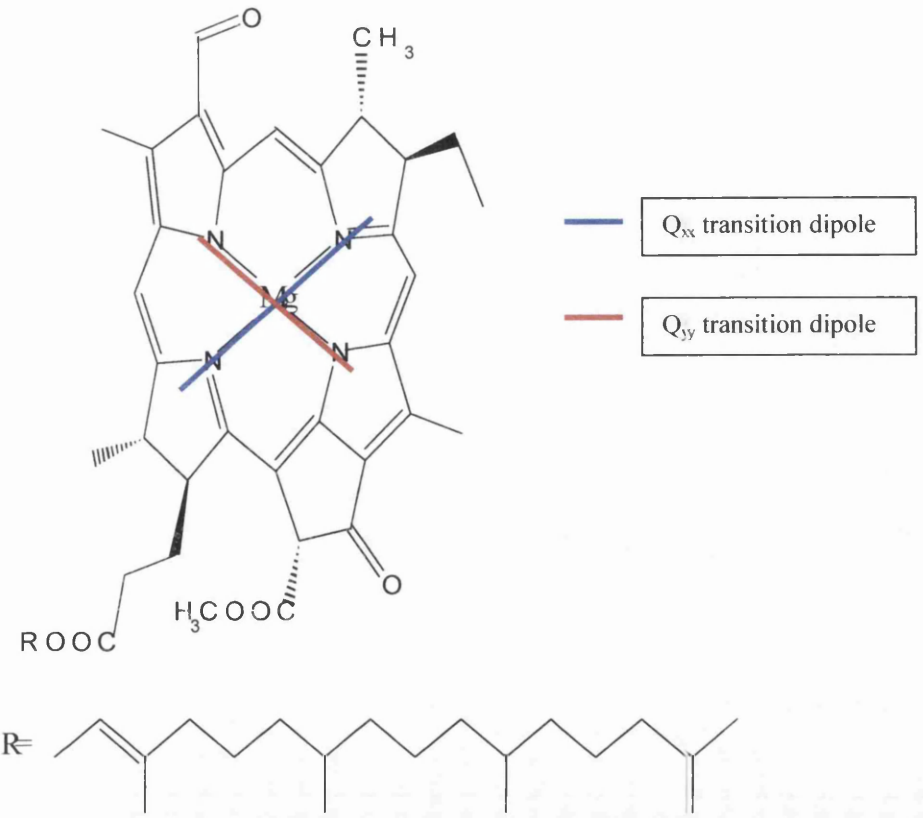

Figure 4. Bchl *a* molecule showing the directions of the Q_x and Q_y transition dipoles. The Q_x and Q_y dipoles are perpendicular. The R group, gerynyl gerynyl, is joined by means of an ester linkage.

Due to the asymmetric conjugated π system of the bacteriochlorin head group, Bchl *a* has two transition dipoles, Q_x and Q_y, which leads to its characteristic absorption spectrum. The Q_x transition dipole results in an absorption band in the visible region of the spectrum and is relatively weak. Q_y is longer, located perpendicular to Q_x, and leads to a stronger absorption band found in the near infrared (NIR). A third absorption band, the Soret band, is located in the blue region of the spectrum. It is due to the overlap of the B_x and B_y absorption bands corresponding to electronic transitions at higher energy levels.

The absorption bands of Bchl *a* are sensitive to the local environment, especially the Q_y absorption that can show the greatest variability in the wavelength of maximum absorption. Monomeric Bchl *a* in organic solvent, such as acetone, has a Q_y absorption maximum at 777nm. In the LH complexes, this has been red-shifted by up to 100nm due to oligomerisation and interactions with the polypeptides. A more in-depth discussion of the interactions required to bring about these changes is discussed in section 1.6.

Bacteriopheophytin is a very similar molecule to Bchl differing only in that it lacks the Magnesium ion in the centre of the bacteriochlorin ring.

Carotenoids are composed of two groups of molecules; carotenes, a class of hydrocarbons, and xanthophylls, oxygenated derivatives of carotenes (Takaichi, 1999 and references therein). They are found throughout nature although only those relating to anoxygenic photosynthetic bacteria shall be discussed here.

Carotenoids are long conjugated molecules (see figure 5) with the extent of the conjugation affecting the absorption characteristics of the molecule. Their synthesis involves four isoprene units being joined head-to-tail creating C_{20} units, with two of these C_{20} units then being joined tail-to-tail to form the C_{40} molecule, phytoene, with a cis-bond in the middle. This is the base for all other carotenoids, which are then formed by various reactions, including desaturation, hydroxylation and methylation (Takaichi, 1999). The carotenoids in the PSU have been shown to fulfil several roles, acting as photoprotective agents, accessory light harvesting molecules and stabilising the structure of some complexes.

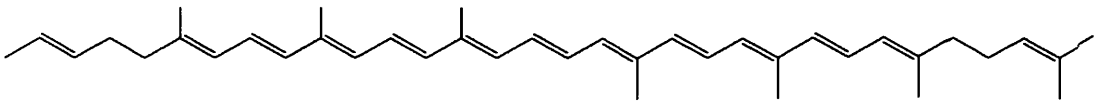

Figure 5. The carotenoid lycopene, showing the extended conjugated double bond system responsible for absorption of light in the visible region.

Ubiquinones are apolar lipid molecules belonging to the quinone family. The characteristic feature of all quinones is their ability to function as redox carriers in electron transport processes within the membranes. The main structural features of quinones are their quinoid ring system and the isoprenoid side chain. The quinoid ring system is used to define the type of quinone (in this case ubiquinone) and the isoprene unit can be used classify the ubiquinone. The only quinone found in the bacteria studied during this work is ubiquinone-10 (Imhoff, 1984b)(see figure 6).

The PSU is made up of the reaction centre (RC) and one or more light harvesting complexes (LHC). The RC is, functionally, the most important and the LHC are produced in order to increase the surface area available for gathering light.

The core light harvesting complex, or LH1 is intimately associated with the RC, and is proposed to sit with the RC in the middle of its ring structure (Papiz et al., 1996; Hu et al., 1997; Hu and Schulten, 1998) (see section 1.5.). Some species of bacteria such as *Rps. viridis* and *Rsp. rubrum* produce only the LH1 complex. Most

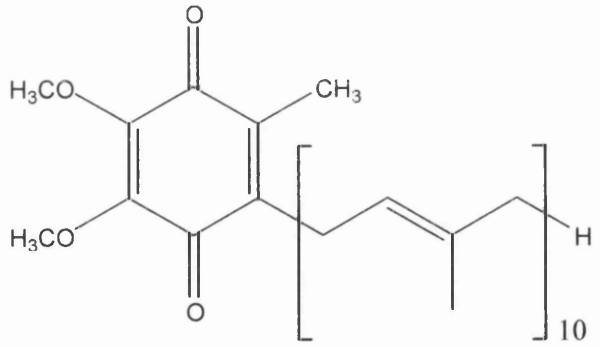

Figure 6. Ubiquinone-10 molecule as found in purple bacteria.

species of bacteria also produce a second LH complex, known as the peripheral light harvesting complex, or LH2. This complex further increases the surface area over which the bacteria can gather photons, and transfers the energy, through the LH1 complex, to the RC. This is discussed in section 1.4.

1.3.1. The Reaction Centre (RC)

The photochemical RC is a protein-pigment complex where the energy from photons is used to drive a proton pump across the membrane that ultimately results in the formation of ATP and NADPH. As with all components of the PSU, the RC spans the depth of the membrane (Sistrom, 1978).

The RC has a characteristic absorption spectrum due to the pigment molecules it contains. An example of the absorption spectrum is shown in figure 7. The RC has been extensively studied, and much is known of its structure and function .

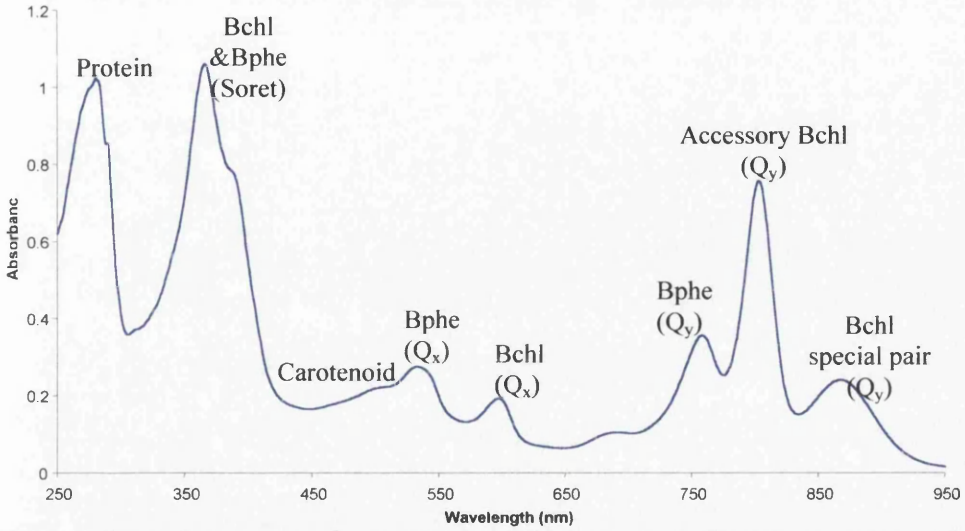

Figure 7. Absorption spectrum from purified reaction centre from *Rhodobacter sphaeroides* showing the pigments responsible for each absorption band.

1.3.1.1.The structure of the Reaction Centre

The RC from *Rps. viridis* was the first integral membrane protein to have its 3-dimensional structure solved by x-ray crystallography (Deisenhofer et al., 1985) followed by that of *Rb. sphaeroides* (Allen et al., 1986; Chang et al. 1986). It was shown to consist of three polypeptides, termed H (heavy), M (medium), and L (light) due to their apparent molecular weight on a SDS-PAGE gel. Some species of bacteria including *Rps. viridis* also have a fourth polypeptide tightly associated with the RC, known as the cytochrome-*c* (cyt c) complex (Thornber et al., 1980). This subunit contains four heme groups and is bound to the rest of the RC by means of a cysteine residue at its N-terminus, linked via a thioether bond to a diglyceride (Weyer et al., 1987). In other species of bacteria such as *Rb. sphaeroides*, the RC consists only of three subunits. There is also found a single heme, water-soluble cyt c_2 complex that can reversibly bind to the periplasmic side of the M-subunit of the RC complex (Adir et al., 1996). The function of this subunit is described in section 1.3.1.2..

There were also found to be several pigment molecules as an integral part of the RC. These are four Bchl molecules, two Bphe molecules, two ubiquinones, a non-heme iron and a carotenoid. These are described in section 1.3.1.1.2.. The reaction centre can be thought of as a scaffold of polypeptides to which the pigment molecules are non-covalently bound (see figure 8).

1.3.1.1.1. The Protein Subunits

The M and L protein subunits have a sequence homology of about 30% (Youvan et al., 1984; Williams et al., 1984; Michel et al., 1986) and the overall fold is very similar. There is pseudo 2-fold rotational symmetry relating these subunits, and there are many similarities between them (see figure 9).

Both subunits have the N-terminus on the cytoplasmic side and contain five trans-membrane α-helices each, which are between 21 and 28 amino acid residues in length. The C-terminus is then located on the periplasmic side of the membrane. There are several α-helical sections located in the loop regions, some of which intrude partially into the membrane region (Lancaster et al., 1995). Together the M and L subunits act as the scaffold to which the pigment molecules are bound.

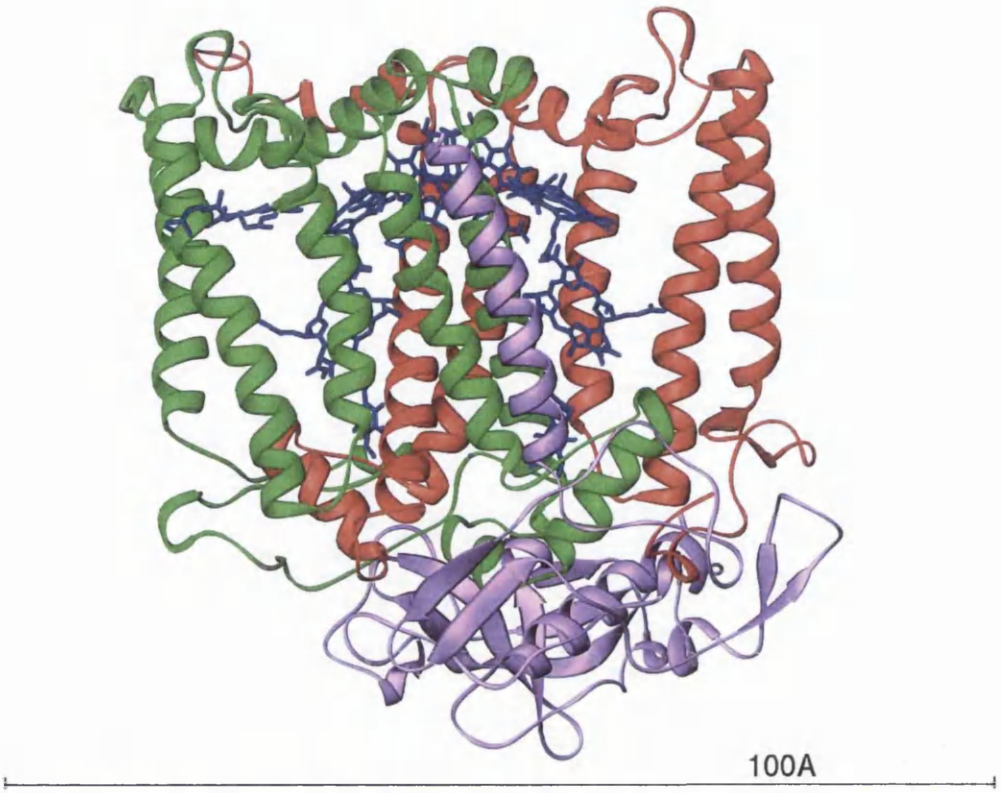

Figure 8. A ribbon representation of the structure of RC from *Rb. sphaeroides* (coordinates from McAuley & Fyfe, unpublished data). The transmembrane helices of the M (green) and L (red) subunits act as a scaffold for the various pigment molecules shown in blue. The H subunit is shown in purple with the one α-helix spanning the membrane and a large cytoplasmic domain. Figures 8-11 were produced using Ribbons3 (Carson, 1997).

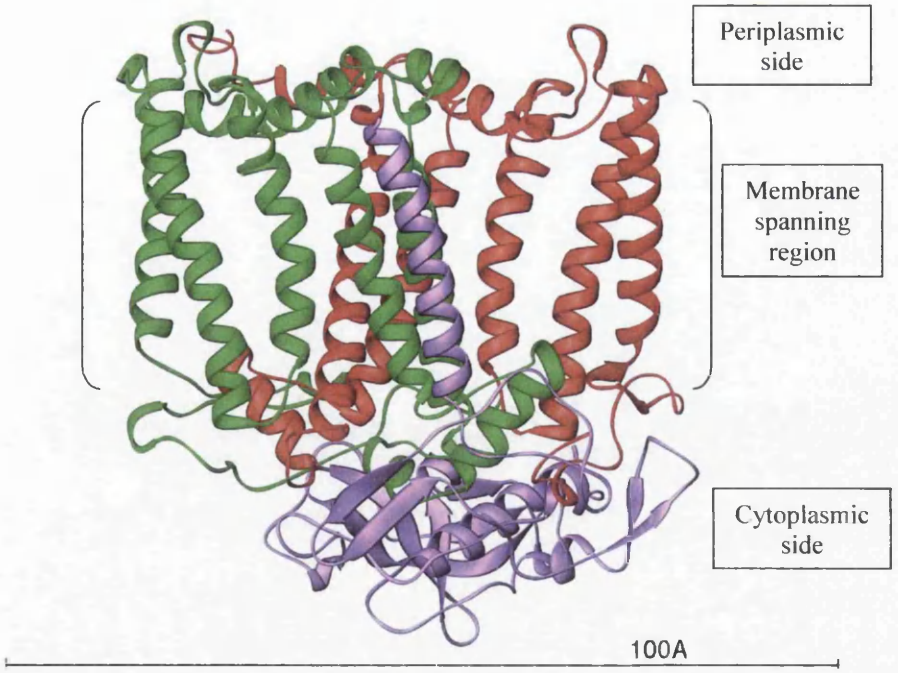

Figure 9. RC polypeptides only (colours as for fig, 8). The M and L subunits each contain 5 transmembrane helices and the H subunit contains one transmembrane helix that serves as an anchor.

The third protein subunit, H, was shown to have the N-terminus located on the periplasmic side of the membrane. This leads into one α-helix spanning the membrane followed by a large cytoplasmic domain. This globular region is composed of parallel and anti-parallel β-sheets and an α-helix which is close to the C-terminus. The H-subunit does not play an important role in the binding of the pigments, instead it seems to be important in orienting the complex correctly in the membrane as it is inserted into the membrane first and the complex then built around it (Chory et al., 1984). The H subunit can be reversibly dissociated from the RC complex in 1.5M LiSCN, with the complex remaining functional (Debus et al., 1986).

1.3.1.1.2. Co-factors

The co-factors present in the bacterial reaction centre are located between the transmembrane helices of the M and L subunits and are arranged in such a way as to share their pseudo 2-fold symmetry. As can be seen in figure 10, there are two branches of co-factors, each containing the same molecules. One branch is associated

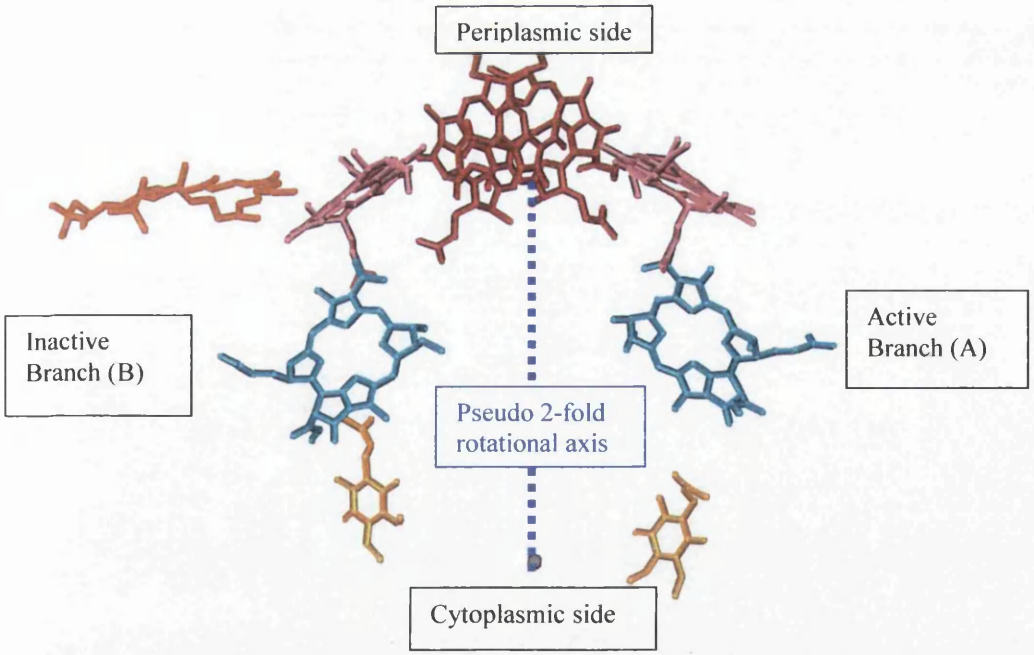

Figure 10. Reaction centre co-factors viewed from within the membrane, showing pseudo 2-fold rotational symmetry axis and the orientation of the complex in the membrane with respect to the co-factors. The Special Pair of Bchl *a* molecules are shown in red, accessory Bchl in pink, Bphe in blue, ubiquinone molecules in yellow and the non-heme iron in grey, The carotenoid, which does not share the pseudo two-fold symmetry is in orange. The tails of the Bchl, Bphe and ubiquinone molecules have been removed for clarity. Electron transfer occurs down the active branch.

closely with the L protein subunit, and one with the M subunit. The function of all the co-factors is discussed in section 1.3.1.2.

Starting at the periplasmic side of the complex, there are two Bchl *a* molecules. These are known as the special pair, or primary donor (D) (Hoff, 1988), as they participate in the first event in the chain of reactions, which are described in the next section. Next comes the accessory Bchl *a* molecules (B) followed by bacteriopheophytin (Bphe or H) molecules. The last pigment molecules in the chain are ubiquinone molecules (Q) which have an Fe^{2+} lying between them. There is also a single carotenoid molecule present that lies to one side of the chain of pigments. This molecule is the exception to the pseudo two-fold symmetry shared by the M and L subunits and the pigment molecules.

1.3.1.2. Function and Energy Pathway

The reaction centre is one of the complexes involved in creating a proton gradient across the membrane, which is described in detail below. The co-factors are involved in the transfer of an electron from the special pair of Bchl *a* molecules down the series of co-factors to the ubiquinone, which becomes reduced. Although there are two similar chains of co-factors, this occurs down only one arm of the chain, which is known as the active chain, denoted by the subscript A, whilst the inactive chain is denoted B (Hoff, 1988). In some papers, the branches are named according to the protein subunit to which they are associated with. In this nomenclature, L is equivalent to the A chain and M is equivalent to the B chain. Much research has been carried out to discover more about the electron transfer processes and it has been quite well characterised, and a review of the x-ray crystallography carried out on site directed mutants can be found in Fyfe and Jones, 2000.

When the special pair absorbs a photon, it forms the excited state of the bacteriochlorophyll, D*. The electron density is proposed to be delocalised over the special pair although the extent of this delocalisation has not been measured due to the short-lived nature of the excited state. An electron is then transferred from D* to the accessory bacteriochlorophyll B_A in ~3.5ps (Holzapfel et al., 1989), which gives rise to the D^+ state, with the charge being shared between D_A and D_B in a ratio of approximately 2:1 (Lendzian et al., 1993). An electron is then transferred from the B_A

onto the bacteriopheophytin, H_A, in a further 0.9ps (Holzapfel et al., 1989; Sporlein et al., 2000). The electron transfer from H_A to ubiquinone, Q_A, occurs in approximately 200ps (Holzapfel et al., 1989; Fleming and van Grondelle, 1994; Hoff and Deisenhofer, 1997) followed by transfer to Q_B in about 150μs giving rise to Q_B^- (Debus et al., 1986). This is summarised in Figure 11.

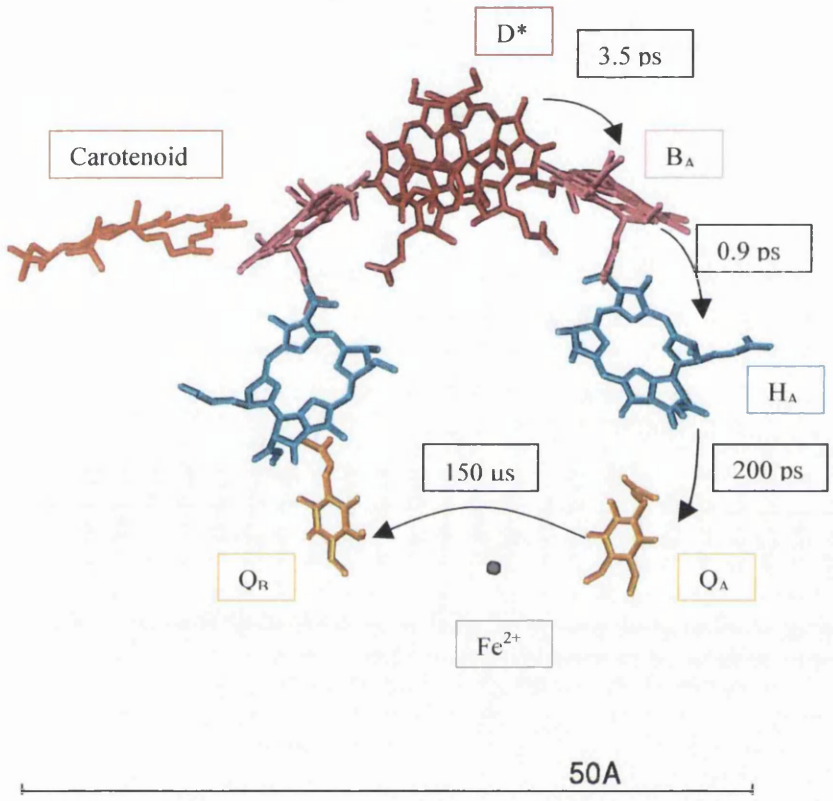

Figure 11. Reaction Centre co-factors showing the electron transfer times. Initially the primary donor (D) is promoted to D* and an electron is transferred down the A chain to Q_A. It is then transferred to Q_B to form the reduced Q_B^-.

The special pair, D^+, is then reduced by the cytochrome c_2 complex and a second electron then transferred down the same pathway which leads to the formation of Q_B^{2-}. The ubiquinone receives two protons from the cytoplasm giving a ubiquinol molecule that dissociates from the complex into the membrane (McPherson et al., 1990). The ubiquinone is replaced in the RC by one from a pool in the membrane whilst the ubiquinol is oxidised by a cytochrome bc_1 complex, which also spans the membrane (Gabellini et al., 1982). The oxidation of the ubiquinol yields two protons, which are released into the periplasm, with the electrons released being taken up by the cytochrome c_2 for return to the RC when reducing the primary donor, D, completing the cycle, as shown in figure 12. Thus a proton or pH gradient across the

membrane comes about from the absorption of photons. This gradient is then used by other molecules situated in the intracytoplasmic membrane to drive further processes, such as the formation of ATP by the ATPase complex.

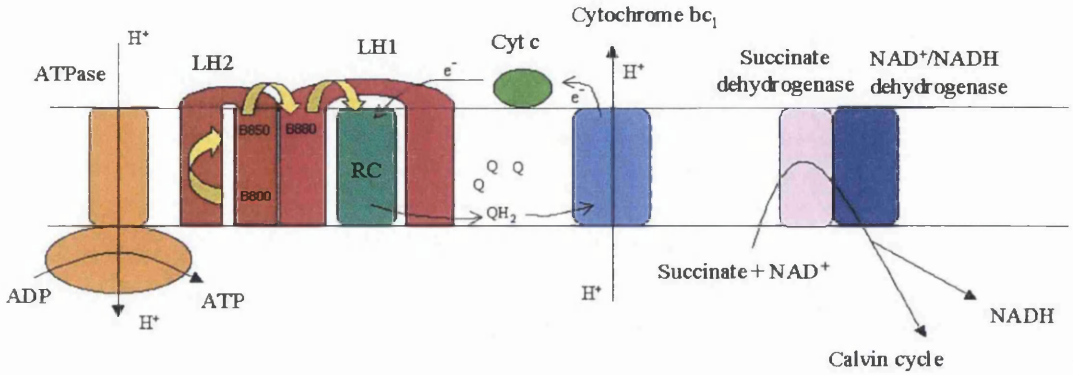

Figure 12. The ICM, which contains the photosynthetic apparatus. The RC and cytochrome complexes create a proton gradient which is then used by other molecules such as the ATPase complex which makes the energy rich molecule ATP. Amended from Kiley and Kaplan, 1988

The Fe^{2+} situated between the Q_A and Q_B plays a role in aiding the transfer of the electron from A to B although it is not essential. A sample of RC from *Rb. sphaeroides* with the iron chemically removed showed that electron transfer times from A to B was slower only by a factor of ~2 (Debus et al., 1986). The efficiency of charge separation from D Q_A to D^+ Q_A^- was also decreased to 63% of the native complex. However, it was shown that Fe^{2+} was not required for rapid electron transfer from Q_A to Q_B. Reconstitution experiments were performed where the iron was replaced by other divalent cations, for example zinc or cobalt. These showed little or no change in the electron transfer rates compared to the native complex thus a metal ion in the iron site is required for native electron transfer properties (Debus et al., 1986).

Although termed the inactive branch, there are only two of the molecules in the B chain that do not play a part in the electron transfer properties of the complex. D_B plays a role in both the delocalisation of the initial charge and in photoprotection (see section 1.3.1.2.2.1.) and Q_B is important in the last step of the charge separation. The question of why the other pigments are there is yet to be answered. Whether it has an evolutionary origin, or is important in the building of the complex or some other reason is unknown at this point.

The carotenoid is the only co-factor not yet dealt with, as it is not involved in the main energy transfer process that leads to the proton gradient. It is, nonetheless, a vital part of the RC complex

1.3.1.2.1. Carotenoids

There are various carotenogenesis pathways that have been well-characterised (see Takaichi, 1999 for overview), although that found most commonly in purple non-sulfur bacteria is the spirilloxanthin pathway, see figure 13. This pathway can be further divided into normal spirilloxanthin, unusual spirilloxanthin, sphaeroidene, and carotenal pathways. In some species of bacteria, there may be several carotenoids produced in similar amounts, for example, under certain growth conditions *Rhodopseudomonas (Rps.) acidophila* strain 7050 produces 37% rhodopin, 34% rhodopin glucoside and 22% lycopene of the total amount of carotenoid along with others in smaller amounts.

Carotenoids play several roles in the PSU, being essential for photoprotection (Griffiths et al., 1955), but also helping in structure stabilisation (Lang and Hunter, 1994) and light harvesting (Angerhofer et al., 1986)(see section 1.4.2.2.).

1.3.1.2.1.1. Photoprotection

One of the main roles carotenoids play is the photoprotection of the complexes in which they are found. In 1955 a mutant of *Rb. sphaeroides*, strain R26, was made that had no carotenoid present and was photosensitive in the presence of oxygen (Griffiths et al., 1955). This was produced by blocking part of the carotenoid biosynthetic pathway such that only the carotenoid phytoene is present. When the bacteria is grown photosynthetically and in the presence of oxygen, this mutation is lethal. The role that carotenoids play is to quench any damaging singlet oxygen present and prevent photo-oxidative reactions taking place.

When a photon hits the Bchl molecule of the special pair, the molecule is promoted from the ground state, S_0, to a singlet excited state, S_1. If an electron is not transferred to another molecule, the S_1 state can rapidly decay to the triplet excited state, T_1 (Parson et al., 1975). The decay from the triplet excited state to the singlet ground

state is spin-forbidden according to the Pauli-exclusion principle, therefore the triplet states has a relatively long lifetime of ~50μs (Cogdell et al., 1975).

Although the concept of allowed and forbidden transitions apply only to polyenes with centres of symmetry, all polyenes seem to exhibit the same electronic

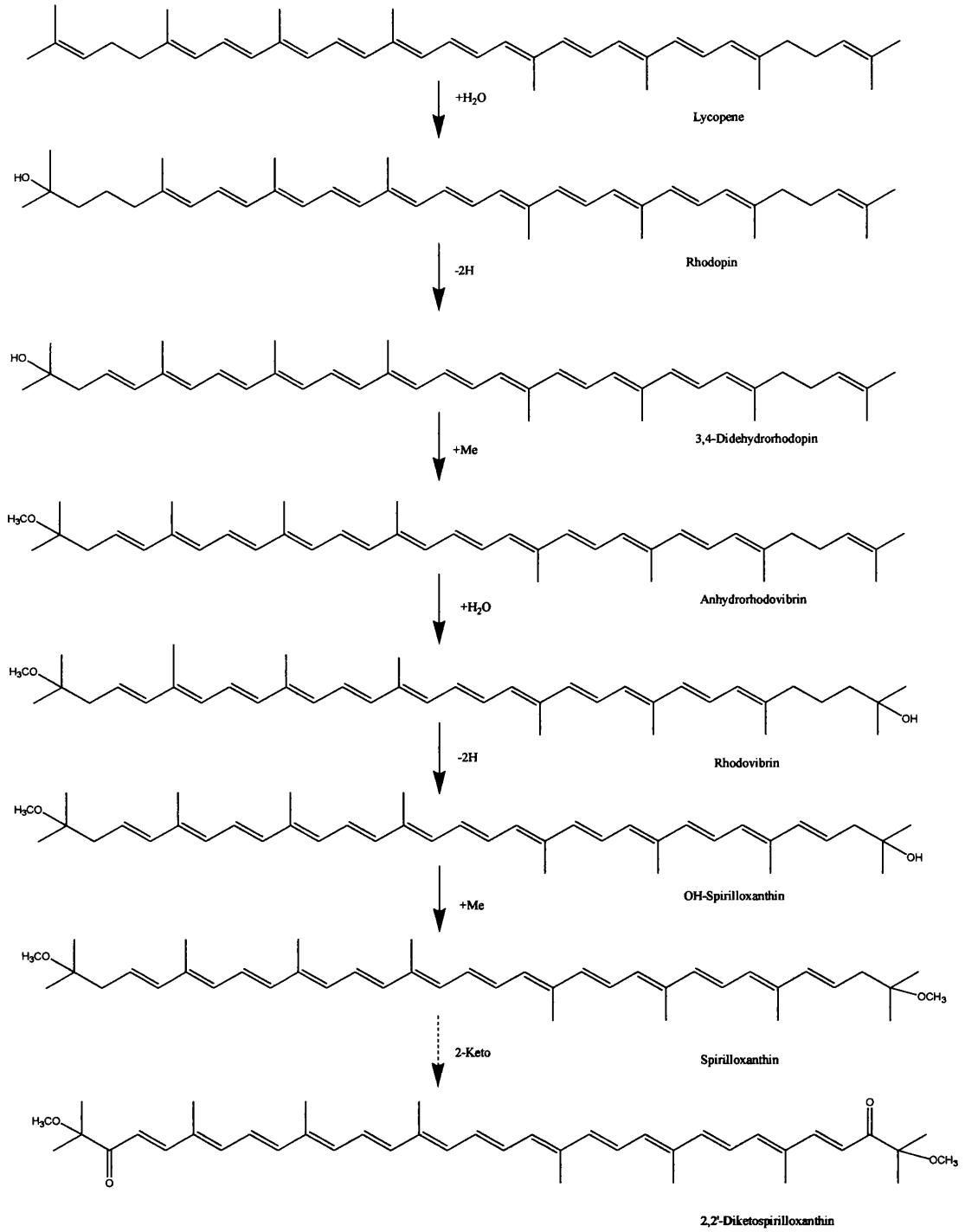

Figure 13. Spirilloxanthin pathway commonly found in purple non-sulphur bacteria. Reproduced from Takaichi, 1999.

energy orderings and similar relative transition strengths (Frank and Christensen, 1995). Thus, the triplet state can either decay back to the ground state, or pass its energy onto another molecule. If that other molecule is oxygen, it is promoted to the singlet excited state, which is a very reactive molecule. Singlet oxygen is a strong oxidising agent, powerful enough to react with many molecules including protein, lipid and nucleic acids (Foote, 1968). Therefore, any singlet oxygen within the cell will cause extensive damage and cells exposed to a high concentration of singlet oxygen die rapidly. If there is a carotenoid in close proximity to the Bchl molecule, when the Bchl is in the triplet state, the carotenoid can accept the energy by triplet-triplet transfer. This gives an excited state carotenoid, which then decays to the ground state by loss of heat, which is shown in figure 14.

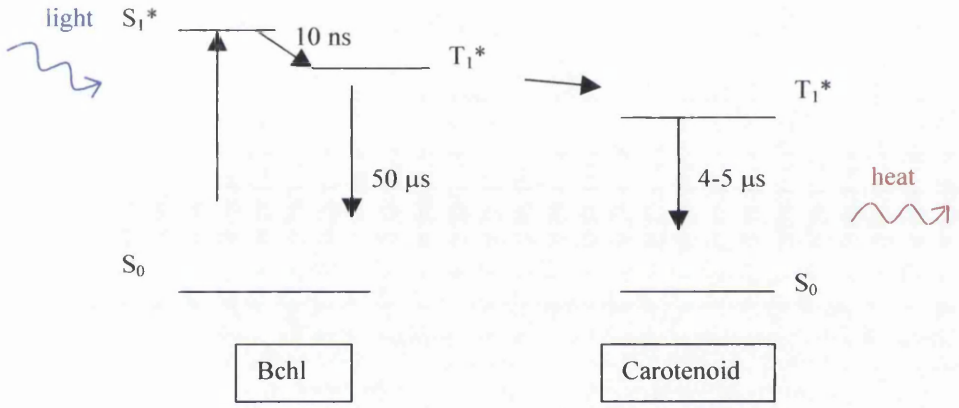

Figure 14. Energy Diagram showing energy transfer within Bchl molecules and from Bchl to carotenoid molecules. Times are given for *Rb. sphaeroides* 2.4.1. taken from Cogdell et al., 1975. The formation of the carotenoid triplet excited state, T_1* was found to occur in approximately 10ns. This implies the triplet-triplet (Bchl to carotenoid) transfer is exceedingly rapid.

Under normal circumstances, electron transfer occurs rapidly down the active branch of co-factors. However, under certain circumstances this process can be interrupted. For example, after the double charge separation occurs in the RC, there is a period of time when the ubiquinol has diffused from the RC complex, but it has not yet been replaced by another ubiquinone molecule from the membrane pool. If the special pair is excited at this time, the electron cannot be transferred down the chain to the ubiquinone. The electron can be transferred to the Bphe, but no further, and from this point, back transfer can occur to the Bchl special pair. The back transfer from Bphe to Bchl special pair also leads to the formation of the triplet state, T_1.

In order to have efficient quenching of the triplet Bchl, which is assumed to occur by an electron exchange mechanism (Dexter, 1953), the carotenoid must be near by, otherwise a reaction with oxygen may occur. The carotenoid is found approximately 4Å from the Bchl on the inactive branch (B_B)(McAuley et al., 2000) and therefore energy transfer from B_A probably occurs through B_B. It is this short distance that allows quenching within a few nanoseconds. It has been shown that if B_B is removed from the complex, the carotenoid is also lost and the cells are susceptible to photo-oxidative damage (Frank et al., 1988).

1.3.1.2.1.2. Accessory Light Harvesting and Structure Stabilisation

Carotenoids can play an important role in light-harvesting and structure stabilisation of some complexes in the PSU. However, these functions are of greater importance in the light-harvesting complexes than in the RC. Therefore the discussion of the light harvesting and structure stabilising properties of carotenoids is presented in section 1.4.

1.3.1.3. Mutations of bacterial RC

Since the successful structure solution of the bacterial RC (Deisenhofer et al., 1985), much work on site directed mutagenesis has been carried out enabling us to have a much more detailed insight to the energy transfer pathways, structure stabilisation and co-factor binding. In all single mutants studied by x-ray crystallography, it has been found that the overall structure of the RC outside the immediate environment of the mutated residue remains unchanged (Fyfe et al., 2001).

Examples where co-factor binding has been studied in *Rb. sphaeroides* include the mutation of the His residue at position 173 of the L chain (L173) to Leu and the mutation of the His residue at position M266 to a Cys residue. The first mutation results in the primary donor Bchl, P_L, being replaced by a bacteriopheophytin molecule. P_M can also be replaced by a bacteriopheophytin molecule by the mutation of the His at position M202 to a Leu residue (Chirino et al., 1994). When His M266 is replaced by a Cys residue, it was found that the RC incorporates Zn^{2+} into the site normally occupied by Fe^{2+} in the wild type (Williams et al., 1991). This mutant was

useful in EPR and ENDOR studies to characterise the electronic structure of the quinones.

A great deal of work has been carried out on electron transfer down the inactive chain through site directed mutagenesis. Charge separation resulting in the $D^+H_B^-$ state has been observed with a quantum yield of up to 23% (Heller et al., 1995; Kirmaier et al., 1999; Roberts et al., 2001). This has been achieved by replacing the Bphe that acts as the primary electron acceptor, H_A, with a Bchl molecule, then adding mutations that modify the environments of H_A, B_A and B_B. A triplet mutant of Phe (L181) to Tyr, Tyr (M208) to Phe and Leu (M212) to His shows 30% electron transfer to H_B. This is proposed to come about from raising the free energy of P^+B_A by the M208 and M212 mutations (Kirmaier et al., 2001)

Electron transfer down the B chain can also be promoted by the mutation of His to Leu at position M182, which results in the Bchl B_B being replaced by a Bphe molecule. 35% B chain electron transfer is observed due to the Bphe being easier to reduce (Katilius et al., 1999).

1.4.Bacterial Light Harvesting Complexes

The theoretical minimum size for the PSU would be one RC complex since the RC is capable of collecting light energy and converting it to a proton gradient. However, this would give a very small area over which the RC could capture light, leading to long periods of time where the RC mechanism was inactive whilst it waited for a photon to "hit" the special pair. Due to the small surface area of the pigments in the RC, and as the RC is composed mostly of protein, a more efficient method of capturing the light energy would be advantageous. In order to increase the surface area available for the capture of light, bacteria also produce light harvesting complexes (LHC), see Freiberg, 1995 for an overview. As the name suggests, these complexes gather in light energy and transfer this energy to the RC where the processes discussed previously take place. The LHC are also situated in the intracytoplasmic membrane beside the RC.

The amino acid sequences of the polypeptides from light harvesting complexes have been reported from many species and strains of photosynthetic bacteria (Zuber and Brunisholz, 1991 and references therein). This information has

made it possible to compare the light harvesting polypeptides from a wide variety of bacteria and gives structural information. A highly conserved transmembrane region has been identified in all the polypeptides, with conserved histidine residues at equivalent points. In the peripheral LHC, the transmembrane domain contains 21 amino acids with the conserved His residue being situated four residues from the cytoplasm boundary. In the core LHC, the transmembrane domain is 23 residues long with the conserved His residue also found four residues from the cytoplasm. The histidines have been shown to ligand the central magnesium atoms of the Bchl molecules, which places all the Bchl molecules at equivalent depths in the membrane. The N- and C-terminal regions show much more variety between species both in length and composition. Some complexes have an extended region such as *Rc. gelatinosus* G151 where the LH2 C-terminal end of the α-polypeptide is extended and may form a helix sitting on the surface of the membrane or may represent a second domain spanning the membrane (Zuber and Brunisholz, 1991). *Rps. viridis* contains an extended region at the N-terminus of the LH1 α-polypeptide.

1.4.1. Peripheral Light Harvesting Complex

Some species of bacteria, such as *Rsp. rubrum*, produce only the RC-LH1 core complex in the PSU, and in response to low light conditions, can only increase the number of PSUs produced per cell (Aargaard and Sistrom, 1972). Other species can, however, produce a second type of light harvesting complex called the peripheral light harvesting complex, or LH2. Like the LH1 complex, the purpose of the LH2 complex is to increase the surface area over which light energy can be collected and to channel it to the RC. This energy transfer occurs from the more distant LH2 complex, through the LH1 complex, to the RC. The peripheral light-harvesting complex is sometimes referred to as B800-850 due to the absorption maximum of the Bchl *a* pigment at 800 and 850nm (see figure 15). The LH2 complex is described first, as there is more information available than from the LH1 structure. The high-resolution structures from LH2 (McDermott et al., 1995; Koepke et al., 1996) have been used to model the structure of the LH1 complex.

When grown photosynthetically under high light conditions, only a small number of LH2 complexes are produced. As the light intensity is decreased, a greater

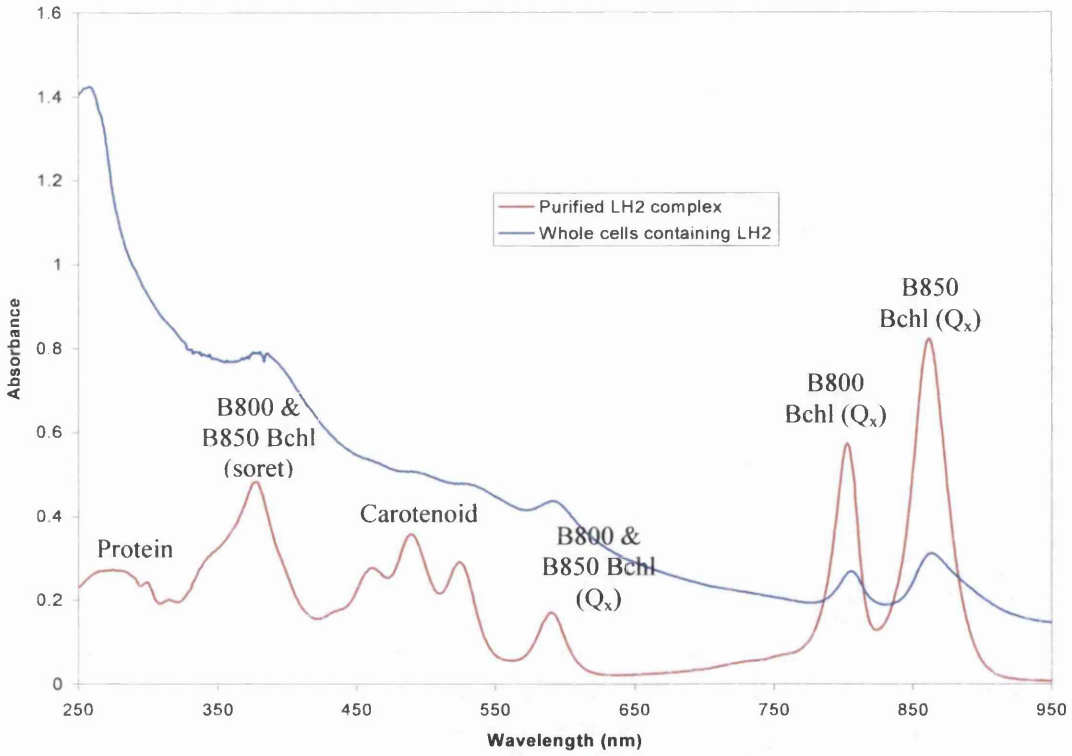

Figure 15. Absorption spectra of whole cells producing LH2 (blue) and purified LH2 complex (red), both from *Rps. acidophila* strain 10050. Each peak is labelled with the pigments responsible for that absorption.

number of LH2 complexes are produced per cell in response to the decrease in incident light.

The LH2 complex spans the depth of the membrane and contains both polypeptides and pigment molecules. In 1995, the 3D crystal structure to 2.5Å of the LH2 complex from *Rps. acidophila* strain 10050 was published (McDermott et al., 1995), and this has now been improved to 2.0Å (unpublished data). This was followed the next year by the structure of *Rsp. molischianum* to 2.4Å (Koepke et al., 1996). These structures have given an insight into how the polypeptides and pigments are arranged within the complexes, how energy transfer occurs, and why the pigments absorb at the wavelengths they do.

1.4.1.1. Structure And Function

The high-resolution structures available for the LH2 complexes enable an in-depth discussion of the structure to take place and the structure can be compared to

functional information. All pigments and polypeptides can be accurately positioned and interactions between and within molecules can be examined.

The LH2 complexes from both species have similarities that are discussed below. The LH2 structure from *Rps. acidophila* is a nonameric ring system composed of two concentric rings of α-helical polypeptides to which the pigment molecules are non-covalently bound. As can be seen in figures 16a and b, the complex consists of 18 polypeptides, 27 Bchl *a* molecules separated into two spectrally distinct populations, and 9 carotenoid molecules.

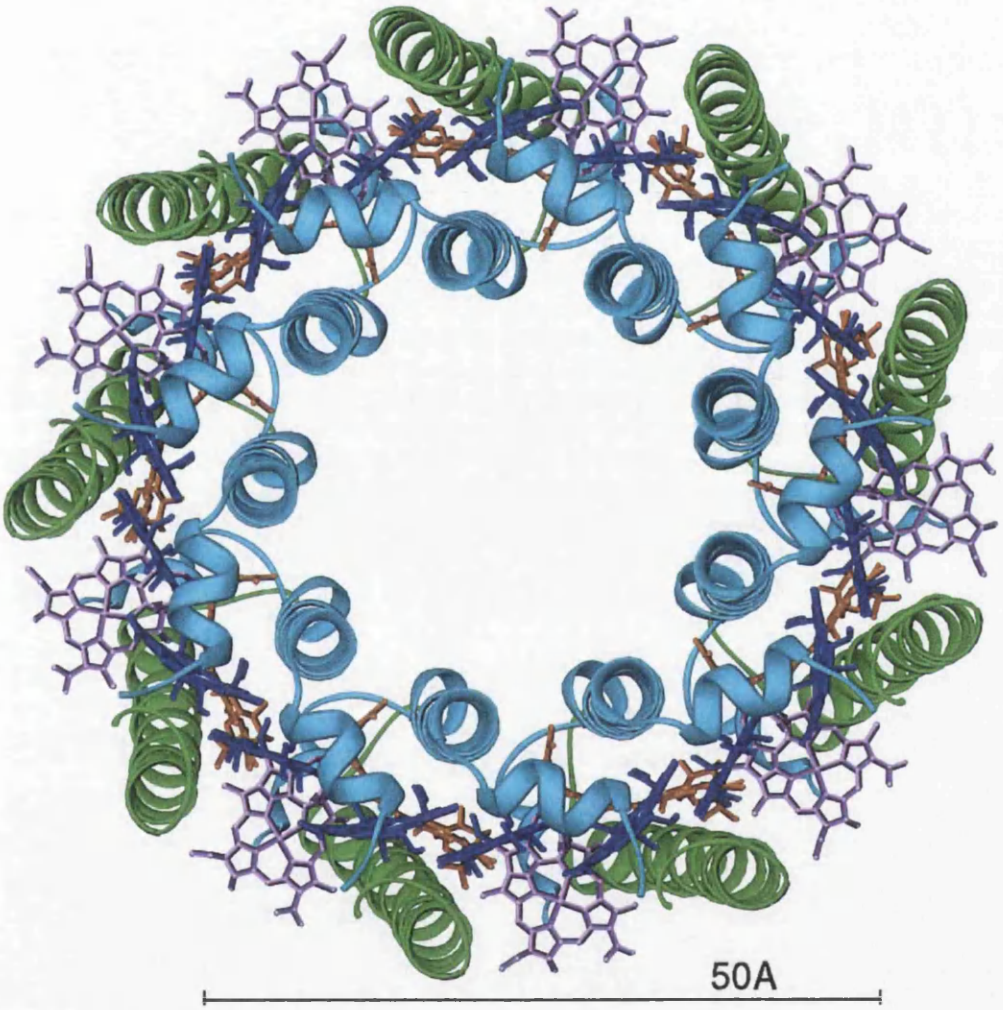

Figure 16a. A ribbon representation of the structure of the peripheral light-harvesting (LH2) complex from *Rps. acidophila* 10050 (McDermott et al., 1995) viewed from above the periplasmic side of the membrane. The α-polypeptides are shown in blue and the β-polypeptides in green both represented by ribbons. The B800 molecules are in purple, B850 molecules in blue and the carotenoid in orange, as stick representations. The phytyl chains from the Bchl molecules have been removed for clarity in figures 16a and b. The co-ordinates used to produce figures 16-20 were taken from the PDB, ref. 1KZU, and the diagrams produced using Ribbons3 (Carson, 1997).

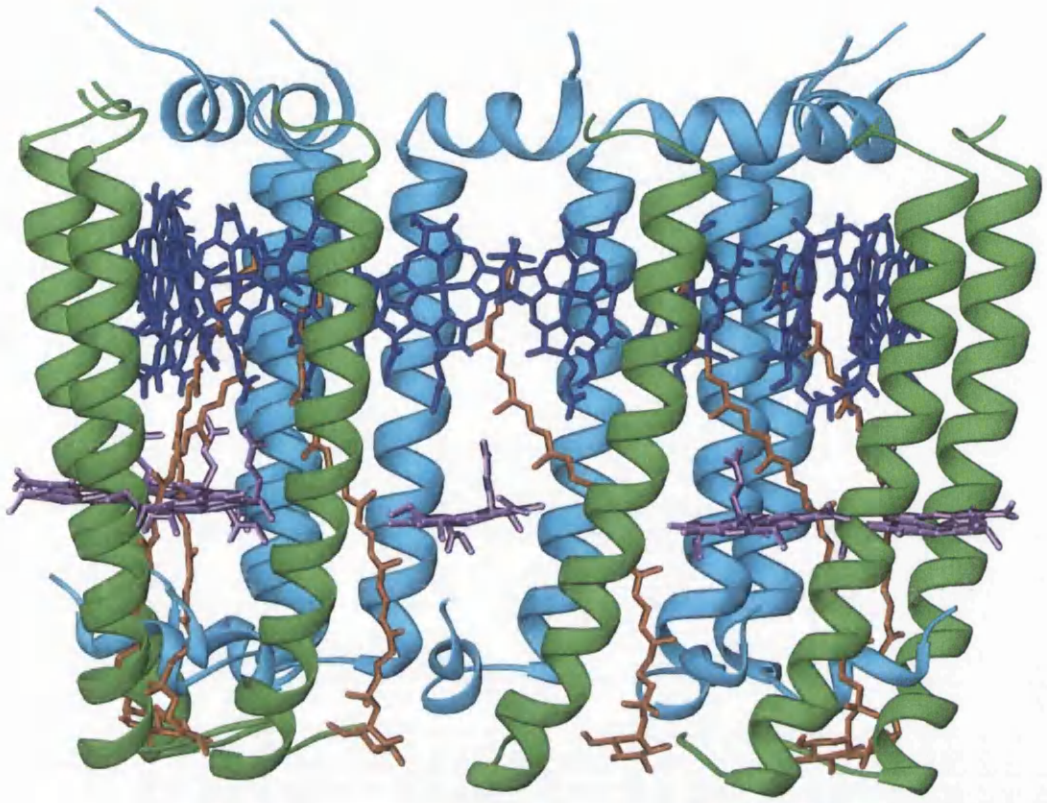

Figure 16b. Structure of LH2 viewed side-on from within the membrane with the periplasm above and the cytoplasm beneath the complex. The rear third of the complex has been removed for clarity.

The inner ring of nine helices, termed the α-polypeptides, have the helical axes almost exactly perpendicular to the membrane surface. The nine helices forming the outer ring, termed the β-polypeptides, are inclined at an angle of approximately 15°. The N and C termini of the apoproteins are bent over, running almost parallel to the membrane surface and closing the structure at the top and bottom.

Situated between the rings of helices are eighteen Bchl *a* molecules that absorb at 850nm, with the plane of their bacteriochlorin ring system running perpendicular to the proposed membrane surface. The nine Bchl *a* molecules that absorb at 800nm are located between the β-polypeptides. The ring system of these pigments is almost parallel to the membrane surface (see figure 17).

There are also carotenoid molecules present in the LH2 structure. From *Rps. acidophila* strain 10050, the major carotenoid is rhodopin glucoside, although several other carotenoids are present in smaller amounts (Gardiner, 1992). Nine of these molecules are modelled, spanning the depth of the membrane and forming van der Waals contacts with the apoproteins and Bchl *a* molecules.

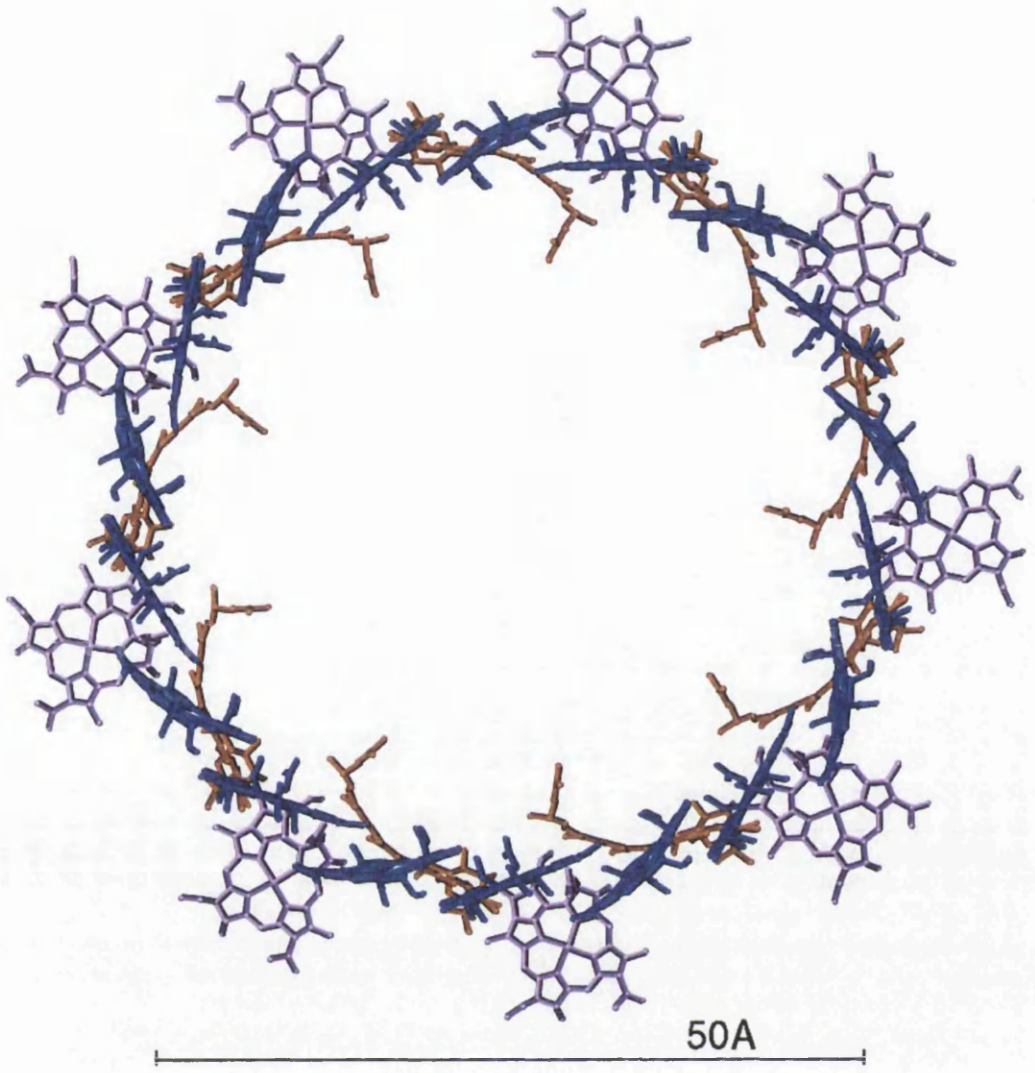

Figure 17. The pigment molecules of LH2 viewed from above the membrane. The phytyl chains of the Bchl molecules have been removed for clarity. 9 B800 molecules are shown in purple and sit with the plane of the bacteriochlorin head group parallel to the membrane surface. The 18 B850 molecules shown in blue form an overlapping ring with the plane of the head group perpendicular to the membrane surface. The 9 carotenoid molecules shown in orange come in contact with all Bchl molecules.

The complex can be split into nine subunits, each containing one α,β-polypeptide pair, one B800 Bchl *a*, two B850 Bchl *a* molecules, and one carotenoid as shown in figures 18.

Of the B850 Bchl *a*s, one is bound to the α polypeptide and one to the β polypeptide, these are referred to as the B850α and B850β respectively and they are therefore not identical. The distance from the central magnesium is different within the subunit (9.53Å) compared to the B850 molecule in the next subunit (9.05Å). The

bacteriochlorin head group and the tail of the of the B850α and B850β molecules adopt slightly different conformations, with the most marked difference in the phytyl chains, which are proposed to act as alignment tools (Freer et al., 1996). The tail of the carotenoid is found between the two B850 Bchl *a* molecules in the monomer, coming within 3.42Å of the Bchl *a* bound to the α polypeptide. The carotenoid also comes into close contact with the B800 pigment (3.57Å).

As mentioned previously, the carotenoid must be in close contact with the Bchl *a* molecules in order to quickly quench the triplet state and prevent production of singlet oxygen. The crystal structure of the LH2 complex confirms the short distances, reinforcing the photoprotective role of the carotenoid from a structural point of view.

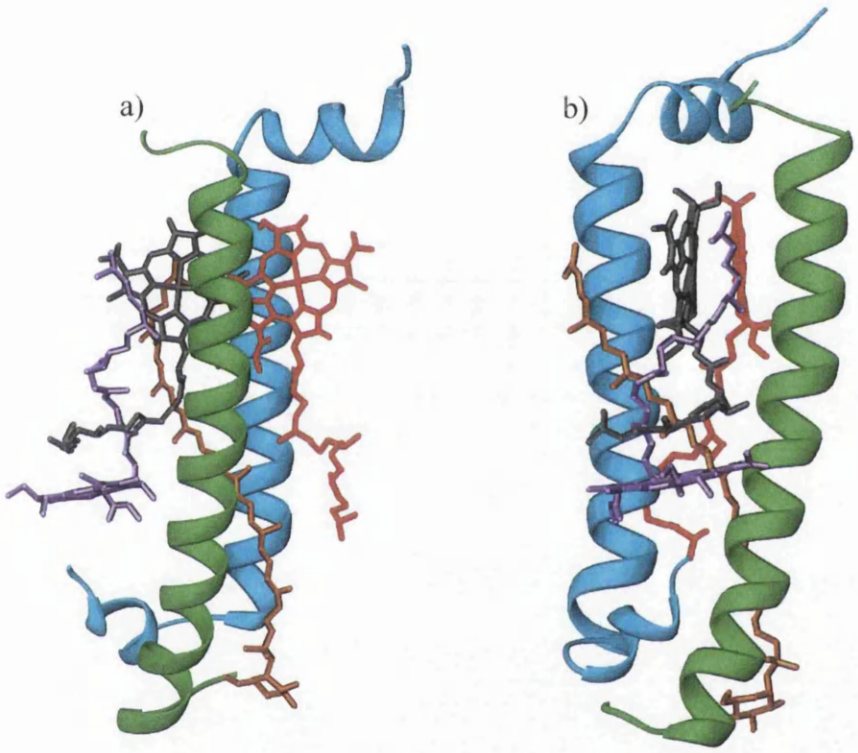

Figure 18a. One subunit of the LH2 complex from *Rps. acidophila* 10050 with the α-polypeptide in blue and the β-polypeptide in green. The bacteriochlorin ring of the B850α (grey) is in a different orientation to the B850β (red), being flipped 180°. The phytyl chain also adopts a different conformation. The B800 molecule (purple) sits with the head group almost normal to the plane of the diagram and the phytyl chain extending up through the complex. The carotenoid can be seen in orange. b)The B850α molecule (grey) can be seen closer to the α-polypeptide (blue) and the B850β (red) closer to the β-polypeptide (green). The B800 molecule (purple) sits with the phytyl chain running up through the complex. The carotenoid (orange) is entwined through the subunit.

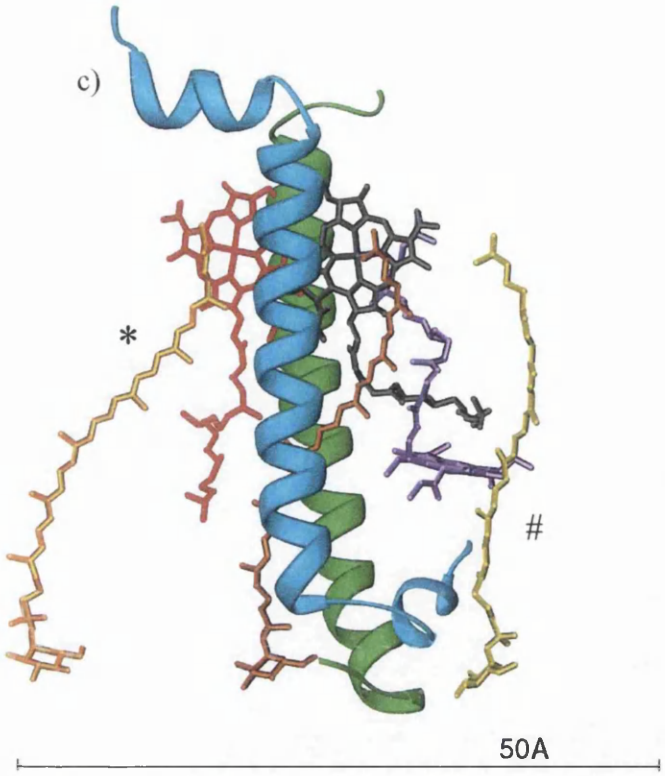

18c) The carotenoids interact with the subunit at either side. The tail of the carotenoid belonging to the next subunit (*) makes contact with the B850β (red) of the subunit shown. The head of the previous subunit (#) contacts both the α-polypeptide and B800 molecules.

1.4.1.2.Pigments and Spectra

When a photon is absorbed by a B800 molecule of the LH2 complex, the Bchl *a* molecule is promoted into the first singlet excited state. The energy is then rapidly transferred to the B850 molecules in 1-2 ps (at 77K) (Bergstrom et al., 1986; Bergstrom et al., 1988; Sundstrom and van Grondelle, 1995) down the energy gradient. The energy can also be transferred around the ring of B800 molecules in around 500 fs.

The alignment of the dipoles of the B850 molecules enables the rapid energy transfer around the ring of B850 molecules, with the structure showing the parallel Q_x dipoles forming a ring "like posts standing erect in a circle" (Freer et al., 1996). The end-to-end Q_y dipoles follow a shallow sinusoidal belt around the ring, leading to highly efficient energy transfer (Freer et al., 1996), with B850-B850 energy transfer occurring in 100-200 fs through the Q_y dipoles (van Grondelle et al., 1994). Excitation can also take place by direct absorption of a photon by the B850 molecules. These energy transfers are represented in figure 19.

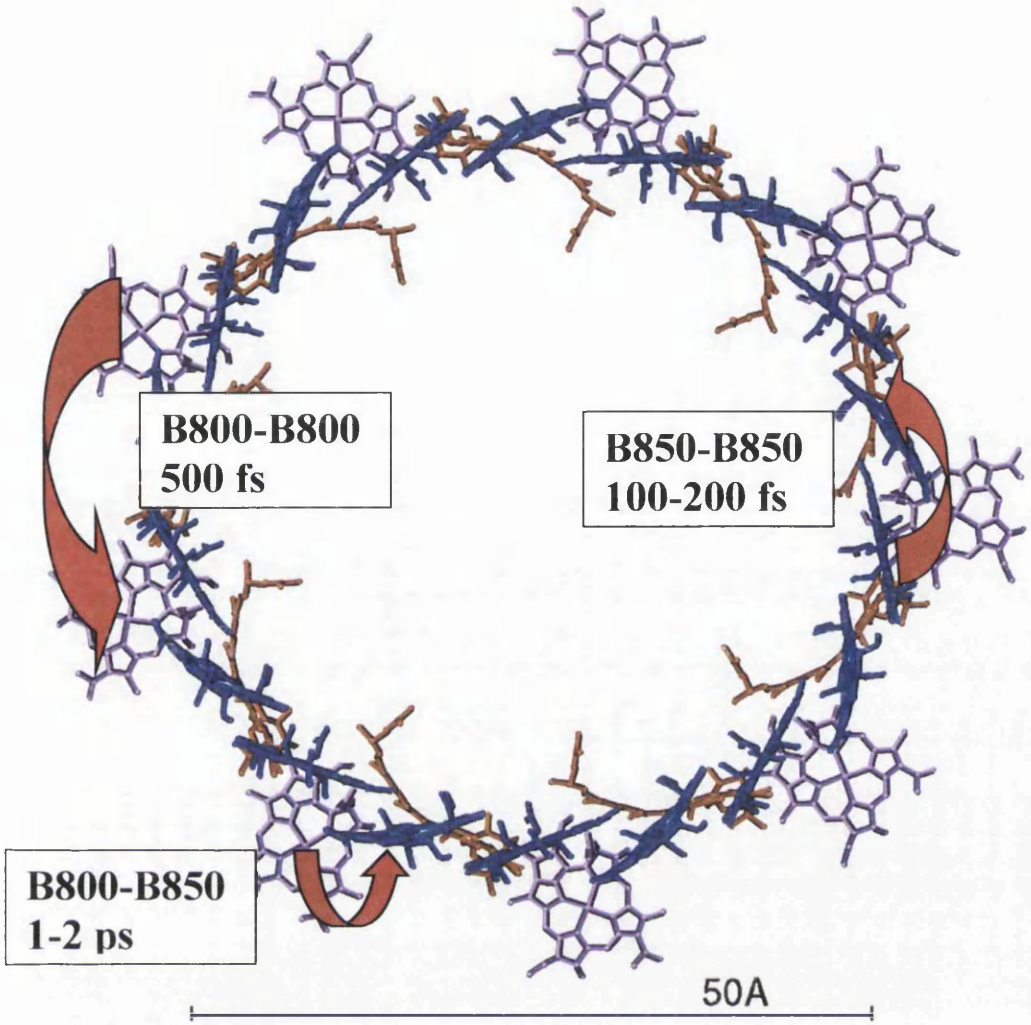

Figure 19. Energy transfer times within the LH2 complex. Transfer between the B800 molecules (purple) occurs in ~500 fs. Transfer from B800 to B850 (blue) occurs in 1-2 ps, and transfer between B850 molecules takes 100-200 fs. References are found in the text.

In effect this rapid energy transfer delocalises the excited state around a "storage ring" (Freer et al., 1996) and is proposed to occur by a combination of Dexter and Forster mechanisms (van Grondelle et al., 1994). The hydrophobic environment of the complex reduces the dielectric constant, which allows coupling over larger distances.

In the LH2 complex, the carotenoid also plays an important part as an accessory light-harvesting pigment (Angerhofer et al., 1986), and in stabilising the complex (Lang and Hunter, 1994).

Carotenoids absorb light in an area of the spectrum that Bchl *a* do not exhibit a strong absorption (450-570nm). Using the carotenoids as light harvesters gives the bacteria an advantage, being able to use incoming light over a broader wavelength

range. Energy is then transferred from the carotenoid to the Bchl. Upon absorption of a photon, the carotenoid is promoted from the singlet ground state, S_0, to the second excited singlet state, S_2. The molecule then rapidly relaxes to the S_1 state in a few 100 fs (Shreve et al., 1991) and then to the ground state in a few ps (Ricci et al., 1996).

As represented in figure 20, energy transfer can occur from both S_2 and S_1 states of the carotenoid. From the S_2 state, energy is transferred to the Q_x band of Bchl *a* and from S_1 to the Q_y band of both the B800 and B850 populations of Bchl *a*. The efficiency of energy transfer from carotenoid to Bchl *a* can be close to 100% in some species e.g. *Rb. sphaeroides* strain G1C (Cogdell et al., 1981). In *Rps. acidophila* it is about 55% (Angerhofer et al., 1986) as energy transfer occurs almost exclusively from the S_2 state (Macpherson et al., 1999).

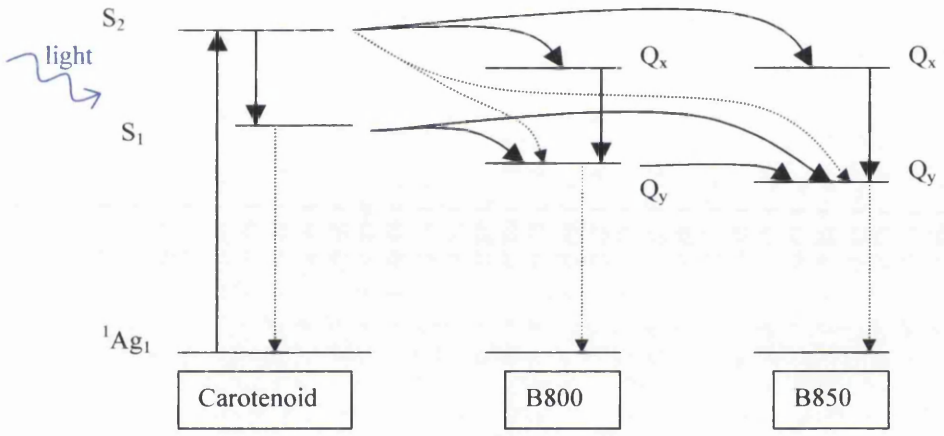

Figure 20. Energy diagram of carotenoid to Bchl transfer. Upon absorption of a photon, the carotenoid is promoted to the S_2 state, which then relaxes to the S_1 state by internal conversion, and then to the ground state. Energy can be transferred from the S_2 state of the carotenoid to the Q_x of Bchl and from the S_1 state to the Q_y band of the Bchl. The dotted lines represent minor transfer/relaxation channels. Taken from Sundstrom et al., 1999.

Carotenoids play an important part in stabilising the structures of light harvesting complexes with the molecule being entwined through the complex and associating with all the other components. It is observed that mutated strains of bacteria with the carotenoid deleted lack LH2 as the complex cannot be assembled without the carotenoid. A carotenoid deficient mutant of *Rb. capsulatus* is found to synthesise the polypeptides and insert them in the membrane, but they are then rapidly degraded (Oberle et al., 1990; Brandt and Drews, 1997). Similar observations have been made in a carotenoidless mutant of *Rb. sphaeroides* (Lang and Hunter, 1994).

1.4.1.3.LH2 Structure From *Rsp. molischianum*

The high-resolution structure of LH2 from the purple bacterium *Rsp. molischianum* (Koepke et al., 1996) shows similarities and differences to that of *Rps. acidophila* (McDermott et al., 1995). They are both ring structures consisting of α and β polypeptide pairs, with 3 Bchl *a* and one carotenoid molecule per subunit.

The most immediately obvious difference in the structures is that whilst the *Rps. acidophila* structure showed a nonameric assembly, that from *Rsp. molischianum* was found to be composed of only eight subunits, see figure 21.

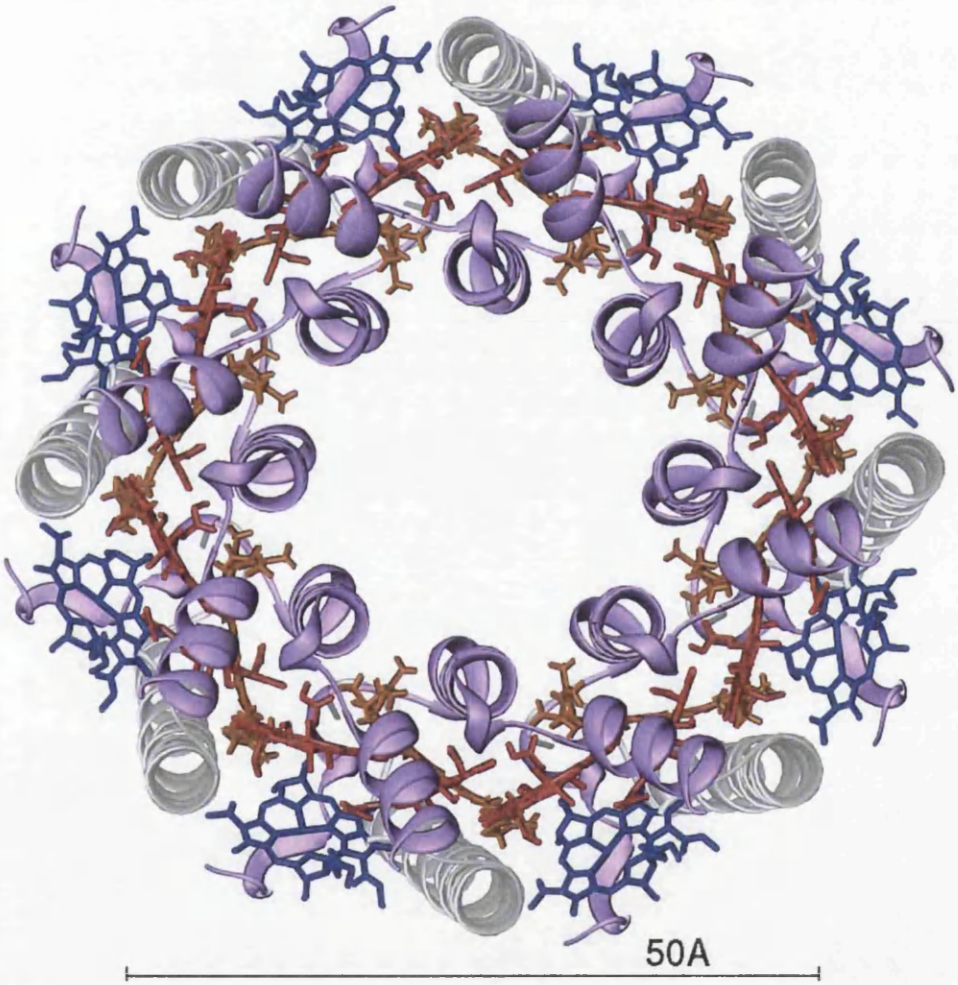

Figure 21a. The octameric structure of the LH2 complex from *Rsp. molischianum* (Koepke et al., 1996) viewed from above the periplasmic side of the membrane. The α-polypeptides are shown in purple and the β-polypeptides in grey both represented by ribbons. The B800 molecules are in blue, the B850 molecules in red and the carotenoid in orange, all as ball and stick representations. The phytyl chains from the Bchl molecules have been removed for clarity. The coordinates used to produce figures 22 and 23 were taken from the PDB, reference number 1CGH, and the diagrams produced using Ribbons3 (Carson, 1997).

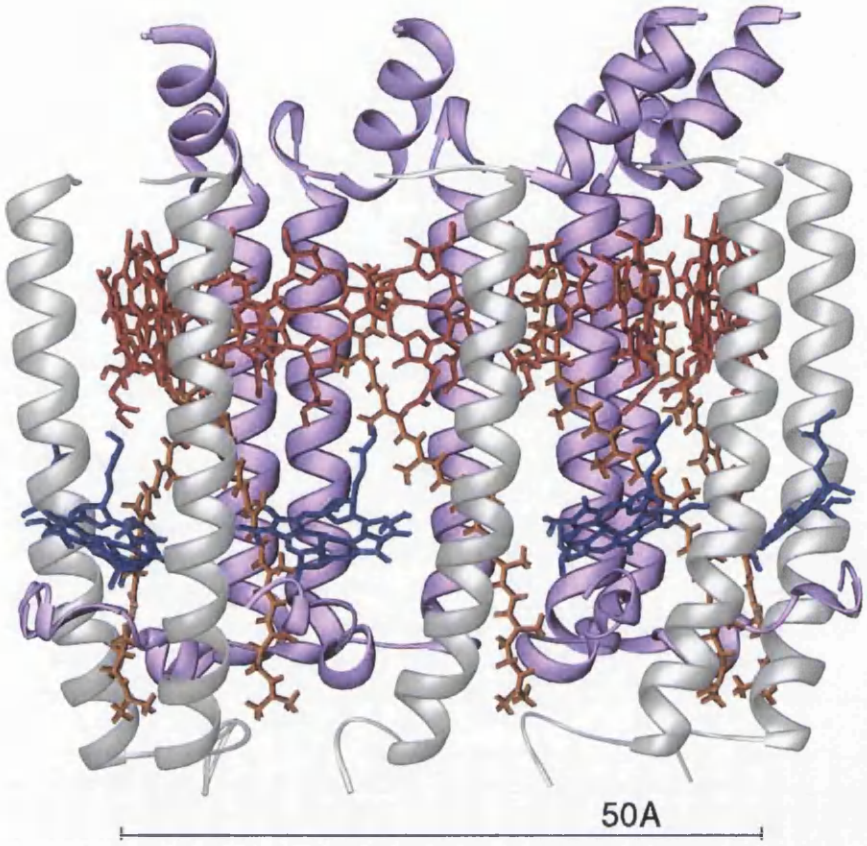

Figure 21a. The LH2 structure viewed side-on from within the membrane with the periplasm above and the cytoplasm beneath the complex. The rear three subunits have been removed for clarity.

The α and β polypeptides show 26% and 31% sequence identity respectively to LH2 of *Rps. acidophila*, with both structures being very similar in the transmembrane helices. Differences occur at both the N and the C termini, the α apoprotein from *Rsp. molischianum* having a longer helix at the C terminal end.

The general locations of the pigment molecules are similar in the two LH2 complexes, however, there are differences in the pigment molecules:
The ligation of the B800 Bchl *a* differs, with the *Rps. acidophila* structure showing the central Mg^{2+} ion ligated to an N terminal extension of the α apoprotein, whilst the *Rsp. molischianum* structure shows the ligand to be Oδ1 of Asp on the α apoprotein. The bacteriochlorin rings of the B800 Bchl *a* are also in a different orientations in the two structures meaning their transition dipoles are in different relative orientations. In the *Rsp. molischianum* structure, although the planes of the B800 molecules are not parallel to the membrane surface (see figure 22), the Q_y transition dipole moments are almost parallel to the membrane. This supports other spectroscopic work in which

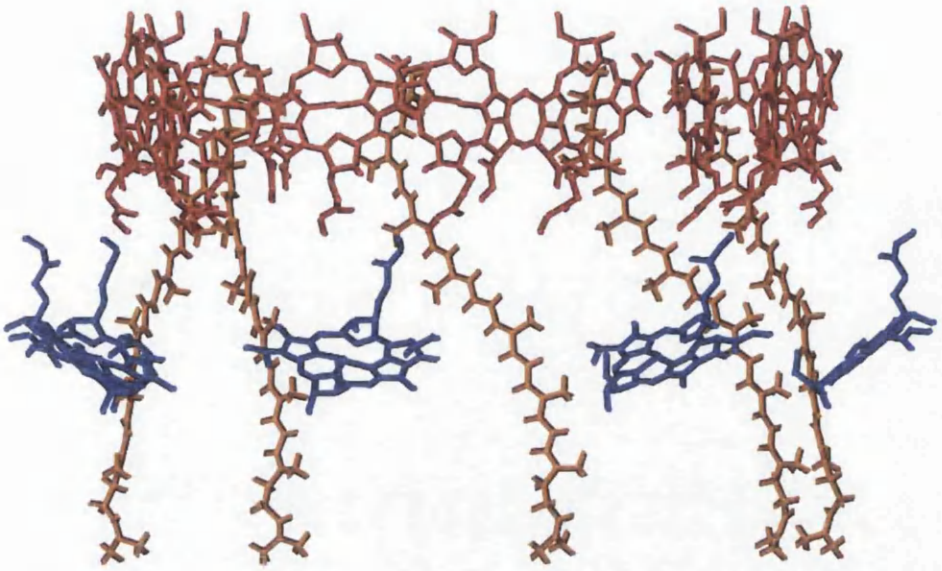

Figure 22. Side-on view of the pigments of the LH2 complex from *Rsp. molischianum*. The rear third of the molecule has been removed for clarity. The B800 molecules (blue) can be seen inclined at a greater angle to the membrane plane than in the LH2 complex from *Rps. acidophila* (see figure 19). Colours used are the same as in figures 21. The phytyl chains have been removed for clarity.

linear dichroism showed the B800 Q_y dipole resides in the plane of the membrane (Visschers et al., 1995). The Q_y transition dipole of the B800 molecule is almost parallel to that of the B850β and the B850α of the next subunit (Koepke et al., 1996). It is when these dipoles are collinear, or at least parallel, that the Forster mechanism is most effective (van Grondelle et al., 1994).

In the *Rps. acidophila* structure, the Q_y transition dipole of the B800 is at an angle of approximately 43° to the Q_y of the nearest B850α and almost perpendicular (about 105°) to that on the B850β molecule (Freer, Prince et al. 1996). This suggests lower energy transfer rates between the B800 and B850 molecules, although coupling amongst the B850 molecules is not taken into consideration, where the transition dipole moment of the ring (in *Rb. sphaeroides*) is enhanced by a factor of $\sqrt{(16 \pm 4)}$ compared to monomeric Bchl *a* (Leupold, Voigt et al. 2000)

Although lycopene is the major carotenoid present in *Rsp. molischianum* and rhodopin glucoside in *Rps. acidophila*, they both adopt very similar orientations (see figure 23).

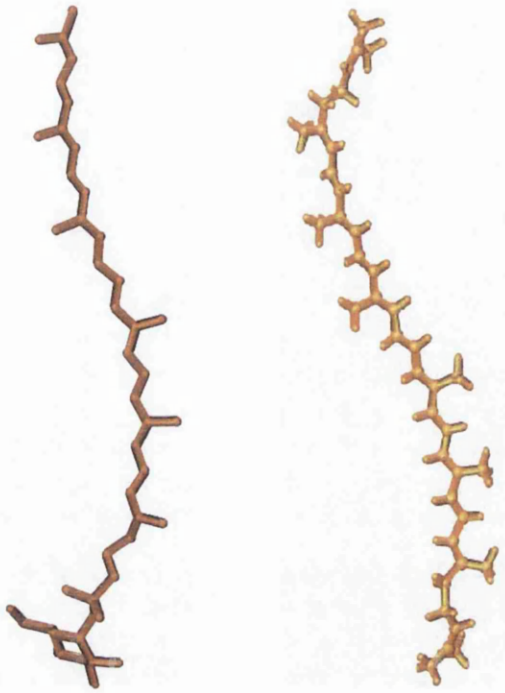

Figure 23. Rhodopin glucoside of *Rps. acidophila* (left) and lycopene of *Rsp. molischianum* (right) adopt similar conformations.

1.4.2. Core Light Harvesting Complex

All species of purple photosynthetic bacteria produce the core light harvesting complex, LH1, which is sometimes referred to as B880 due to the maximum absorption of Bchl *a* at 880nm as seen in figure. 24.

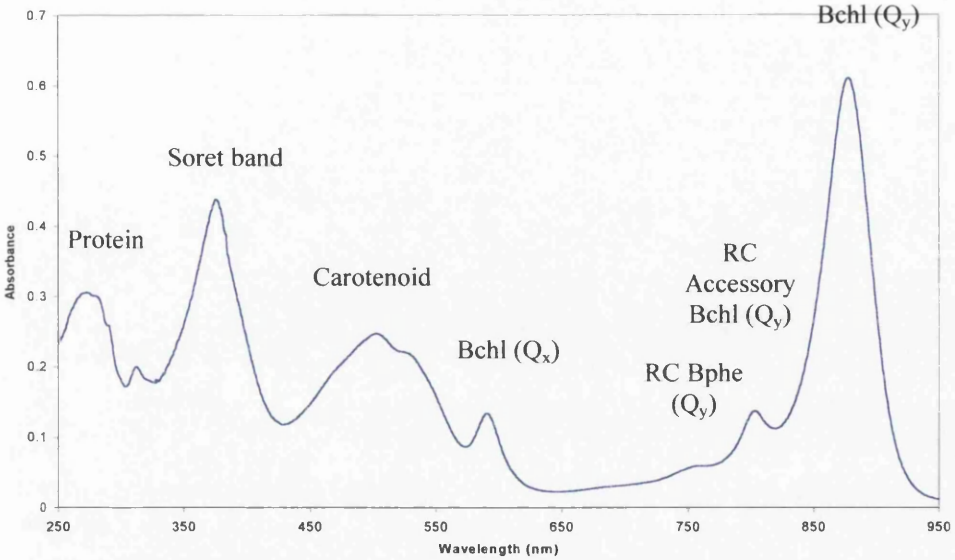

Figure 24. Absorption spectrum of RC-LH1 core complex from *Rps.* palustris, strain French, showing the pigments responsible for each absorption band. The absorption is due mostly to the LH1 complex as there are relatively few pigment molecules in the RC compared to the LH1 complex.

1.4.2.1.Structure And Function

The two-dimensional structure of the LH1 complex from *Rsp. rubrum* has been published as an 8Å projection map (Karrasch et al., 1995). This low resolution model was produced using electron microscopy and comparisons have been made between it and the peripheral light harvesting complex (McDermott et al., 1995) (see section 1.4.2.). It shows a ring system, 116Å in diameter with a large hole in the middle with a diameter of 68Å. This hole is large enough to accommodate the RC complex and this is the basis of many models of the PSU.

A model of the LH1 structure has been built (Papiz et al., 1996), (Hu and Schulten, 1998), the former using the subunit of the LH2 structure from *Rps. acidophila* (McDermott et al., 1995), and the latter using the subunit from *Rsp. molischianum.* The symmetry has been extended (which entails expanding the subunit radially) to fit the data available for the LH1 complex (Karrasch et al., 1995). See figure 25.

The LH1 and LH2 complexes share many features, with the most predominant one being the general composition of a ring assembly made up of pairs of α-helices, one ring inside the other with the helical axes almost normal to the membrane surface. The LH1 complex is apparently composed of 16 pairs of α-helices, with the inner helices termed the α-polypeptides, and the outer termed the β-polypeptides(Karrasch et al., 1995). It is proposed the pigment molecules, 32 Bchl *a* molecules and 16 carotenoids, are arranged between the α and β polypeptides with the plane of the bacteriochlorin ring system of the Bchl *a* molecules lying in the same direction as the helices. However, as it is only a low-resolution model, the positions of the pigments are uncertain (Karrasch et al., 1995).

There is some discussion as to whether the LH1 structure is a complete ring system or if there is a gap containing some other molecules. This is discussed more in section 1.5..

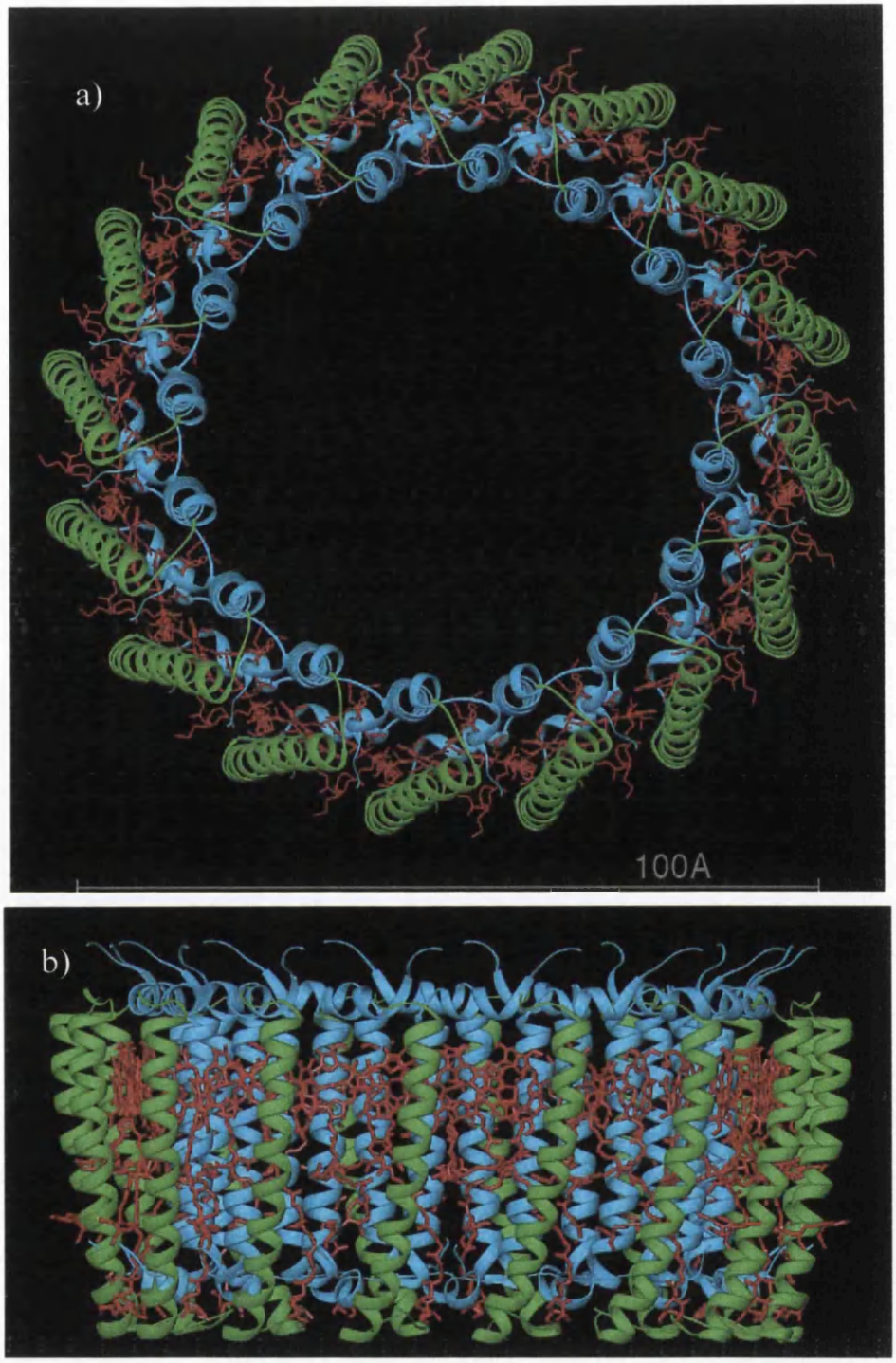

Figure 25a) Model of the core light-harvesting (LH1) complex (Papiz et al., 1996) viewed from above the periplasmic side of the membrane. The α-polypeptides (blue) have the α-helix almost perpendicular to the membrane surface. The β-polypeptides (green) are tilted at an angle of approx. 15° to the normal. The pigment molecules (Bchl *a* and carotenoid, in red) are situated between the polypeptides. b) The LH1 complex viewed side-on from within the membrane with the periplasm above and the cytoplasm beneath the complex. The coordinates used are from N. Isaacs (personal communication), and the diagrams produced using Ribbons3 (Carson, 1997).

1.4.2.2.Pigments And Spectra

The pigment molecules found in LH1 are bacteriochlorophylls and carotenoids, present as approximately 20% of the molecular weight of the complex. The low resolution of the structure makes it difficult to accurately place any of the pigments(Karrasch et al., 1995). However, it has been modelled that the 32 Bchl molecules are arranged such that the bacteriochlorin ring systems overlap, giving an overlap of the transition dipoles (Papiz et al., 1996). This would lead to the rapid and efficient energy transfer around the Bchl *a* molecules, effectively delocalising the energy until it is passed onto the special pair of the RC.

It can be seen in the absorption spectrum of LH1 in figure 23 that the Bchl molecules absorb at approximately 880nm (depending on species) which is at lower energy than the special pair in the RC absorb at (865nm). It is not yet clear why energy is being transferred in an "up-hill" manner from a greater wavelength to a shorter one rather than the other way around.

1.5.Model Of The Photosynthetic Unit

The high-resolution structures of RC and LH2 complexes along with the low-resolution projection maps of the LH1 complex enable a model of the whole PSU to be assembled (Papiz et al., 1996; Hu et al., 1997). In this, the RC is placed inside the ring of the LH1 complex, forming the core complex, with the LH2 complexes arranged peripherally around LH1 (see figure 26).

It has been shown that at high light levels, the PSU in *Rb. sphaeroides* contains about 30 Bchl *a* molecules per RC whereas at low light levels, 200-250 Bchl *a* molecules per RC are synthesised (Aargaard and Sistrom, 1972). This corresponds approximately to one LH1 complex per RC at high light, and an additional eight LH2 complexes at low light.

There are several unresolved points regarding the proposed model of the PSU, with one being the actual size and shape of the LH1 complex. The projection map of LH1 (Karrasch et al., 1995) shows that the hole in the centre of the complex is of a suitable size to place a RC complex inside the LH1 ring, and indeed some electron density was seen. This is supported by the projection structure of the RC-LH1 core

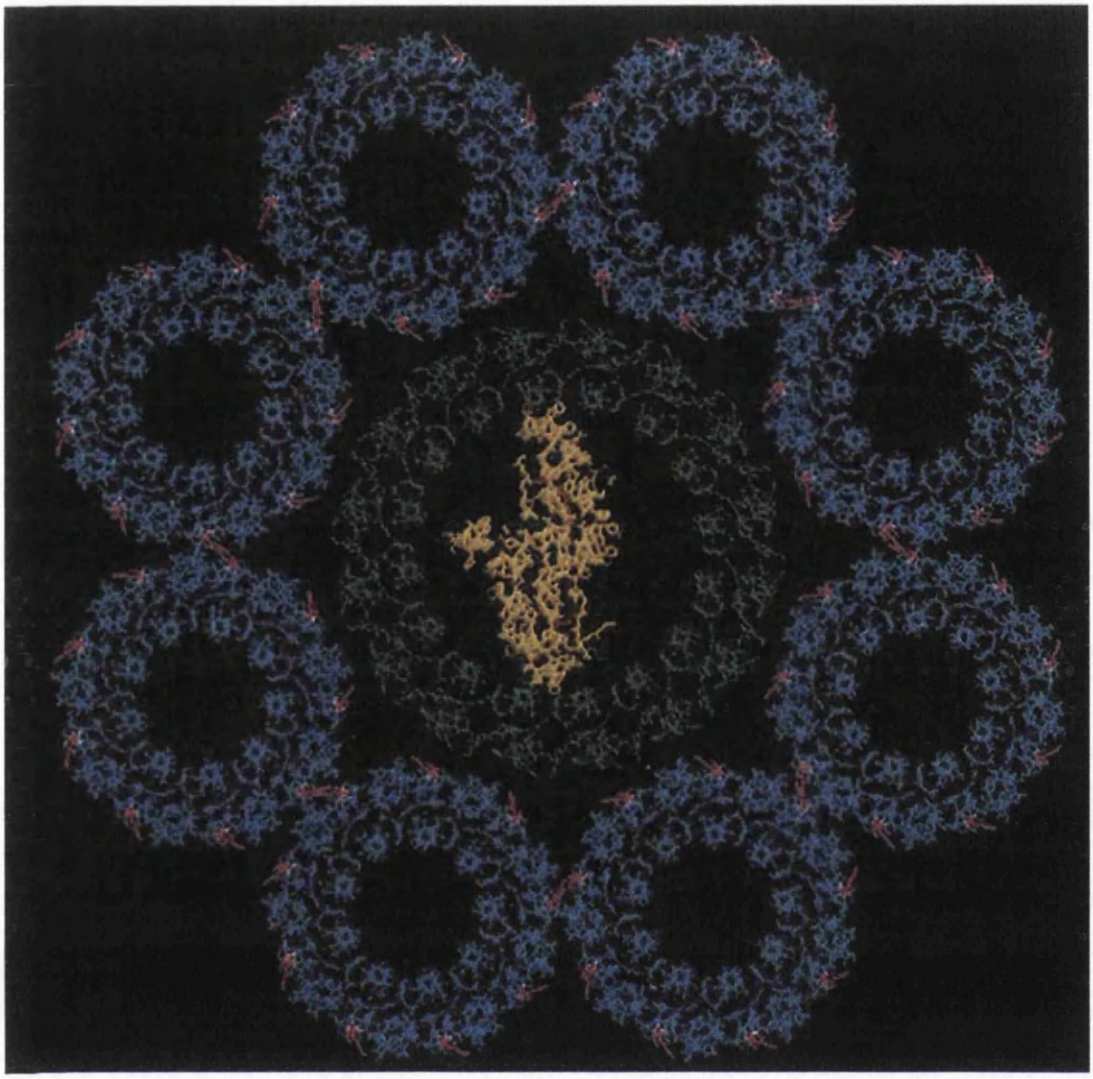

Figure 26. Model of the PSU viewed from above the membrane. The RC in yellow (from *Rb. sphaeroides*) is placed inside the LH1 complex drawn in green (based on data from *Rsp. rubrum*), and this is surrounded by LH2 complexes drawn in blue (from *Rps. acidophila*). This diagram is taken from Papiz et al., 1996. Eight LH2 complexes would only be seen in the PSU under very low light conditions.

complex at 25Å (Walz et al., 1998). However, if the LH1 complex were a complete ring with the RC inside, this would prevent the reduced ubiquinol from the Q_B site of the RC diffusing out of the complex and into the membrane and a new ubiquinone molecule filling the site. The function of the RC depends on this ubiquinone being replaced (Cogdell et al., 1996). The authors of the RC-LH1 core complex paper (Walz et al., 1998) note that the samples were prepared from RC-LH1-only mutants where the PufX gene was deleted (McGlynn et al., 1994; McGlynn et al., 1996). This means that the PufX polypeptide, which may prevent the LH1 complex from completely encircling the RC, is absent. Electron micrographs have demonstrated the presence of

quasi-crystalline arrays in the photosynthetic membranes of *Rb. sphaeroides* (Jungas et al., 1999) and this organisation depends on the presence of PufX (Frese et al., 2000). It is also suggested that PufX acts as a portal between the RC and cyt bc_1 complex (Frese et al., 2000). A higher resolution structure of the RC-LH1 core complex from a native strain of bacteria, and elucidation of the membrane organisation would help to answer this question.

There are also several proposed ways of arranging LH2 complexes around the core, ranging from a regular, ordered arrangement, to a random arrangement. In the regular arrangement, there could be up to eight LH2 complexes surrounding the core, and in the random arrangement, there is no set number of LH2 complexes to each core and an individual LH2 could be several units away from LH1.

In order to have rapid and efficient energy transfer between the complexes of the PSU that have been reported (van Grondelle et al., 1994), the Bchl *a* pigments must be close. In all the complexes of the PSU, the Bchl *a* molecules are found at the same depth in the membrane. The energy transfer from LH2 to LH1 takes place in 3-5ps and from LH1 to RC in 30-50ps (van Grondelle et al., 1994). However, work carried out on the whole PSU has been on crude membranes that may contain many forms of PSU and therefore must be considered an average.

It would be of benefit if the high-resolution structure of all complexes in the PSU could be determined from the same bacterium. At the moment, high-resolution RC crystal structures from *Rps. viridis* and *Rb. sphaeroides* have been solved. The 8Å map of LH1 is from *Rsp. rubrum* and the high resolution LH2 crystal structures are from *Rps. acidophila* and *Rsp. molischianum*. There are also low-resolution projection structures of the LH1 and RC-LH1-core complexes at 25Å from *Rb. sphaeroides* (Walz et al., 1998), a 6Å structure of the LH2 complex from *Rb. sphaeroides* (Walz et al., 1998) and a 7Å structure of LH2 from *Rhodovulum sulfidophilum* (Savage et al., 1996). Although these lower resolution structures are of interest, they do not show the details required to answer many questions such as what the arrangement of the LH1 complex is around the RC, and what the structural changes which lead to the different Bchl absorption are.

1.5.1. Energy Flow In The PSU

The photons absorbed by the Bchl *a* pigments in the LH2 complex is at wavelengths of 800nm and 850nm. That energy absorbed at 800nm is transferred to the Bchl *a* that absorb at 850nm which is at lower energy, therefore travelling down an energy gradient. This in turn is transferred to the LH1 Bchl *a* that absorb at 880nm, again travelling down an energy gradient. This downhill energy gradient leads to an almost uni-directional flow towards the RC, although the last transfer, from LH1 to RC is energetically uphill (see figure 27). The electron transfers of the RC have already been discussed in section 1.3.1.2.

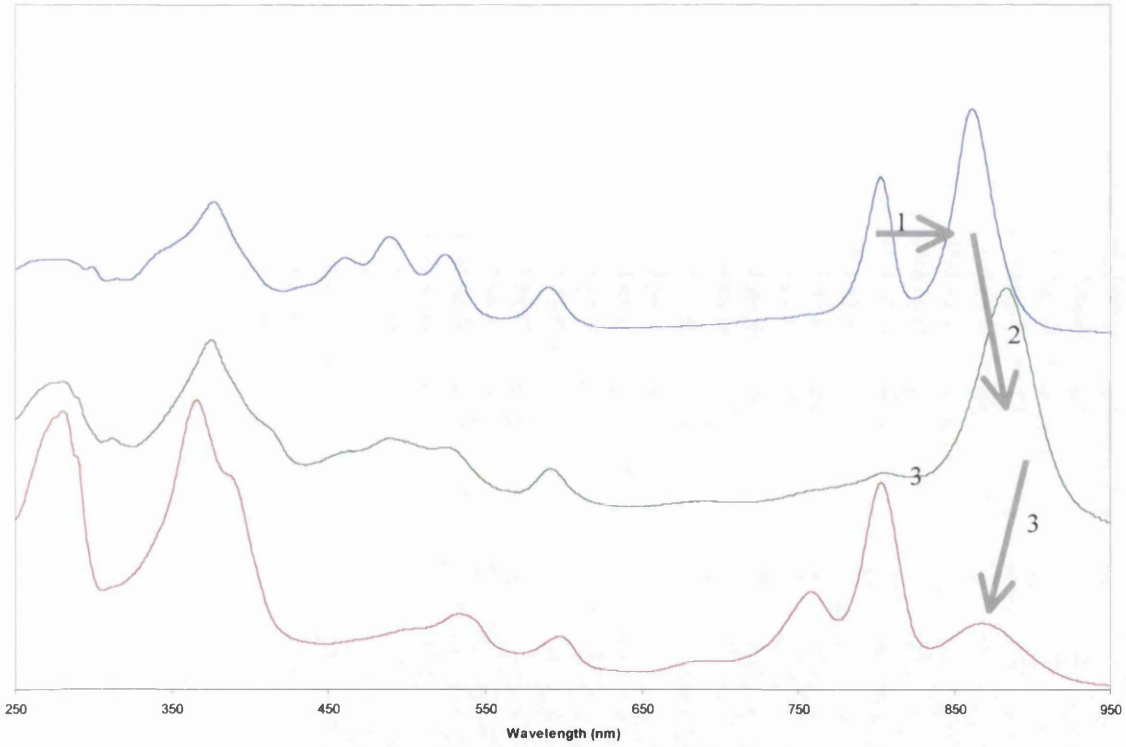

Figure 27. Overlaid absorption spectra of the components of the PSU (LH2 in blue, LH1 in green, RC in red) with the arrows showing energy and electron transfer.
1-B800 (LH2) to B850 (LH2). 2-B850 to B880 (LH1). 3-B880 to Primary Donor, D (RC).

The energy transfer process can be thought of as an energy "funnel" with the LH2 complexes positioned at the top of the funnel, covering a wide area and feeding into the LH1 complex which sits lower down the "funnel." The LH1 complex covers a smaller area, and surrounds the RC, which sits in middle of the funnel. However, as stated earlier, the energy transfer from LH1 to RC occurs in an "uphill" manner.

1.6.The B800-820 Light Harvesting Complex

In response to low light conditions, some species of bacteria such as *Rb. sphaeroides* produce LH2 complexes in varying amounts; few LH2 complexes at high light and more at lower light (Angerhofer et al., 1986). Other species of bacteria have the ability, at very low light, to produce a third light harvesting complex, LH3. This complex is very similar to the LH2 complex but instead of the Bchl *a* maximum absorption at 800 and 850nm, it is shifted to 800 and 820nm, hence it is sometimes referred to as the B800-820 complex (see figure 28). The reasons for the absorption change are discussed in section 1.6.2.

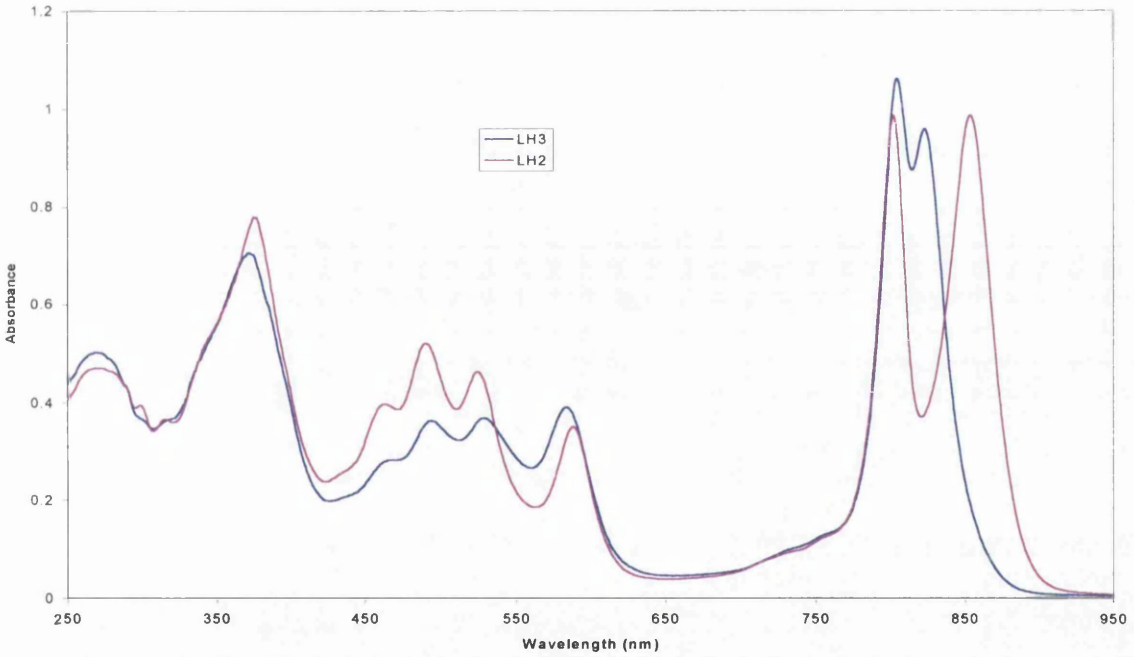

Figure 28. Overlaid spectra of LH2 and LH3 complexes from *Rps. acid* 7050. The LH2 complex shows absorption maxima at 800 and 850nm. The LH3 complex shows absorption maxima at 800 and 820nm. The three peaks between 450 and 550nm show incorporation of different carotenoids in the complexes.

Rps. acidophila strain 7050 and 7750 along with *Rps. cryptolactis* are amongst the bacteria able to produce this spectrally different form of the antenna light harvesting complex (Hawthornwaite and Cogdell, 1991).

It can also be seen that this peak height is of lower intensity in the low light (LL) form (peak at 820nm) than in the high light (HL) form (peak at 850nm). This is due to the wavelength dependence of the extinction coefficient of Bchl *a* but may also

be partly due to lower occupancy levels of the Bchl sites within the LH3 complex compared to the LH2 complex.

The absorption in the visible region, due to the carotenoid, is also slightly different. In *Rps. acidophila* strain 7050HL, the major carotenoid is rhodopin whilst in 7050LL, rhodopinal glucoside is the major carotenoid (Takaichi, 1999).

1.6.1. Production Of LH3 Complex

The production of these different complexes is mediated by a two component regulatory system where the external environment (incident light and/or temperature) is detected and a second messenger regulates the synthesis of the complexes. As the light and/or temperature decreases, firstly there is an increase in the production of LH2, and as the light level and/or temperature falls further, the production of LH3 is instigated. A review of this transcriptional regulation can be found in Phillips-Jones, 1998.

Several studies have been carried out to find under what conditions the bacteria produce the LH3 complex. It has been shown that different two different strains of *Rps. acidophila*, strain 7050 and 7750 require different conditions to produce the LH3 complex.

Strain 7050 will produce the LH2 complex at light conditions down to 110μmol/s/m^2 (Gardiner, 1992), whereupon there is a transition period where both LH2 and LH3 complexes are produced until LH3 is produced almost exclusively at 40μmol/s/m^2 (Gardiner, 1992). In order to differentiate between the different strains and complexes produced, *Rps. acidophila* strain 7050 will be referred to as 7050HL when producing the LH2 complex at high light (HL), and 7050LL when producing the LH3 complex at low light (LL). It should be noted that the bacteria also produce different carotenoids at HL and LL (Takaichi, 1999) and that the transition from production of the HL carotenoid to the LL carotenoid occurs at a slightly greater light intensity.

Strain 7750 reacts slightly differently as it also displays temperature dependence for producing the LH3 complex. When grown at 30°C, under low light conditions 50μmol/s/m^2 (Gardiner, 1992), 7750 will still produce a sizeable amount of LH2 complex. However, when the temperature is decreased to 22°C with the same

incident light of 50μmol/s/m^2, the bacteria produce mostly LH3 (Gardiner, 1992). It is seen that for the production of the LH2 and LH3 complexes, the light-dependence is dominant over the temperature dependence. When cultured at HL intensity and decreasing temperatures, the production of LH2 predominates, even at temperatures down to 20°C. A basal level of LH3 complex was always evident (Gardiner, 1992).

The production of a second peripheral light-harvesting complex can be rationalised by looking at the energy transfer from LH2 and LH3 to LH1. Since there is an energy gradient from the B850 of LH2 to B880 of LH1, energy transfer occurs in a mostly unidirectional way. However, there is some back transfer from LH1 to LH2. With LH3, the energy gap between this form of the peripheral light harvesting complex (820nm) and LH1 (880nm) is greater, therefore back transfer is restricted (Deinum et al., 1991).

However, the lifetime of the excited state Bchl *a* is in the order of a few ns whilst energy transfer from LH2 to LH1 takes only 2-20ps (van Grondelle et al., 1994; Hess et al., 1995). Even if energy is transferred back to LH2, it is likely that the equilibrium of the transfer would lie very much towards the LH1 complex. Therefore there may also be an evolutionary or other basis to production of the LH3 complex.

1.6.2. Structure Of LH3 Complex

The 3D crystal structure of the LH3 complex from *Rps. acidophila* strain 7050 has been solved to 3.0Å (McLuskey et al., 2001). It shows a complex similar in composition to the nonameric LH2 complex from *Rps. acidophila* strain 10050 (McDermott et al., 1995).

Like the LH2 structure, the LH3 complex consists of a ring made up of two cylinders of nine α-β apoprotein pairs with Bchl *a* and carotenoid molecules bound non-covalently. The apoproteins are almost exactly superposable from the LH2 and LH3 complexes, with the only major differences being in the pigment molecules.

The B800 Bchl *a* is found in the same environment in both complexes, with nine identical apoprotein-pigment interactions (<4.2Å) each. As with the B850 molecules of the LH2 complex, the B820 molecules can be split into two populations according to their associated polypeptide, referred to as αB820 and βB820.

It is the differences between the B850 molecules in the LH2 complex and the B820 molecules in the LH3 complex that are of the greatest interest as they show how the bacteria modulate the absorption maximum. In the LH3 structure, it is seen that the phytyl chains of both the αB820 and βB820 molecules adopt different, more extended conformations when compared with the analogous B850 molecules in the LH2 structure (see figure 29)(McLuskey, 1999).

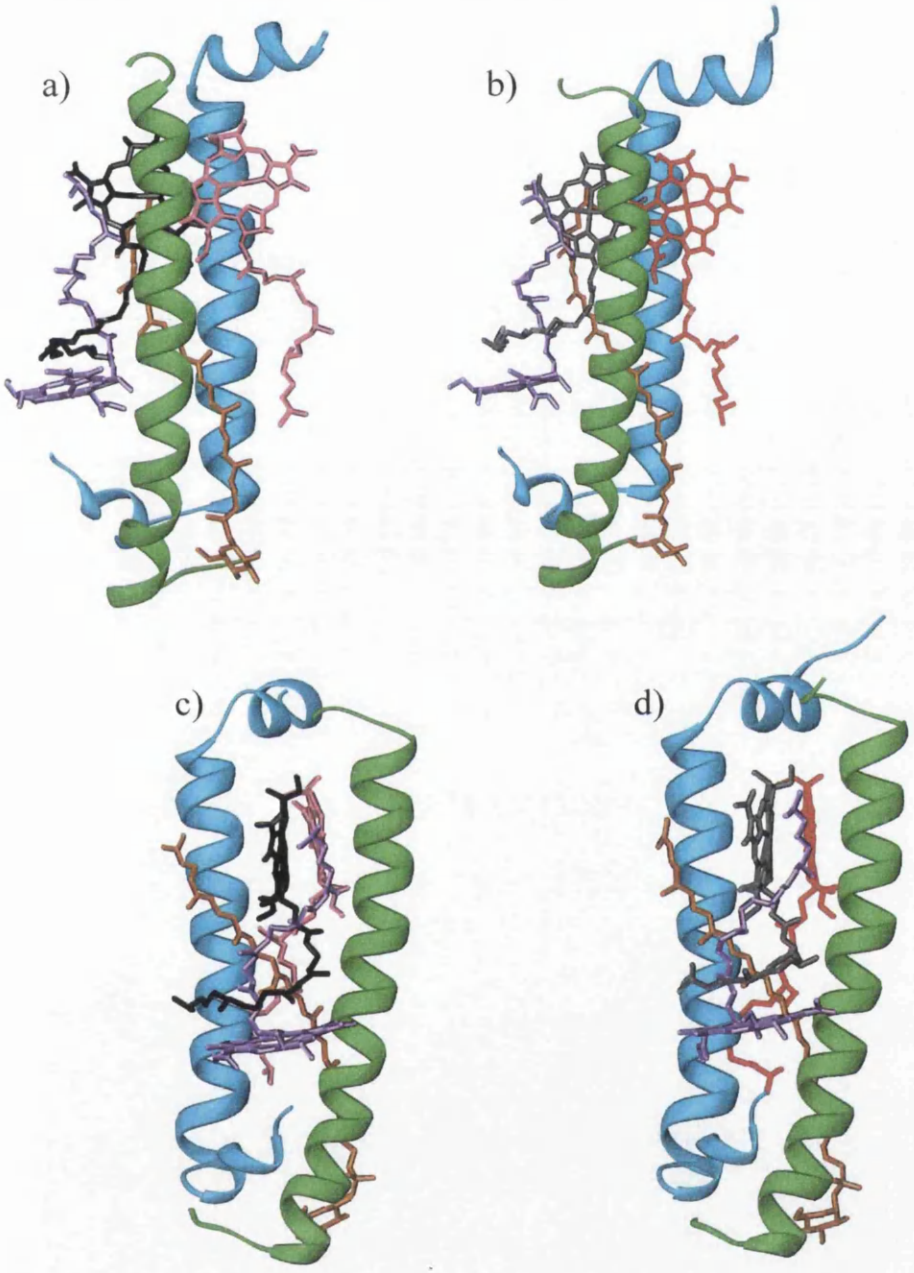

Figure 29. Subunit of LH3 (a & c)and LH2 (b&d). The αB820 (black and grey) and βB820 (pink and red) molecules adopt slightly different conformations in the complex. The carotenoid (orange) and B800 molecule (purple) are in similar positions in the LH2 and LH3 complexes.
Subunit of LH3 (c) and LH2 (d). The αB820 is seen closest to the α-polypeptide (blue), and the βB820 closest to the β-polypeptide. At this angle, the differences in conformation are not so obvious.

However, the conformation of the phytyl chain has little effect on the absorption characteristics of bacteriochlorophyll, which results from the transition dipoles of the bacteriochlorin ring.

There are many factors that affect the absorption maximum of Bchl *a* and could account for the observed change from the LH2 complex at 850nm to LH3 complex at 820nm. These have been recently reviewed (Cogdell et al., 2002) and can be either environmental or structural.

A more polar environment results in a red shift of the Q_y transition dipole, and buried point charges in the hydrophobic membrane could result in large shifts of the Q_y absorption (Eccles and Honig, 1982).

There are several structural factors that can affect the Q_y absorption. The bacteriochlorin ring system of the Bchl *a* can adopt a number of slightly different structures (see Barkigia & Fajer, 1993. for a review), the main ones being planar, bowed and saddled, each of which affects the absorption characteristics (Gentemann et al., 1997). Hydrogen bonding can also affect the Bchl absorption, with the LH3 structure showing the loss of two hydrogen bonds to the acetyl groups on Bchl (from α44 and α45) and a subsequent rotation of the acetyl groups out of the plane of the bacteriochlorin ring (McLuskey, 1999). This is due to amino acid changes at positions 44 and 45 of the α-polypeptide from Y and W (hydrogen bonding) in LH2 to F and L (non-hydrogen bonding) in LH3 being important. The rotation of the acetyl group removes it from the conjugated bond system of the Q_y dipole, thus decreasing the length of the conjugation and decreasing the wavelength.

1.7 Protein Crystallography

Protein crystallography is a technique that uses x-ray diffraction techniques on single crystals of a protein in order to determine its 3-dimensional structure. A crystal is a structure composed of many unit cells, which are the basic building blocks of crystals. These unit cells are arranged in a regular 3-dimensional array, with every unit cell within a crystal being identical.

1.7.1. Protein Classification

Proteins can be classified according to their location within the cell. If a protein is found in the aqueous environment of the interior of the cell, it is classified as a soluble protein. If it is found in, or associated with, the cell membrane, it can be classified as a membrane protein. As stated earlier, the pigment-protein complexes that comprise the PSU are membrane bound. Soluble proteins are described below as many techniques developed on soluble proteins have been adopted for the membrane bound species.

1.7.1.1.Soluble Proteins

Soluble proteins are reasonably well understood from a structural point of view, with the first 3D crystal structure of a soluble protein (that of myoglobin) being published in 1958 (Kendrew et al., 1958)

The first proteins to have their structures determined were ones that are reasonably abundant in the cell, as a sufficient quantity must be extracted and purified in order to grow crystals. As the targets for protein crystallography expanded, those proteins being targeted have not all been in high abundance within the cell, and different ways of producing the protein have been developed. Protein overexpression has been pivotal in producing a sufficient amount of proteins in order to study them by many techniques including x-ray crystallography.

Although by no means an exact science, the crystallisation of soluble proteins is also quite well characterised, and there are many documented techniques and principles that can be applied to increase the chances of growing crystals.

The numbers of protein structures available has increased dramatically with over 3000 structures of soluble proteins deposited in the Protein Data Bank (PDB) in 2001 (http://www.rcsb.org/pdb/).

1.7.1.2.Membrane Proteins

The cell membrane (also known as the phospholipid bi-layer) is a non-aqueous environment of amphipathic molecules, and this is where membrane proteins can be

found. Membrane proteins can be classified according to their interaction with the membrane. Some proteins are only loosely associated with the membrane, generally interacting with the head groups of the phospholipids through ionic bonds. Some have a small section protruding into the membrane, often an α-helix which acts as an anchor, tying the protein to the membrane. The remaining proteins are classed as integral membrane proteins, and these are intimately associated with the membrane, often spanning the entire depth of the lipid bi-layer.

Just as the field of soluble protein structure determination was dominated in early years by those proteins available in abundance, this has also been the case in the field of membrane protein crystallography. Membrane proteins are very difficult to overexpress in their native form, as many cells do not express large amounts of membranes or membrane proteins. Work into this area is ongoing in order to develop systems that can regularly provide mg quantities of membrane proteins.

1.7.2. Basic Crystallisation Theory

Crystallisation is where molecules are brought from a supersaturated solution into the solid state. A super-saturated solution is a temporary, unstable state when too many molecules in a solution are competing for solvent interactions, therefore some molecules must come out of solution. The aim is to bring out the protein molecules in a solid crystalline state (the other main states being precipitation and phase separation).

There are three stages to crystallisation; nucleation, growth and termination of growth of crystals.

Nucleation is when crystals appear spontaneously and occurs when a sufficient number of molecules aggregate to form a nucleus, the minimum sized thermodynamically stable aggregate. This occurs in the nucleation region of the supersaturated area of the phase diagram (see figure 30).

The growth phase of the crystal is when protein molecules are added to the surface of the nucleus and the crystal is enlarged. Much work, using both practical and modelling techniques, has been carried out on the growth of crystals in order to understand convection currents and sedimentation flow within protein drops (Haas and Drenth, 2000; Qi and Wakayama, 2000). The presence of a "liquid film" around the crystal, with high protein concentration, enhances the sticking probability of new

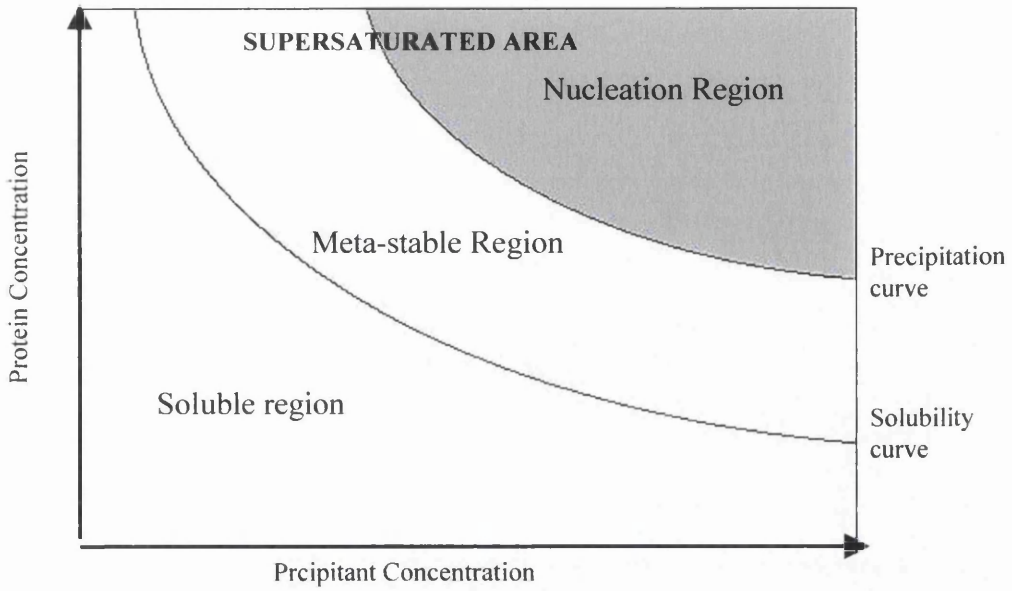

Figure 30. Phase diagram for protein in solution.

molecules (Haas and Drenth, 2000). Crystal growth occurs in the meta-stable region of the phase diagram.

The termination of growth of the crystal is when no new protein is added to the crystal. This can be due to several reasons including that there is not enough protein in solution (the protein concentration has passed through the solubility curve) and the crystal drop is no longer in the meta-stable region of the phase diagram or due to defects in the crystal packing. Generally, crystals can selectively incorporate homogeneous molecules during growth, but as the growth phase progresses, the concentration of heterogeneous molecules increases, and therefore the likelihood of their incorporation increases.

If the solution is taken too far or for too long into the nucleation zone of the phase diagram, a lot of nucleation will occur, and many very small crystals may result. Ideally, there should be two or three sites of nucleation enabling large, single crystals to grow. If nucleation is proving problematic, a technique known as seeding can be attempted. Seeding provides a template on which further molecules can be assembled. There are two main methods of seeding, both requiring that the protein solution to be seeded is at equilibrium, and in the supersaturated region of the phase diagram.

Firstly, if previous crystallisation has yielded many small crystals, these can be used as the "seeds" from which to grow larger crystals. The small crystals can be

washed in mother liquor to partially dissolve them and give a fresh surface, on which other protein molecules can bind, and then transferred to a pre-equilibrated protein drop. This is known as macro-seeding.

Micro-seeding (or streak seeding) is where a hair or fibre is gently touched against a crystal that has already formed. This hair will pick up microscopic fragments of crystal where it has touched the crystal. The hair is then drawn across a protein drop that has already been equilibrated against well solution. Crystals may form on the line where the hair was streaked and deposited micro-crystals.

The phase diagram can be affected by many factors, including vibration, temperature and additives, and changing one parameter can radically alter the behaviour of a protein solution with regards to crystallisation.

There are several methods of crystal growth of which vapour diffusion is the most commonly used and was employed in this study. Other methods include the batch method, whereby protein and precipitant molecules are mixed and left, and the related microbatch technique where small volumes (about 2μl) are used under oil, which prevents evaporation. It should be noted that generally this is not suitable for membrane proteins due to interaction between detergents and oils. The other commonly used method is dialysis whereby the protein solution is equilibrated with mother liquor through a semi-permeable membrane.

Of the vapour diffusion techniques, sitting drop is most commonly used for membrane proteins and larger volumes can be used. Hanging drop is not commonly used for membrane protein crystallisation as the detergents used can make hanging drops spread out by decreasing the surface tension. The use of sandwich drops can slow down the rate of equilibrium when required.

Supersaturation and crystal growth can be obtained in two ways, salting out and salting in. Salting in occurs when a protein becomes less soluble as the ionic strength of the solution decreases. If the protein drop has a low initial ion concentration, the protein will fulfil some electrostatic bonding requirements with protein-ion interactions. As the ion concentration is decreased, the protein molecules form interaction between molecules to fulfil their electrostatic requirements. This leads to a lower solubility and is used to grow crystals. Dialysis is often used for salting in as low ionic strength buffers or even distilled water can be equilibrated against the drop.

With salting out, the protein becomes less soluble as the ionic strength of the solution increases. The initial salt concentration of the well solution is much higher than that in the drop, therefore water vapour diffuses from the drop to the well thus decreasing the drop volume and increasing the concentration. As the concentration increases, the solution eventually reaches super-saturation, with the intention being that the protein molecules will come out of solution in well ordered crystals. Vapour diffusion is commonly used for salting out.

Many additives can be used to change the characteristics of the phase diagram. Precipitants can help by possibly providing nucleation sites or competing interactions with solvent molecules. The phase diagram is also dependant on pH, temperature, time and vibration and all of these parameters must be accurately controlled.

Although not always the case, if a crystal has good morphology (sharp edges and corners, well-defined shape, consistent colour throughout) it will often diffract better.

1.7.3. Membrane Protein Crystallisation

Crystallising a membrane protein is complicated further by use of detergents. Since the proteins exist in the membrane, if they are removed from the membrane into an aqueous solution, they will rapidly precipitate and therefore detergents are used to mimic the lipid bi-layer. This can lead to a more complicated system with detergents affecting the phase diagram, solubility and properties of some additives commonly used for soluble proteins.

1.7.3.1.Use Of Detergents In Membrane Protein Crystallisation

Detergents are amphipathic molecules comprising a hydrophobic tail and a hydrophilic head group. They are used to remove the proteins of interest from the membrane, which is rather heterogeneous, containing many types of lipids and other molecules. Homogeneous detergents are used to replace the membrane (although mixtures of detergents are sometimes used) and also have the ability to form micelles (an aspect lacking in lipids). Micelles are thermodynamically stable colloidal aggregates that form above a certain concentration of detergent known as the critical

micelle concentration (CMC). Micelles can be used to displace the lipid and isolate protein molecules. As detergent is added to the membranes, it is firstly incorporated into the membrane. As the detergent concentration is increased, the membrane breaks down and as more detergent is added, proteins from the membrane become isolated in detergent micelles. The intention is to completely replace the membrane with detergent and isolate individual protein molecules within a homogeneous detergent micelle. Detergents are used throughout the protein preparation, which enables the work to be carried out in aqueous solutions, negating the necessity of more difficult solvent conditions.

However, there are also disadvantages to using detergents. Since detergent molecules surround the hydrophobic region of the protein molecule, it is those detergent molecules rather than the protein that may interact with the surroundings and the properties may be changed by use of different detergents. The hydrophilic regions of the protein should still be free to interact as is seen in the crystal packing of the LH2 complex (McDermott, 1997).

In crystallisation, changing detergents can also affect many parameters. The phase diagram may be altered, different crystal forms may grow, phase separation may occur, or there may be an adverse reaction with a precipitant molecule or other additive. Sometimes, a protein may be found to not crystallise successfully until the correct detergent is found. Due to cost constraints, ease of working/measuring, and the particular requirements of individual steps within the protein preparation, it may be necessary to change detergents during the experiment. This has often been the case prior to crystallisation (Koepke et al., 1996; McLuskey, 1999).

With regards to protein crystallisation, liquid-liquid phase separation is the situation where a crystal drop has separated into two different phases, often recognisable due to the appearance of "oily" droplets within the drop. One of the phases, normally the oily droplet, is generally rich in protein and precipitant whilst the other is mainly solvent. Although there have been reports of some protein crystals growing from phase separated drops, in most cases crystal growth does not occur.

Phase separation is especially a problem in membrane protein crystallisation where many non-optimised parameters can lead to rapid and significant phase separation. One of the phases is generally very rich in detergent, which can denature the protein, and the other is detergent poor, which can lead to precipitation. Some detergents may be more prone to phase separation under different conditions so in

addition to the usual parameters that must be investigated for soluble protein crystallisation, detergent type and concentration must be optimised for membrane proteins.

1.7.3.2.Use Of Amphiphilic Molecules In Membrane Protein Crystallisation

Many small amphiphilic molecules are used in membrane protein crystallisation although their exact role is uncertain. It is proposed that they are incorporated into the detergent micelles, disrupting the packing and decreasing the size of the micelle enabling more crystal packing contacts (Deisenhofer et al., 1985). This is further characterised in work carried out on the use of heptane-1,2,3-triol in detergent micelles of LDAO (Timmins, et al., 1991). It could also be possible that the amphiphiles themselves play a part in the crystal contacts although there has been no crystallographic evidence of this. As with the addition of many other molecules to the crystal drop, small amphiphiles also affect the phase diagrams. Commonly used small amphiphilic molecules include benzamidine and heptane-1,2,3-triol. Some membrane proteins have been crystallised in the absence of a small amphiphile but the majority of reported conditions do contain some. Again, the choice of this molecule can have major effects on the crystallisation of the protein, and care must be taken in choosing it so that there is no reaction with protein, detergent, or any other molecule present.

1.8.X-Ray Crystallography

When a beam of x-rays is focused on a crystal, some of these x-rays will be diffracted. It is these diffracted x-rays that are measured, and the field of x-ray crystallography is based upon. X-rays are of wavelengths between 1000 and 0.1Å although those used for x-ray crystallography are generally between 0.7Å and 1.6Å.

If we firstly consider a single molecule subjected to an x-ray beam, it would give such a small diffraction as to be undetectable. The reason the crystal diffracts x-rays to a sufficient degree to be detected is due to its composition. A crystal can be though of as a series of molecules repeating in all directions. Planes could then be imposed on this model (see figure 31). When x-ray are diffracted from one plane of

the crystal, they are also diffracted by the next plane. As x-rays are wave functions, they have a phase as well as amplitude, and according to the angle at which the diffraction occurs, these x-rays will lead to constructive or destructive interference.

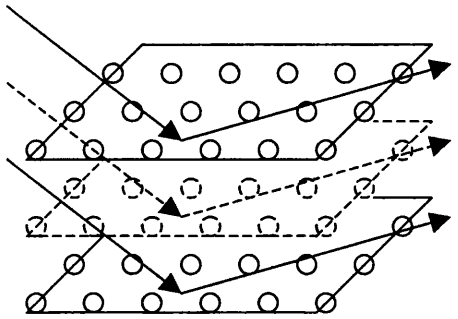

Figure 31. Simplified diagram of three planes of a crystal with molecules represented by circles. Incident x-rays are diffracted by all planes.

This has been characterised by Bragg's Law:

$$2d\sin\theta = n\lambda$$

where d=distance between two crystal planes, θ=angle of incident radiation with respect to crystal plane, and λ=wavelength of radiation.
Therefore, in order to be coherent (constructive interference), the phase difference must be an integral number, n.

Well ordered crystals are essential for good diffraction, with small defects accounting for poor resolution as well as the termination of growth of crystals.

When exposing crystals to an intense beam of x-rays as is used in modern crystallography, there can be significant radiation damage to the crystal. There are two types of radiation damage, primary and secondary radiation damage. Primary damage occurs when an x-ray hits a protein or solvent molecule and forms a radical. Secondary radiation damage occurs when this radical diffuses through the crystal and comes into contact with other molecules thus damaging them, and creating more radicals. In order to limit the radiation damage caused, it is common to collect data at cryo-cooled temperatures of about 100K (Rodgers, 1994). This does not decrease the amount of primary radiation damage, but reduces secondary radiation damage, by preventing the diffusion of molecules and radicals through the crystal (Garman and Schneider, 1997).

When collecting and measuring the diffraction pattern from an experiment, only the intensity of the spot produced is measured. Since it is known that the spot is caused by constructive interference, the waves must be in phase, however, it is not possible to measure the phase of x-rays, and they could be in any part of the phase cycle. This means that the phase of the x-rays must be calculated by some other means. This is known as the phase problem. There are several methods of solving the phase problem for protein crystallography. These include Direct Methods (DM), heavy atom methods and Molecular Replacement (MR).

Direct methods is a *de novo* way of determining the structure of a molecule, originally used in small molecule crystallography but rapidly becoming a vital tool for protein crystallographers. Although constantly improving, programmes such as SHELX and ShakeNBake, work best on very high-resolution structures (≤1.2Å) of smaller proteins (<100aa).

Of the several heavy atom methods currently in use for solving the phase problem, the most commonly used techniques are multiple isomorphous displacement (MIR) and multiple-wavelength anomalous dispersion (MAD).

MIR involves incorporating a number of heavy atoms into the crystal, often by soaking a crystal in mother liquor containing heavy atoms compounds, such as K_2PtCl_4 or $KAu(CN)_2$. Several different heavy atom soaks are performed on separate crystals in order to bind heavy atoms to specific sites within the unit cell. If there are too many heavy atoms incorporated in the unit cell, the signal will be swamped by the heavy atoms, and if they are not bound specifically, there will be disorder about their position.

A dataset is taken from the native crystal and each of the heavy atom derivatives. If it is assumed the crystals are isomorphous, the differences in diffraction patterns will be due to the heavy atoms and this can be used to determine the phases.

MAD also uses heavy atoms within the unit cell, although this often uses seleno-methionine derivatives or intrinsic metal ions, for example copper or iron within the protein. For selenium derivatives, the protein is overexpressed in a system in which selenium can be incorporated into all methionine residues in preference to the sulfur atom, which is normally present. Since methionine residues rarely play a part in the chemistry of the proteins, the structure of the protein should remain unaffected.

The MAD technique uses the fact that heavy atoms differentially absorb photons of different wavelengths, with each element displaying a characteristic absorption maximum. At energies below this peak, the absorption drops rapidly and this is known as the absorption edge and atoms display anomalous scattering close to this absorption edge. Light atoms normally found in proteins such as carbon, nitrogen and oxygen do not have an absorption edge close to the wavelengths used in crystallography, however, heavy atoms such as copper and selenium have absorption edges with wavelengths around the 1Å region.

Three, or sometimes four, datasets are collected at different wavelengths corresponding to the peak wavelength, the inflexion point, a high energy remote point, and sometimes a low energy remote point. These different wavelengths produce datasets with very small differences in the anomalous signal that can be used to determine the heavy atom sites, either through a Patterson search or by direct methods. MAD experiments can only be carried out on beamlines with a tuneable wavelength and it is important to accurately know the wavelength at which each dataset is collected.

Molecular Replacement (MR) relies on the previous structure solution of a similar protein by one of the methods mentioned above. As more structures become available, MR is becoming an increasingly popular method of solving the phase problem. If there is a similar protein structure in the protein database (PDB), the phase information from that protein may be used to provide initial information on the phases from your target protein. In this case a similar structure may be >25% amino acid identity, although this value can vary dramatically. In order to solve the structure of the target molecule, a model is placed in the unit cell and manipulated by translation and rotation functions so that it best matches that of the target structure.

Firstly the rotation function compares the Patterson self-vectors of the known and unknown structures. Patterson functions can be calculated from amplitudes only, and translation vectors can be discounted as intramolecular vectors are shifted to the origin. The rotation function provides the α, β and γ angles and once these are optimised, the translation function is considered.

The translation function determines where in the unit cell the search model should be placed after the application of the rotation function. Depending on the space group, a lower dimensional search may be possible (in a monoclinic cell, only a search on the x- and z-axes are required due to the arbitrary position along the y-axis).

As the structures of several RC complexes are available, it was possible to use MR to solve the phase problem in the work carried out here.

1.8.1. Types Of Radiation

The x-rays used in protein crystallography can either be generated in the home lab or from a synchrotron radiation (SR) source.

The most commonly used home source employs a rotating anode, normally copper, to provide x-rays at a wavelength of 1.54Å from the Kα edge. The advantages of a home source include ease of timetabling (crystals can be used as and when they become available), generally data can be collected slower and over longer time periods and the beam is consistent over long time periods.

SR comes from an electron storage ring where electrons are accelerated to emit electromagnetic radiation of different wavelengths according to the extent of the acceleration. This acceleration can either be caused by a bending magnet, which is used to guide the electron beam and produces "white" radiation, or by an insertion device.

Insertion devices are magnets inserted into the electron pathway to disrupt the normal flow, and produce x-ray radiation. The most basic type of insertion device is a wavelength shifter which provides radiation of shorter wavelength and higher intensity. A multipole wiggler, as used in beamline 9 at the SRS uses a series of wavelength shifters to produce a more intense x-ray beam which is of tuneable wavelength.

An undulator like that used on ID14 at the ESRF is similar to a multipole wiggler, but uses magnets with moderate power and a large number of poles. This gives radiation with a coherent sum and is almost monochromatic, although this wavelength is not tuneable.

SR produces a much stronger and less divergent beam (high brilliance) which leads to faster data collection from smaller crystals. Synchrotron beams are, however, less stable and fluctuate throughout the day, as the synchrotron requires regular injections of electrons to maintain an output. Trips must be planned in advance and crystals must either be grown in time for the trip, or frozen and stored.

1.9.Mass Spectrometry of peripheral light harvesting complexes

Matrix Assisted Laser Desorption Ionisation mass spectrometer with Time of Flight detector (MALDI-TOF) mass spectrometry has been used since the late 1980s as a useful tool for analysing the mass of macromolecules (Karas et al., 1987). It's advantages over other methods, like electrospray, is that very small amounts of sample can be used, and it is relatively tolerant to buffers and other additives. This means the sample can be analysed in a less harsh environment rather than extracting into the polar, volatile solvents required for electrospray.

The sample is mixed with a solution containing matrix molecules where the matrix molecules are small sublimable molecules. A small drop of this mixture is placed on a target plate and allowed to dry. The basis for this method is that the drop will form a "solid solution" whereby each sample molecule is isolated and surrounded by matrix molecules and ions that will provide the necessary charge to enable analysis. The plate is then placed in the analyser and the dried droplet is targeted by a laser pulse that excites the matrix, which in turn excites the sample molecule. If the laser were used to excite the large polypeptide directly, a higher energy would be required, which may decompose the sample molecules. The excitation of the sample leads to a charged species, $[M+X]^+$ where M=sample molecule and X=H, Li, Na, K etc. Negatively charged species can also be detected although only positively charged ions were used in this study. The matrix molecule is chosen as one that absorbs at the wavelength of the laser used to provide the excitation energy (in this case a nitrogen laser at 337nm).

A voltage is then applied to the flight tube, which accelerates the charged species according to their charge and mass. These species are detected and categorised according to their time of flight.

1.10. Aims

The work detailed in the remainder of this thesis was undertaken in order to provide more information on the structures of purple bacterial Reaction Centres (RCs) and peripheral light harvesting (LH3) complexes.

Firstly, work was carried out on the LH3 complexes from *Rps. acidophila* strains 7050 and 7750 in order to try to improve on the 3.0Å resolution limits of the structure currently available (McLuskey, 1999). This was to look at the binding of the 820nm absorbing Bchl *a* molecules to clarify the structural changes compared with the LH2 complex.

Mass Spectrometry was employed to identify contaminating polypeptides present within the native complexes, and to identify the main component by comparison with published sequences.

The structure of a carotenoidless RC mutant was investigated in which the carotenoid had been chemically reconstituted. This was carried out in order to determine the presence of the reconstituted carotenoid, it location in the same binding pockets and the same orientation as that found in the wild type structure. This will confirm from a structural viewpoint the validity of other spectroscopic work previously carried out.

2. Chapter 2 Materials and Methods

2.1.Cell Culture

The growth of all bacteria took place in temperature controlled conditions (either a constant temperature growth room at 30°C or a water bath at 22°C) and light controlled conditions (set distances from a row of incandescent light bulbs). Bacteria were grown anaerobically either in Pfennig's media for *Rps. acidophila* (Pfennig, 1969) which uses succinate as the carbon source for photosynthesis, or a different succinate media for *Rb. spharoides* (Subir, 1963).

Starter cultures were prepared by pouring fresh media on top of a culture stored in agar and incubated for 3-4 days. This sample was used to inoculate a larger vessel, incubated for 3-4 days and the process repeated until the bacteria were growing in 500ml flat-sided bottles. If required, these 500ml bottles were used to inoculate 10 litre glass bottles.

In order to grow bacteria with the low light form of light harvesting complex, LH3, the bacteria was grown firstly under high light conditions until well established in 500ml bottles. When transferred into new 500ml bottles, the bacteria were placed in low light conditions, which stressed the bacteria into producing the LH3 complex. The bacteria had changed to low light growth after approximately four transfers, and could be made to produce the high light form again by returning the bacteria to the high light conditions.

All inoculations were performed under aseptic conditions in a laminar airflow cabinet. At regular intervals, the bacteria were checked for contamination by streaking out the bacteria onto agar plates and being left for 3-4 days in anaerobic jars. The colonies grown were then visually inspected for impurities. If impurities were detected, single colonies that appeared pure were picked, streaked onto new agar plates and incubated. This process was repeated until there were no obvious alien colonies. Single colonies were then selected, put into agar stabs and incubated for 3-4 days. These stabs from single colonies were used to start further cultures.

Cells were either harvested as described in section 2.2, or stored in the dark at 4^0C until required.

During this project, most work was carried out on two complexes of the purple non-sulphur bacteria, *Rps. acidophila*: the B800-820 LH complexes from strains 7050 and 7750.

2.2.Cell Harvesting

When twenty litres of cells had been grown, they were centrifuged at 4000rpm (4600xg) for 20 min at 4°C (MSE Mistral 6000 Coolspin Centrifuge). The supernatant was discarded and the pelleted cells resuspended in minimum volume of 20 mM Tris HCl pH8.0 using a hand homogeniser to ensure the cells were thoroughly resuspended. The suspension of cells was then diluted to give an optical density at 800nm (OD_{800}) of about 100. This was achieved by measuring the OD of a diluted sample and working out the dilution needed to give the cells a final OD of 100. This gave a volume of 200-250ml from 20 litres cells, with approx. 50ml being required for each preparation. The remaining cells were stored at -20^0C in aliquots of approx. 50ml.

This large volume of cells was grown so that consecutive preparations were from the same batch and therefore slight differences in growth could be eliminated.

A small amount of DNase and $MgCl_2$ were added to the suspension of whole cells and, this was homogenised. The cells were then passed through a French Pressure cell twice at 950 lb/inch^2 to break up the cell walls and release the membranes.

2.3.Solubilisation

Once the membranes containing the light harvesting complexes were released by French press, they were solubilised by the addition of detergent. The suspension of disrupted cells was diluted to give an OD_{800} of 50 using 20mM Tris HCl pH8.0. Enough N,N-dimethyldodecylamine-N-oxide (LDAO) was added drop-wise to the stirred solution to give a final concentration of 1.5%, and then incubated for 3 hours at 4^0C. Other detergents were investigated and the structure of those used: LDAO, N,N-dimethylundecylamine-N-oxide (UDAO), and n-octyl-β-D-glucopyranoside (β-OG) are shown in figure 32.

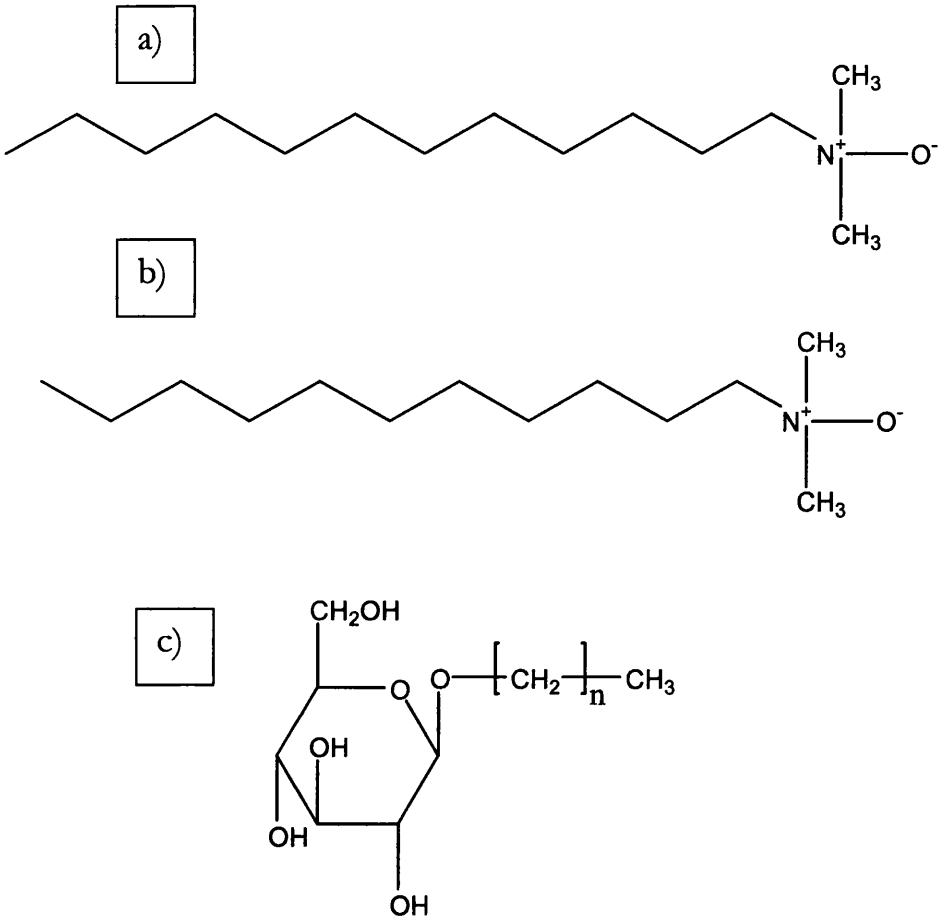

Figure 32. Structure of detergents used during this work. a) LDAO (Fluka, Gillingham, UK) b) UDAO (Fluka, Gillingham, UK) and c) β-OG where n=7 (Anatrace, Maumee, OH, USA)

The solubilised membranes were centrifuged at 15000xg for 20 minutes at 4°C to remove any unsolubilised material (whole cells, cell walls etc.). The supernatant, which contained the solubilised complexes, was collected whilst the pellet containing the unsolubilised material was discarded.

2.4.Isolation of LH2 Complex

The LH2 complex was isolated from other components by use of discontinuous sucrose density gradients (Hawthornwaite and Cogdell, 1991).

The gradients were prepared by slowly layering 8ml 0.9M then 0.6M followed by 0.3M sucrose solution into 27ml polycarbonate ultracentrifuge tubes. The sucrose

solutions were made up in 20mM Tris HCl pH8.0 and contained 0.1% v/v detergent (LDAO). The remaining space in the tube was filled completely by carefully layering approximately 3ml solubilised complexes, and the gradients were centrifuged overnight (16hours) at 45000 rpm (146,000xg) at 4°C (Beckman L7 Ultracentrifuge).

When the spin was finished, the pigmented moieties were resolved into three distinct bands (see Fig 33). The top layer consisting of denatured complex, protein molecules, carotenoid and other small molecules. The middle layer, the LH2 complex of interest and the lower band, the RC/LH1 core complex. The middle LH2 band was removed from the gradient using a Pasteur pipette.

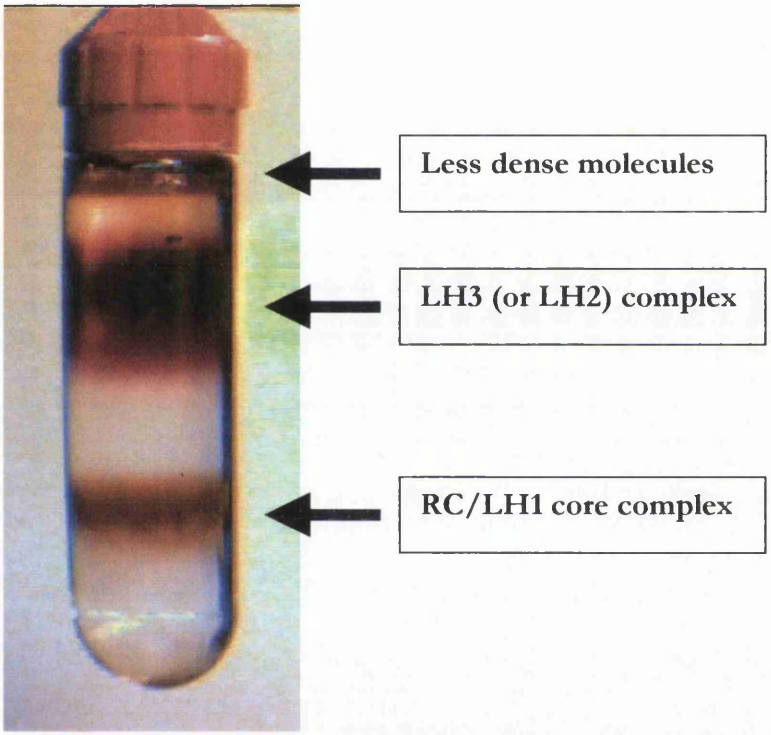

Figure 33. Sucrose gradient consisting of 0.9 (bottom), 0.6 & 0.3M sucrose (top) after centrifugation at 110,000xg for 16 hours at 4°C. There are three distinct bands. The lowest band contains the RC/LH 1 complex, the middle band contains the LH2 complex and the top band contains the least dense molecules.

2.5. Analysis of Protein complex purity

In order to determine the purity of the LH2 samples, a ratio from the absorption spectrum was used. The absorption of the sample at 280nm was compared to that at 800nm. The absorption at 280nm is due to amino acid residues in the protein

containing aromatic rings i.e. tyrosine, phenylalanine and tryptophan. The absorption at 800nm is due entirely to Bchl *a* molecules bound within the complex. This means that the higher the $^{800nm}/_{280nm}$ ratio, the more bound Bchl *a* molecules compared to protein moieties. This ratio has been termed the integrity ratio (I_r) (McLuskey, 1999), and any reduction in this ratio, suggests either a decrease in bound Bchl *a* molecules (due to denatured complexes) or extraneous protein contaminants. Figure 34 shows the absorption spectra of two LH3 samples at different points in the purification protocol. Sample A is considered pure (I_r=3.6), whilst sample B is from an early step in the purification procedure and still contains protein impurities (I_r=1.7). In practise, a value of approximately 3 (depending on the strain of bacteria) was used as a cut off point below which the sample was not considered pure enough for crystallisation.

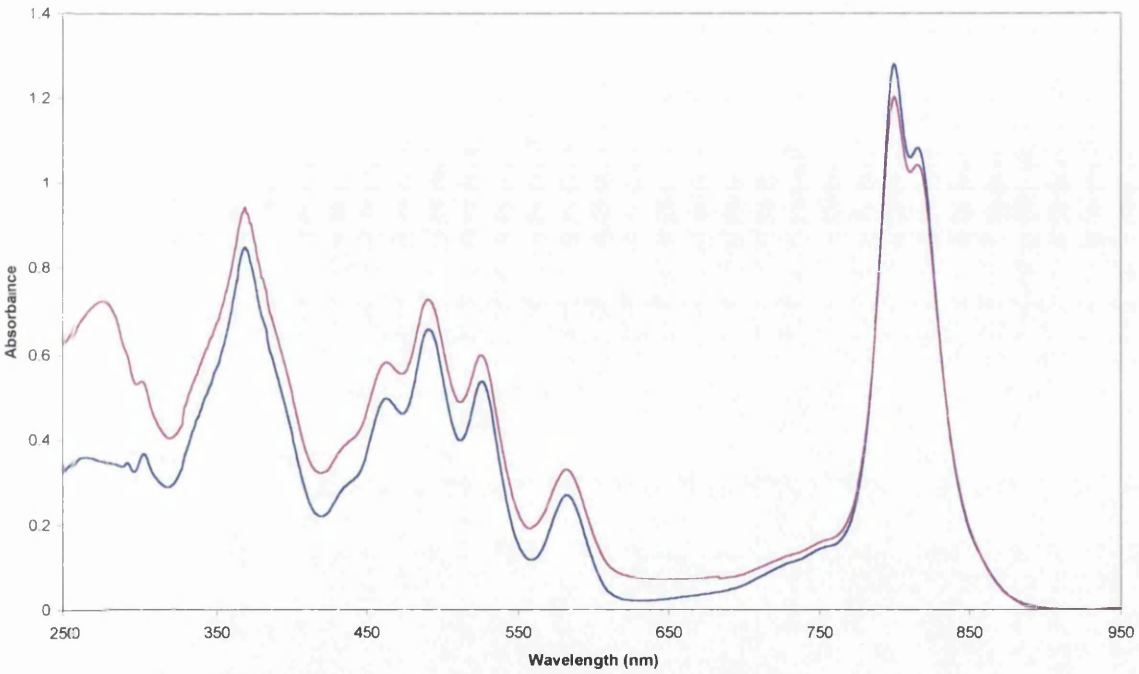

Figure 34. Absorption spectra of a purified LH3 sample (sample A in text, here in pink) and LH3 sample containing protein contamination (sample B in text, here in blue) from *Rps. acidophila* strain 7050. I_r of the purified sample is 3.6 whilst that of the contaminated sample is 1.7.

Whilst I_r is a useful method of determining the general purity of the complex, it was found to be insufficient in defining the separation of the B800-850 and B800-820 complexes. If, for example, when attempting to purify a B800-820 complex there was a large B800-850 complex, there was a readily apparent "shoulder" at 850nm. However, as this impurity becomes smaller, it is more difficult to see, and another method of measuring it is needed. This involves comparing the absorption peak at

800nm to that at 820nm. Since both types of the LH2 complex contain Bchl *a* molecules which absorb at 800nm, a B800-850 impurity will increase the peak height at this wavelength, relative to the 820nm peak which should remain unaffected. This has been termed the peak ratio (P_r) (McLuskey, 1999) and values of around 0.9 were used (depending on the complex). Figure 35 shows the absorption spectra of two samples with the same I_r, however, sample C is considered to be purely B800-820 complex (P_r=0.85), whilst sample D contains a small amount of B800-850 complex P_r=0.82).

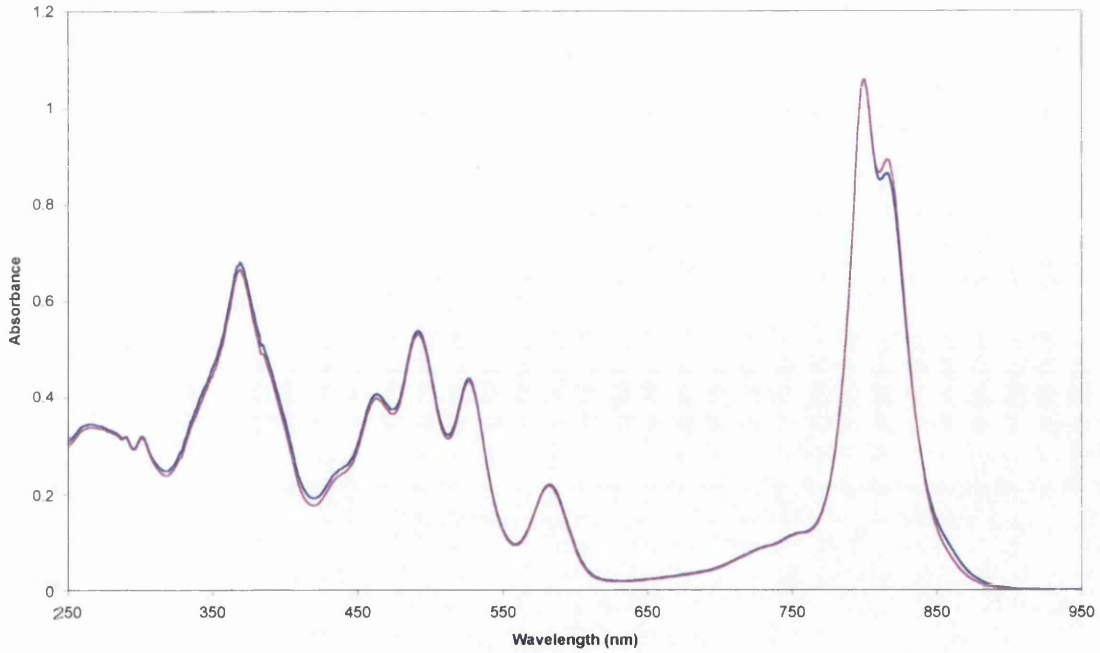

Figure 35. Absorption spectra of a purified LH3 sample (sample C in text, here in pink) and LH3 sample with slight LH2 contaminant (sample D in text, here in blue) from *Rps. acidophila* strain 7750. I_r of both samples is 3.1. However, the P_r differs, with values of 0.82 (contaminated sample) and 0.85 (LH3 only sample)

2.5.1. Ion Exchange

2.5.1.1. Whatman DE52 column

A gravity fed Whatman diethylaminoethyl cellulose (DE52) anion exchange column was initially used in the preparation. A slurry of DE52 media was prepared in 20mm Tris HCl pH8.0 buffer and poured into a 5cm diameter glass chromatography column to a height of about 15cm. This was allowed to pack down and was then

washed with about three column volumes of the buffer containing detergent (20mM Tris, pH 8.0 + 0.1% LDAO). The LH2 sample was then slowly pipetted onto the column straight from the sucrose gradient (with an OD_{800} of about 10).

The sample was eluted from the column using a NaCl gradient in 20mM Tris HCl pH8.0 + 0.1%LDAO from 0-250mM in steps of 50mM. Fractions were collected in 1ml aliquots and assayed spectrophotometrically. This ion exchange method was found to not resolve the LH2 and LH3 complexes sufficiently, with resultant I_r and P_r values of around 2.9 and 0.9 respectively depending on the bacteria, so other methods were employed.

2.5.1.2.Resource Q

The anion exchange step, which was used to replace the Whatman DE52 column, was carried out using a 1ml Resource Q column attached to an FPLC system (both Amersham Pharmacia Biotech, Uppsala, Sweden). The Resource Q column has 10µm beads with quaternary ammonium groups which is known as a strong group because it is active over a wide pH range. All solutions used in the FPLC system were filtered through a 0.22µm membrane and the buffers degassed under vacuum prior to use. The column was washed with 10ml 20mM Tris HCl pH8.0 0.1%LDAO buffer, the LH2 layer extracted from the sucrose gradients and then loaded onto the column. When the sample was extracted from the sucrose gradients it typically had an OD_{800} of 10 in which case approximately 10ml could be loaded for each run. The column was washed with 10ml equilibration buffer before a programmed salt gradient of 0-500mM NaCl in 20mM Tris HCl pH8.0 +0.1%LDAO was used to elute the sample.

Due to the small column volume and rapid flow rates, it was possible to optimise the salt gradient for each complex and steps were introduced where necessary. The elution profile was monitored (see Fig 36), and the eluant collected in 1ml fractions which were assayed spectrophotometrically.

Initially, the purest fractions from this column were then used in crystallisation trials. However, when a further purification step was introduced, the P_r and I_r were found to improve.

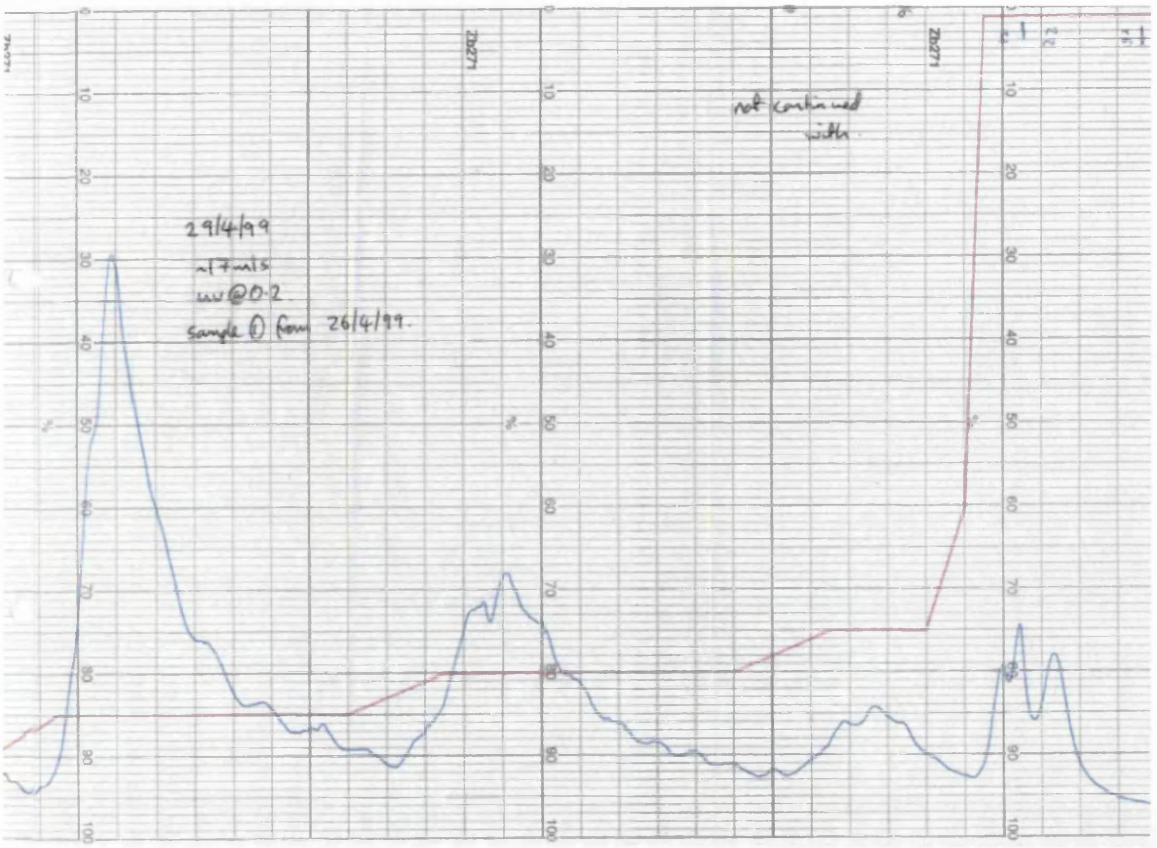

Figure 36. A trace of the elution profile from a Resource Q column run on the FPLC system. Approximately 10 mls of sample at OD_{800} of ~10 was removed from sucrose gradients loaded onto the column and eluted at 2.0ml/min. The horizontal axis represents volume, with the start of the experiment on the left of the trace. The chart recorder was set at 0.5cm/ml. The vertical axis represents the 500mM NaCl gradient with 0% at the bottom and 100% at the top (for the red line), and the absorption at 280nm of the output from the column (the blue line).

2.5.2. Gel Filtration

The fractions from the Resource Q column with the best I_r and P_r ratios were pooled and concentrated prior to separation on a Superdex 200 (S200) gel filtration column (Amersham Pharmacia Biotech, Uppsala, Sweden) attached to the FPLC system. The sample was concentrated until an OD_{800} of about 80 was obtained using a 30,000 molecular weight cut off (MWCO) membrane in an Stirred Ultrafiltration Cell for larger volumes, or a 50,000 MWCO centricons (both Amicon Inc., Beverly, MA, USA) for smaller volumes.

1ml aliquots were spun in a microcentrifuge for 5 minutes at 13000 rpm to pellet any solid material- filtering was diffucult due to the small volumes involved. The sample was then loaded onto an 80cm long S200 column, equilibrated with two column volumes of 20mM Tris HCl pH8.0 +0.1%LDAO buffer, and eluted at 0.5ml/min. The elution profile was monitored (see Fig 37) and the eluant collected in 1ml fractions. These fractions were again assayed spectrophotometrically for their suitability in crystallisation trials.

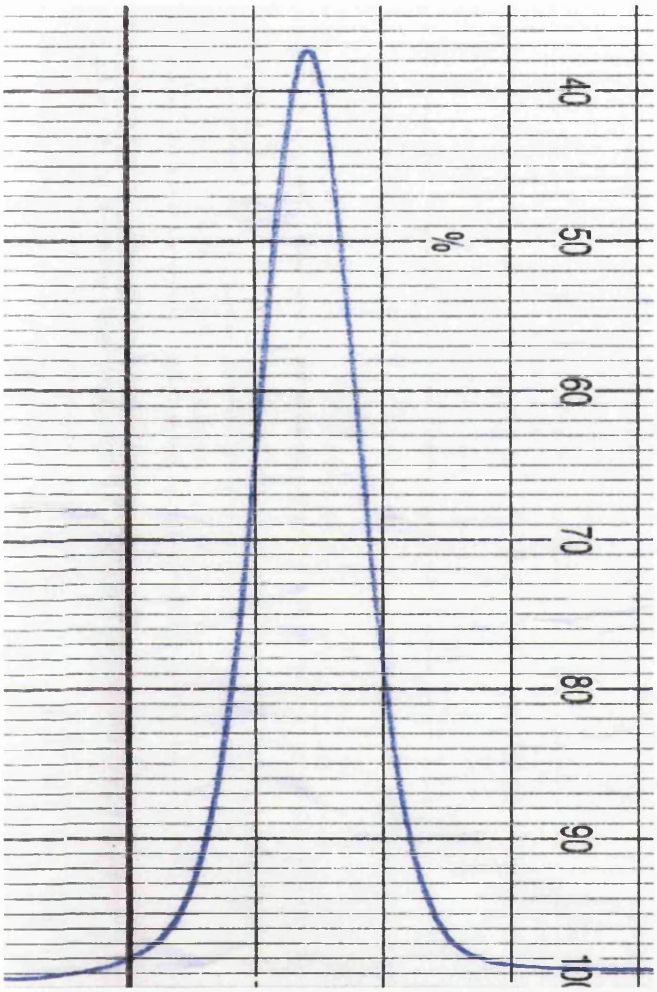

Figure 37. Elution profile of S200 column showing symmetrical single peak. The horizontal axis represents volume, with the start of the experiment on the left of the trace. The chart recorder was set at 0.5cm/ml. The vertical axis represents the absorption at 280nm of the output from the column (the blue line. 1ml sample (OD_{800} of ~100) was loaded onto the column and eluted with a flow rate of 0.5ml/min.

2.6.Crystallisation

2.6.1. Detergent Exchange

For the B800-820 LH complex of *Rps. acid.* strain 7050, in order to obtain good quality crystals, it had been found to be necessary to exchange the working detergent (LDAO) for one more suited to crystallisation, in this case 1% ß-OG (McLuskey, 1999). Detergent exchange was used in order to test different crystallisation detergents

In order to change the detergents, the sample was concentrated to a minimum volume. This was then diluted with detergent free buffer and the sample respun. This was repeated to ensure as much of the original detergent was removed as possible, but had to be done quickly in order that the protein did not precipitate during the time when there was little or no detergent present. The sample was then diluted with buffer containing the new detergent, concentrated and again diluted to ensure as much new detergent had been substituted as possible. This was then concentrated to the OD required for crystallisation.

2.6.2. Crystallisation Method

Initial crystallisation conditions were based on those in figure 38 that were used to obtain diffraction quality crystals from LH2 complexes of *Rps. acid.* strain 10050 (McDermott, 1997).

Drop Solution		Well Solution	
LH2 complex OD_{850}	100	[AMS]	2.2M
Detergent	1% β-OG	AMS pH	9.3
NaCl	350mM		
Amphiphile	2.5% (w/v) BA		
KP_I	1.0M		
Drop size	15µl		

Figure 38. Table of crystallisation conditions used to grow LH2 crystals of *Rps. acidophila* strain 10050 (McDermott, 1997). These conditions were used as the starting crystallisation conditions for this work.

The sitting drop method of vapour diffusion was used for growing crystals. Cryschem trays (NBS Biologicals, Huntingdon, UK) consisting of 24 wells with polypropylene platforms were used. The well solution was used to equilibrate against a drop containing the protein complex, detergent, precipitants and small amphiphilic molecules.

After detergent exchange, the complex was adjusted to a concentration of about 4.5mg/ml (OD_{800} ~100) although different concentrations were tried. Crystallisation parameters were investigated and details are given in chapter 3. Here, a typical crystallisation procedure is listed.

Enough NaCl to make the solution 350mM was weighed into an eppendorf tube, the desired volume of protein complex added, and this was vortexed until dissolved. 2.5% (w/v) benzamidine (BA) was also dissolved in this manner. A stock solution of 4M Di-potassium hydrogen phosphate (KPi) solution at pH8.0 was used to make the final solution 1M. One quarter of the final volume of solution was added slowly from the stock and then vortexed. This means the protein and other molecules in the final solution had a concentration of 0.75 of the initial value i.e. 4.5mg/ml of protein becomes 3.4mg/ml. This solution was then spun in a microcentrifuge for 5 minutes to sediment any solid material.

1ml of ammonium sulphate (AMS) at known concentration (eg 2.2M) and pH (eg 9.3) was placed in the well and a 15 or 20µl drop of the prepared sample was pipetted into the bridge. The tray was carefully sealed using Crystal-clear adhesive tape (Hampton Research) and the trays incubated at constant temperature (eg 16°C). Each crystallisation tray contained a concentration gradient and a pH gradient of well solution.

It should be noted that rapid purification was deemed essential and the entire procedure, from cell harvesting to setting up crystal trays, was carried out in 3 days. This is because it was noted that the I_r (and to a lesser extent P_r) ratio decreased over several days.

2.7.Crystal Handling

2.7.1. Capillary Mounting

The most traditional method of mounting protein crystals is to mount them in a small sealed glass capillary tube with a small reservoir of mother liquor, see figure 39. Depending of the size of the crystal, 0.1-1.0mm diameter capillaries were used. A small reservoir of mother liquor was drawn into the capillary by applying a small amount of suction to one end until it was about 15mm from the end. The crystal, with a minimal amount of liquid, was then drawn into the tube by suction. Fine paper wicks were used to draw excess moisture away from the crystal until it was isolated from any large amounts of liquid. Extremely thin, drawn Pasteur pipettes were also found to be useful for drawing off small amounts of liquid by capillary action. The end off the capillary was sealed with several small additions of beeswax. The capillary was carefully cut about 10mm above the reservoir and this end also sealed with beeswax.

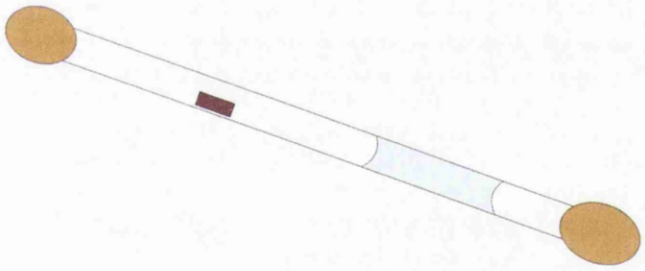

Figure 39. Diagram of a capillary mounted crystal. The crystal is drawn into the capillary and excess liquid drawn off with paper wicks or drawn-out pasteur pipettes. A small amount of mother liquor is then drawn into the capillary to prevent the crystal dehydrating, and the end sealed with beeswax. The capillary is then cut above the crystal and that end also sealed with beeswax.

2.7.2. Artificial Mother Liquor

Artificial Mother Liquor (AML) is a solution that aims to mimic the liquid in which the crystals grow. It contains the ingredients required to maintain the crystals in a steady state, and must be at the correct pH and temperature. If the concentration of any of the ingredients is too low, the crystals may dissolve, and if it is too high, they may break up. AML is often required when a well is opened as its minimal volume

(15 or 20μl) leads to rapid evaporation, especially under the heat of a microscope. AML can therefore be added to "top up" the drop to prevent dehydration and it has been shown that steeping crystals in AML can improve the resolution of diffraction shown by the crystals (McLuskey et al., 1999). AML is also required to introduce cryo-protectant into the system.

AML had previously been used for the B800-850 LH complex from *Rps. acidophila* strain 10050 (McDermott, 1997) and the B800-820 complex from *Rps. acidophila* strain 7050 (McLuskey, 1999) and these protocols were adapted for this work.

If a crystal drop had contained protein at initial OD_{820} of 90, 350mM NaCl, 2.5% (w/v) BA, 1% β-OG (w/v), and 1.0M KPi, the AML would contain half the amount of β-OG (0.5%), the same amount of NaCl (350mM), and 1.5 times the amount of KPi (1.5M), in 20mM Tris HCl pH8.0. The addition of BA was found to not be required. If LDAO was used as the crystallisation detergent, it was left out of the AML recipe as it was found to lead to phase separation problems. Three x 300μl drops of this solution were equilibrated against 10ml AMS in a 10cm diameter vapour diffusion dish for at least 36 hours. The AMS was of the same pH and concentration as the well yielding crystals.

2.7.3. Cryo-protectant

In order to expose the crystals to the x-ray beam at cryogenic temperatures, a solution which prevents regular ice structure formation must be introduced to the crystals. This is known as a cryo-protectant (cp) and one containing 50% saturated sucrose had been used for the LH2 and LH3 complexes from *Rps. acidophila* (McDermott, 1997; McLuskey, 1999). This cp was also used in this work and was prepared by making an AML solution but at 2 times concentration, and mixing it with saturated sucrose in a 1:1 ratio. This solution was then corrected to the pH of the equilibrated AML using 85% (w/v) phosphoric acid.

In the case of crystals grown in the presence of LDAO and glycerol, a cp solution containing glycerol (Mitchell and Garman, 1994) was investigated. This was prepared similar to above, but mixing the 2 x [AML] with 100% glycerol in a 1:1 ratio.

Other cryoprotectants including paraffin oil and ethylene glycol were investigated, and these are described in Chapters 3 and 5. Several methods of introducing the cp were investigated.

Dialysis was used to slowly introduce the cryoprotectant into the crystals. Using a micropipette, a crystal was taken from the drop and placed in a 10µl dialysis button (Cambridge Repetition Engineers Ltd., Cambridge, UK) containing 5µl AML. Low molecular weight dialysis membrane (3,500 MWCO) was dampened and secured over the top of the dialysis button using a rubber o-ring. The button was then placed upside down in a sealed vial containing the cp. The buttons were incubated at 16°C for at least 10 hours. The crystals were then loop mounted and flash frozen in the cryostream. Dialysis is not a suitable method for some cryoprotectants, e.g. glycerol, that have a lower molecular weight, and are found to pass through the membrane rapidly and "shock" the crystal- when the cp is added too quickly to the crystal and it may crack and break up or dissolve. This is due to the sudden change in osmotic pressure in the system.

As an alternative method of introducing the cp, a crystal tray was set up with a number of solutions containing an increasing concentration of glycerol, made by mixing the cp solution with decreasing amounts of AML. A crystal was looped from the drop and placed in the first solution (of lowest glycerol concentration) for a given length of time (5-30 seconds). It was then looped into the next solution and so on until it was in the cp containing 50% glycerol. The crystal was then loop mounted and frozen.

Various volumes (1-5µl) of cp (50% glycerol) were also added at timed intervals to a drop containing crystals. A small volume (1-5 µl) of the mother liquor from the drop was removed at this time to ensure that eventually it would almost all be replaced by the cp. When about 50µl had been added, it was assumed the mother liquor had been replaced.

The concentration gradient as the cp is added can be lessened by replacing the mother liquor firstly with 10% glycerol in AML (small addition and removal) then 20%, 30% 40% and finally 50%. This involves more handling & risk due to more movements, but if done carefully, can subject the crystals to less stress.

2.8.Collection of X-Ray Diffraction Data

In this project x-ray diffraction test data has been collected on crystals of the LH2 and LH3 complexes from *Rps. acidophila* and RC crystals from *Rb. sphaeroides* R26-1. Trials of the crystals have been carried out both at room temperature and cryotemperature using the in-house rotating anode facilities at University of Glasgow. A Siemens multi-wire area detector used with a Siemens rotating anode x-ray generator, and a Nonius system with DIP 2020 and DIP 1030 image plates were available. Trips were also made to stations 9.5, 9.6, 7.2, and 14.1 at the Daresbury Laboratory Synchrotron Radiation Source (SRS) in order to test smaller crystals. Crystals were also taken to stations 14-2 and 14-4 of the European Synchrotron Radiation Facility (ESRF) at Grenoble, France. Test images of each crystal were taken and analysed.

The crystals were tested by mounting the crystal and recording an x-ray diffraction pattern of the crystal, with two images being taken, the second at 90° to the first. The two images were taken at 90° to each other in order to assess the overall diffracting quality of the crystals. The resolution limits of the diffraction pattern were considered along with the shape of the spots, any obvious splitting of crystals, and presence of ice rings if cryocooling was employed.

2.9.Mass Spectrometry

In order to measure the masses of the polypeptides within the light harvesting complexes, and investigate the composition of those present, mass spectrometry was employed. A Voyager DE Pro (Applied Biosystems) Matrix Assisted Laser Desorption Ionisation mass spectrometer with Time of Flight detector (MALDI-TOF) was used.

2.9.1. Sample preparation

The samples of light harvesting complexes were purified according to the protocol used for crystallisation (section 2.5). The purified complex was then exchanged into a solution suited for MALDI-TOF analysis using the centricon method

described in section 2.6.1. In practise, this was found to be 0.2% ß-OG in 20mM Tris, pH 8.0 although slightly higher concentrations of detergent were required to stop some complexes, especially the LH3 complex from *Rps. acidophila* strain 7750, from precipitating.

MS was being used to investigate any impurities within the crystals, which may be preventing formation of crystals that diffract to high resolution. Therefore crystals were also taken from the crystal wells, washed in AML and redissolved in buffer containing ß-OG. It was also found to be necessary to wash the samples through a centricon to improve the I_r ratio.

A matrix solution was then prepared by weighing 10 mg α-cyano-4-hydroxycinnamic acid (CHCA) into a 1.5 ml eppendorf tube and adding 1ml of 50% acetonitrile (Beavis and Chait, 1992). The solution was made acidic by the addition of 0.2% (v/v) trifluoroacetic acid (TFA) giving a pH of approximately 4. This was vortexed for 5 minutes until no more CHCA would dissolve, then spun in a benchtop microcentrifuge at 13,000 rpm for 2 minutes to pellet the undissolved matrix. When using this solution, only the supernatant was taken. Two main methods of sample preparation are described in the Biosystems manual and both were used with apparent equal success.

In the first method, 1 µl of the sample solution is placed in an eppendorf tube and 1 µl of matrix solution is added to it. This is mixed then spun briefly before 1 µl of the mixture is placed on the target plate and allowed to dry. However, sometimes a solid was formed inside the mixing tube so a method in which the mixing occurs on the target plate was employed.

In the second method, 0.5 µl of the solution containing the sample was dropped into the target plate and allowed to dry in the air (approximately 5 minutes), A 0.5 µl drop of the matrix solution was placed on top of this drop and again allowed to dry.

There was no noticeable difference in the results from either method so the second method was used preferentially as it involved less handling.

Calibration standards were used for each sample, being placed close to the drop so that any plate imperfections were similar. The standards were prepared in the same way to the samples; mixed with matrix molecules and dropped into the target plate. The standards contained a mixture of polypeptides of known mass varying from

1300 Da to 5700 Da. A standard was taken for each sample and the resulting spectrum callibrated according to the standard. The polypeptides being investigated are known to be in the 4-7kDa range.

3. Chapter 3 Crystallisation of the B800-820 light harvesting complex (LH3) from *Rps. acidophila* strains 7050 & 7750

3.1. The B800-820 light harvesting complex from *Rps. acidophila* strain 7050

The crystal structure of the B800-820 complex from *Rps. acidophila* strain 7050 has already been solved to a resolution of 3.0Å (McLuskey et al., 2001). The aim of this part of the project was to collect higher resolution data in order to see more clearly the details of the differences between this complex and the B800-850 light harvesting complex of strain 10050. This is in order to understand more clearly the structural factors that change the absorption maximum of the Bchl *a* molecules.

It has been found that the rapid purification of the complex is vital in order to successfully grow crystals that diffract to high resolution (McLuskey, 1999). The purity of the complex is measured according to the peak ratio (P_r) and integrity ratio (I_r)) as discussed in section 2.5. Throughout preparations, these ratios were monitored in order to ensure the complex was as pure as possible with the ratios being at least equal to those that gave the 3.0Å dataset.

Growth of *Rps. acidophila* strain 7050 was carried out as described in section 2.1, with the 500ml bottles being placed approximately 70cm from a single 40W incandescent light bulb. The bacteria showed a change in carotenoid composition after only one transfer (by visual inspection, see figure 40) from an orangish-purple colour to a deep violet colour. Differentiation of the carotenoids in whole cells by comparison of the absorption spectra is difficult as the characteristic "three-fingered" carotenoid peaks are less apparent due to scattering by other cell components (see figure 41). Although the bacteria change their carotenoid composition after one transfer, production of the B800-820 complex occurs only after three or more transfers.

Figure 40. When *Rps. acidophila* strain 7050 is grown at high light conditions it has an orangish-red colour, and low light conditions has a deep violet colour.

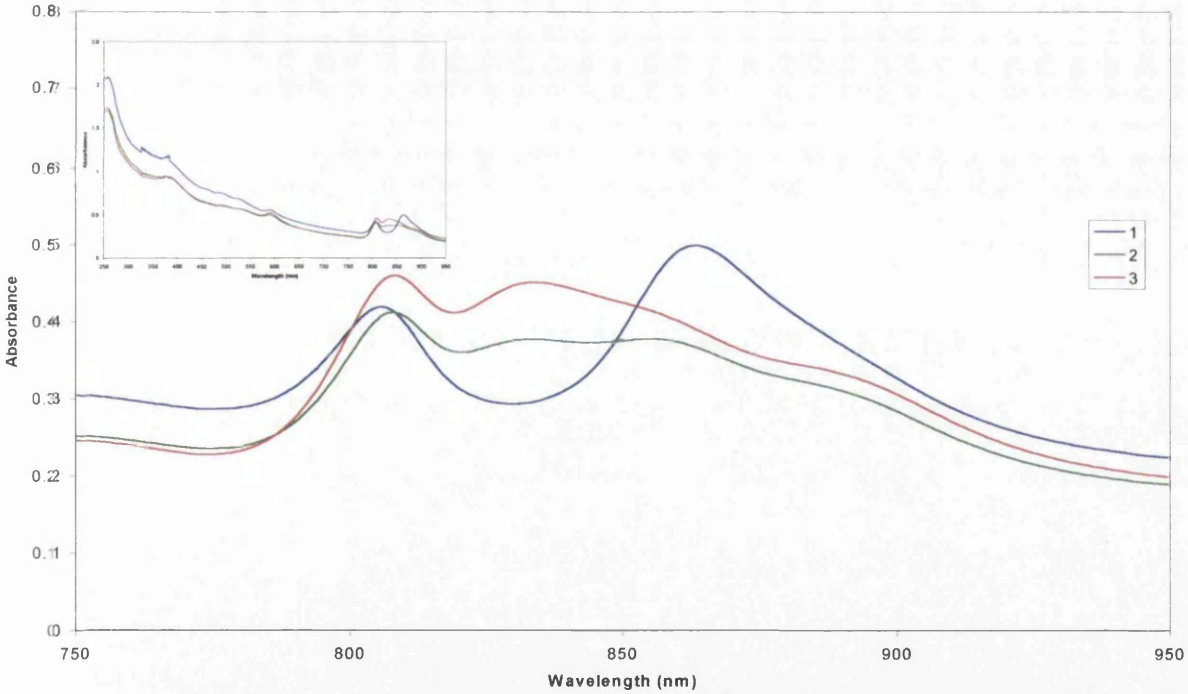

Figure 41. Absorption spectra of whole cells showing change of 7050 HL to LL. 1) Growth at high light. 2) Production of LH2 and LH3 in approximately the same amounts (growth after two transfers at low light conditions). 3) Bacteria produces mostly LH3 after four transfers at low light. The inset shows the absorption spectra of the same samples over the 250-950nm wavelength range.

The absorption spectra of whole cells apparently showed production of only B800-820 complex, with no visible 850nm shoulder to the 820nm peak. However,

upon purification it was found that a basal level of the B800-850 complex was always present. As the light intensity was further decreased, there appeared to be a slight increase in the proportion of B800-820 complex produced, but this was accompanied by a dramatic decrease in the rate of growth. Subsequent purification appeared to completely separate the LH2 impurity from the LH3 complex, therefore, it was decided to persist with growth at a distance of 70cm from the light-bulb.

The effects of minor differences in growth conditions became apparent upon purification (as discussed below). It was observed that purified LH3 complex from different batches of bacteria displayed slightly different absorption spectra, with differences in P_r values, even though the purification procedure was identical. This could be due to anomalies in the purification, for example selecting different fractions from the anion exchange or using different batches of detergent, although all efforts were made to minimise these errors. It is therefore most likely there are slight differences in the growth conditions, resulting in small differences in production of the light harvesting complexes. In order to minimise this, larger volumes of cells were prepared before harvesting, with aliquots of harvested cells being frozen.

Solubilisation was investigated systematically using 1-2% LDAO with a sample OD_{800} of 25-100 with the solution incubated at 4°C or room temperature for 1-4 hours. After solubilisation, the purification was carried out in an identical manner each time, in order to assess the effect different solubilisation conditions have on the LH3 purity (measured by I_r and P_r). Crystallisation trials were also set up with each preparation and the quality of crystals obtained was recorded. The changes in solubilisation conditions did not have a noticeable effect on the P_r and I_r values, or on subsequent crystallisation. After investigation of these parameters, solubilisation was carried out using 1.5% LDAO with OD_{800} of 50, and incubated for 2 hours at 4°C.

The purification was based on the protocol described in chapter 2. After the initial stages of cell harvesting, solubilisation and sucrose density centrifugation, which extracted and isolated the peripheral light harvesting complexes (LH2 and LH3), separation of the two complexes was required. Previously the best results of this separation had been being obtained using anion exchange only (McLuskey, 1999).

Anion exchange was carried out on a Resource Q (Pharmacia, Uppsala, Sweden) 1ml column. Although the values of I_r and P_r were maintained at the same

levels and the crystallisation conditions were also kept constant (see figure 42), it was not found to be possible to repeat the growth of single crystals.

Drop solution	Initial values investigated
Initial protein OD_{800}	90
Detergent	1% β-OG
Amphiphile	2.5% BA
NaCl	350mM
KP_i	0.8 & 1.0M, (pH not corrected)
Incubator temperature	16°C
Drop size	15µl
Well solution	Values investigated
AMS concentration	2.1-3.0M
AMS pH	9.3-9.9

Figure 42. Initial crystallisation conditions investigated for LH3 complex from *Rps. acidophila* strain 7050

The majority of wells resulted in amorphous precipitate, however, some wells yielded small needle-like crystals, at most 100µm long or very thin round plate-like crystals, approximately 200µm in diameter. Larger plate-like crystals were observed, but as the size increased, their shape became more irregular, with maximum diameter being 0.6mm. The crystals were observed under several conditions over the whole range of wells, however, it was noted that AMS well solution at the lower end of the pH range resulted in more crystals. Crystallisation conditions were therefore expanded to screen lower pHs, different AMS well solution concentrations, and crystal drop parameters. No improvement in the quality of crystals was observed. As the solubilisation conditions had been investigated, a review of the purification procedure was undertaken.

In an attempt to improve the purification procedure, a different anion exchange column was investigated. A DE52 column was used in place of, and then in addition to the Resource Q column. Using only the DE52 anion exchange column resulted in lower P_r and I_r values, with crystallisation trials resulting in the rapid precipitation and denaturation of the complex. When the DE52 column was used in conjunction with the Resource Q column, there seemed to be no improvement in ratios compared to using only the Resource Q. The difference in time of the preparation, however, resulted in a slight decrease in the I_r value.

A return to using only the Resource Q was then implemented and attempts were made at optimising the elution of the complex from the column. Rapid increases in salt concentration (0-200mM in 10 minutes) to elute the complex quickly and save on time resulted in incomplete separation of the LH2 and LH3 complexes and a corresponding decrease in P_r values. A more gradual salt gradient with steps when different peaks appeared to elute resulted in many peaks and when assayed spectrophotometrically, many appeared to be identical according to the I_r and P_r values. The purest fractions eluted at higher salt concentrations (~150mM), so eventually a combination gradient was used whereby a rapid initial increase in salt concentration was used to elute those fractions of poor ratio values, followed by a slow increase including steps to elute the best fractions. The ratios of the fractions were measured, and the best fractions pooled for crystallisation. Crystallisation trays were set up using the expanded conditions, however, when this again failed to yield good single crystals, a further step of gel filtration was introduced.

Gel filtration using an S200 column (Pharmacia, Uppsala, Sweden) was investigated before, after and instead of anion exchange (using the Resource Q column). The use of gel filtration resulted in a single, almost symmetrical peak, however, a secondary peak was observed to elute after the main peak. This second peak was very slight and could only be detected if the sensitivity of the UV recorder was increased (see figure 43). The fractions collected over this peak were very dilute and were not investigated further. It was also noted in the use of gel filtration that P_r values remained fairly constant throughout the run, although I_r values increased slightly in the centre of the peak.

Use of gel filtration as the sole purification step resulted in particularly poor P_r values (of ~0.75) similar to those of the sample applied to the column. However, the I_r values were slightly improved (typically from 2.5 before gel filtration to 3.0 after). When gel filtration was used followed by anion exchange, there was a slight improvement in the ratio values, but the best values were obtained when anion exchange was followed by gel filtration, typically resulting in I_r and P_r values of 3.0 and 0.9 respectively.

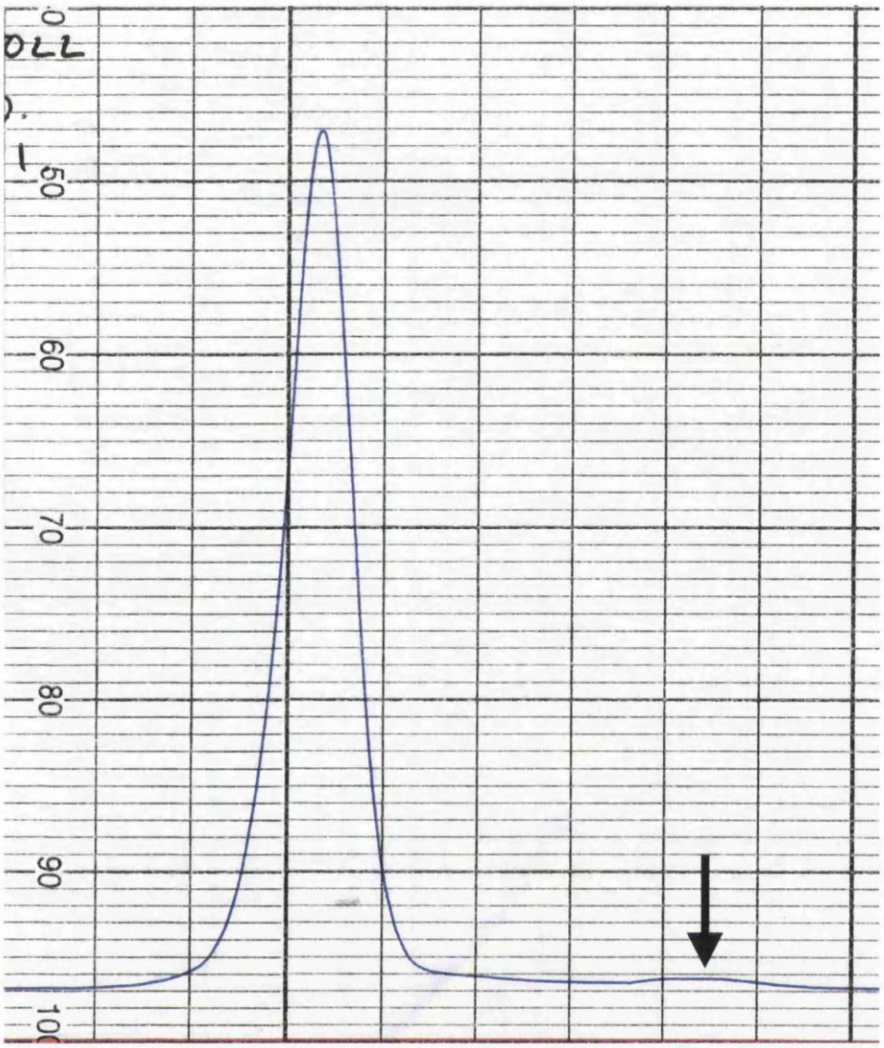

Figure 43. Elution profile of LH3 complex from *Rps. acidophila* eluting from S200 column. The major peak is followed by a second, minor one at the right hand side of the trace.

The anion exchange column appears to separate the LH3 complex from the LH2 complex, leading to an improvement in P_r values. However, there does not seem to be sufficient separation of the complex from extraneous protein or from heterogeneous complexes. It is possible that some complexes with lower occupancy of the Bchl sites (perhaps due to denaturation of the complex) would have the same charge (due to the same polypeptides) and would elute from the Resource Q column at the same salt concentration as the main complex.

The gel filtration column appears to remove any extraneous protein moieties, or complex heterogeneities such as those complexes with lower Bchl occupancy, due to their differing molecular weight. This leads to an increase in I_r values but not in P_r as it does not appear to separate the LH2 and LH3 complexes sufficiently.

The theoretical mass difference of the two complexes is almost 6,000 Da (assuming a nonameric complex) from the amino acid sequences (Zuber and Brunisholz, 1991)). This mass difference should be resolved on a gel filtration column. The observation that these complexes are not resolved could be accounted for by the size of the complex (it elutes almost in the void volume of the column), by different detergent micelles forming, or could indicate slight errors in the sequences.

When the purification procedure of anion exchange (Resource Q column) followed by gel filtration (S200 column) was used, single crystals were obtained approximately 200 x 100 x 50 μm in size. The conditions yielding the single crystals were not those found to be most promising before the introduction of the S200 purification step. Single crystals were only observed in approximately 25% of wells with identical conditions.

3.1.1. Crystallisation conditions.

Crystallisation was carried out using sitting drops and many different crystallisation parameters were changed in order to improve the diffraction quality of the crystals. The starting conditions (see figure 42) were altered methodically in an attempt to find the optimum conditions. Each well was checked regularly for the appearance of crystals, and the wells were graded according to observations made. When it was established that most crystals took 3-6 weeks to appear, trays were left undisturbed during the first 3-4 weeks in order to allow crystallisation under constant conditions. Parameters affected by too frequent checking include temperature (as the incubator door is opened and under the heat of the microscope), and vibration (picking up and setting down of trays).

Firstly, different well conditions were investigated as this was the starting condition with the greatest variability, which reported crystals grew with 2.2M-3.2M ammonium sulphate (AMS) at pH 8.5-9.5. Trays were set up over this range and it was consistently found that most wells produced crystals of some sort. These crystal forms included microcrystalline precipitate (see figure 44a), thin discs and plates (see figure 44b), thin needles, twinned crystals and occasionally, single crystals (see figure 44c). The single crystals, and the best of the other crystal forms, were tested in an x-ray beam. See section 3.1.3. for the results of these test exposures. The well conditions were expanded to cover concentrations of 2.0-3.5M with pH of between

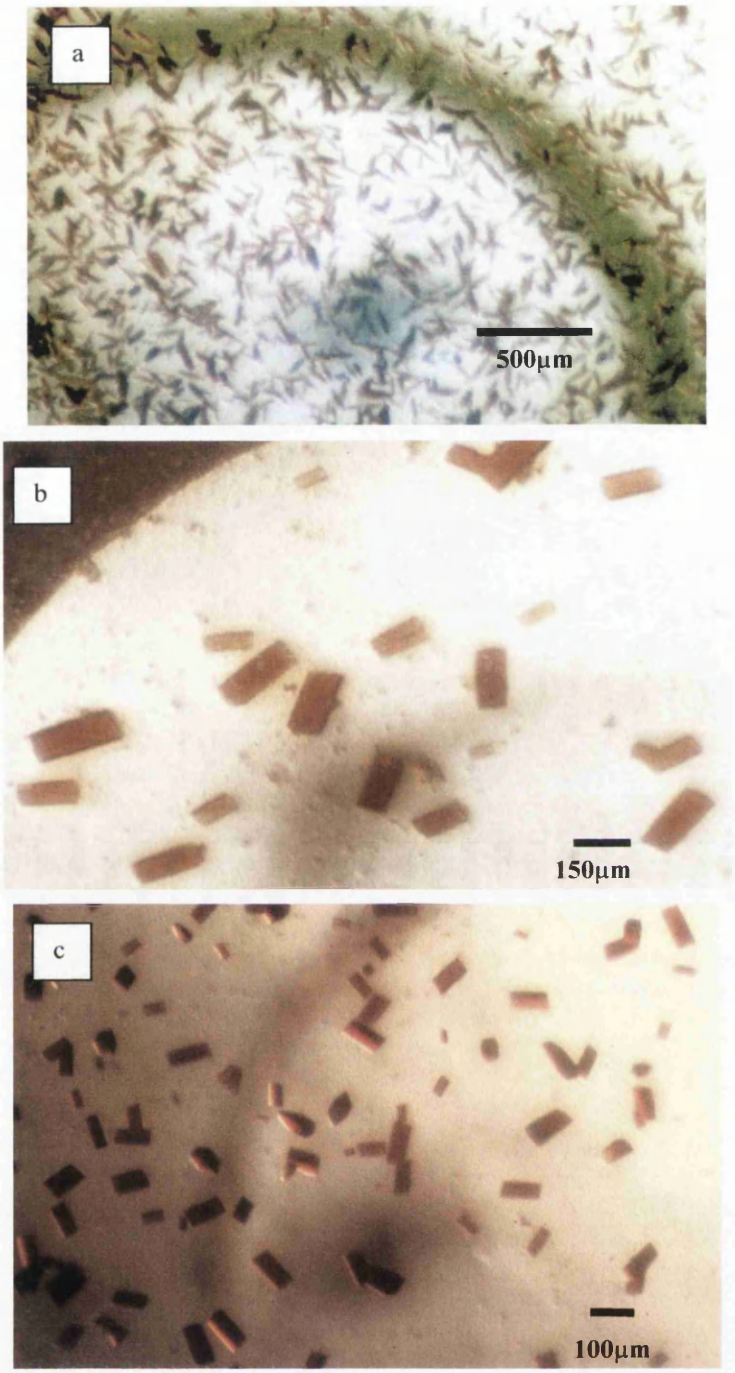

Figure 44. Photos of 7050LL crystals

a) Microcrystalline precipitate. Drop: complex initial I_r =3.0, P_r =0.91, OD_{800} =92, 1% β-OG in 20mM tris pH8.0, 300mM NaCl, 2.5% BA, 0.8M Kpi pH10.0, drop size =15µl. Well: 2.8M AMS pH9.2. Incubated at 16°C. After 6 weeks.

b) Very thin plate-like crystals, maximum size: 150 x 75 x 20µm. Drop: complex initial I_r =2.8, P_r =0.93, OD_{800} =90, 1% β-OG in 20mM tris pH8.0, 300mM NaCl, 2.5% BA, 1.0M Kpi pH10.0, drop size =15µl. Well: 2.5M AMS pH9.5. Incubated at 16°C. After 4 weeks.

c) Small single crystals, maximum size: 100 x 60 x 60µm. Drop: complex initial I_r =3.0, P_r =0.92, OD_{800} =92, 1% β-OG in 20mM tris pH8.0, 300mM NaCl, 2.5% BA, 0.8M Kpi pH10.0, drop size =10µl. Well: 2.6M AMS pH10.2. Incubated at 16°C. After 6 weeks.

6.0 and 10.5. AMS concentrations of 2.2-2.7M with pH 8.5-10.5 were found to most regularly yield crystals, and these conditions were used to investigate the other parameters. A summary of crystallisation conditions investigated and the optimised conditions can be found in figure 45.

Crystals had also been reported to grow in different amounts of KPi (0.8M and 1.0M) either at an unadjusted pH (McDermott, 1997), or at pH 8.0 (McLuskey, 1999). The effects of changing the concentration (0.6-1.2M) and pH were investigated (unaltered pH was typically 9.5, solutions were corrected to 8.0-10.6 using H_3PO_4 or NaOH). The best condition was found to be 1.0M KPi at pH 10.0, although crystals were regularly observed in drops containing KPi over a wider pH range (9.0-10.5) and of 0.8M.

Drop solution	Values investigated	Conditions yielding single crystals	Optimised values
Initial protein OD_{800}	75-120	90	90-100
Detergent	0.1-0.2% LDAO	-	-
	0.5-1.2% β-OG	1% β-OG	1% β-OG
Amphiphile	0-3% BA	2.5% BA	2.5% BA
NaCl	0-350mM	350mM	300mM
KPi	0.6-1.2M, pH 8.0-10.6	0.8M (pH uncorrected)	1.0M, pH10.0
Glycerol	1-4%	-	-
Incubator temperature	4-20°C	16°C	16°C
Well solution	Values investigated	Conditions yielding single crystals	Best values
AMS concentration	2.0-3.5M	2.3M	2.2-2.7M
AMS pH	6.0-10.5	9.7 & 9.9	8.5-10.5

Figure 45. Crystallisation conditions investigated for LH3 complex from *Rps. acidophila* strain 7050,(2nd column), conditions yielding single crystals after the introduction of the gel filtration purification step (3rd column), and the optimised conditions over which good single crystals were observed in the last column.

Detergent type and concentration was also investigated with LDAO (0.1-0.2%) being found to be a poor detergent for crystallisation. The best crystals were found using β-OG (1%) as reported previously (McLuskey, 1999). When

investigating the detergent concentration, consideration had to be given to maintaining the critical micelle concentration, CMC.

The addition of 1-4% (v/v) glycerol to the protein drop was investigated as it is thought to slow down crystal growth by slowing down diffusion of protein molecules through the solution (S. Prince, pers. comm.). It was found that the addition of 1-2% glycerol improved the crystals when grown in the presence of LDAO.

However, these crystals were not of as high quality as those grown in the presence of β-OG. The addition of glycerol to protein drops containing β-OG as detergent was not found to improve the crystals formed. The initial concentration (OD_{800}) of the LH3 complex was also investigated and found to be an important factor in size and quality of the crystals. Too low an OD_{800} (75-90) resulted in few single crystals, with more drops showing amorphous precipitate or thin, 2D discs. Too high an OD_{800} (100-120) generally resulted in many nucleation sites and therefore small crystals, with many twinned or higher aggregated forms. Values of 90-100 were found to give the best crystals.

BA was the only amphiphile investigated during crystallisation trials. Addition of enough BA to make the final solution 0-3% (w/v) was investigated with 2.5% being found to be optimal. Crystals grew both with and without BA, although in the presence of BA, the crystals were larger and had fewer defects.

The addition of a small amount of NaCl (350mM) was found to improve the quality of the crystals. Crystal trials with and without NaCl yielded crystals, although those grown in the presence of NaCl were slightly larger and more regular in appearance.

The size of the hanging drop was also investigated although a typical drop was 15µl, 10 and 20µl drop were also tried. Drop size did not appear to have a major effect on the crystal quality. As expected, smaller drops produced crystals quicker, but the drops showed signs of denaturation more rapidly. In drops where there were few nucleation sites, larger crystals resulted from the larger drops. 20µl drops were used in an attempt to grow larger crystals once conditions had been optimised.

Incubator temperature during crystal growth was also investigated varying from 4°C to 25°C. It was found that at higher temperatures, phase separation became a major problem, and any temperature above 20°C led to rapid phase separation in a

few days. The complex also became denatured after 1-2 weeks, compared with more than 8 weeks for temperatures of 16°C or below.

The crystals chosen for testing in the x-ray beams were orthorhombic and plate like, with one dimension being smaller. For testing on the home source, crystals of 0.5 x 0.5 x 0.2mm were used with smaller crystals (down to 0.05 x 0.05 x 0.02mm) being taken to synchrotron sources.

It was observed throughout all preparations that crystals of LH3 from *Rps. acidophila* strain 7050 were very fragile. Extreme care was exercised when looping crystals but many were broken upon handling, even when drawing a crystal into a capillary. The estimated solvent content of the crystals is 55% (McLuskey, 1999).

3.1.2. Cryoprotectant

Various cryoprotectants and methods of introducing them were investigated during this work. Initial conditions were those used to obtain the 3.0Å dataset (McLuskey, 1999) which was to introduce 50% saturated sucrose solution through a low molecular weight cut off dialysis membrane. Using this method, diffraction data extending to 3.5Å resolution was obtained at beamline 9.5 at the SRS, Daresbury. However, this resolution was never replicated despite extensive trials, and typical diffraction using this method of cryoprotection was to approximately 5Å. For a typical diffraction pattern obtained, see figure 46.

When a reasonable supply of crystals was established, these cryoconditions were investigated further. Rather than dialysing in the sucrose solution, which involves transferring the crystal to a small dialysis button, other methods were investigated. Sequential addition/extraction using saturated sucrose, and soaking experiments were carried out.

Sequential additions of cryoprotectant and extraction of mother liquor was investigated to see if the decrease in handling of the fragile crystals could improve the diffraction data obtained. Unfortunately, it was found that additions of small volumes of sucrose solution, even of low concentration (10% saturated sucrose), resulted in the sucrose solution sitting on the bottom of the drop and not mixing easily with the mother liquor. If the crystal was sitting on the bottom of the drop it was subjected to an immediate and rapid increase in sucrose concentration and often cracked, whilst

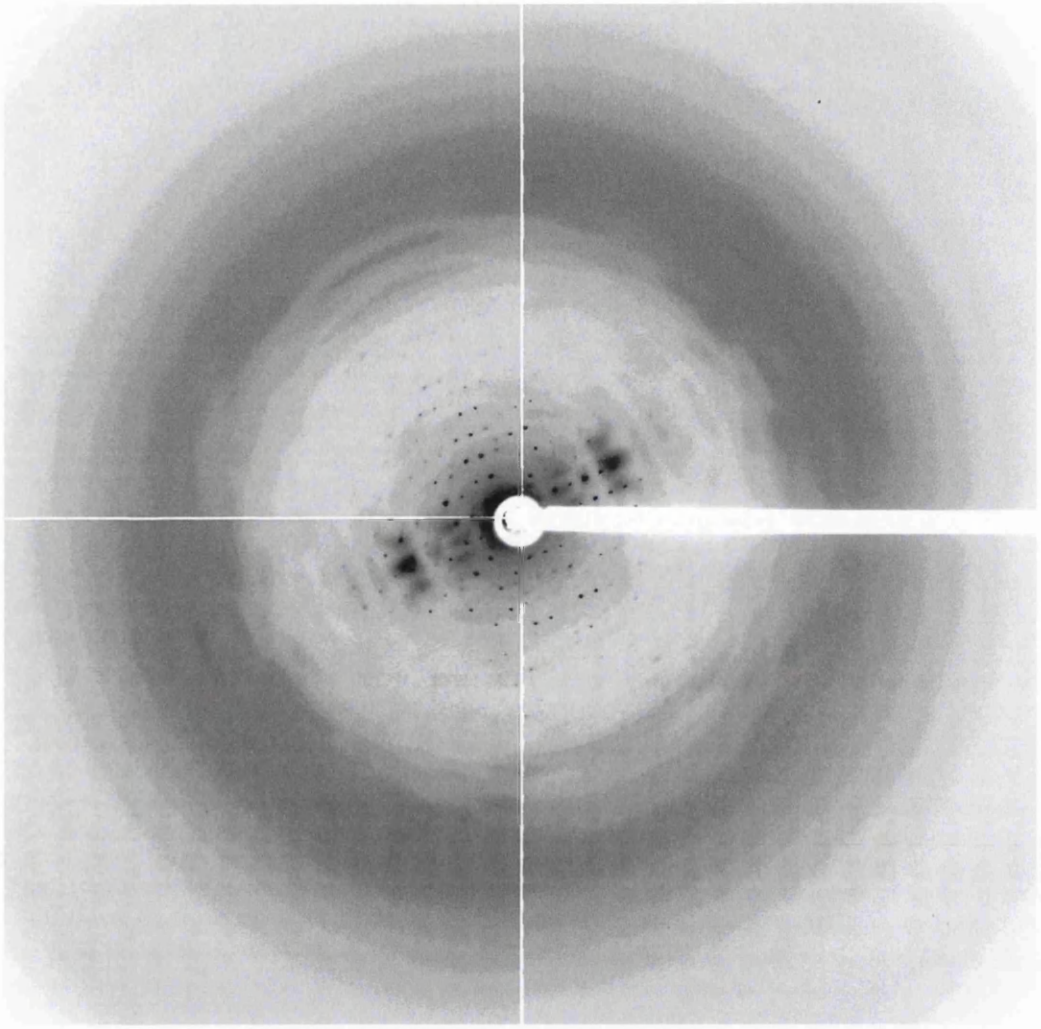

Figure 46. Test exposure of LH3 crystal from 7050. Diffraction pattern recorded at station 14-2, ESRF, Grenoble on ADSC Quantum-4R CCD detector. Ethylene glycol was used as a cryoprotectant, the data recorded at 100K with a 10 second exposure and oscillation of 0.5°. The resolution at the edge of the detector is 2.1Å, lowest resolution observed is 31Å. Data is detectable to approximately 12Å.

those on the surface had little change in environment. It was attempted to gently mix the solutions, both by stirring with the pipette tip, and by drawing and re-injecting a small volume of solution several times. The hazard in this was that the crystals may dissolve or break under the physical stress which some did, but others were then successfully loop mounted and flash frozen. Diffraction was observed in the best case, to 6Å using the Siemens multi-wire detector at Glasgow University.

Crystals were also soaked for short periods in sucrose solutions. It was found to be very difficult to draw a crystal rapidly through a high concentration sucrose solution as, due to the high viscosity, the crystal was usually dislodged from the loop, and therefore more time was taken whilst re-looping. In an effort to combat this,

crystals were rapidly drawn through several solutions of increasing sucrose concentration This method was found to result in crystals that were even more fragile and often disintegrated when trying to loop them. The best diffraction observed was to approximately 5Å resolution at beamline 9.6 at the SRS, Daresbury.

Glycerol as a cryoprotectant was also investigated by addition of small volumes of solutions of varying concentrations and soaks in glycerol solutions. As with the sucrose, even low concentration glycerol solutions (10%) were found to remain in a separate layer from the mother liquor when added to drops, resulting in the same problems of very fragile and cracked crystals. The best diffraction seen with glycerol cryoprotectant was approximately 8Å using the Siemens multi-wire detector, Glasgow University. The dialysis method was not investigated as glycerol passes rapidly through dialysis membrane due to its size.

Other cryoprotectants such as paraffin oil, ethylene glycol and high salt concentrations of Na formate and Na acetate were investigated.

Crystals were drawn through drops of dry paraffin oil with a limited success rate. It was observed that the time taken to draw the crystal loop through the oil was critical, with rapid transfer giving the best results. However, too rapid and the procedure was not effective, resulting in ice rings in the diffraction patterns. Care was exercised to ensure that no droplets of aqueous solution remained stuck to the crystal or loop, whilst looping the crystal through the oil as rapidly as possible. It was often found to be necessary to use several fresh drops of oil to adequately remove the aqueous solvent from the crystals.

Using paraffin oil as cryoprotectant, diffraction was regularly observed to 6Å in one direction and 8Å in the other, with no ice rings present. However, no improvement on this resolution was achieved.

The use of ethylene glycol and high concentrations of Na formate and Na acetate as cryoprotectants was investigated as an addition to Reaction Centre work (see chapter 5). Crystals were looped from the drop and rapidly drawn through solutions containing cryoprotectant, made up in AML (see section 2.7.2). Different solutions were investigated, however, none of these cryoprotectants resulted in diffraction of higher resolution than about 6Å in one direction and 9Å in the other, on the Siemens mulitwire, University of Glasgow. It was found that high salt concentrations of Na acetate were particularly bad, resulting in diffraction of less than 10Å at the synchrotron source of ID 14-2, ESRF, Grenoble.

Commercially available sparse matrix screens of cryoprotectant crystallising conditions, Cryo I and Cryo II (Emerald Biostructures), were also used (see Appendix 2). These contain a wide variety of conditions with different buffers, precipitants, additives and pH. These screen have been produced mainly for soluble proteins, therefore slight amendments were made to the conditions. These were the inclusion of detergent (1% β-OG) and the drops being set up with and without an amphiphilic molecule (2.5% BA). From the screens, only those conditions between pH 7.0 and 10..5 were used, as the complex is known to rapidly denature at lower pH. It was found that many drops denatured or resulted in phase separation. Other drops yielded amorphous precipitate or resulted in no observable change after 6 months. A few wells showed signs of producing crystal-like precipitate and these conditions were investigated further. These were conditions 26, 28, 36, and 38 from Cryo I and condition 25 from Cryo II and they contain a variety of different precipitants, buffers and additives at pH between 7.0 and 10.5 see figure 47. None of the conditions produced single crystals and upon repeating the experiment, it was apparent that the precipitate was amorphous. As the cryo-screens did not provide any leads, this investigation was abandoned.

Cryo-screen condition	Precipitant	Buffer	Additives
Cryo-I, no. 26	40% (v/v) PEG-300	CHES pH 9.5	0.2M NaCl
Cryo-I, no. 28	40% (v/v) PEG-600	HEPES pH 7.5	0.05M Li_2SO_4, 10% (v/v) glycerol
Cryo-I, no. 36	50% (v/v) PEG-200	Tris pH 7.0	0.05M Li_2SO_4
Cryo-I, no. 38	30% (v/v) PEG-400	Tris pH 8.5	0.2M Li_2SO_4
Cryo-II, no. 25	40% (v/v) 2-methyl-2,4-pentanediol	CAPS pH 10.5	none

Figure 47. Cryo-screen conditions providing possible leads for the LH3 complex from *Rps. acidophila* strain 7050. These conditions were further investigated but did not show any promising leads.

As the changes in cryoprotectant did not appear to have any improvement in resolution of the diffraction, several crystals were mounted at room temperature in order to discover if the crystals were inherently poor at diffraction or whether it was the method or type of cryoprotectant causing the poorer diffraction.

Crystals were mounted in quartz capillary tubes (0.1-1.0mm depending on size) with a reservoir of mother liquor and the tube sealed. Crystals were very difficult to handle and many shattered within the capillary when the excess mother liquor was drawn off with a paper wick or drawn Pasteur pipette. Although extreme care was

taken in mounting the crystals, and they were inspected under the beamline optics for shape, there is no guarantee that the crystals were undamaged. Upon exposure, it was seen that room temperature mounted crystals diffracted to approximately 4Å in one direction and 6Å in the other on the home source using the DIP2020 image plate, Glasgow University.

3.1.3. Conclusions

Despite extensive testing of crystals at 100K and room temperature, it was not found possible to equal or better the resolution obtained by McLuskey (1999). Of the cryoprotectants investigated, sucrose was found to be the best, and dialysis, the best method of introduction. Cryoconditions still remain a problem area for these crystals, and no conditions could be found under which the crystals diffracted beyond 5Å (after the initial 3.5Å resolution seen).

It was found that crystals diffracted slightly better at room temperature without cryoprotectant (to 4Å resolution), but the efficiency of mounting crystals in capillaries was very low. Room temperature exposure of crystals at beamline 14-1 of the SRS, Daresbury was undertaken, however, no improvements on the 4Å resolution observed in the home lab were obtained. The lower resolution obtained for these crystals could be due to less efficient handling and mounting (for example too long being taken to transfer the crystal from the drop into the cryostream) or due to less perfect crystals.

3.2.The B800-820 light harvesting complex from *Rps. acidophila* strain 7750

The LH3 complex from *Rps. acidophila* strain 7750 was investigated as it provides an alternative low light complex for comparison with that currently available from strain 7050. The regulation also differs, as this strain produces the LH3 complex in response to low light and low temperature, and it would be of interest to find any structural differences accompanying this.

Crystals of the LH3 complex from strain 7750 had previously been grown (Guthrie et al., 1992; McLuskey, 1999), however, no diffraction has been seen beyond 6Å (K. McLuskey, pers. comm.).

The purity of the complex was monitored (by P_r and I_r values) throughout the preparation. The values used as cut-off points for crystallisation were taken as approximately 0.8 for P_r and 3.0 for I_r (McLuskey, 1999). The purification procedure employed for this complex shall only be described where it differs from that detailed in chapter 2.

The bacteria were grown in flat-sided 500ml bottles in a temperature controlled water tank at 22°C. They were illuminated by one 40W incandescent bulb at a distance of 40cm . Growth and reversion to production of LH3 was monitored using absorption spectroscopy. It was apparent by visual inspection that the carotenoid composition changed when growth was switched from high light (orangish-purple) to low light (reddish-purple), which occurred after 1-2 transfers to low-light conditions. It was noted that this strain of *Rps. acidophila* was more difficult to change to production of the LH3 complex than strain 7050, with the majority of the light harvesting complexes being LH3 only after 5-6 transfers (by comparison of absorption spectra).

Differences in the growth of the bacteria were more apparent for strain 7750, with different bottles showing slightly different colouration (by visual inspection) and slightly different peak ratios. In an attempt to minimise this, growth using stirred 10 litre pots was investigated as it was thought that with a larger volume, the entire vessel would contain the same form of cells, and the differences in many 500ml bottles could be eliminated. It was found that the absorption spectra were more consistent, however, it was much more difficult to control the production of LH2 and

LH3 complexes. Growth was therefore carried out in 500ml bottles, large quantities (30-40 litres) harvested together and aliquots frozen so subsequent preparations were from the same batch of cells.

Solubilisation conditions were investigated systematically using 1-3% LDAO and an initial sample OD_{800} of 40-80. Incubation was carried out at 4°C or room temperature for 1-4 hours. After solubilisation, the purification was carried out in an identical manner each time, and I_r and P_r values along with results of crystallisation trials were compared. It was found that solubilisation conditions appeared to make little difference to the I_r and P_r values and subsequent crystallisation. After initial investigation, solubilisation was carried out using 2% LDAO at a complex OD_{800} of 50. The solution was incubated for 2 hours at 4°C.

Previous purification had been carried out using anion exchange (Resource Q) or gel filtration columns, although crystallisation trials showed only microcrystalline precipitate (McLuskey, 1999). Anion exchange using the Resource Q column was used as a starting point for investigations into the purification procedure.

It was reported that LH3 complex from strain 7750 binds only very weakly to an anion exchange column in 20mM Tris at pH 8.0 (McLuskey, 1999) and this was confirmed. This suggests that this pH is one at which the complex has very few exposed, charged residues. It may also be true that the complex is close to the PI, the pH at which the protein has no net charge, although this does not take account of areas of positive and negative charge which may cancel each other out. Inspection of the amino acid sequences for the polypeptides did not show any reason for the different binding, with LH3 from 7050 and 7750 both having similar charged residues. The pH of the buffer solution was increased slightly to 8.5 to adjust for this weaker binding. This slightly higher pH was maintained throughout the preparation.

Even at this slightly higher pH, it was seen that some material did not bind to the column. The absorption spectra of these fractions showed a larger LH2 contamination than in the complex that bound to the column. The complex was eluted from the column using a NaCl gradient, with the fractions containing the purest LH3 eluting at ~100mM NaCl. Absorption spectra of the fractions were inspected and the purest collected and pooled for further purification. These fractions typically had P_r = 0.9 and I_r = 2.6 (compared with values of 0.8 and 3.0 published (McLuskey, 1999))

As the salt concentration was further increased (to 250mM), it was observed that the absorption peak at ~820nm decreased until there was only a peak at 800nm

apparent. The fractions displaying this B800 only absorption were rather dilute with a very low I_r value (of around 1) and were considered a contaminant. This B800-only complex (if that is what it is) would be interesting to investigate further, although whether it is a distinct complex produced by the bacteria or an artefact of the purification is unknown. The low-resolution structure of a B800 only LH2 complex from *Rps. palustris* has recently been published (Hartigan et al., 2002).

The purest fractions were pooled and concentrated, and initial crystallisation trials set up to screen around the best conditions reported previously (McLuskey, 1999) (see figure 48)

Drop solution	Values reported (McLuskey, 1999)	Values investigated
Initial protein OD_{800}	(OD_{820}) 90 (≈110 OD_{800})	90-100
Detergent	1% β-OG	1% β-OG
Amphiphile	2.5% (w/v) BA	2.5% (w/v) BA
NaCl	350mM	350mM
KP_i	0.8M, pH 9.2	0.8-1.0M, pH9.2 & 10.0
Incubator temperature	16°C	16°C
Well solution	Values reported	Values investigated
AMS concentration	2.3M	2.1-3.0 M
AMS pH	9.0	8.5-9.5

Figure 48. Crystallisation conditions reported for LH3 complex from *Rps. acidophila* strain 7750 (McLuskey, 1999), and conditions screened in the last column.

No crystals were observed under these conditions, with most wells showing amorphous precipitate in 2-3 weeks. This could be due to more contaminated samples (represented by the lower I_r values), and care was exercised to use only the purest fractions. However, when using only the Resource Q column, typical I_r values rarely exceeded 2.9. As the introduction of gel filtration had proven essential in growing crystals of LH3 from strain 7050, this additional purification step was also introduced for strain 7750.

The purest fractions from the Resource Q column were concentrated and loaded onto an S200 column pre-equilibrated with 20mM Tris pH8.5. As with the LH3 from 7050, the majority of the sample eluted in a single, almost symmetrical

peak. Also apparent was a minor second peak that was very dilute. When the resulting fractions from the main peak were inspected, it was seen that the P_r values remained fairly constant throughout, and that the I_r values varied more, with the purest fractions occurring underneath the peak. The fractions with the best I_r and P_r values (normally >2..9 and >0.85 respectively) were pooled, concentrated, and used for crystallisation.

Crystallisation trials were set up using the parameters described in figure 48. However, these trials did not result in single crystals, therefore a more in depth investigation into the crystallisation conditions was carried out.

3.2.1. Crystallisation Conditions

Much of the experience gained from working on the LH3 complex from strain 7050 was applied to strain 7750. Crystallisation was carried out using sitting drops and the starting conditions (see figure 48) were altered methodically in an attempt to find the optimum conditions. Wells were checked regularly for the appearance of crystals, and graded according to the observations made. Crystals typically appeared in 6-8 weeks.

When the initial conditions yielded only thin, imperfect needles and star-shaped aggregations (see figure 50a), the crystallisation parameters were widened (see figure 49).

The first crystallisation conditions to be investigated further were those of the well solution. It had been noted that the best results obtained were from drops with well solution at the lower end of the pH range and higher concentrations of AMS. Therefore the parameters were widened to cover concentrations of 2.0-3.5M AMS at pH 5.5-10.0. It was found that crystals grew over many conditions with the best between pH 6.5 and 9.0 and at higher concentrations (between 2.6 and 3.0M). Crystals were long, very thin needles (up to 1 x 0.05 x 0.05 mm) which were found to be extremely fragile, and upon close examination (using polarised light), most were found to be composed of several smaller needles.

The addition of 1-2µl of AMS well solution to the 15µl protein drop was also investigated, with and without the addition of KPi. It was thought that using AMS instead of KPi would give a less complicated system, easier to understand and manipulate. However, it was found that KPi is required for crystal growth, and

Drop solution	Values Investigated	Optimised values
Initial protein OD_{800}	75-120	100-120
Detergent	1% β-OG	-
	0.1-0.2% LDAO	0.1% LDAO
	0.1-0.4% UDAO	0.2-0.3% UDAO
Amphiphile	0-3% (w/v) BA	2.5% (w/v) BA
NaCl	0-350 mM	0-350 mM
KP_i	0.6-1.2 M, pH 8.0-10.6	0.8-1.0M, pH10.0
Incubator temperature	4-20°C	16°C
Well solution	Values Investigated	Optimised values
AMS concentration	2.0-3.5 M	2.6-3.0 M
AMS pH	5.5-10.0	6.5-9.0

Figure 49. Crystallisation conditions investigated for LH3 complex from *Rps. acidophila* strain 7750 and the optimised conditions in the last column.

only amorphous precipitate resulted from use of only AMS. The addition of 1-2µl of AMS to the drop that already contained KPi was carried out in the hope the drop and well solutions would be closer to equilibrium, and fewer, larger crystals would result. It was observed that large salt crystals, probably AMS, grew in the drops where AMS had been added. This did not prevent the formation of LH3 crystals, but it did not seem to improve their size or likelihood of formation either. This can be seen in figure 50b.

The concentration and pH of KPi in the drop was investigated, with 0.6-1.2M KPi at pH 8.0-10.6 (and at unadjusted pH) being used. The optimised concentration was found to be between 0.8 and 1.0M at pH 10.0 although crystals were observed under other conditions.

KPi was also investigated as the well solution (as it is present in the drops), and trays were set up using 2.3-2.9M KPi at pH 8.0 and 10.0. Most drops showed precipitate after 6-9 weeks, mostly in the form of starry aggregates, and phase separation became apparent after 12 weeks. No single crystals or promising leads had deweloped from these trials, and the use of KPi as well solution was not investigated further.

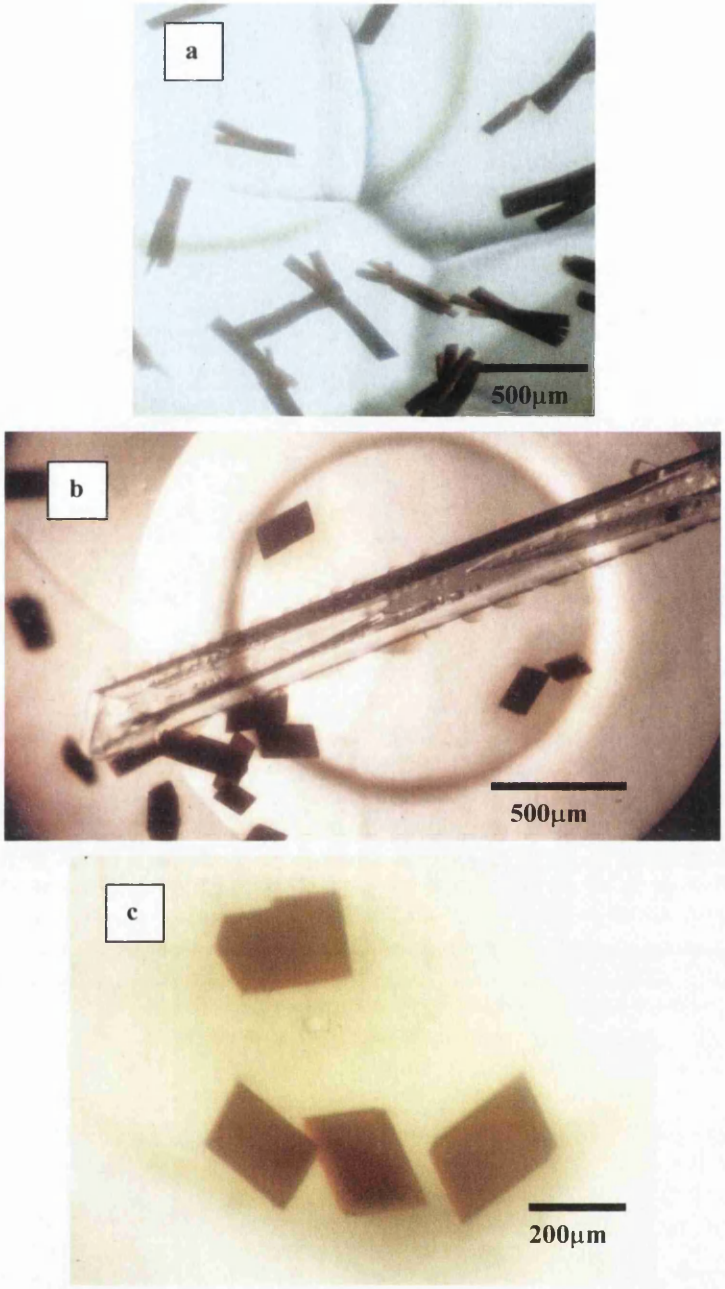

Figure 50. Photos of 7750LL crystals

a) Chunky needles composed of twins or higher aggregates. Drop: complex initial I_r =3.4, P_r =0.89, OD_{800} =120, 0.1% LDAO in 20mM tris pH8.5, 2% glycerol, 300mM NaCl, 3% BA, 1.0M KPi pH10.3, drop size =15µl, pH of drop =8.9. Well: 2.6M AMS pH9.0, 1.5µl AMS well solution added to drop. Incubated at 16°C. After 3 weeks.

b) Single crystals, maximum size: 200 x 100 x 50µm in same well as AMS crystal. Drop: complex initial I_r =3.2, P_r =0.90, OD_{800} =120, 0.1% LDAO in 20mM tris pH8.5, no glycerol, 300mM NaCl, 2.5% BA, 0.8M KPi pH10.0, drop size =15µl. Well: 2.8M AMS pH8.5. Incubated at 16°C. After 4 weeks.

c) Single crystals approx. 200 x 150 x 75 µm Drop: complex initial I_r =3.2, P_r =0.86, OD_{800} =120, 0.3% UDAO in 20mM tris pH8.5, 1% glycerol, 150mM NaCl, 2.5% BA, 1.0M KPi pH10.0, drop size =20µl. Well: 2.8M AMS pH7.0. Incubated at 16°C. After 16 weeks.

The initial concentration (OD_{800}) of the complex was again found to be an important factor in determining the quality of the resulting crystals. Values of 75-120 were investigated with the more concentrated sample with OD_{800} of 110-120 giving the best crystals. This compares favourably with those published in McLuskey, 1999, where an OD_{820} of 90 was used- since the average P_r value in that work was 0.8, an OD_{820} of 90 is approximately equal to OD_{800} of 112.

Crystals were mostly observed in drops in which BA was present, although some crystals grew without this amphiphile. 0-3% (w/v) was used, and 2.5% was found to be optimal for size, quality and reproducibility. No other amphiphiles were investigated, although this may be an area worthy of further research.

The addition of varying concentrations of NaCl to the drop (0-350mM) was not found to be required for crystal growth. The addition of NaCl did not seem to affect the size or quality of the crystals, but did apparently affect the reproducibility of crystallisation. However, this observation may be linked to the fact that more crystallisations were carried out in the presence of NaCl.

15µl and 20µl hanging drops were used, with equal success rates. Drop size did not appear to have an effect on the crystal quality, although 20µl drops were used in an attempt to grow bigger crystals once conditions had been optimised.

Incubator temperature during crystal growth was also investigated varying from 4°C to 20°C. As for the LH3 complex from strain 7050, it was found that at higher temperatures, phase separation became a major problem, and any temperature above 18°C led to phase separation. The complex also became denatured after 2-3 weeks, compared with more than 8 weeks for temperatures of 16°C or below. Incubation was carried out at 16°C.

The crystallising detergent was not investigated until later on in the project as, taking into account the experiences with strain 7050, and previously published data (Guthrie et al., 1992; McLuskey, 1999), β-OG was seen as the preferred crystallisation detergent. However, after extensive crystallisation trials using β-OG with no successful results, the use of 0.1% LDAO as crystallisation detergent was investigated (as the preparation was carried out using this detergent). Single crystals were observed in several wells, and these conditions were expanded upon. In conjunction with both LDAO and β-OG, glycerol was investigated as an additive, with 1-4% glycerol being added to the light-harvesting complex solution. No

improvement was observed in the β-OG conditions. However, it was observed that the addition of 1-2% glycerol gave the best results with LDAO. Large needle crystals grew in several drops, with some appearing to be twinned or made up of multiple crystals. However, some conditions yielded single crystals approximately 0.3 x 0.3 x 0.1 mm (see figure 50c).

Optimisation of these conditions could not determine more accurately the crystallisation parameters. Crystals grew in approximately 10% of wells over a wide range of similar conditions and the conditions producing crystals were not consistent. No conditions produced crystals that diffracted to higher resolution than 7Å in one direction and 10Å in the other on the home source.

Crystals from *Rsp. molischianum* were reported using N,N-dimethylundecylamine-N-oxide (UDAO) as the crystallisation detergent (Koepke et al.,, 1996). Therefore, this was investigated in place of LDAO as the crystallisation detergent.

The critical micelle concentration (CMC) of UDAO is higher than that for LDAO and therefore several UDAO concentrations were investigated for crystallisation. 0.1% (w/v) UDAO resulted in rapid precipitation of the complex after only a few days. 0.2 and 0.3% (w/v) UDAO yielded crystals over a wide range of conditions. In general the crystals appeared in more wells (approximately 20%) and diffracted to the same resolution or better than those grown in the presence of 0.1% LDAO. Single crystals up to 0.6 x 0.2 x 0.2 mm were grown. At 0.4% (w/v) UDAO, phase separation became a problem in most wells.

In an attempt to improve the crystals, the entire preparation, from solubilisation to crystallisation was carried out using UDAO. The membranes were solubilised using 2.5% UDAO and incubated for 2 hours at room temperature. The buffer used throughout the preparation was 20mM Tris, pH 8.5 + 0.3% UDAO, and the method the same. There was no improvement in the reproducibility of crystal growth, or the size and shape of the crystals however. Therefore subsequent preparations were carried out in 0.1% LDAO, and the detergent exchanged for 0.2-0.3% UDAO prior to crystallisation.

3.2.2. Cryoprotectant

Different types of cryoprotectant and the methods of their introduction were also investigated for crystals of the LH3 complex from 7750. The same cryoprotectants were used as for 7050 crystals therefore only the results shall be discussed here.

It was noted throughout that the crystals of LH3 from strain 7750 were very difficult to handle. Although crystals were grown under a variety of conditions, all crystals were found to be very "sticky" and the slightest contact from a loop, hair or acupuncture needle (used to manipulate crystals within the drops) resulted in the crystal fragmenting, and pieces sticking to the foreign body. This was obviously found to be major problem, and all mounting had to be carried out with the utmost care. The amino acid sequences of the polypeptides were examined to see if the residues responsible for crystal contacts in the LH2 structure from strain 10050 (McDermott, 1997) and the LH3 structure from strain 7050 (McLuskey, 1999) had different charges in this complex. No major differences could be found to explain the exceedingly fragile crystals.

Initially, 50% saturated sucrose in AML was used as cryoprotectant (as described in section 2.7.2), and was introduced by dialysis. However, despite numerous attempts, most crystals did not survive their time in the dialysis buttons. When the dialysis membrane was removed after incubating, most crystals had dissolved, with the best case being severe fragmentation. Diffraction was once observed to approximately 5Å at station 9.6, SRS, Daresbury (see figure 51 for a typical diffraction pattern). However, this was never repeated and the fragments did not show any diffraction upon exposure to x-rays.

Crystals were steeped in AML and cryoprotectant in order to discover where the problem lay. When crystals were taken from the drop and placed in AML or in cp, they were observed to dissolve, or break up. When small amounts of AML or cp were added to the drop, the crystal appeared to be stable for a longer period of time. It was therefore thought that the perturbation caused by removing the crystal from one solution into another was enough to cause the break up. However, since the crystals

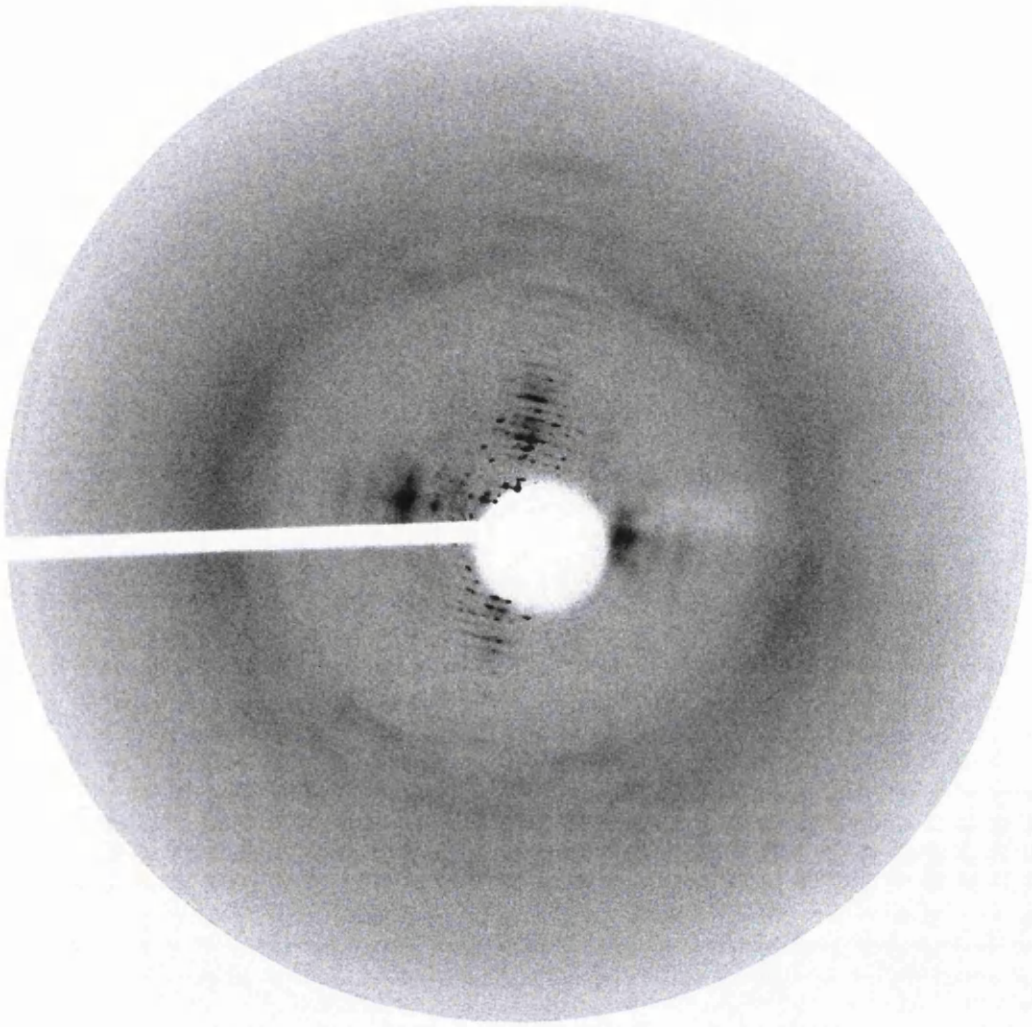

Figure 51. Test exposure of LH3 crystal from 7750. Diffraction pattern recorded on the home source using the DIP2020 image plate with a 20 minute exposure and 0.5° oscillation. Sucrose cryoprotectant was introduced to the crystal by sequential additions/extraction to the drop, the crystal was then looped and flash frozen at 100K. The edge of the image plate is at 2.5Å, the highest resolution visible is 8Å. The diffraction observed is "smudged" with the spots not clearly visible. This was typical in many cases.

did eventually dissolve in their drop after addition of AML, it was also assumed that the recipe was not optimised.

Time was therefore spent trying to find AML conditions that fully mimicked the drop conditions. Care was taken in finding the correct pH of the drop, using all the components from the drop or a mixture of them, yet no conditions were found that the crystals were stable in over a long period of time. The best AML found was simply a KPi solution at 1.5 times the concentration of that in the drop. When saturated sucrose

was added to a 2 x concentration of this AML in a 1:1 mix, crystals appeared stable in this solution for several minutes- enough time to freeze them.

Diffraction was seen to approximately 12Å in one direction and 7Å in the others upon sequential addition/extraction of sucrose/AML solutions. Crystals quickly looped through this solution showed, at best, diffraction to 5Å in all directions at station 9.6, SRS, Daresbury.

Paraffin oil was investigated as cryoprotectant with crystals being looped through several drops in order to remove the aqueous solution. It was found that a short soak (less than 1 minute) or looping the crystal through the oil resulted in poor diffraction to only 8Å, along with the appearance of ice-rings. A longer soak (up to 5 minutes in order to fully cryoprotect the crystal) appeared to give a slight improvement in diffraction to approximately 6Å in one direction and 7Å in the other at station 9.6, SRS, Daresbury. Paraffin oil was only used as cryoprotectant with a few crystals but none showed diffraction beyond 6Å at any time.

It was found to be very difficult to mount these crystals at room temperature in order to assess if the poor diffraction is due to the cryoprotectant or inherently poorly diffracting crystals. Despite many attempts at capillary mounting LH3 crystals of 7750, the best diffraction obtained was very low resolution to approximately 15Å using the Nonius DIP2020, Glasgow University.

Co-crystallisation with cryoprotectant was investigated using the Cryo I and Cryo II screens (Emerald Biostructures). None of the conditions investigated showed promising signs of crystallisation despite attempts in the presence of LDAO, UDAO and β-OG, with and without the presence of benzamidine.

3.2.3. Conclusions

There are many parameters that effect the crystallisation of the LH3 complex from *Rps. acidophila* strain 7750, and finding the correct crystallisation detergent was found to be critical in this case. For some membrane protein-pigment complexes, the detergent has not proven critical (McDermott, 1997), whilst for others it is essential to find the right detergent (Michel, 1990). A regular supply of crystals has been established through rapid and high quality purification

The crystals have been found to be exceedingly fragile and "sticky." It has also been very difficult to determine AML conditions in which these crystals are stable. Extensive x-ray testing of LH3 crystals from *Rps. acidophila* strain 7750, both at 100K and room temperature has so far failed to deliver high-resolution diffraction. The x-ray diffraction patterns have generally been of poorer quality and resolution in one direction.

Unfortunately, these problems mean that it is uncertain whether the lack of x-ray diffraction obtained is due to inherently poor crystals or the handling and mother liquor/ cryoprotectant solutions employed. Therefore, until artificial mother liquor and cryoprotecting conditions are optimised, it is difficult to test (by exposure to x-rays) which purification procedure and crystallisation conditions give the best diffracting crystals. However, until more robust crystals are grown, it seems difficult to find good AML and cp conditions.

4. Chapter 4 Mass Spectrometry of peripheral light harvesting complexes

4.1.Introduction

Previously, both MALDI-TOF and Electrospray mass spectroscopy have been employed on light harvesting complexes to investigate possible impurities (McLuskey, 1999) but mass spectroscopy has yet to be used extensively as a tool to look at the polypeptides comparing them to the amino acid sequences available.

The amino acid (aa) sequences are available from many species of purple bacteria, and some strains of *Rps. acidophila* are known to produce many polypeptides for the light harvesting complexes (Zuber and Brunisholz, 1991). These polypeptide sequences were obtained by Edman degradation.

Even for those species that are reported to express only one α-, β-polypeptide pair for the peripheral light harvesting complex, there are often several polypeptide genes. For example, *Rps. acid* strain 7050 is reported to produce only one α- and one β-polypeptide in the LH2 complex (Bissig et al., 1990) and one different α- and β-polypeptide in the LH3 complex (Zuber and Brunisholz, 1991). However, experiments on the genes of this strain show there are 4 gene sequences for expression of α light harvesting polypeptides (termed puc1A to puc4A) and 4 gene sequences for β-polypeptides (termed puc1B to puc4B) (Gardiner, 1992). The puc4A and puc4B were found to be responsible for the polypeptides produced under high light conditions (the LH2 complex). However, comparison of the amino acid sequences for which theses genes encode, and the polypeptide sequences of the α- and β-polypeptides show 4 different residues in the α-polypeptide and 4 differences in the β-polypeptides. The other 3 aa sequences derived from the pucA genes differ in between 10 and 15 residues from the published α-polypeptide sequence of the LH3 complex. The other 3 aa sequences from the pucB genes differ between 13 and 15 residues from the published β-polypeptide sequence of the LH3 complex. It would therefore be useful to know for certain the amino acid sequence of the polypeptides present in the light harvesting complexes.

How the expression of the redundant polypeptides may be induced is unknown, as is the role they play. The amino acid sequences and calculated masses are shown in figure 52.

Polypeptide	N-terminus	C-terminus	Calculated mass (Da)
Ac7050 LL α	MNQGKIWTVVPPAFGLPLMLGAVAITALLVHAAVLTHTTWYAAFLQGGVKKAA		5546.7
Ac7750 LL α	MNQGKIWTVVNPAVGLPLLLGSVAITALLVHLAVLTHTTWFPAFTQGGLKKAA		5567.7
Ac7050 HL α	MNQGKIWTVVNPSVGLPLLLGSVTVIAILVHAAVLSHTTWFPAYWQGGLKKAA		5656.7
Ac7750 HL α	MNQGKIWTVVNPAIGIPALLGSVTVIAILVHLAILSHTTWFPAYWQGGVKKAA		5654.8
Ac10050 HL α	MNQGKIWTVVNPAIGIPALLGSVTVIAILVHLAILSHTTWFPAYWQGGVKKAA		5654.8
Ac7050 LL β	AEVLTSEQAEELHKHVIDGTRVFLVIAAIAHFLAFTLTPWLH		4726.5
Ac7750 LL β1	ADKPLTADQAEELHKYVIDGARAFVAIAAF HVLAYSLTPWLH		4651.3
Ac7750 LL β2	AVLSPEQSEELHKYVIDGARAFLGIALVAHFLAFSATPWLH		4507.2
Ac7050 HL β	ADDVKGLTGLTAAESEELHKHVIDGTRVFFVIAIFAHVLAFAFSPWLH		5279.1
Ac7750 HL β	ATLTAEQSEELHKYVIDGTRVFLGLALVAHFLAFSATPWLH		4555.2
Ac10050 HL β	ATLTAEQSEELHKYVIDGTRVFLGLALVAHFLAFSATPWLH		4555.2
Ac7050puc1A	MNQGKIWTVVDPAVGIPLLLGSVAVTALLVHLAILQNTTWFPAFMQGGLKKAA(AIVQVVG)		5602.7 (6269.5)
Ac7050puc2A	MNQGKIWTVVNPAVGFPLLLGSVAITALLVHLAVLTHTTWFPAFMQGGLKKAA(AIEHVVG)		5631.8 (6337.6)
Ac7050puc3A	MNQGKIWTVVNPAIGLPLLLGSVAITALLVHLAVLTHTTWFPAYMQGGLKKAA(AIEHVVG)		5627.8 (6333.6)
Ac7050puc4A(HL)	MNQGKIWTVVNPSVGLPLLLGSVTVIAILVHLAVLSNTKWFPAYWQGGLKKAA(AIETTIVG)		5702.8 (6487.7)
Ac7050puc1B	MADKPLTADQAEELHKYVIDGARAFVAIAAFAHVLAYSLTPWLH		4853.6
Ac7050puc2B	MAVLSPEQSEELHKYVIDGARVFLGIALVAHFLAFSMTPWMH		4744.6
Ac7050puc3B	MAVLTPEQSEELHKYVIDGARVFLGVALVAHFLAFSATPWLH		4666.4
Ac7050puc4B(HL)	MADVKGLTGLTAAEAEELHKYVIDGTRVFFVIAIFAHVLAFAFSPWLH		5305.2
G151 α	MNQGKVWRVVKPTVGVPVYLGAVAVTALILHGGLLAKTDWFGAYWNGGKKAAAAAAAVAPAPVAAPQAPAQ		7136.4
G151 β	MADDANKVWPSGLTTAEAEELQKGLVDGTRVFGVIAVLAHILAYAYTPWL(H)		5404.2 (5541.3)

Figure 52. Amino acid sequences and calculated masses of the α- and β-polypeptides from light harvesting complexes studied during this project. Ac = *Rps. acidophila*, G151 = *Rv. Gelatinosus* G151, puc 1A, 2A, 3A and 4A = sequences derived from gene sequences encoding light-harvesting α-polypeptides and puc 1B, 2B, 3B and 4B = sequences derived from gene sequences encoding light-harvesting β-polypeptides. The N-terminus is at the left-hand side. Calculated masses are for the averaged $[M+H]^+$ ion which is the particle detected during MALDI-TOF MS. For the puc A genes, the cleavage site on the gene sequence is found 7 or 8 residues beyond the C-terminus usually seen in the polypeptides. Therefore, the masses have been calculated assuming this cleavage. Those values in brackets relate to the additional residues being present. The β-polypeptide aminona acid sequence for G151 shows the mass without the C-terminal H residue, the value including the H residue is given in brackets.

Due to the difficulties encountered in growing large single crystals that diffracted to high resolution, the possibility of polypeptide impurities was considered. Mass spectrometry has been employed to look at the polypeptides present in purified light harvesting complexes.

4.1.1. Screens And Matrices

There are several matrices available according to the type and size of molecule being investigated. For polypeptides less than 8kDa, CHCA is the recommended matrix molecule, for slightly larger polypeptides, sinnapinic acid can be used. Both matrices were investigated but CHCA was found to yield better results.

The ratio of sample: matrix can be critical in inducing flight in the sample molecules, at a lower ratio, there are not enough matrix molecules surrounding each complex and at higher ratios, there is not enough sample to register an accurate reading. Typically, a concentration gradient on the target plate was performed by diluting the sample with varying amounts of buffer then mixing this solution with the matrix in a 1:1 ratio. It was found that using a sample diluted with buffer to an OD_{800} of 2 was best for inducing the polypeptides to fly.

4.1.2. Parameters for optimising the MALDI-TOF

There are many parameters that can be changed with the Voyager MALDI-TOF system in order to optimise the spectra obtained. An in depth description of these can be found in the manual (Applied Biosystems), but an overview of those used are presented here.

The laser power is that which actually hits the target. If this is too low, very few molecules will fly and the background signal will be higher as seen in figure 53a. However, if the laser power is set too high, the polypeptides may disintegrate leading to a large percentage of low molecular weight fragments which leads to very inaccurate readings, especially at lower molecular weights shown in figure 53b. Typical values of laser power used were 2400-2900 on the Voyager DE Pro system although this value was optimised for each sample.

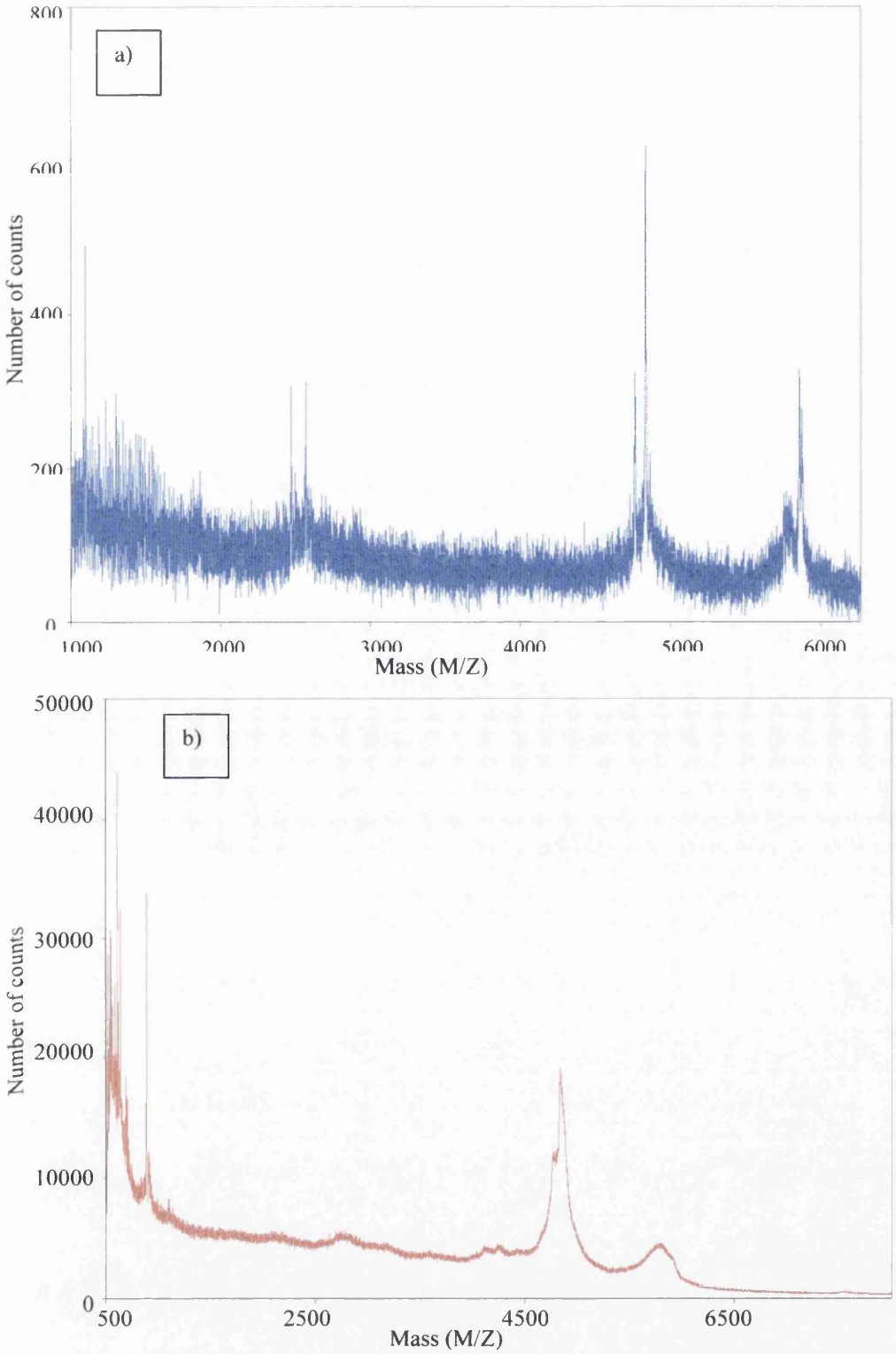

Figure 53. Mass spectrum of *Rps. acidophila* strain 7050 LH3 with the laser power of the MALDI-TOF instrument. a) Laser power too low (1900) in blue- signal to noise ratio is very poor. Peaks of interest cannot be resolved. b) Laser power too high (3100) in red- the peaks of interest are small compared with the whole spectrum, which increases at lower mass values due to an increase in fragmentation by ISD. The laser power used was optimised for each sample, with typical values used being between 2400-2900.

The delay time is the delay between the laser hitting the sample at which point a low voltage is applied to the plate thus desorbing material from the target and the moment when a high voltage is applied to the target in order to induce the charged particles to fly. This can be critical, as with too short a delay, some particles may still have kinetic energy from their desorption, leading to less accurate readings. If the delay is too long, the particles may fall back onto the plate and therefore not fly at all. It was found that a delay time of approximately 100ns was optimal for these polypeptides.

In linear mode, the flight path the charged particles follow is straight. In reflector mode, a second voltage is applied when the particles are already in flight, which reverses their direction, and they are detected on a second detector. If there are non-charged particles flying with the charged particles, these will not be reflected but instead crash into the inactive detector. It is only particles of the correct charge that will reverse direction and therefore be detected. However, in reflector mode, the sample detected (number of counts) is usually smaller, and linear extraction mode was found to be best for the LH polypeptides.

4.1.3. Sequencing using MALDI-TOF

Sequencing using MALDI-TOF is a powerful tool enabling partial sequences of polypeptides to be derived from only μg quantities of protein. This MS technique has been employed to provide experimental data of the polypeptide sequences, rather than using data often derived from the gene sequences (Zuber and Brunisholz, 1991) that does not take account of production of different complexes or post-translational modifications.

The fragmentation of peptides occurs in a reasonably well-documented manner (Johnson and Biemann, 1989). The differences in mass of these fragments are then used to find which amino acid residues have been cleaved, and to assign partial sequences. There are several methods that can be employed to study this peptide fragmentation from proteins and polypeptides using MALDI-TOF.

The most simple of these is in-source decay (ISD) (Brown and Lennon, 1995) in which a higher than usual laser power is employed to desorb the analyte from the target. This results in the polypeptides having more energy and as they travel down the flight path they often break, mostly along the peptide backbone. Since the analyte was charged, one fragment will be neutral, and one will maintain the charge, with the charged species then

being detected. This process is aided by selecting a matrix that is more favourable to promoting fragmentation.

Collision-induced dissociation (CID) is where there are two mass analysers, with a chamber in between. This chamber contains a gas, often xenon, at a temperature and pressure sufficient that when the analyte hits the xenon molecules, the energy from the inert gas is passed onto the analyte, which then fragments. One of these particles will be charged and can be detected. This method was not employed during this study.

The method that has been employed mostly in this work is that of enzymatic digestion whereby the analyte is premixed with an enzyme over various concentrations or times, the sample is spotted onto the target plate with matrix molecules, and the mixture analysed. Depending on the enzyme used, ladder sequences can be obtained in which differences of one amino acid fragment can be detected. A sequazyme^{TM} C-peptide sequencing kit (PerSeptive Biosystems, Foster City, USA) was used which contains carboxypeptidase Y (CPY) and carboxypeptidase P (CPP). Both these enzymes are known to cleave amino acids from the c-terminus, the number being dependant on the concentration used. CPY has been reported to cleave all residues from the c-terminus, including proline. However, certain combinations of residues can inhibit digestion. CPP was used to provide extra information where polypeptides were resistant to CPY. If there is inhibition of the enzyme, this can sometimes be overcome by changing the pH at which the experiment is carried out.

Proteinase K was used as a general proteinase with broad cleavage specificity, useful for the general digestion of protein samples. The sample of LH2 was placed in a cuvette under the correct buffering conditions for the enzyme. Proteinase K has optimal activity at 42°C, therefore the cuvette was placed in a water bath at this temperature and the solution corrected to an OD_{800} of about 1. An absorption spectrum was recorded and the cuvette returned to the water bath after a 0.5 µl sample was taken out and dried on the MALDI-TOF plate. Enough proteinase K to make the final solution 100µg/ml was then added and another sample taken and spectrum recorded. The cuvette was returned to the water bath to maintain temperature and this process was repeated over approximately two hours. When the absorption spectrum showed completely denatured complex (see figure 54), the experiment was stopped. Matrix was then added to each of the drops, dried in the air and the time-course experiment analysed using MALDI-TOF. A control experiment was also carried out whereby a sample was maintained at the same temperature of 42°C and absorption spectra recorded to assess the amount of denaturing due only to the heat applied (see figure 55).

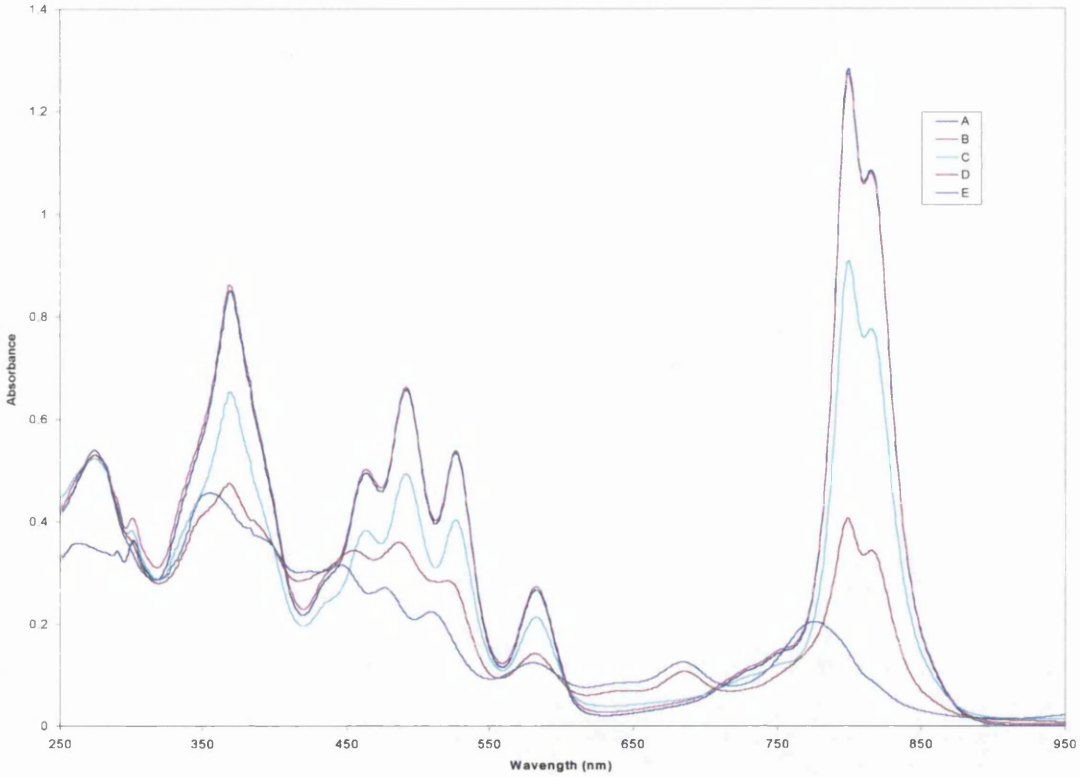

Figure 54. Absorption spectra of dissociation of the LH3 complex from *Rps. acidophila* strain 7050 at 42°C, before and after addition of proteinase K.

A= before addition of proteinase K

B= immediately upon addition of proteinase K (to make the final solution 100µg/ml), time = 0 mins. The increase in absorption at 280nm at time = 0 is due to the addition of the enzyme, proteinase K.

C= 32 mins D= 68 mins E= 110 mins

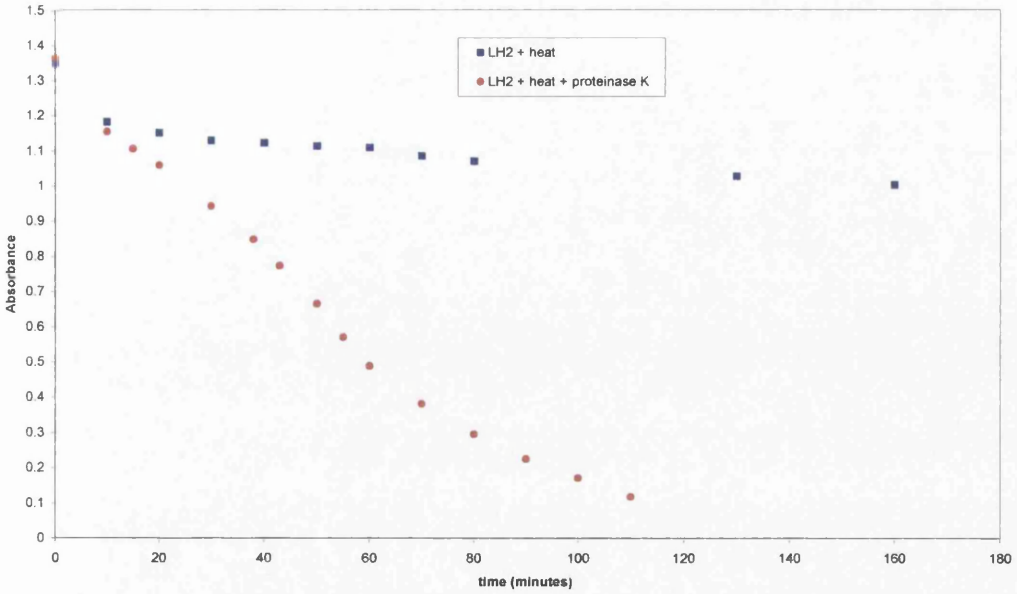

Figure 55. Absorbance at 800nm due to Bchl *a* bound within the LH2 complex plotted against time, with (red) and without proteinase K (blue) at 42°C

4.2.The B800-850 complex from other light harvesting complexes.

To verify the validity of using this technique for analysis of the polypeptides, mass spectra of other light harvesting complexes were measured. *Rhodocyclus gelatinosus* strain G 151 is known to express only one α-, β-polypeptide pair with the α-polypeptide having an extended C-terminal sequence. Analysis of a sample of the purified LH2 complex from this bacterium confirmed the presence of two single sharp peaks suggesting the presence of only one α-, β-polypeptide pair as seen in figure 56.

The peak at 5404.5 Da corresponds well to the calculated mass of an amended β-polypeptide sequence of 5404.2 Da. The published sequence has a calculated mass of 5541.3, although if the N-terminal histidine residue is removed, the calculated mass is 5404.2. Why the β-polypeptide should be present in this form, and whether it is an artifact of the purification procedure or as is found in the native complex is uncertain and further investigation would be useful. There is a smaller peak at 4785.5 Da, which could correspond to the β-polypeptide with several other residues removed: if the Leu and Trp residues are removed from the C-terminus and the Met, Ala and Asp residue from the N-terminus, the calculated mass of the polypeptide is 4787.4. Why this may be occurring is again unknown.

The peak at 7128.3 is close to the calculated mass of the α-polypeptide of 7136.4 Da although this slight difference of 8.1 has not been accounted for. There are no other peaks visible in this region.

A purified LH2 sample from *Rps. acid.* strain 10050, which is known to produce only one α- and one β-polypeptide was also analysed. The mass spectrum showed a sharp peak at 4555.9 which corresponds to the calculated mass of the β-polypeptide of 4555.2, see figure 57. There are also minor peaks in this area, one at a higher mass/charge value of 4573.0, which, with a difference of 17.1Da, could correspond to the addition of an OH group. The minor peak at 4538.9 (a difference of 17Da) could be accounted for by the loss of an OH group.

Only a minor peak was observed in the region in which the α-polypeptide was expected. It could not be accurately placed although it was at approximately 5650 Da so was assigned to the α-polypeptide, which has a calculated mass of 5654.8 Da.

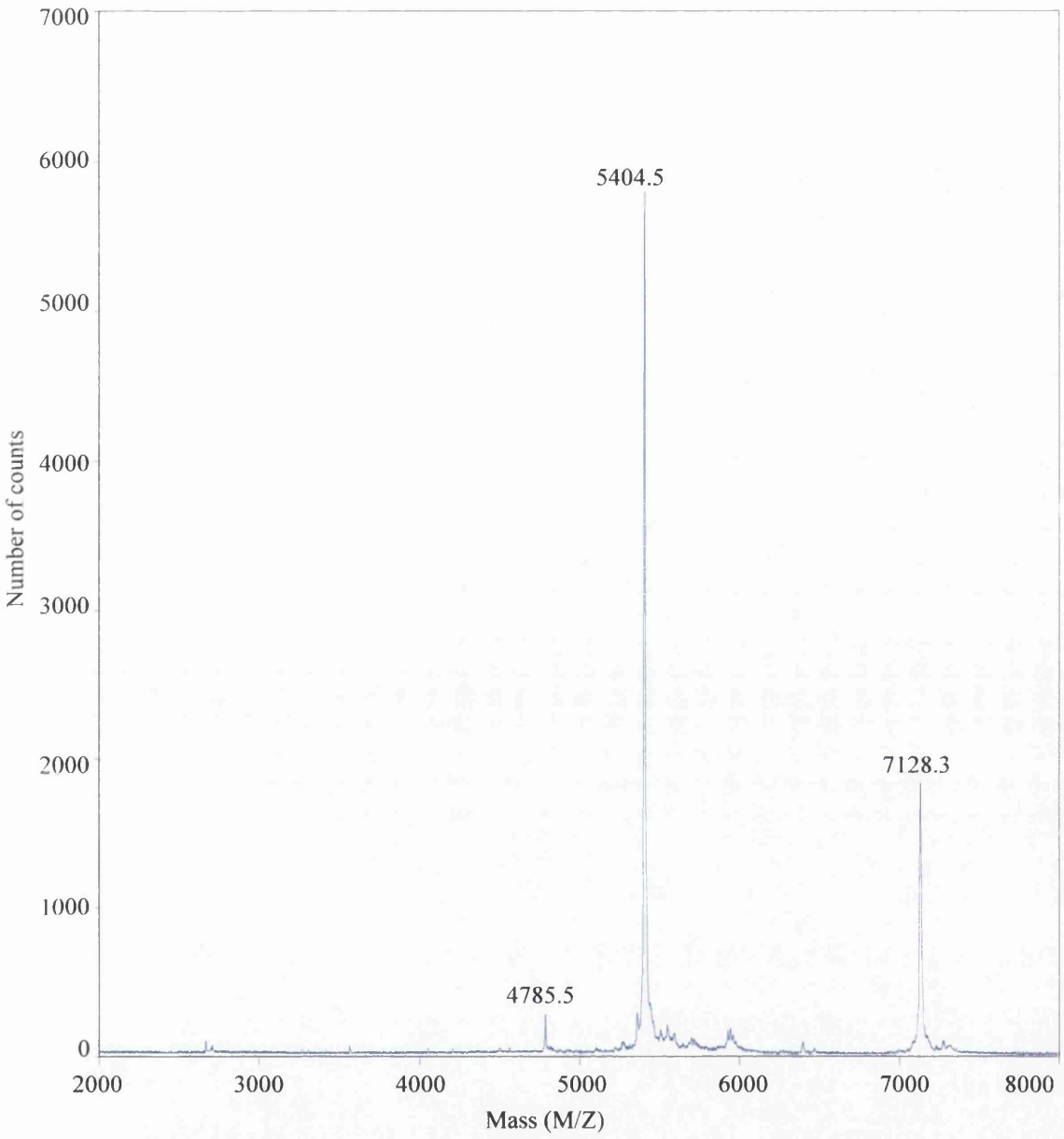

Figure 56. Mass spectrum of LH2 from *Rc. gelatinosus* G151. 0.5µl of purified complex at OD_{800} of 2, in 0.2% β-OG solution was placed on the target plate and allowed to dry. 0.5µl CHCA matrix solution dropped on top of this dried droplet. Linear extraction mode was employed with an accelerating voltage of 20,000V. Delay time was 100 nsec. The spectrum was accumulated over 200 laser shots with a laser intensity of 2282. Two sharp single peaks are observed corresponding to the β-polypeptide at 5404.5 Da, and the α-polypeptide with an extended C-terminus at 7128.3 Da. The minor peak at 4785.5 is discussed in the text.

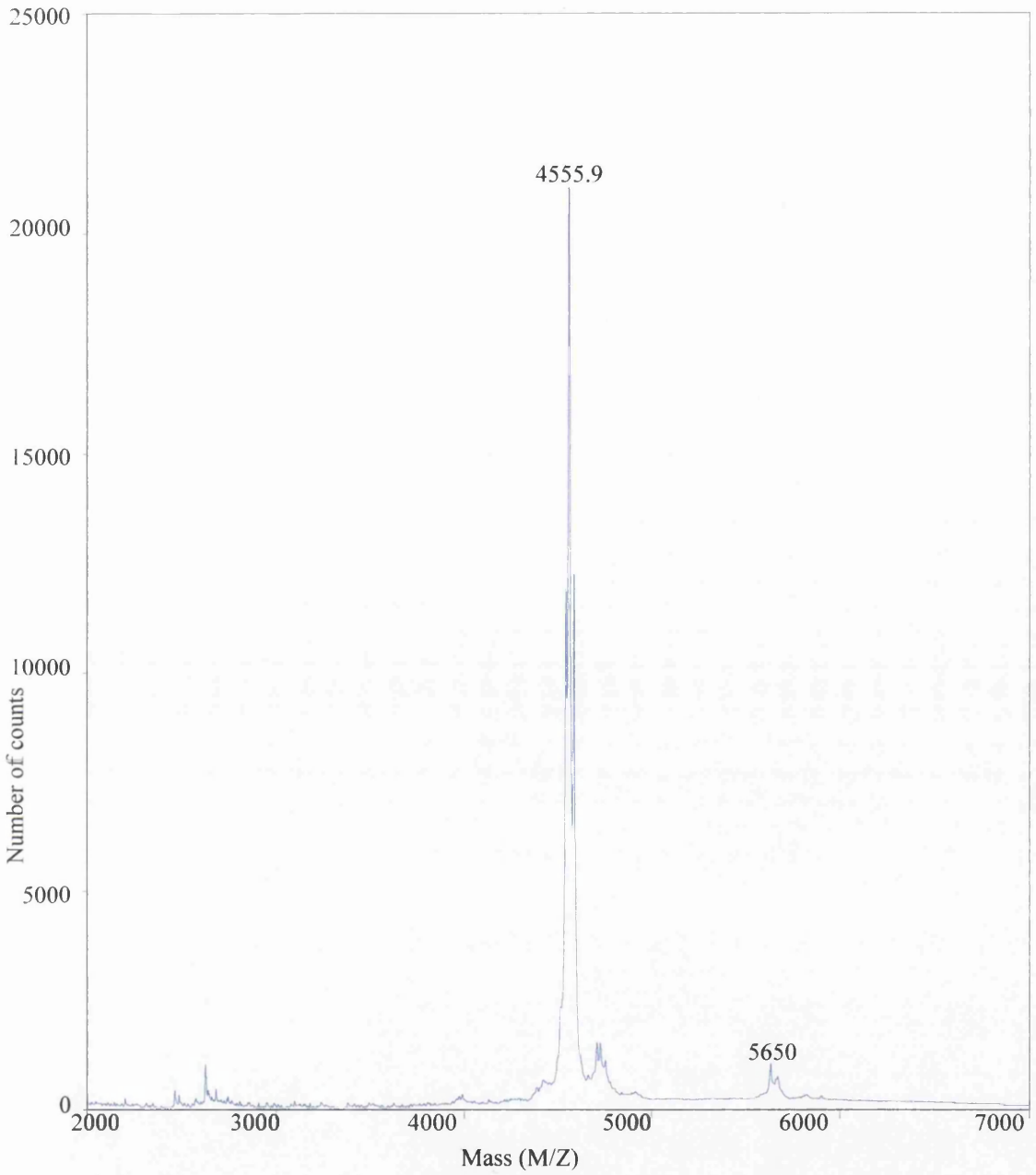

Figure 57. Mass spectrum of LH2 from *Rps. acidophila* strain 10050. 0.5µl of purified complex at OD_{800} of 2, in 0.2% β-OG solution was placed on the target plate and allowed to dry. 0.5µl CHCA matrix solution dropped on top of this dried droplet. Linear extraction mode was employed with an accelerating voltage of 20,000V. Delay time was 100 nsec. The spectrum was accumulated over 200 laser shots with a laser intensity of 2542. A large peak corresponding closely to the β-polypeptide mass of 4555.2 Da is observed at 4555.9 Da along with two minor peaks approximately 17 Da above and below the main peak. These have been tentatively assigned to the loss and addition of a hydroxyl group. A small peak is observed at approximately 5650 Da which is due to the α-polypeptide (calculated mass of 5654.8 Da).

4.3.The B800-820 complex from *Rps. acidophila* strain 7050

There is reported to be only one α-, β-polypeptide pair present in the LH3 complex from strain 7050 (Zuber and Brunisholz, 1991), therefore, mass spectrometry was expected to be used as a tool to confirm the presence of a single α- and β-polypeptide and hopefully match the masses of the sequences published. It was also thought that mass spectrometry would be ideal to detect small quantities of heterogeneous polypeptides, and to identify them by comparison with the sequences from other polypeptides. However, this was not found to be the case and several enzymes were also used in an attempt to cleave of the terminal amino acid residues and partially sequence the polypeptides (see section 4.2.2.).

4.3.1. Results And Discussion

Several mass spectra were recorded on the same samples in order to minimise any errors in the preparation. Also, mass spectra were recorded of several samples from different batches in order to further minimise any heterogeneities between batches (although the purification procedure is thought to do this).

As can be seen in figure 58, which is a typical mass spectrum of LH3 from *Rps. acid.* strain 7050, there are two groups of peaks, with those in the region of 4800Da corresponding to the shorter β-polypeptides and the longer α-polypeptides showing at approximately 5800Da.

The main β-polypeptide peak is observed at 4832.0 Da, which does not correspond to the molecular weight of the published β-polypeptide published of 4726.5 Da, a difference of 105.5 Da. There are no cysteine residues (103.1 Da) at either terminus of the β-polypeptide sequence whose loss could possibly account for this difference. Matrix molecules can become bound to polypeptides and the mass of the matrix must therefore be considered. However, the matrix used, CHCA, has a mass of 189.2 Da therefore the peak cannot be assigned to the sequence published. Comparison with the other puc genes for the β-polypeptide also fails to show a match.

There is also a secondary peak 71.2 Da from the main peak, which could be due to the loss of the N-terminal alanine residue (mass 71.1 Da). This could be caused by ISD or the polypeptide may be present in two populations due to post-translational modifications. It

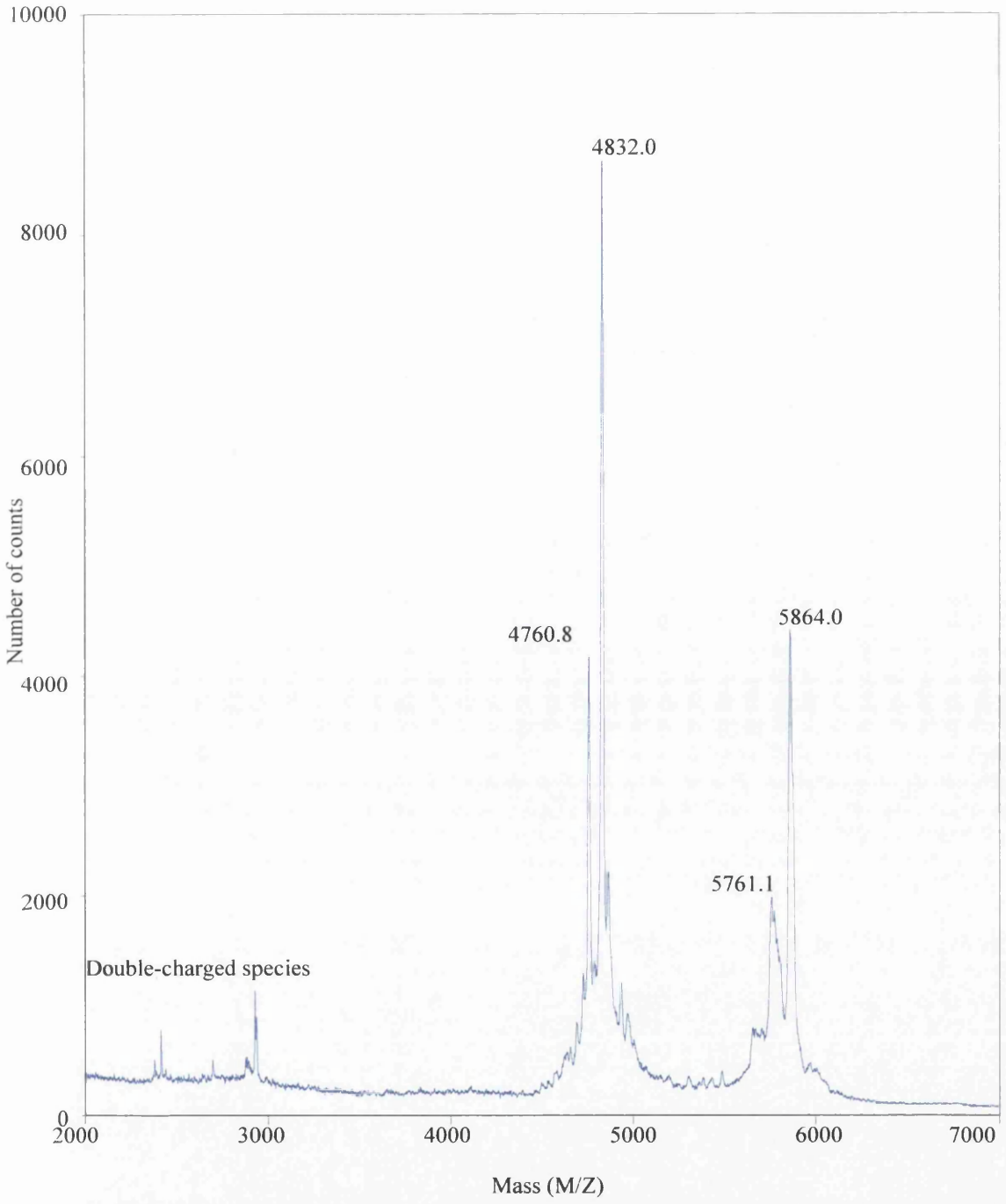

Figure 58. Mass spectrum of LH3 from *Rps. acidophila* strain 7050. 0.5µl of purified complex in 0.3% β-OG at OD_{800} of 5 was placed on the target plate and allowed to dry. 0.5µl CHCA matrix solution was then placed on top of this dried droplet and allowed to dry. Linear mode of operation was employed with an accelerating voltage of 20,000V. Delay time was 100 nsec. The spectrum was accumulated over 200 laser shots with the laser intensity of 2442. The peaks from the α-polypeptides are observed between approximately 5600 and 6000. Those from the β-polypeptides are between approximately 4600 and 5100. The peaks to the left of the spectrum are due to the doubly charged species, with their major and minor peaks corresponding exactly to half the mass/charge value of the main peaks.

was observed that the peak could not be removed by adjusting the parameters to reduce ISD.

The peaks due to the α-polypeptide are less well resolved despite attempts at optimising the parameters, and therefore the conclusions drawn from them can be even less certain. However, the observed mass of 5864.0 Da does not correspond to the molecular weight of the sequence published of 5656.7. The difference of 207.3 Da could be generously accounted for if the N- and C-terminal residues (methionine and alanine respectively) were both lost (202.3 Da). However, the difference in mass does not suggest this, and the peak does not match the molecular weight of any of the other puc gene sequences.

The secondary peak visible is not resolved well enough to show an exact mass, but the difference of approximately 103 Da cannot be accounted for by the loss of any of the terminal residues.

4.3.2. Enzymatic Digestion

As the results of these MALDI-TOF experiments proved inconclusive in the assignment of the α- and β-polypeptides, enzymatic digests were carried out in order to find partial ladder sequences which could be used to identify the polypeptides. A sequazyme™ sequencing kit (PerSeptive Biosystems) was used, which employs carboxypeptidase P and Y (CPP and CPY respectively). However, these enzymes failed to cleave the polypeptides, possibly due to the hydrophobic or complex-bound nature of the polypeptides. Proteinase K, which is known to cleave light harvesting polypeptides, was then used in an attempt to derive partial sequences to aid in the identification of the polypeptides. With proteinase K, the complex could clearly be seen to denature by observing the absorption spectra. The mass spectra remained constant during the first few samples then appeared to undergo a rather sudden change, showing mostly low molecular weight fragments as can be seen in figure 59.

Due to the data observed from the MALDI-TOF experiments carried out on 7050 LH3, it was not possible to assign the peaks to particular amino acid sequences, therefore which polypeptides are actually present and the presence of contaminating polypeptides is uncertain. However, the fact that the peaks are not sharp and single suggests there is some heterogeneity in the polypeptide composition. Whether this is due to the presence of different polypeptides within the native complex due to some post-translational modifications, or whether there are other contaminating complexes is unknown. If it is the former, then the production of high-resolution diffracting crystals may prove difficult, as

some residues required for crystal contacts may not be present in some complexes. If it is the second option, then the purification procedure is not separating these impurities sufficiently, despite repeated effort to obtain only homogenous complexes.

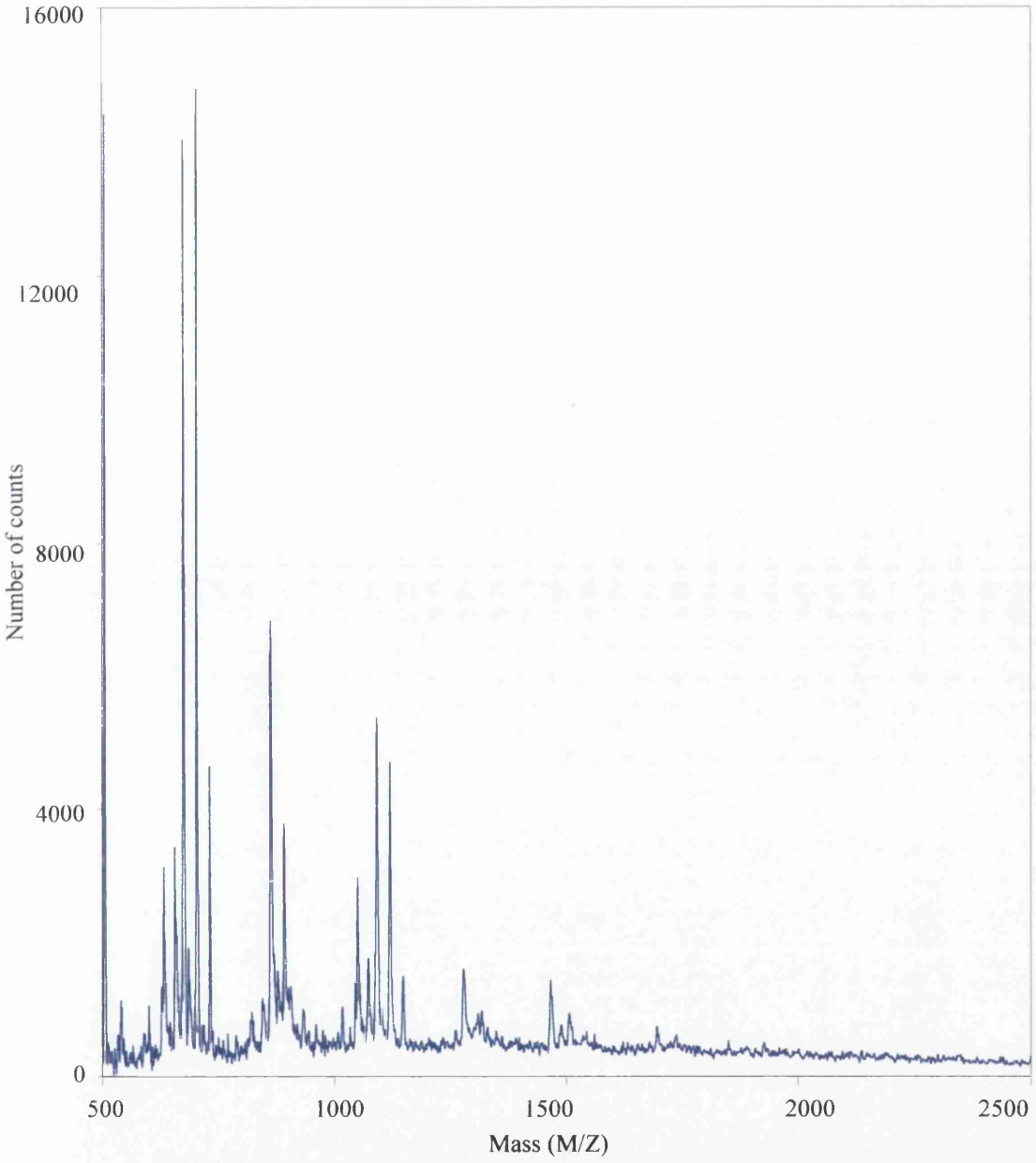

Figure 59. Mass Spectrum of LH3 from *Rps. acidophila* strain 7050 + proteinase K (100μg/ml) showing only low molecular weight fragments. 0.5μl of purified complex in 0.2% β-OG at OD_{800} of 1.5 was removed from the sample cuvette (see section 4.1.4. for details of preparation) and allowed to dry on the target plate and 0.5μl CHCA matrix solution dropped on top of this dried droplet. Linear extraction mode was employed with an accelerating voltage of 20,000V. Delay time was 100 nsec. The spectrum was accumulated over 200 laser shots with a laser intensity of 2461. The only peaks observed were below 1500 Da, corresponding to small fragments of polypeptides that have been fragmented too much to be of use in determining partial sequences.

4.4.The B800-820 complex from *Rps. acidophila* strain 7750

The B800-820 complex from *Rps. acid.* strain 7750 is reported to produce two β-polypeptides, β_1 and β_2, and two α-polypeptides, α_1 and α_2, The sequences of the α_1, β_1 and β_2-polypeptides are known although that for the α_2-polypeptide is undetermined (Zuber and Brunisholz, 1991). It was expected that the mass spectra would show the presence of two α- and two β-polypeptides, and that if the samples were impure, any polypeptide impurities would also be detected. It was expected that the mass spectra of LH3 samples of *Rps. acidophila* strain 7750 would be more complicated than those from the LH3 complex of strain 7050.

4.4.1. Results and Discussion

The mass spectra from samples of the LH3 complex from strain 7750 showed several peaks between 4500 Da and 5650 Da generated by the ionisation of α- and β-polypeptides, see figure 60. Peaks in the region between 4500 and 4800 Da are due to the β-polypeptides whilst the peaks between 5500 and 5650 Da are due to the α-polypeptides.

There are two main peaks in the region where the β-polypeptides were expected to be observed, which occur at 4722.2 and 4584.7 Da. The peak at 4722.2 Da corresponds well to the published β_1-polypeptide sequence mass of 4722.4 Da. There are no secondary peaks of significance around this peak. The other major peak at 4584.7 Da is close to the calculated mass for the β_2-polypeptide of 4567.4. The mass difference of 18.2 could correspond to one oxygen and two hydrogen atoms being lost from the published β_2-polypeptide. However, this secondary peak is found 137.5 Da from the peak assigned to the β_1-polypeptide, which is very close to the histidine mass of 137.1 Da. Therefore, the possibility exists that this secondary peak is due to the loss of the C-terminal histidine residue of the β_1-polypeptide. This second peak has been left unassigned due to this ambiguity.

There are several minor peaks both above and below this mass value that are difficult to assign and may be due to small amounts of extraneous polypeptide or due to modifications to the polypeptide either within the cell or in the mass spectrometer by ISD.

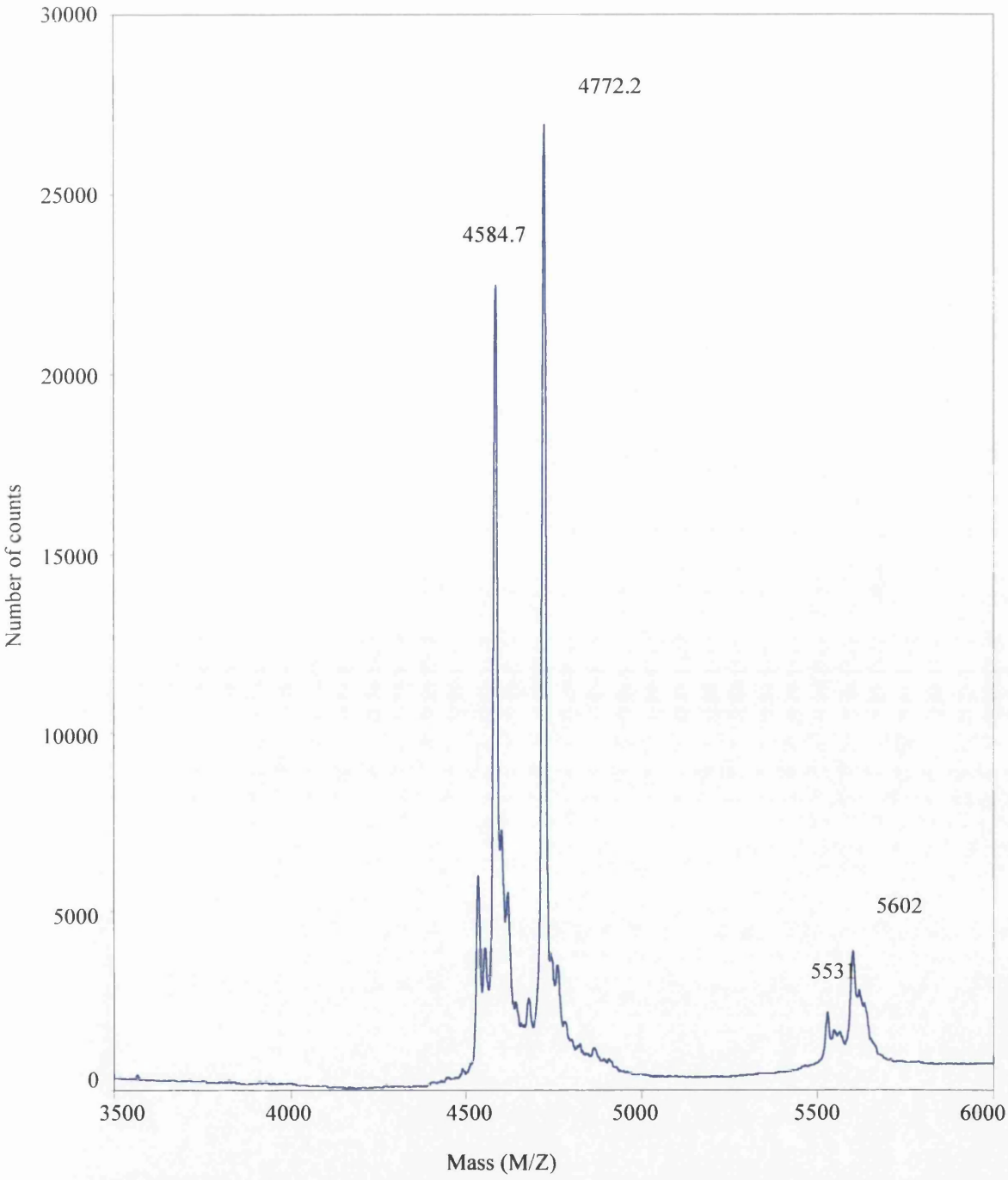

Figure 60. Mass spectrum of LH3 from *Rps. acidophila* strain 7750. 0.5µl of purified complex at OD_{800} of 2, in 0.4% β-OG solution was placed on the target plate and air-dried. 0.5µl CHCA matrix solution was then placed on top of the sample droplet and again allowed to dry. Linear mode of operation was employed, with an accelerating voltage of 20,000V. Delay time was 100nsec. The spectrum was accumulated over 200 laser shots with a laser intensity of 2304. The peaks observed between 4500Da and 4800Da are due to the β-polypeptides, and those in the region of 5500-5650 are due to the α-polypeptides. There were no peaks from the double-charged species observed.

Due to the smaller peaks detected in the region where the α-polypeptides are expected to be observed, the masses are more difficult to identify. The main peak can be seen at approximately 5600 Da with a smaller secondary peak at 5530 Da. Unfortunately, neither of these peaks correspond with the calculated mass of the published sequence which would occur at 5567.7 Da. The mass difference between the major peak observed and the calculated mass is 32.3 Da which could correspond to the addition of two oxygen atoms. However, the difference between the two peaks is seen to be approximately 71 Da, which could correspond to the removal of the C-terminal Ala residue that all the LH α-polypeptides from *Rps. acid.* have. If this is the case, it would suggest that the peak at 5600Da did not correspond to the addition of two oxygen atoms, instead was the full amino acid sequence, with the peak at 5530Da being a truncated form of the polypeptide.

4.4.2. Enzymatic Digestion

As with the LH3 complex from strain 7050, the results of these MALDI-TOF experiments were inconclusive in identifying the α- and β-polypeptides, although more success was achieved with this, the LH3 complex from the 7750 strain. Enzymatic digests were again carried out using CPP and CPY from the Sequazyme^{TM} kit in an attempt to obtain partial ladder sequences that could be used to identify the polypeptides. However, these enzymes failed to cleave the polypeptides, lending weight to the possibility that the hydrophobic or complex-bound nature of the polypeptides prevents them working in their usual or optimal way.

Proteinase K, was therefore used in an attempt to derive partial sequences to aid in the identification of the polypeptides. With proteinase K, the complex again could clearly be seen to denature by observing the absorption spectra. However, in contrast to the LH3 sample from strain 7050, this LH3 sample from strain 7750 showed more gradual degradation, leading to partial ladder sequences, especially in the area of the β-polypeptides, see figure 61.

Assignment of the peaks for the β-polypeptide digestion was not found to be possible due to the number of the peaks and the distances (in Da) between them. The pattern of peaks in the β-polypeptide region of the mass spectra without the addition of proteinase K has led to an overlap of the degradation product peaks. Analysis of the digestion of the α-polypeptide was not possible, as the signal detected was small.

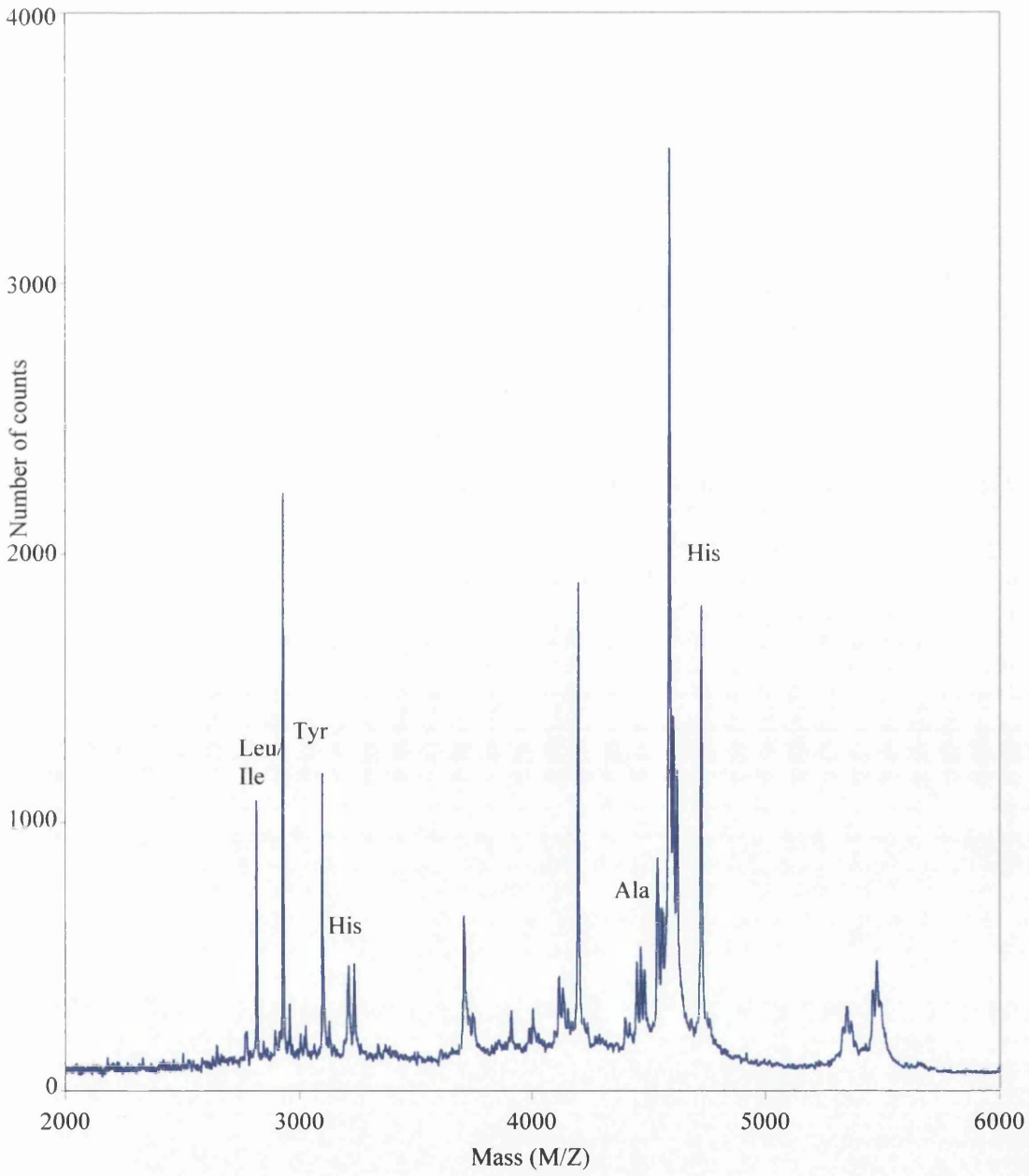

Figure 61. Mass spectrum of LH3 from 7750 + proteinase K (100μg/ml) showing partial ladder sequences. 0.5μl of purified complex in 0.2% β-OG at OD_{800} of 1.5 was removed from the sample cuvette (see section 4.1.4. for details of preparation) and allowed to dry on the target plate and 0.5μl CHCA matrix solution dropped on top of this dried droplet. Linear extraction mode was employed with an accelerating voltage of 20,000V. Delay time was 100 nsec. The spectrum was accumulated over 200 laser shots with a laser intensity of 2462. Differences between adjacent peaks can give tentative assignment of residues (examples given), but these provisional sequences do not match the published sequences.

In order to overcome this problem, first a sample containing only one kind of α- and β-polypeptide would have to be obtained. This does not seem possible given current purification procedures (if it is at all possible).

The mass spectra obtained from this 7750 LH3 suggest two α- and two β-polypeptides, although not necessarily corresponding to the published sequences. The mass spectra show reasonably well-resolved peaks for the β-polypeptides, but less so for the α-polypeptides.

4.5.Conclusions

Mass spectrometry using MALDI-TOF was found to be a useful technique and highlighted that the complexes being investigated did not contain single polypeptide elements. Although the α- and β-polypeptides are present in the LH complexes in equal amounts, in this mass spectrometry analysis, it was often found that one polypeptide would be induced to fly much more readily than the other. The shorter β-polypeptide showed a stronger signal and this may be due to several reasons. Firstly, the β-polypeptide is situated on the outside of the ring that the complex forms. It may be that as the complex dissociates, the α-polypeptide is unable to interact with the matrix molecules as it is hindered by steric interactions. It is also possible that the amino acid composition of the α-polypeptide leads to it being less likely to pick up a positive charge at the given pH and conditions.

The analysis of the β-polypeptides was found to be quite accurate, although the multiple peaks did not allow full identification. Despite extensive investigation into the MALDI-TOF parameters, sample preparation and concentration and matrix type, it was not found to be possible to obtain a signal from the α-polypeptide of equal intensity to the β-polypeptide.

The results obtained from these experiments were found to support the accuracy of 0.05% of the molecular weight claimed in the documentation, which would be ±2.4 Da with a polypeptide mass of 4700Da. Separate mass spectra were taken of the same samples in order to assess this accuracy. In the majority of cases, each mass spectrum showed the same values for the β-polypeptide peaks, within these errors.

However, the peaks were not found to be sharp and single in the majority of cases and this may be due to the membrane bound nature of the complex. If lipid or detergent molecules are bound to the complex, this may prevent rapid dissociation of the complex that

enables the polypeptides to become charged and analysed. The pigment molecules present may hinder the flight path of the polypeptides, thereby spreading the data over a wider area. Despite these problems, mass spectrometry using MALDI-TOF was found to be a very useful tool in analysing the polypeptide composition of light harvesting complexes.

This technique was to be used to identify any contamination of purified samples of LH complexes by heterogeneous polypeptides. However, it was found that the purified LH complexes did not display the mass spectra expected. This could be due to inadequacies of the technique when used with membrane proteins, especially within large complexes, or inaccuracies within the published amino acid sequences, most of which are derived from gene sequences.

Unfortunately, the α-polypeptide could not be detected sufficiently for identification in many cases despite extensive optimisation work. Further work could be carried out in order to detect the α-polypeptide, however, this problem has been previously reported (McLuskey, 1999).

As the initial mass spectra were difficult to interpret, and single peaks were not observed, fragmentation studies carried out in order to partially sequence the polypeptides resulted in even more complicated mass spectra.

When using ISD as a tool for peptide sequencing, it was very difficult to find a laser power whereby the polypeptides were not broken down into low molecular weight fragments, yet were sufficiently fragmented to provide accurate identification. It was found that ISD was not a useful technique for these light-harvesting complexes and after initial investigation, was not used.

Enzymatic digestion was most commonly used in an attempt to provide sequencing information on the polypeptides and thus aid in their identification.

The enzymatic degradation of the polypeptides in order to identify them from amino acid sequences did not give the desired results. Many of the enzymes available were found to be inactive with the light harvesting polypeptides, possibly due to their hydrophobic or complex-bound nature.

4.6.Future work

Due to time constraints, several aspects of this investigation were unable to be carried out. This sections aims to show which further experiments should be carried out, and give possible methods.

As stated, the most immediate experiment to carry out would be MALDI-TOF MS on isolated polypeptides. In order to isolate the polypeptides, a solvent extraction could be carried out on the purified complex using a 1:1 mixture of chloroform and methanol. This would then be passed down a molecular sieve column to separate polypeptides from pigment molecules.

At this point, the sample could either be analysed using MS or further purified using HPLC. If the sample was analysed at this point, it would contain the same polypeptides as the whole complex. This could be used to assess the effect the complex-bound nature has on this technique, but is unlikely to resolve the problems of identifying the polypeptides.

In order to be certain of identifying individual polypeptides, they could be isolated using RP-HPLC which elutes each polypeptide at a different time. The separate peaks could be collected and MS analysis carried out on each individually. This should give a definitive mass for each polypeptide present. If, however, this information is not enough to identify all polypeptides, enzymatic degradation could then be used. Since the starting polypeptide is now pure, the resulting ladder sequences should give a clear indication of the primary structure of the polypeptide and help in identifying it.

It may be necessary to try different solvents as some polypeptides, especially membrane bound hydrophobic ones, can aggregate on the MALDI-TOF sample plate and therefore not fly well.

It may also be desirable to take samples from earlier on in the purification protocol, eg. from the sucrose gradients, to observe the polypeptides present throughout, and which are being eliminated at each stage of the purification. This could also show changes that different growth conditions can produce.

These procedures using organic solvents should not truncate any residues or change the primary structure. However, care must be taken in analysing the MS data as some changes may have taken place, for example the oxidation of cysteine or methionine residues.

At all points in these experiments, standard polypeptides (eg. the standards kit from Applied BioSystems) should be used to should for calibration purposes. Another standard

from a similar organism should also be used to check the validity of these techniques for LH complexes, perhaps using *Rc. gelatinosus* G151 which contains only one α-, β-polypeptide pair.

5. Chapter 5 Studies on the Reaction Centre from *Rhodobacter sphaeroides* R26-1 with a reconstituted carotenoid

5.1. Introduction

The RC from *Rb. sphaeroides* has been studied extensively through various biophysical techniques, such as flash photolysis, and site directed mutagenesis. Of particular interest has been electron transfer pathway and many studies have been carried out into the rates of electron transfer. Several point mutations in the M and L subunits of the RC have been made to study the differences that small changes in the bonding of pigments can affect the transfer pathway. Unfortunately, not all of these mutations have been studied through x-ray crystallography so how these changes in, for example rate of electron transfer from ubiquinone Q_A to Q_B, relates to a structural change is uncertain.

Such an example of detailed study is in the Reaction Centre for *Rb. sphaeroides* R26-1, a mutation where the carotenoid biosynthetic pathway has been deleted. It has been shown that this mutation is lethal to the bacteria in the presence of oxygen due to the photoprotective role the carotenoid usually plays. Many studies have been carried out on strain R26-1, including reconstitution experiments where a carotenoid purified from other strains of bacteria is inserted chemically into the RC. There have been many experiments performed on these reconstituted complexes, such as fast transient absorption, fluoresence and EPR spectroscopic studies (see Frank, 1999 for a review) which show the carotenoid carries out the same transfer processes and is in the same orientation. However, no x-ray crystallography experiments have been carried out in order to support the orientation and to determine the exact structure of the complex, with particular attention to the carotenoid. The aim of this section of the thesis is to introduce and present the structure of the Reaction Centre from a carotenoid reconstituted sample of *Rb. sphaeroides* R26-1.

RC from strain R26-1 was purified, samples were sent to collaborators in the laboratory of Prof. Frank, University of Connecticut, USA, where carotenoid was inserted into the RC. The sample was returned whereupon crystals were grown and x-ray diffraction data collected. The crystal structure was then solved by molecular replacement using a model of a high-resolution structure of a reaction centre complex from *Rb. sphaeroides* (M^{c}Auley & Fyfe, unpublished data)

5.2. Cell growth

Cells were cultured in a similar way to that described in section 2.1. with the amendments described below.

Rb. sphaeroides can be grown anaerobically under light conditions in a media using a succinate carbon source (Subir, 1963). However, since strain R26-1 contains no carotenoid, it sensitises it's own death even in the presence of small amounts of oxygen. In order to overcome this problem, fresh bottles of bacteria were grown in the dark overnight so that any oxygen present was consumed through respiration. The bottles were then placed in light conditions so that photosynthetic growth could occur. Transfer into fresh media was performed every 2-3 days and large volumes of bacteria were grown using 10litre flasks. A typical preparation involved 20 litres. The lack of carotenoid present also affects the colour of the bacteria, with the Bchl resulting in the cells appearing a bluish green (compared with reddish brown when carotenoid is present) as shown in figure 62.

Figure 62. Cells of *Rb. sphaeroides* R26-1 (on right) appear bluey-green due to the Bchl absorption. In the presence of carotenoid, (*Rb. sphaeroides* wild type on the left) these cells appear reddy-brown.

Due to the smaller number of Bchl molecules within the RC compared to that within the LH2 complex, protein concentrations, as measured by the OD, differs. In the absorption spectrum of whole cells and purified complexes, the peaks due to RC pigments are partly concealed beneath the peak from the LH1 complex occurring at approximately 865nm in this case (see figure 63). Therefore, the OD_{865} was used as a measure of concentration for

the first steps of the protocol until the solubilisation was carried out which preferentially solubilises RC, whereupon the peaks from the pigments molecules bound in the RC are visible.

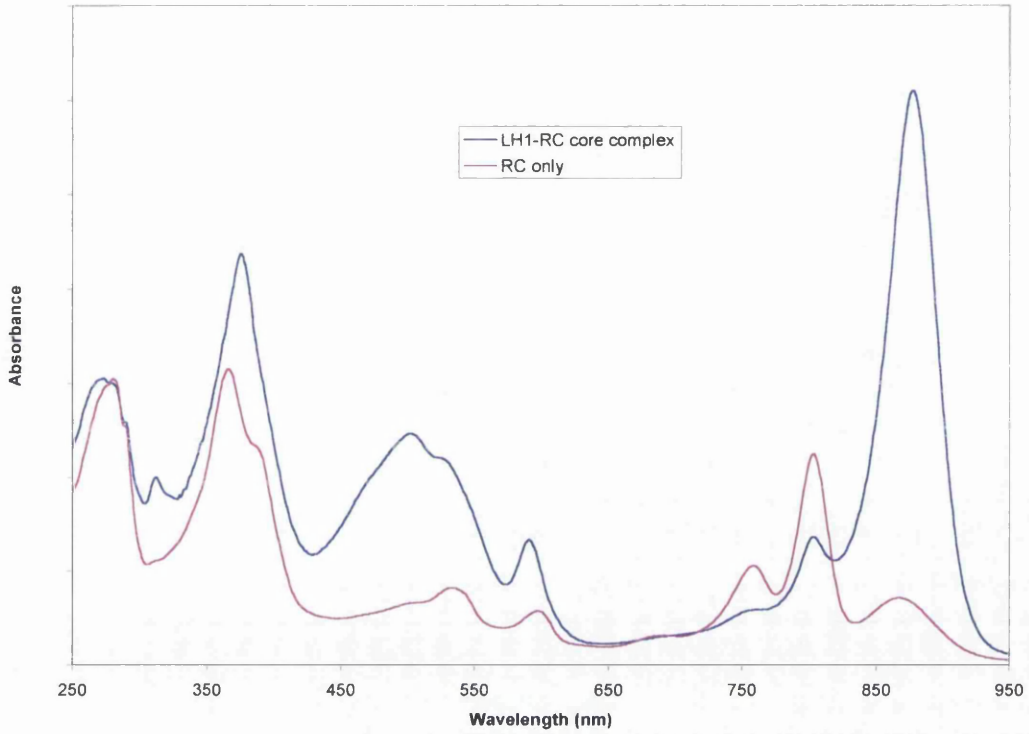

Figure 63. Absorption spectra of LH1-RC core complex from *Rps. palustris* (blue) and RC complex only (pink) from *Rb. sphaeroides* overlaid showing that only a small proportion of the absorption of the core complex is due to the RC complex.

5.3. Purification

Throughout the RC preparation, purity of the complex was measured using a ratio of peaks similar to the I_r used for determining the integrity of the LH2 complex. For the RC, the peak at 800nm was compared to the peak at 280nm. A value of $(^{280}/_{800}) \leq 1.4$ was considered pure enough for crystallisation (Fyfe, 1997).

The cell harvesting, and disrupting of the cell walls was performed as stated in section 2.2. The disrupted cells were then centrifuged for 1hour at 50,000rpm in a Beckman Ultracentrifuge which resulted in three distinct layers. The bottom layer is a very hard pellet containing the cell walls, the middle sponge-like layer contains the membranes, and the supernatant contains the water soluble elements. The supernatant was poured off and the

middle layer removed and resuspended in a minimal volume of 20mM Tris using a hand homogeniser.

To solubilise, the suspension was corrected to an OD_{865} of 50 and 0.3% LDAO was added dropwise to a stirred solution. 150mmol NaCl was also added, then the suspension incubated for 1hour at room temperature. The solution was then centrifuged again for 1hour at 50,000rpm in a Beckman Ultracentrifuge which resulted in a supernatant containing the detergent solubilised moieties, and a large sponge-like pellet containing the unsolubilised material. The absorption spectra of both the supernatant and the pellet were taken and if RC was still present in the pellet, it was resuspended and the solubilisation process repeated. It commonly took 2 or 3 solubilisations before all the RC was released from the membranes.

The supernatant was then pooled and an ammonium sulphate (AMS) precipitation performed. 30% (w/v) AMS was added gradually to the sample and stirred for 10minutes. The sample was then centrifuged in 1litre wide-necked pots at 4700xg for 10minutes which resulted in a floating pellet of RC. The supernatant was discarded and the pellet resuspended in 20mM Tris + 0.1% LDAO. This was dialysed overnight against a large volume of 20mM Tris + 0.1% LDAO to remove the AMS.

The solution was then purified using a DE52 column as described in section 2.5.1.1. The purest fractions were pooled (generally the fractions that eluted between 150mM and 200mM NaCl) and again dialysed overnight against 20mM Tris + 0.1% LDAO to remove the salt.

This crude sample of RC complex was then loaded onto a Sepharose Q (Pharmacia, Uppsala, Sweden) anion exchange column and eluted with a NaCl salt gradient. Fractions were tested for purity and those with an $^{280}/_{800}$ ratio ≤ 1.4 were pooled and concentrated using centricon concentrators. Due to the small volumes, salt could be rapidly removed by repeated addition of salt free buffer and centrifuging down to a small volume, negating the need for another dialysis step.

5.4. Reconstitution of Carotenoid

At this point, the samples were frozen and sent to collaborators in the laboratory of Prof. H. Frank, University of Connecticut where the sample was reconstituted with carotenoid (Frank, 1999). This method used is described below.

The RCs are placed in a small vial (8ml) and 1% Triton X-100 in 15mM Tris buffer, pH 8 is added to obtain a final solution of 0.67% Triton X-100. A 15-fold molar excess of the carotenoid in petroleum ether relative to Bchl is layered onto the surface of the RC solution. The petroleum ether is then evaporated with a stream of nitrogen. The resulting mixture is sonicated for 30-45 min at room temperature in the dark. The solution is then diluted 1:5 with 15mM Tris buffer, pH 8.0, and loaded onto a 1 x 8 cm DEAE Sephacel column. The RCs now containing the carotenoid, are washed using a buffer containing 15mM Tris, 0.1% Triton X-100 and 100mM NaCl at pH 8.0 to remove the excess unbound carotenoids. The purified RCs are then eluted using a buffer containing 15mM Tris, 0.1% Triton X-100 and 300mM NaCl at pH 8.0, and then dialysed overnight using Spectrapor standard cellulose dialysis tubing (25mm, M.W. cutoff 12,000-14,000 Da) against 15mM Tris buffer containing 0.03% Triton X-100, at pH 8.0. Finally, the RCs with the carotenoid incorporated are concentrated for subsequent use by centrifugation at 3,000 x g using an Amicon microconcentrator (M.W. cutoff 10,000 Da).

The carotenoid used for reconstitution was spheroidene, which is the carotenoid occurring naturally in wild type *Rb. sphaeroides.*

5.5. Further Purification

When the reconstituted RC sample was returned, it required further purification by gel filtration before crystallisation. The sample was run through an 80cm Superdex 200 (S200) column which gave a single, almost symmetrical peak. The fractions were sorted according to their $^{280}/_{800}$ ratio with fractions displaying a value less than 1.4 being pooled and concentrated for crystallisation.

5.6. Crystallisation

Crystallisation was carried out using the sitting drop method of vapour diffusion. Sodium citrate was used as precipitant, LDAO as the crystallising detergent, and heptane triol (HPT) as the amphiphilic molecule.

The RC solution was adjusted to OD_{800} of 45 using 20mM Tris + 0.1% LDAO. Enough HPT to make the final solution 3.5% (w/v) was weighed into an eppendorf tube, RC solution was added and the solution vortexed. If required, 4% (v/v) ethylene glycol was

added and the solution again vortexed. The addition of this small amount of cryo-protectant is proposed to ease the further addition of ethylene glycol to act as cryo-protectant once the crystals are grown. Several other cryo-protectants were investigated so the addition of ethylene glycol was not always required. Na citrate was then added from 1.7M stock solution to make the solution 0.35-0.5M and then vortexed. The eppendorf was spun in a microcentrifuge at 13,000rpm for 5 minutes at 4°C. Whilst this was spinning, 1ml Na citrate at a concentration of 1.1-1.6M was added to the wells of the crystal trays. 15µl of the RC solution was then added to the bridge, the wells sealed and the trays incubated at 18°C.

Crystals appeared after 3 days and grew up to 0.3 x 0.3 x 0.8 mm after approximately 1 week (see figure 64 for crystallisation conditions, and figure 65 for photos of RC crystals). It had been previously found that larger crystals of RC complexes do not react well when cryocooled (P. Fyfe, pers. comm.), and this corresponds to other work suggesting that crystals will not react well to cryocooling when they have a $^{(\text{surface area})}/_{(\text{volume})}$ value of greater than 12 mm^{-1} (Garman and Schneider, 1997).

Drop Solution	Values used (without cryoprotectant)	Values used (with cryoprotectant)
Initial complex OD_{800}	45	45
Amphiphile	3.5% HPT	3.5% HPT
Na citrate	0.35M, 0.4M, 0.45M, 0.5M	0.4M, 0.45M, 0.5M
Ethylene glycol	-	4%
Drop size	15µl	15µl
Incubator temperature	18°C	18°C
Well Solution	1.1M, 1.15M, 1.2M	1.4M, 1.5M, 1.6M

Figure 64. Crystallisation conditions used for purified RC from *Rb. sphaeroides* R26-1. Work had previously been carried out on the crystallisation of this RC, and therefore the starting crystallisation conditions were known (K. M°Kendrick, pers. comm.).

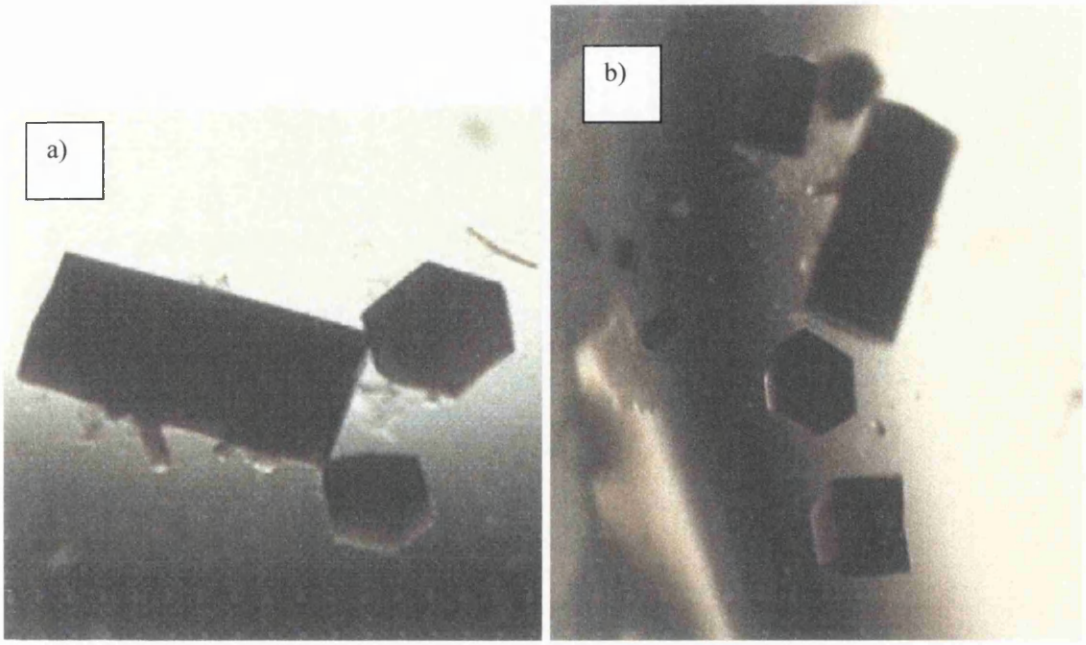

Figure 65a) and b). Photos of RC crystals. The longer dimension of the crystals can clearly be seen in both photographs, as can the hexagonal cross section of the crystal.

5.7.Crystal Handling

5.7.1. Artificial Mother Liquor

As with crystals of the LH3 complexes, AML was required in order to keep crystal drops hydrated when opened to manipulate the crystals, and contained the following:

3.5% (w/v) HPT

0.06% (v/v) LDAO

15mM Tris

Na citrate at the concentration of the well solution.

It should be noted that for the higher concentrations of Na citrate, some HPT was insoluble, even when heated.

5.7.2. Cryo-protectant

Cryoprotection has long been a problem with the cryocooling of RC crystals which results in greatly increased mosaic spread (P. Fyfe, pers. comm.). Several cryoprotectants were investigated during this study.

Ethylene glycol has been frequently used in the past and a small amount (4%) was added to some protein drops to facilitate further addition. In order to increase the concentration of ethylene glycol in the crystals to provide cryoprotection (about 25 % is required), several solutions of increasing ethylene glycol concentration were prepared. 5, 10, 15, 20, 25, and 30% of ethylene glycol was added to 1.7M Na citrate solution and 0.06% LDAO added. Several methods of introducing the cryo-protectant were investigated.

Small volumes (2μl) of solution containing 30% ethylene glycol were added to the crystal drop and a similar amount of mother liquor extracted. This was repeated several times until most mother liquor had been replaced by cryo-protectant. The crystals were then looped from the drop and flash frozen. This method of repeated addition and extraction was also used with solutions of increasing cp concentration (from 5-30%) until the drop contained 30% ethylene glycol. This was performed in order to decrease the concentration gradient the crystal was being subjected to.

Crystals were also looped from the drop and soaked sequentially in 5-30% cp solutions. Soaking times varied from less than 1 second required to draw the crystal through the drop to more 2 minutes. Soaking the crystals straight into 30% solution was also investigated although this did not give good results.

It was found that the best results were obtained from crystals drawn rapidly through several solutions containing increasing concentrations of ethylene glycol. Typical test exposures of 20 minutes from the Nonius DIP 2020 system resulted in diffraction to ~5Å.

The crystals were grown in high salt concentrations, with the final concentration of Na cit in the drop being 1.1-1.2 M in the case of crystals grown without cryoprotectant. The use of high salt concentration as a cryoprotectant was therefore investigated. Sodium formate and sodium acetate were used as the small ions are capable of easily diffusing through the solvent channels. The cryoprotectants also contained 0.06% LDAO and 3.5% HPT.

It was found that 5M Na formate was sufficient to provide cryoprotection, with a saturated solution being approximately 8M. Soaking experiments involving changing the

time and concentration of cryoprotectant soaks similar to those used for ethylene glycol were carried out. It was discovered that a rapid transfer to a high concentration of Na formate (5-8M) for a short time (10-20seconds) gave higher resolution diffraction than long soaks or sequential additions of increasing concentrations of cryoprotectant. However, there was limited diffraction observed beyond ~5Å.

Na acetate acts as a cryoprotectant at concentrations above 2.5M and is saturated at approximately 4M. A short soak of the crystals (10-20 seconds) in 3M Na acetate was found to give the best diffraction with resolution extending to approximately 3.0Å.

5.8.Data Collection

Three datasets were collected from crystals of RC containing reconstituted carotenoid.

The first was collected by K. McKendrick at beamline ID14-3 at the ESRF in Grenoble (Dataset 1). This dataset contained two sets of 60 frames in 0.5° oscillations from a single crystal and was measured at 100K using ethylene glycol as the cryoprotectant. The two sets of frames were collected such that the crystal orientation was maintained and data was collected from 28-2.8Å (see figure 66). Upon processing, it was seen that there were many overloaded reflections resulting in incomplete data, especially in the highest resolution shells (28 – 7Å), see section 5.8 and figure 67. Much phase information is derived from the lower resolution data that was missing in this case. In an attempt to overcome this difficulty, further datasets were collected, with particular attention paid to the low-resolution data.

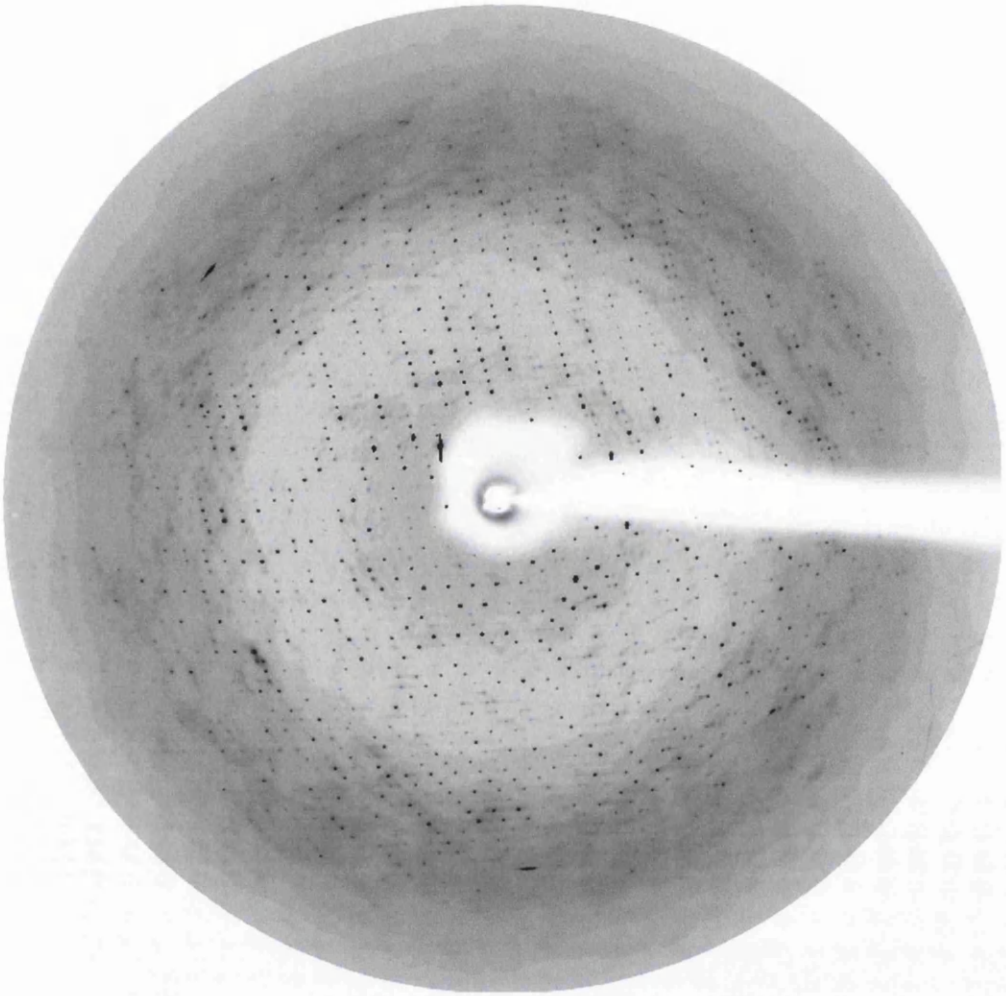

Figure 66. Typical diffraction pattern from a RC crystal, dataset 1. Recorded at station 14-1, ESRF, Grenoble on a Mar 345 image plate. The resolution at the edge of the diffraction is 2.8Å, the lowest resolution is 28Å.

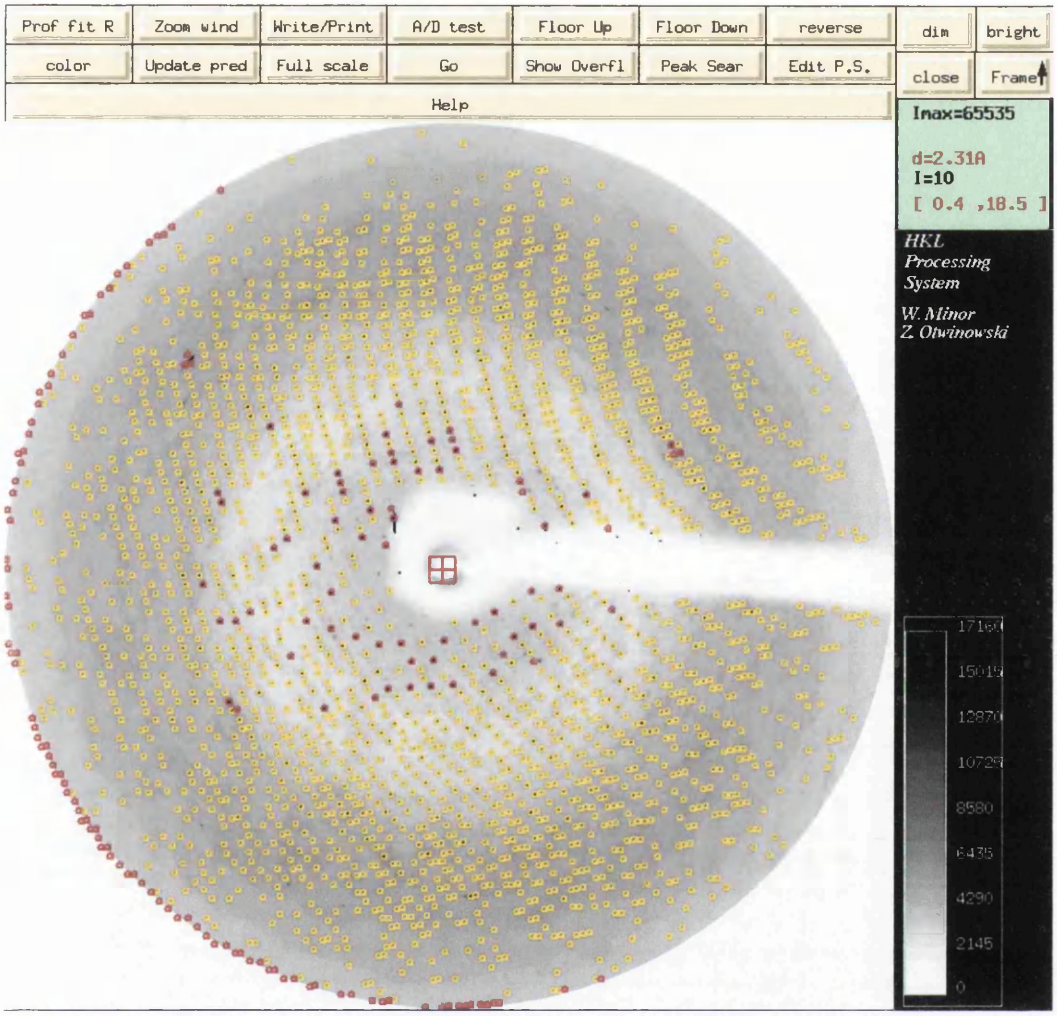

Figure 67. The same image as shown in figure 68, after processing. Reflections used in the processing are surrounded by a yellow square (representing partial reflections). The reflections surrounded by a red square are not used in the processing- those on the outside of the image due to being on the edge of the image plate, and those in the centre, mostly due to overloaded reflections where the image plate is saturated. Data was processed using Denzo and displayed using Xdisp (Otwinowski and Minor 1997)

The second dataset was collected on beamline ID 14-2 at the ESRF in Grenoble from a single crystal measuring approximately 0.1 x 0.1 x 0.2mm (Dataset 2). The crystal was soaked in 3M Na acetate for approximately 20 seconds prior to flash freezing in the cryostream at 100K. 233 images with 0.5° oscillations were collected with diffraction apparently extending to 3.0-3.4Å. Data was collected over a resolution of 31-2.1Å (see figure 68).

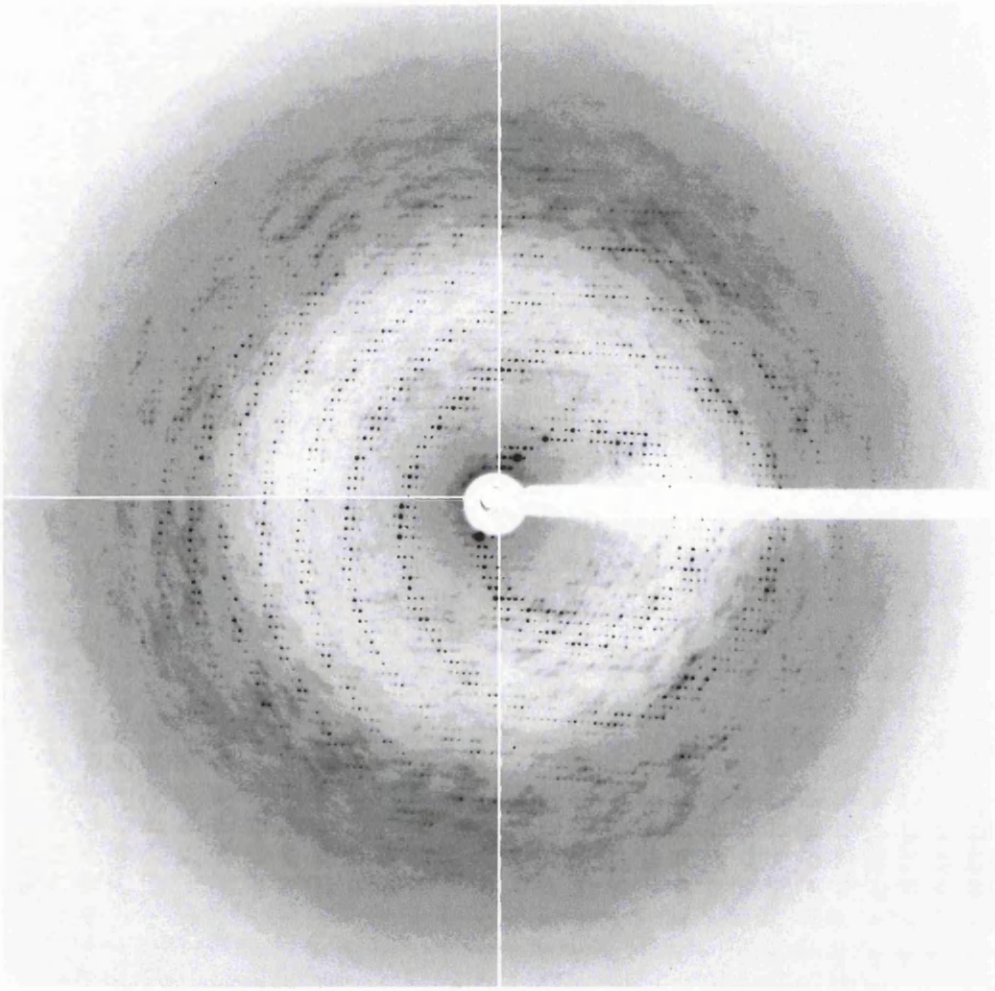

Figure 68. Typical diffraction pattern from dataset 2. Data collected on station 14-2, ESRF, Grenoble. Na citrate was used as cryoprotectant, the dataset was recorded at 100K. 10 second exposures were used, with an oscillation of 0.5°, data was collected on ADSC Quantum-4R CCD detector. The resolution at the edge is 2.1Å and the lowest resolution observed is 31Å

A third dataset was collected using the in house rotating anode x-ray source and the DIP 2020 image plate (Dataset 3). This was collected using a single crystal approximately 0.2 x 0.2 x 0.7 mm, capillary mounted at room temperature with oscillations of 0.5° (see figure 69). The beam size of 0.2 x 0.2 mm meant that once diffraction became poorer due to radiation damage, the crystal could be translated along it length twice to expose a fresh area to the beam. The crystal was aligned perpendicular to it's longest axis with respect to the beam so subsequent positions would maintain the crystal orientation.

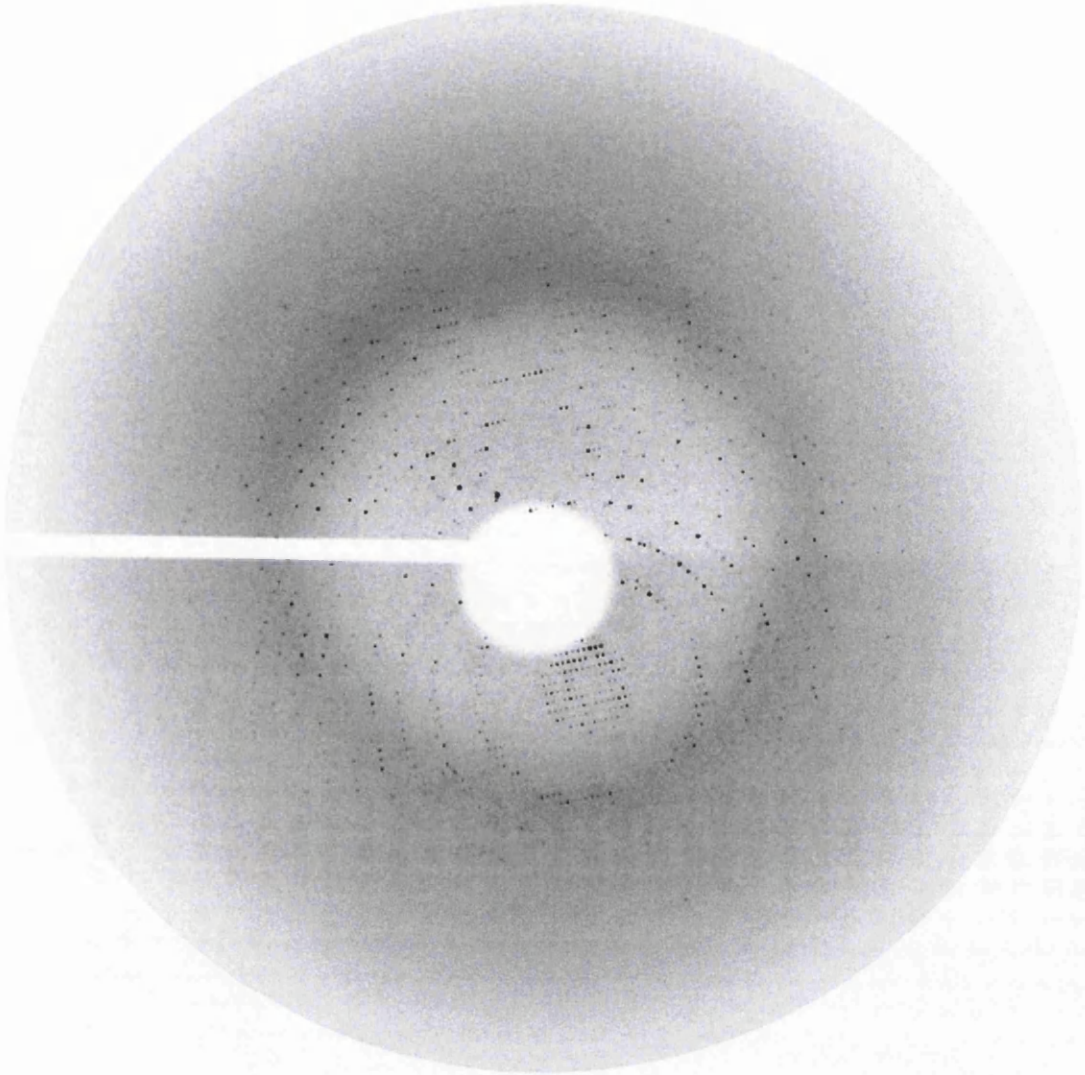

Figure 69. Typical diffraction pattern from dataset 3. Data collected at room temperature on the home source using the DIP2000 image plate. 30 minute exposures were used, with an oscillation of 0.5°. The edge of the image plate is at 2.4Å, with the lowest resolution being 30Å.

5.9. Data Processing

Data processing and all further computational work was carried out using programmes from the Collaborative Computational Project Number 4 (Bailey,1994) unless otherwise referenced.

Dataset 1 was processed using Denzo (Otwinowski and Minor, 1997), and the resulting xfiles were scaled using Scalepack. The data extended from 30.0Å to 2.8Å and overall completeness was 89.0% (91.4% in the highest resolution shell 2.85-2.80Å).

However, the lowest resolution shell (30.00-7.56Å) was only 51.6% complete and the next shell (7.56-6.02Å) only 86.1% complete. This was due to many overloaded reflections due to a high dosage of x-rays. The x-ray dose delivered to the crystal was increased so that diffraction data could be observed to as low resolution as possible, however, the strongest spots (those of low resolution) also increase in intensity, resulting in these overloaded reflections. See figure 69 for a typical RC diffraction pattern with the processed reflections overlaid. Figure 72 lists some data processing statistics from this dataset.

Truncate was then used which produces a .mtz file as used by CCP4 programs from the .sca file produced by SCALEPACK (Otwinowski and Minor, 1997). Data reduction was carried out to convert the experimental intensities (I) into structure factors (F).

5.10. Molecular Replacement

There are many high resolution structures available for RC complexes from *Rb. sphaeroides*, therefore molecular replacement was the obvious choice for deriving phase information. However, since the structures are so similar, an initial attempt was made to fit the coordinates of the search model, a high resolution structure of a wild-type reaction centre, straight into the unit cell of the experimental data using rigid body refinement. In order to minimise any bias towards the model structure, the carotenoid coordinates were removed from the pdb file before using these coordinates. The entire search model was used as a rigid body, but when this failed to provide a solution, the individual parts (polypeptides and cofactors) were used as separate rigid bodies. However, this also failed to provide a solution so molecular replacement using AMoRe (Navaza and Saludjian, 1997)was carried out.

Mtzdump was used to put the information into ascii format required by AMoRe, and AMoRe provided rotation and translation function. Only one rotation function was highlighted, and one translation function stood out above the rest. The solution was fitted and gave a correlation-factor of 66.3% and R-factor of 36.0%. The next best solution had correlation-factor and R-free values of 40.8% and 46.8% respectively.

A subset of 5% of the structure factors were removed as the R_{free} set in order to provide an impartial correlation between the model and the data during refinement. The R-free set used was the same as that for the search model in order to provide as impartial an R-factor as possible. If a new R-free set had been chosen, some reflections would not have

been in the R-free set when refining the search model, and therefore the R-free set would not truly represent unrefined data.

5.11. Refinement and Model Building

Rigid body refinement was performed on the solution from AmoRe using REFMAC version4 (Murshudov et al., 1997). After each round of refinement which contained 7 cycles of normal refinement followed by one cycle of rigid body refinement, the point which gave the best fitting model, as judged by the R-factor and R_{free} values was selected.

Modelling was then carried out in QUANTA (Accelerys, USA) using $f_o - f_c$ and $2\ f_o - f_c$ electron density maps. The 2fo-fc map was contoured in different colours at 1σ and 2σ. The difference map (fo-fc) is used to show areas where there is too high or too low an area of electron density modelled in the coordinate file, and was contoured at $+2\sigma$ and -3.5σ. The position of each residue was inspected in QUANTA for good fit into the electron density map and any amendments that better fitted the model to the electron density were made. The output was written as a new pdb file, which was then used as the input for subsequent rounds of refinement.

As the search model (the high resolution Reaction Centre structure used in molecular replacement) contained a carotenoid molecule, there was the possibility of model bias, whereby the new calculated electron density maps contain a "ghost" carotenoid. In order to minimise this model bias, the first rounds of refinement were carried out without the carotenoid present. Only when it was obvious there was enough electron density (in both the $2f_o - f_c$ and the positive $f_o - f_c$ maps) to support the carotenoid, was spheroidene inserted into the coordinate file. Several further rounds of refinement and model building were then carried out to most accurately place the carotenoid.

Final refinement statistics were as follows:

R-factor = 22.2%

R_{free} = 29.0%

Bond length RMS deviation = 0.028Å

Bond angle RMS deviation = 5.618°

As can be seen, the geometries of the model were poor, and after inspection of the Ramachandran Plot it was found that 3 residues lay in the disallowed regions and 17 in the generously allowed regions (see figure 70). It was also noted that the highest R-factors were from the low resolution shells (30-7Å), therefore constraints on geometry had to be tightened and it was decided to collect other datasets in order to merge the low resolution data and calculate a better model.

However, when subsequent processing and scaling failed to merge Dataset 1 with either dataset 2 or 3 (see section 5.11.), it was decided to look again at dataset 1 using Refmac version 5 which was not available at the time of initial refinement.

TLS refinement was used to further improve the model. Refinement was carried out using 5 cycles of TLS refinement, using each protein chain and pigment molecule as a separate entity for refinement. This was followed by 20 cycles of normal refinement with a low diagonal weighting factor (0.08). At this value, reasonably tight constraints are placed on the geometry of the model calculated and this was used in order to improve the poor bond lengths and angles. At this resolution, it was found that the electron density does not support accurate placing of all side chains, although it does support the placing of them, so standard geometries were used. The geometries of the residues were improved, as can be seen in the Ramachandran plot in figure 71.

The final model (which is discussed in section 5.12) containing the carotenoid had the following statistics:

R-factor = 19.1 %

R_{free} = 23.6 %.

Bond length RMS deviation = 0.019Å

Bond angle RMS deviation = 1.993°

Chiral bond angle RMS deviation = 0.106°

Overall FOM = 0.8349

Overall correlation coefficient = 0.9450

(free correlation coefficient) = 0.9181

Cruickshank's DPI for co-ordinate error =0.4

Ramachandran Plot

frank_ref6tls

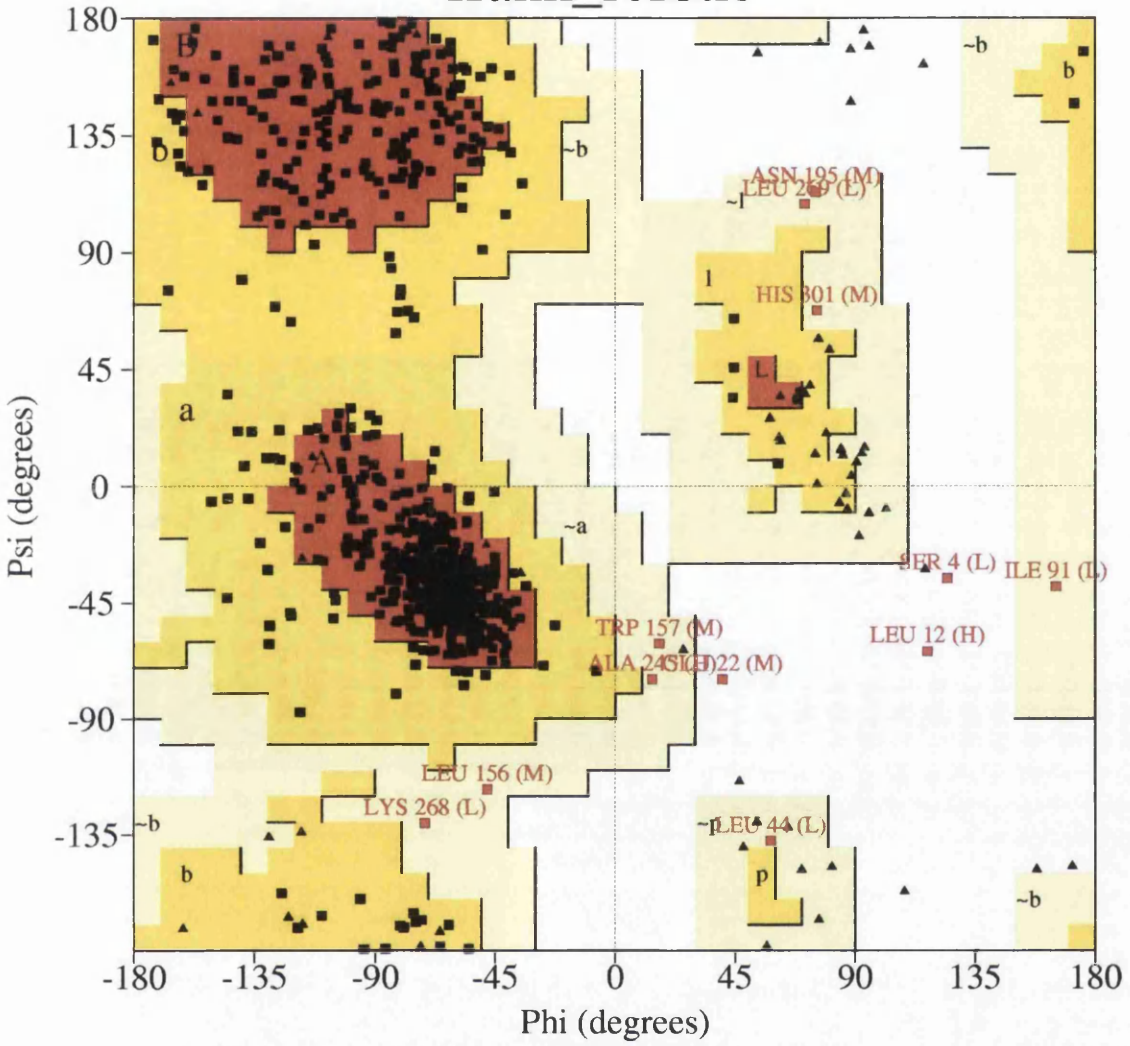

Plot statistics

Residues in most favoured regions [A,B,L]	569	83.7%
Residues in additional allowed regions [a,b,l,p]	99	14.6%
Residues in generously allowed regions [~a,~b,~l,~p]	9	1.3%
Residues in disallowed regions	3	0.4%
Number of non-glycine and non-proline residues	680	100.0%
Number of end-residues (excl. Gly and Pro)	193	
Number of glycine residues (shown as triangles)	91	
Number of proline residues	48	
Total number of residues	1012	

Figure 70. Ramachandran plot of initially refined RC coordinates from dataset 1. As can be seen, the geometry of several residues is rather bad despite tight geometrical constraints.

PROCHECK

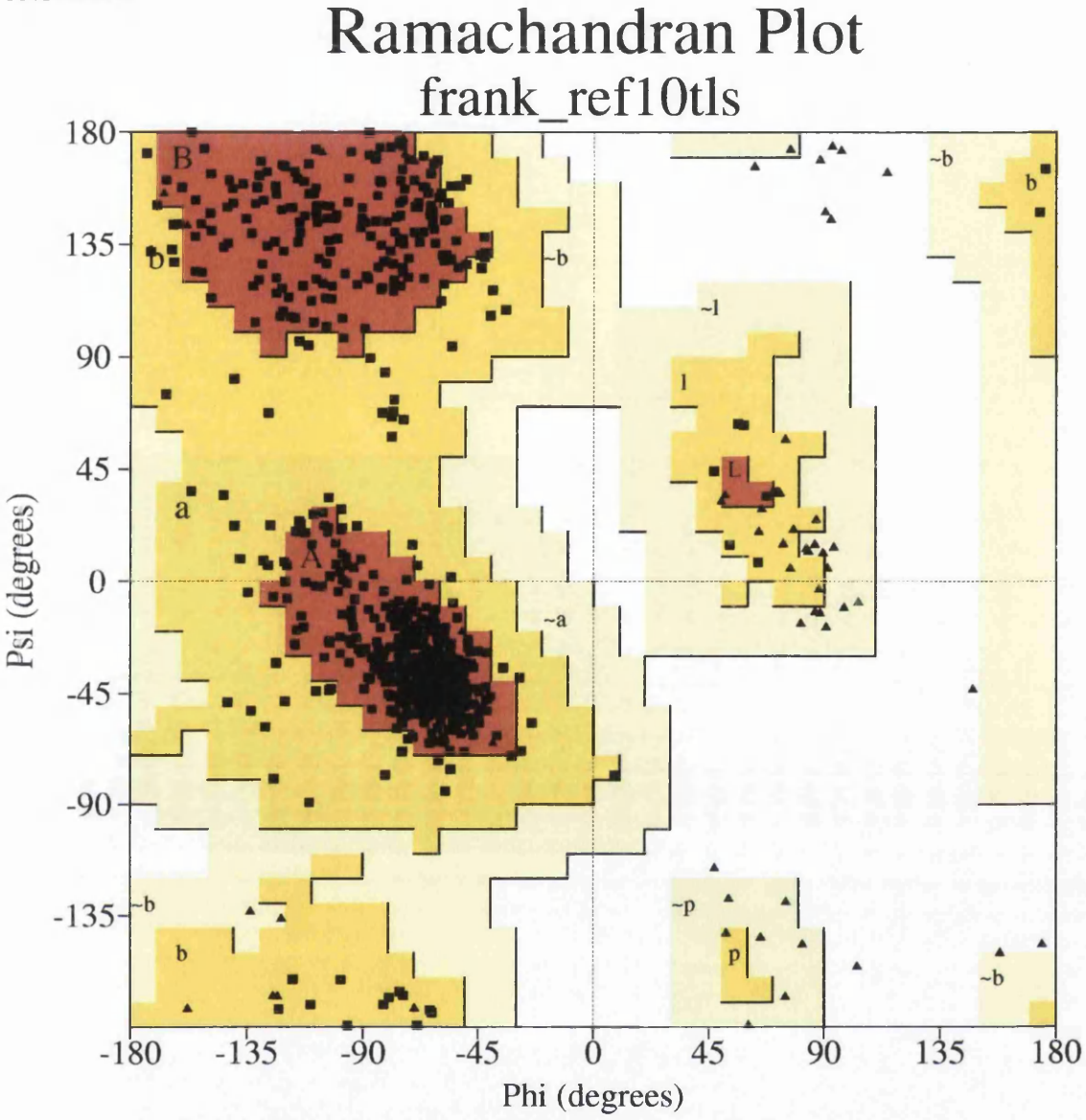

Plot statistics

Residues in most favoured regions [A,B,L]	589	86.6%
Residues in additional allowed regions [a,b,l,p]	91	13.4%
Residues in generously allowed regions [~a,~b,~l,~p]	0	0.0%
Residues in disallowed regions	0	0.0%
	----	------
Number of non-glycine and non-proline residues	680	100.0%
Number of end-residues (excl. Gly and Pro)	189	
Number of glycine residues (shown as triangles)	91	
Number of proline residues	48	

Total number of residues	1008	

Figure 71. Ramachandran plot of refined RC final coordinates from dataset 1. As can be seen, the geometries of the residues is generally good with 86.6% within the most favoured regions.

5.12. Dataset 2 and Dataset 3

When dataset 2, containing 233 images of 0.5° oscillations, was processed using DENZO, it was found to have the same space group of $P3_121$ with a similar unit cell. The resulting xfiles were scaled using SCALEPACK. Figure 69 shows a diffraction image from dataset 2. The data extended from 35-2.9Å with an overall completeness of 99.2% (91.8% in the outer shell of 2.95-2.90Å). Listed below are some of the data processing statistics.

Redundancy = 7.2

Space group $P3_121$

Unit Cell: a = 139.53 b = 139.53 c = 185.91

$\alpha = \beta = 90^\circ$ $\gamma = 120^\circ$

$chi^2 = 0.995$

linear R-factor (R-merge) 8.2%

Mosaicity 0.8°

As dataset 2 appeared to contain useful data and had scaled well, SCALEPACK was used to scale the .sca files (SCALEPACK output) from dataset 1 and dataset 2. However, the datasets did not scale well with overall R-merge = 18.7% and $chi^2 = 37.2$. All the indexing matrices for this space group were used in an attempt to scale the datasets more succesfully, but all failed.

An alternative method is to scale the original .x files together and SCALEPACK was again used to scale the .x files from dataset 1 and dataset 2. This was unsuccessful, with scaling statistics of $chi^2 = 117$ and R-merge of 52.1%, with values being especially poor at the highest resolution.

Dataset 2 was not strong in the 4.0-2.9Å range so the dataset was reprocessed using the resolution limits 35-4.0Å and scaling again attempted. However, this was also unsuccessful, with scaling statistics of $chi^2 = 2.15$ and R-merge of 13.7%

As the two datasets could not be scaled properly, the reciprocal lattice was examined using hklplot. It was thought that there might have been a major indexing problem between the two datasets such as a wrongly positioned beam centre in one of the datasets. This was investigated as it can result in the mis-indexing of data, but the beam position was found to be correct after the successful scaling of another dataset collected at the same beam at the same time. No shift could be identified that would align the two datasets and further scaling attempts were abandoned.

Dataset 3 consisted of three sets of 30 frames, each with a 0.5° oscillation. The resolution extended from 30Å to 3.5Å. After processing the first frames, work was transferred back to dataset 1 using Refmac 5, and no further work was carried out on dataset 3. It may be interesting to look back at dataset 3 to find out if it can be scaled successfully, and if so, what effect it has on the subsequent refinement.

5.13. Overall Assembly

The overall assembly of the RC complex from the reconstituted R26-1 is nearly identical to that of the wild type RC from *Rb. sphaeroides* (see figure 72).

It has been shown that RC from R26-1 with no carotenoid present has slight structural differences in the carotenoid area when compared with the wild type structure. As well as there being no electron density in the crystal structure for the carotenoid, the M162 residue rotates into the space usually occupied by the carotenoid (A. Rosak, pers. comm.).

5.13.1. Co-factors

The majority of the co-factors within the RC structure for the reconstituted R26-1 adopt near identical positions when compared to the WT structure. The special pair of Bchl *a* molecules can be seen in the same positions, as can the accessory Bchl and Bphe molecules. It should be noted that the Bchl molecules are ligated through the central magnesium atom, with all ligating amino acid residues adopting similar distances in both structures. The distances between the pigment molecules and the closest residues are given in figure 73. Figure 74 shows Bchl 303 binding to the histidine at position 202 of the M subunit.

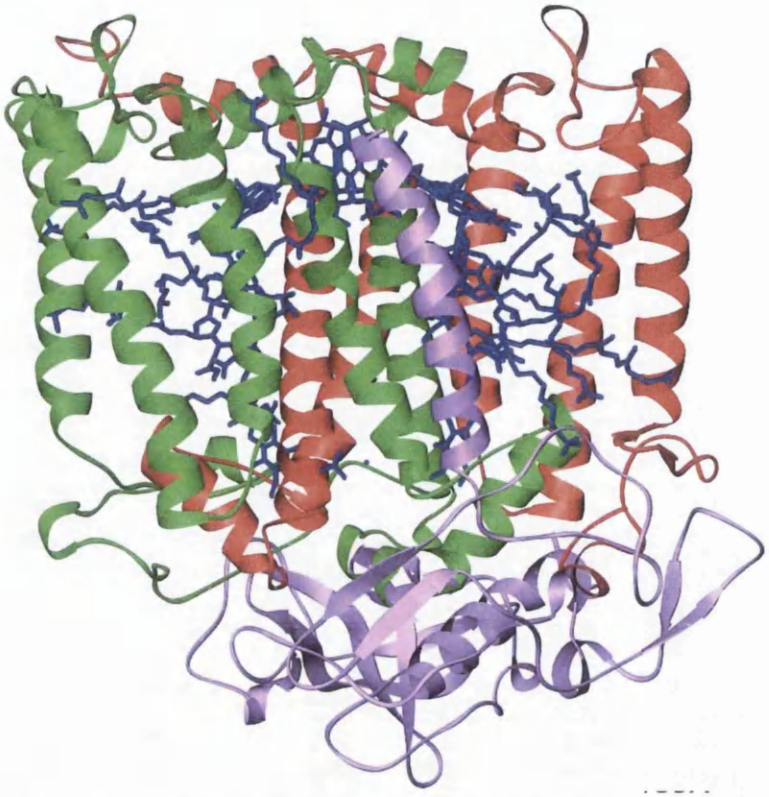

Figure 72. Structure of RC from *Rhodobacter sphaeroides* R26-1. The L, M, and H protein subunits are shown in red, green and purple respectively and the pigment molecules in blue. The figure was produced using Ribbons3 (Carson, 1997).

Pigment molecule	Closest residue(s)	Distance (Å)	Comparative distance in MR model (Å)
Bchl 301	M 182 His	2.09	2.22
Bchl 302	L 173 His	1.91	2.22
Bchl 303	M 202 His	2.37	2.25
Bchl 304	L 153 His	2.47	2.42
Bphe 401	M 150 Phe	2.99	-
	M 129 Trp	2.90	-
	B 301 tail	3.17 at closest	-
Bphe 402	L 104 Glu	2.78	-
	L 121 Phe	3.36	-
	B 302 tail	3.18 at closest	-

Figure 73. Table showing closest distances from the pigment molecules to amino acid residues, and similar distances to the same residues in the search model.

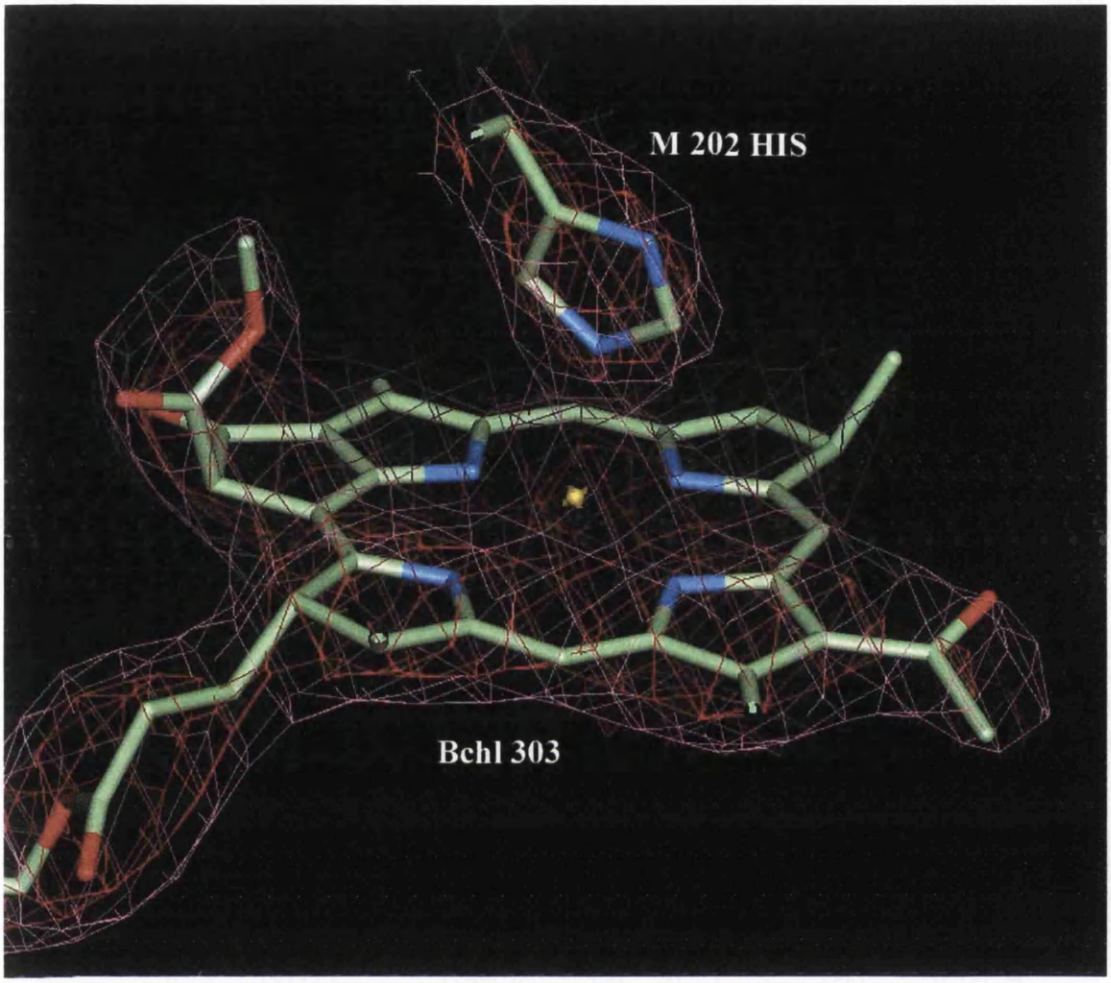

Figure 74. The Bchl *a* molecules are liganded through the central magnesium atom to histidine residues. In this case the Bchl 303 magnesium is 2.4Å from the histidine at position 202 on the M subunit. The electron density is contoured at 1.5σ (pink) and 3σ (orange). Other areas of electron density and other side chains have been removed for clarity. Figures 76-82 are drawn using Quanta (Accelerys, USA).

The Fe^{2+} is also in almost exactly the same position in the two structures and is ligated to the same residues as seen in figure 75

Distances from Fe^{2+} to closest residues:

L230 His	2.27Å
M 219 His	2.07Å
M234 Glu	2.23Å & 1.83Å
M 266 His	2.08Å
L 190 His	2.06Å

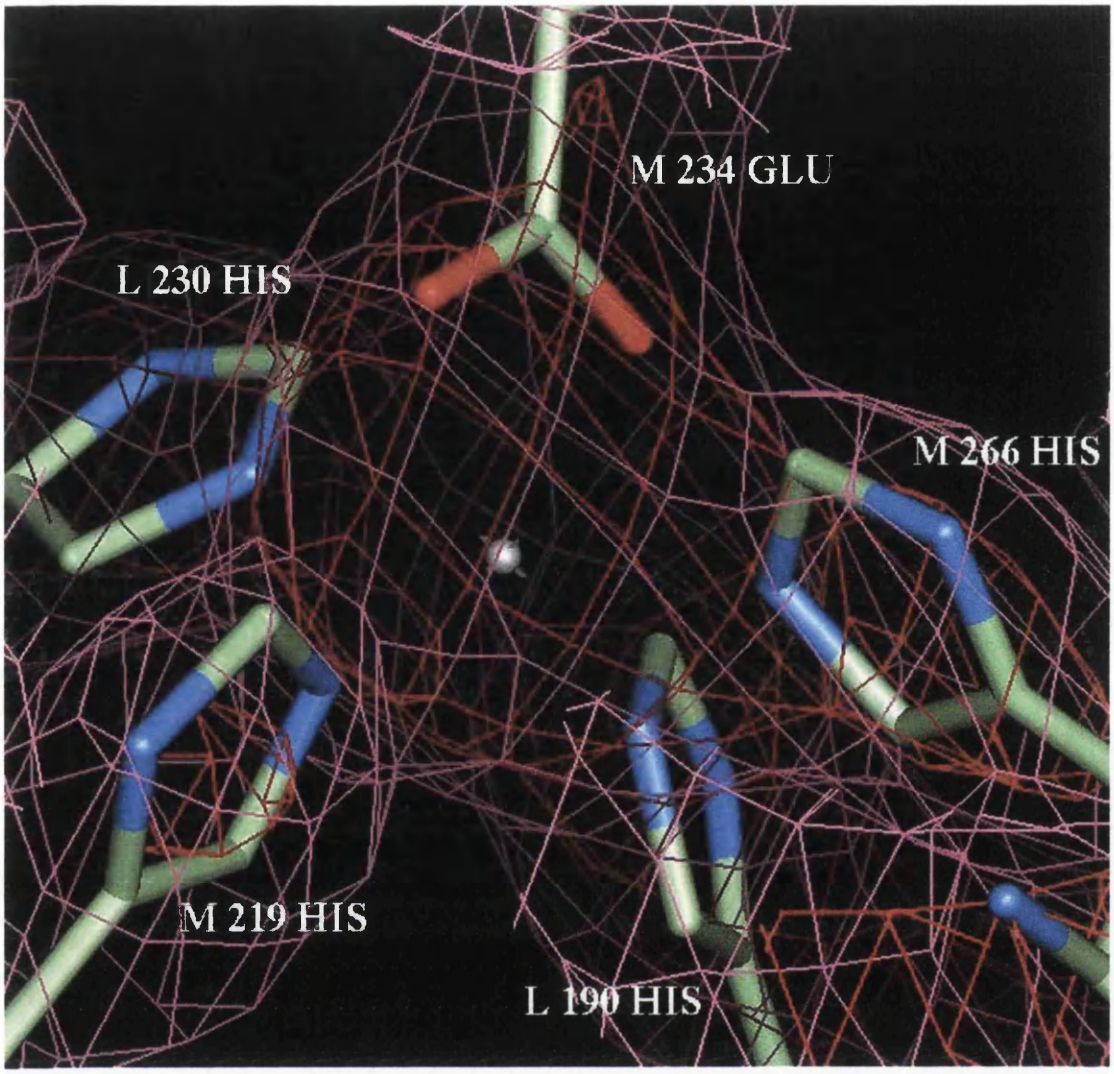

Figure 75. The non-haem iron (grey sphere in the centre) is coordinated through five ligands. Closest distances are as follows: L190His 2.06Å, M219 2.07Å, L230His 2.28Å, M234Glu 2.23Å and M266His 2.08Å. The electron density is contoured at 1.5σ (pink) and 4σ (red).

In several RC structures, a cardiolipin molecule has been found occupying a groove along the surface of the L subunit. It was first seen in the 2.7Å structure of a mutant, AM260W (McAuley et al., 1999), and upon re-inspection of several other structures, there has been found density for at least part of this lipid. As cardiolipin is not used in the preparation, it must remain bound to the complex from the membrane. Whether it has any function is, as yet, uncertain, but its common appearance is interesting. Upon inspection of the area in which cardiolipin is usually found, there was to be insufficient density to support the placing of this molecule. However, there was a strong area of density noted where the head group of the lipid is situated and several area of density in the area where the tails of the lipid would be expected. The density at the head group was initially modelled as a

chloride ion but after several rounds of refinement, a phosphate group was found to fit the density better. The cardiolipin molecule has a phosphate head group, and this molecule fits the density well, making hydrogen bonds to 2 other residues (see figure 76).

Distances from phoshate group to closest residues:

M 145 His 2.620Å

M 267 Arg 2.752Å

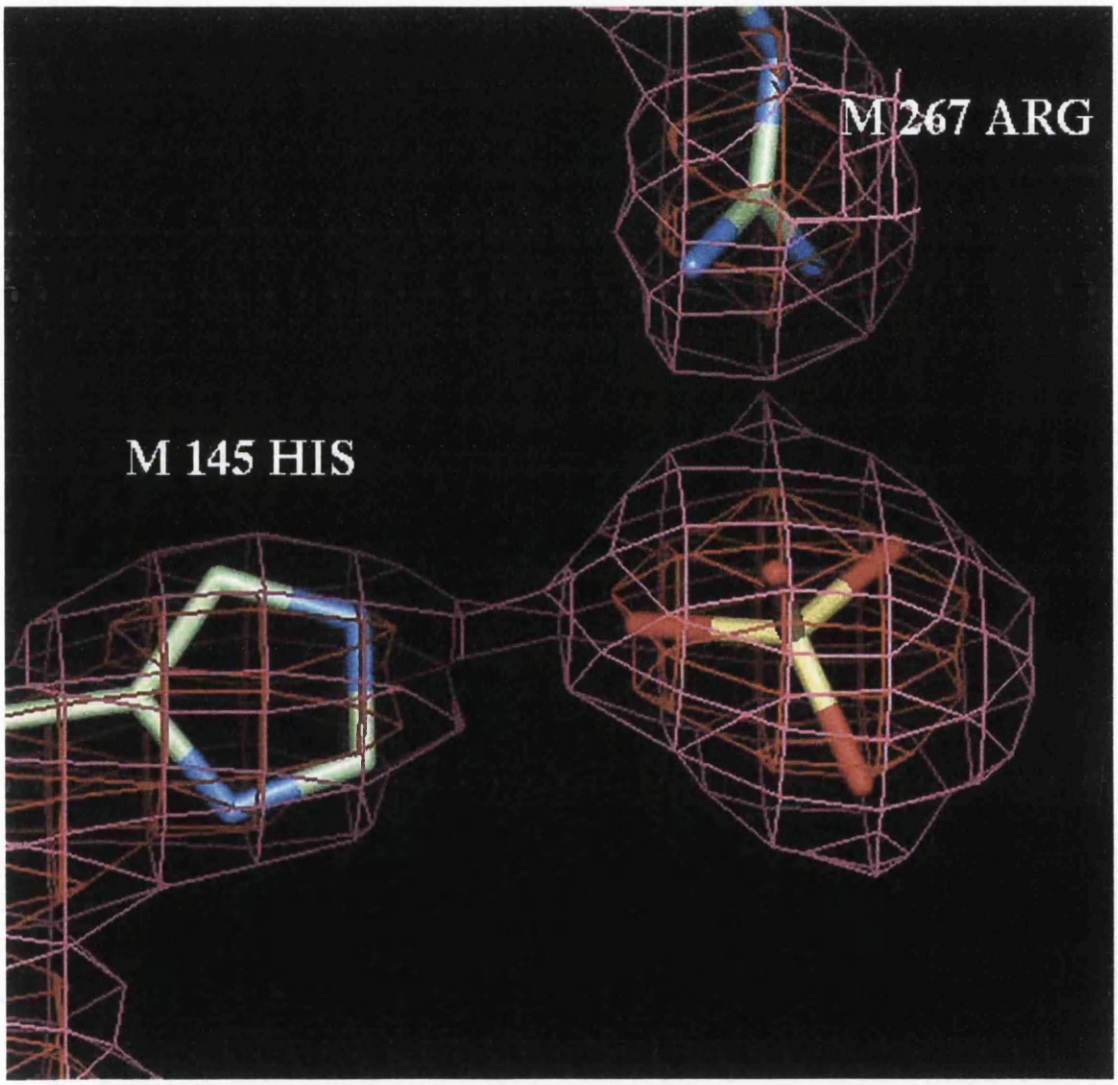

Figure 76. Phosphate group in the position where the head group of the cardiolipin would be. Strong density supports the placing of this phosphate. The group was rotated such that an oxygen was in close contact to both M145His and M267Arg, however, in subsequent refinement, the phosphate returned to the position in which it is seen here. It is 2.62Å from M145His and 2.75Å to the closest N on M267Arg. The electron density is contoured at 1.5σ (pink) and 3.0σ (orange).

There were 104 water molecules placed in the structure with nearly all of these being around the areas that would be exposed on either the periplasmic or cytoplasmic side of the membrane. Only where there were good hydrogen bond contacts were waters inserted.

Six LDAO detergent molecules were also placed in the structure (see figure 77), being found in approximately the same position to those in other structures. They are located only in the membrane bound section of the RC as would be expected.

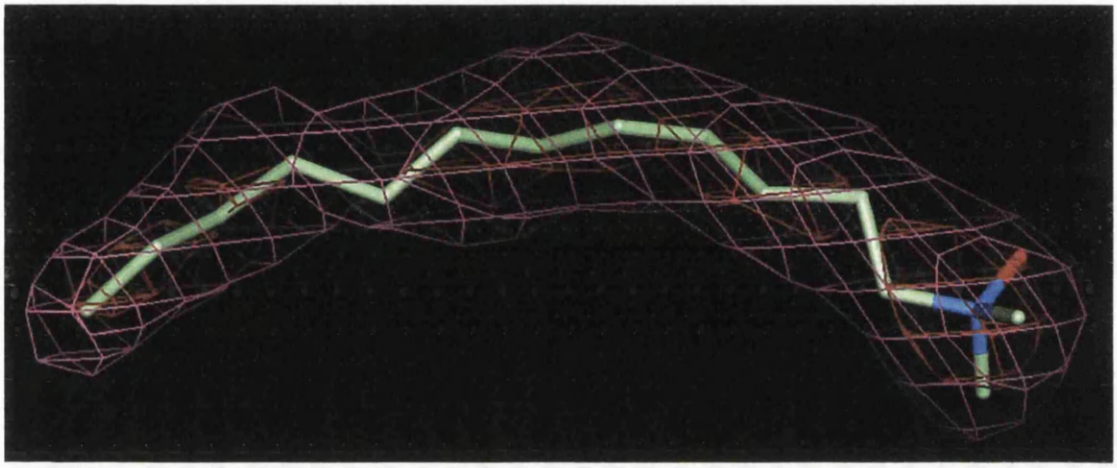

Figure 77. LDAO detergent molecule modelled into electron density contoured at 1.5σ (pink) and 2.5σ (orange).

5.13.1.1. Ubiquinone

The ubiquinone on the active chain, Q_A, is found in the same position in most RC structures, as it is in this structure (see figure 78).

Distances from U501 (Q_A) to closest residues (numbering used is the same as in the co-ordinate (pdb) file):

Q_A ring	M 252 Trp ring	3.19Å
O2	M 219 His	2.72Å
O5	M 260 Ala (backbone N)	2.78Å
C4M	M 260 Ala (backbone O)	2.99Å (although this is out of the plane)

The Q_B ubiquinone adopts a different conformation when it becomes charged, undergoing a 180° propeller twist around the isoprene chain (Stowell et al., 1997). When it has a double charge, it diffuses from the complex, into the membrane to be replaced with another ubiquinone. This results is large amounts of disorder of the U_B molecule in the crystal structure.

Several rounds of refinement were carried out with no ubiquinone in the Q_B position in order to remove any model bias from the wild type structure, however, electron density continued to show the presence of the ubiquinone. There were two possible positions to place the head group, but after modelling and refinement, one was ruled out.

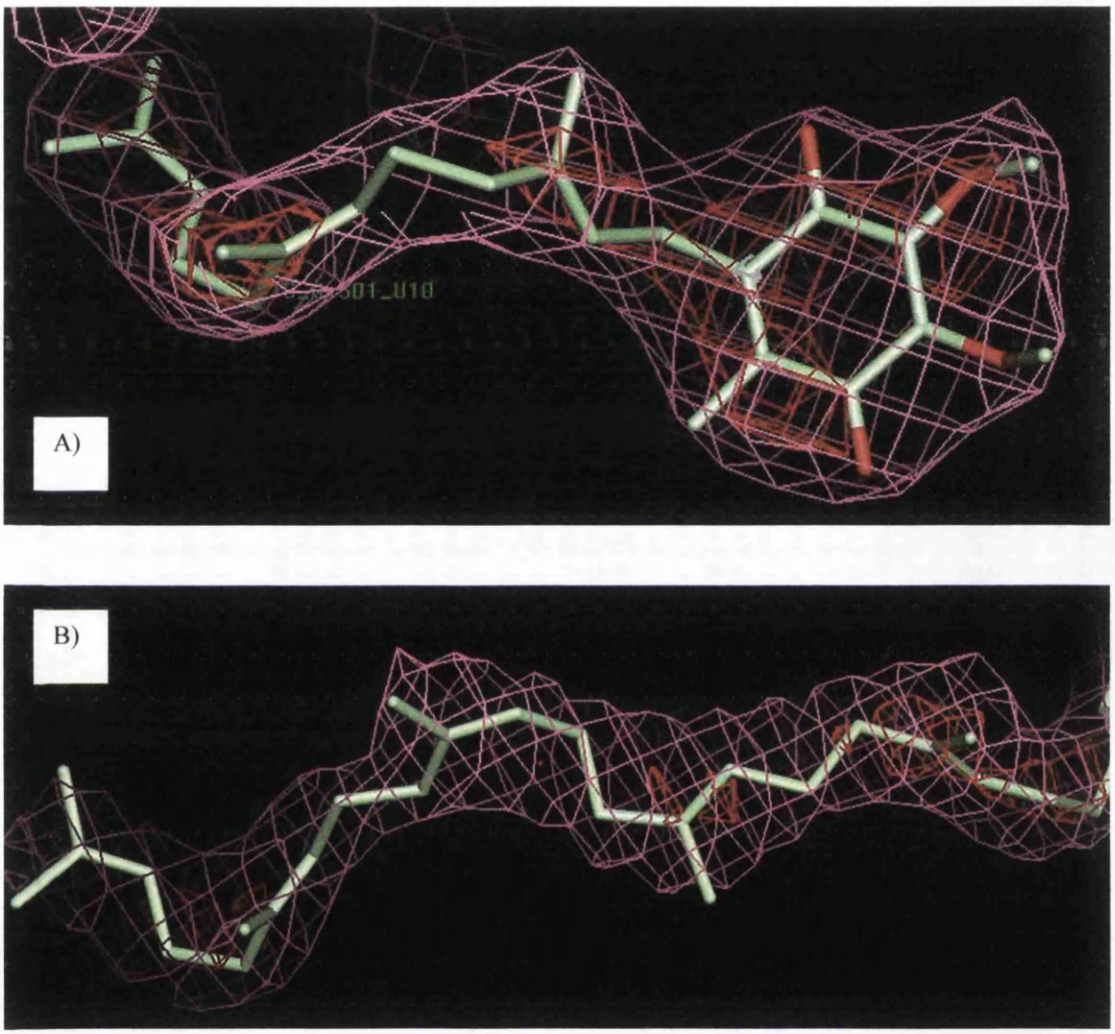

Figure 80. Electron density for ubiquinone, Q_A. This ubiquinone molecule is seen in the same position throughout RC structures A) The head group up to C16 is shown (at C16, the tail projects away from the reader and it was easiest to show the molecule in two parts). The position of the head group was well resolved. Electron density is contoured at 1.5σ (pink) and 3.5σ (red). B) The tail of the ubiquinone (C16 – C41) is also well resolved (although less well so than the head group due to more potential freedom in the flexible hydrocarbon chain. Electron density is again contoured at 1.5σ (pink) and 3.5σ (red).

Distances from U502 (Q_B) to closest residues (numbering used is the same as in the coordinate (pdb) file):

O2	L 190 His	2.94Å
O4	L 226 Thr	2.91Å
O5	L 224 Ile	2.73Å
O5	L 223 Ser	2.90Å
O5	L 225 Gly	2.92Å

The remaining position did not support full occupancy of the ubiquinone with electron density being especially poor from C26-41 which is the end of the tail. Occupancy was set at 0.5 for the entire molecule. Figure 79 shows the electron density in the Q_B binding pocket with the best position found for the ubiquinone molecule.

5.13.1.2. Carotenoid

As molecular replacement used the model from a structure containing a carotenoid, the initial model calculated will contain a certain amount of bias, resulting in electron density showing for the carotenoid, even if there is no molecule present in the structure. In order to overcome this bias, the first rounds of refinement were carried out with no carotenoid in the pbd file, and indeed, no molecule in the area proposed to contain the carotenoid. After two rounds of refinement using no carotenoid in the model, it was apparent from both the fo-fc and 2fo-fc maps that the density supported the insertion of the carotenoid, sphaeroidene.

As can be seen in figure 80, the carotenoid adopts the 15-cis orientation identical to that from the wild-type structure and there is good electron density supporting the positioning of the carotenoid for the entire length. The only slight difference is that the head group has been rotated approximately 100° in order to form a better hydrogen bond to the nitrogen of M 75 Trp (2.76Å), which can also be seen in other RC structures.

The binding pocket for the tail of the carotenoid was found to consist of hydrophobic amino acid residues and the hydrocarbon tail of the B 301 molecule. The residues found were M 66 Trp, M 67 Phe, M 85 Phe, M 74 Phe, M 105 Phe, M 115 Trp, M 120 Phe, M 123 Phe, M 157 Trp, M161 Phe, M 163 Phe and M177 Tyr.

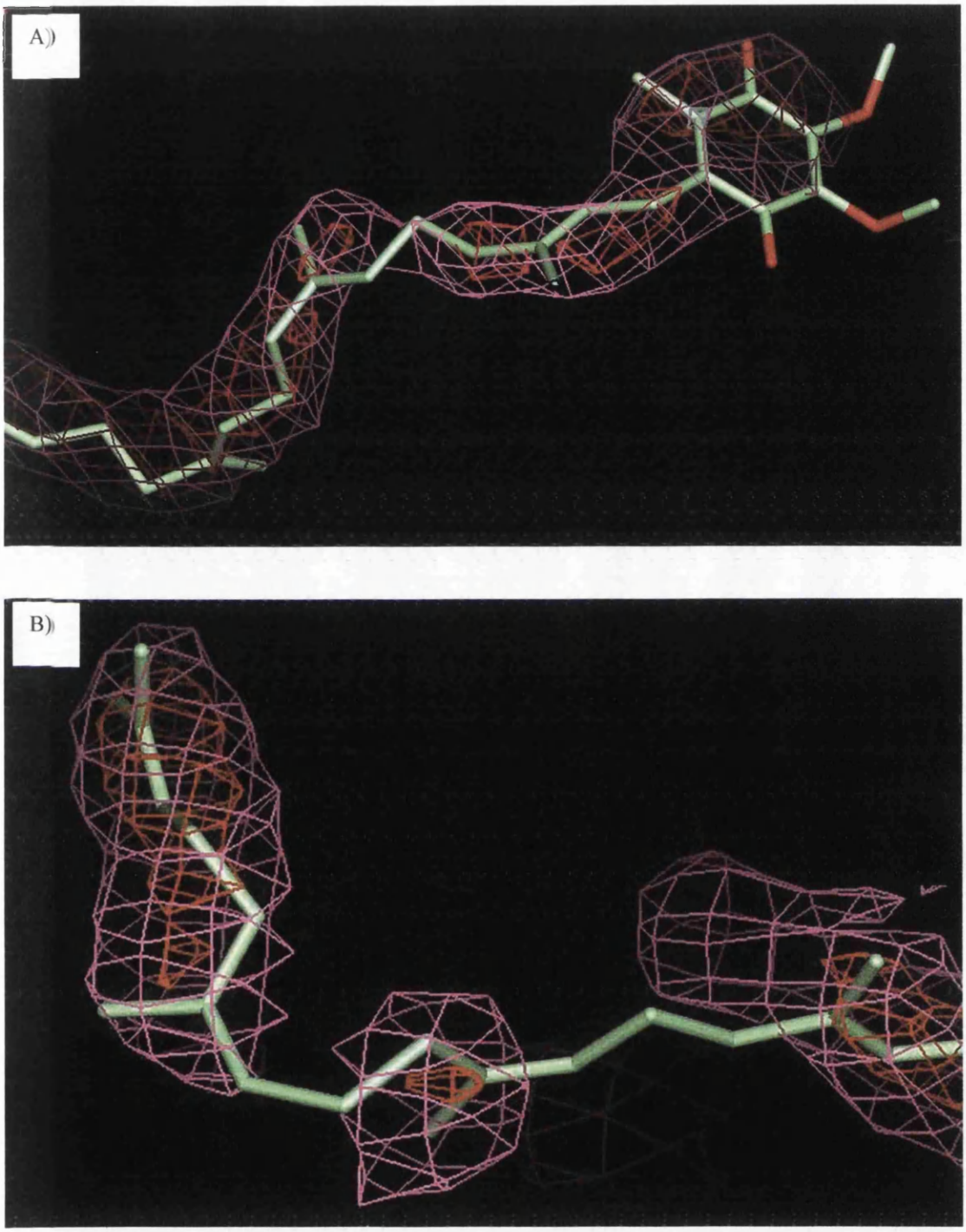

Figure 79. Electron density for ubiquinone, Q_B. This molecule is often seen in a disordered state in RC structures. A) The head group up to C23 is shown . The position of the head group was changed manually to better fit the observed density, however, during refinement, it returned to the position seen here. Electron density is contoured at 1.0σ (pink) and 1.5σ (red). B) The tail of the ubiquinone (C23 – C41) is less well resolved. Electron density is contoured at 0.7σ (pink) and 1.5σ (orange). There was no negative density observed in the fo-fc map at –2.0σ despite a lack of positive density in this 2fo-fc map. The occupancy of the entire molecule was set at 0.5, and the atoms are found to have high B-factors (46-60).

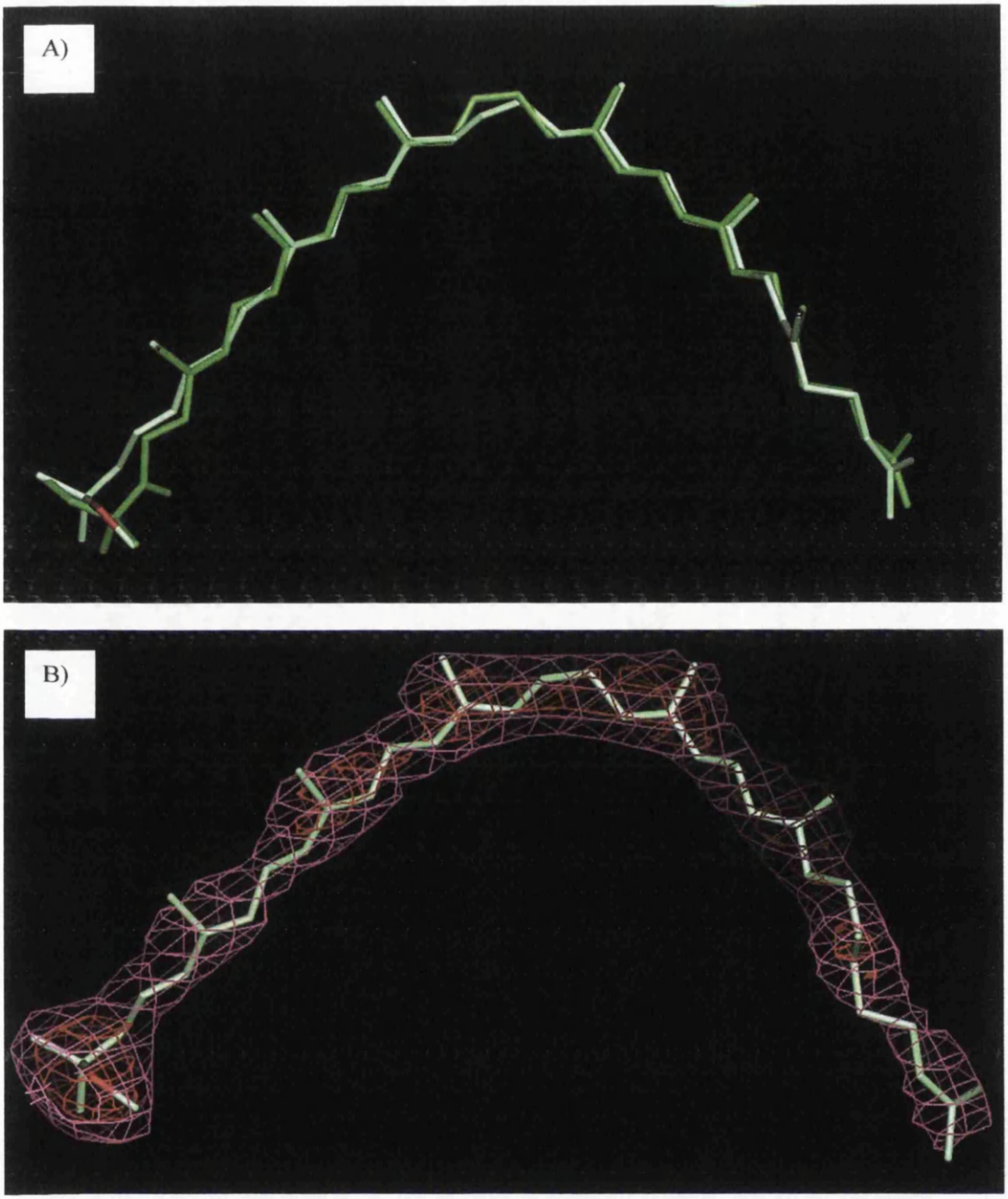

Figure 80.A) Spheroidene molecule from the solved RC structure overlaid with the matched coordinates of the carotenoid, spheroidenone, from a high resolution structure. The carotenoids are seen to adopt almost identical positions and orientations. B) Sphaeroidene molecule placed in the usual binding pocket. There is good electron density over the entire length of the molecule, which adopts the same 15,15'-cis conformation as in the WT structure. Electron density is contoured at 1.5σ (pink) and 3.0σ (orange).

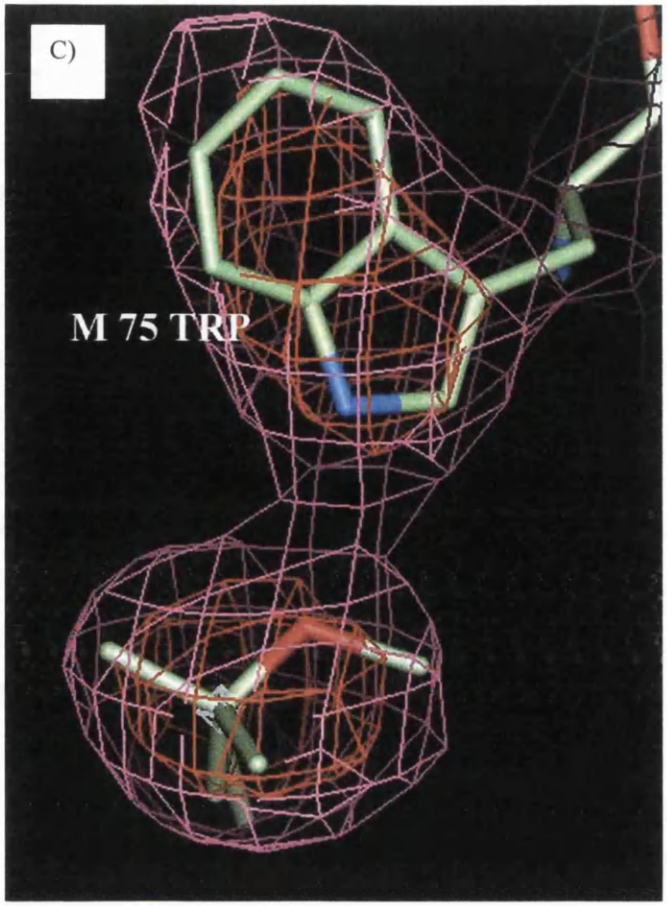

Figure 82 C) Enlargement of the head group of the carotenoid shows hydrogen bonding to the N of M75 Trp with a distance of 2.76Å. Electron density is contoured at 1.5σ (pink) and 3.0σ (orange).

5.14. Conclusions

It can be concluded from the experiment carried out on the reconstituted RC from *Rb. sphaeroides* strain R26-1 that previous experiments suggesting the reconstitution experiments inserted a carotenoid molecule in the same position and orientation as the WT structure are correct. Structural studies using x-ray crystallography support the placing of sphaeroidene in the same position in the R26-1 RC as the WT.

6. Chapter 6. Conclusions

The structures of the LH2 complexes currently available (McDermott et al., 1995, Koepke et al., 1996) answered many questions about the absorption and energy transfer characteristics. However, the 3.0Å resolution LH3 structure (McLuskey et al., 2001) did not show sufficient detail to accurately describe the changes in the Bchl *a* molecules responsible for the wavelength shift from 850nm in the LH2 complex to 820nm in the LH3 complex.

The work carried out on both strain 7050 and strain 7750 of *Rps. acidophila* yielded similar results, and therefore the LH3 complexes are summarised together here. When initial crystallisation trials did not yield single crystals that diffracted to high resolution, a review of the purification procedure was undertaken. Many parameters were investigated in order to separate best the pure LH3 samples from all contaminating moieties. These included growth conditions, solubilisation conditions and chromatography columns. Throughout the preparations, the purity was monitored by the peak ratios, I_r and P_r and only the purest fractions from each stage were used in subsequent steps.

Various crystallisation parameters were also investigated, including detergent type and concentration, additives, and incubation temperature. Crystals of apparently good morphology were grown in many wells of differing conditions, however, upon exposure to x-rays, none were found to diffract to high resolution. Crystals were exposed to an x-ray beam using both room temperature capillary mounting and loop mounting at cryogenic temperature (100K) using a cryoprotectant. Capillary mounting was found to be extremely difficult with crystals being very sticky and breaking up easily. Artificial mother liquor and cryoprotectant conditions were found to not be optimal and time was spent investigating these solutions with limited success.

As it appeared that the fault perhaps lay with the crystals, despite the careful purification and crystallisation procedure, another method of determining the complex purity was required. MALDI-TOF mass spectrometry was employed initially to identify the polypeptides and any contaminating heterogeneous polypeptides according to their masses.

The mass spectra of the purified complexes showed a complex mixture of peaks suggesting many different sizes of polypeptides, although whether this is due to different amino acid residues, or slight fragmentation is unclear at the moment.

When it was discovered that the apparently pure complexes contained several polypeptides in varying amounts, another way of identifying the polypeptides was required. Enzymatic digests were carried out in order to fragment the polypeptides and match the partial ladder sequences obtained to the published sequences. However, the polypeptides either degraded very rapidly, giving only low molecular weight fragments, or showed many overlapping peaks due to several polypeptides present. These factors made the resulting mass spectra impossible to interpret.

There are several areas of this work that would bear further investigation. In particular, the ability of the MS to identify large amounts of heterogeneous polypeptides in an allegedly pure LH3 sample raises questions about the purification procedure and the peak ratios currently in use to determine the purity. If the purified complex actually contains different polypeptide subunits, some residues required for crystal contact may not be present in some complexes, thus creating crystal defects, which could account for the poorly diffracting crystals. However, if the complex is simply not purified enough by the procedure used during this work, then a new purification protocol must be investigated.

One way to test this would be to carry out MS experiments on the polypeptides extracted into organic solvent. This route was not pursued here as it was considered better to record the MS of the purified complex, in the same form as it was for crystallisation, thus giving a greater insight into any impurities present.

It would appear from the crystallographic and MS experiments that purer LH3 complex is required in order to grow crystals that diffract to high resolution. However, in order to test the crystals, they have to be either made more robust, or AML and cryoprotectants need to be found in which the crystals are stable over a longer period of time. Hopefully with an improved purification, and more homogeneous polypeptide populations, more crystal contacts may be made which should give a more robust crystal.

Also, in order to carry out the enzymatic digests, it is apparent that the starting sample must display only a single peak for each of the polypeptides. If this is not the case (as was seen here), the resulting ladder sequences overlap (as seen with LH3 from strain 7750), making identification of the polypeptides impossible. Only a

limited number of enzymes were investigated for digesting the polypeptides and this could also be looked into further.

The structure determination of the carotenoidless RC mutant, reconstituted with spheroidene was successfully completed. Of the three datasets collected from crystals of this mutant, only the original one was ultimately used to provide the final solution. It was found that the second dataset collected could not be scaled, although the reason for this is unknown. The third dataset could be taken further to see if it improves the model, although the potential advantages of this are perhaps limited. The new version of Refmac (v5) was found to be vastly superior to Refmac4 in the refinement of this RC, and the final geometries and refinement statistics are good for data of this resolution.

The structure showed the presence of the carotenoid spheroidene in the same binding pocket and in the same 15-cis orientation as the wild type. It has therefore been concluded that the carotenoid is inserted back into the same binding pocket occupied by the carotenoid in the wild-type structure.

Appendix 1- Growth Media

Pfennigs media for growth of *Rps. acidophila*

Per 1 litre of media

Potassium dihydrogen orthophosphate	1 g
Magnesium sulphate.$7H_2O$	0.4 g
Sodium chloride	0.4g
Sodium succinate	1.5 g
(or succinic acid	0.65 g)
Calcium chloride.$2H_2O$	0.05 g
Ammonium chloride	0.5 g
Ferric citrate solution (see below)	5 ml
Trace element solution (see below)	10 ml

The pH of the media was adjusted to 5.2 using HCl and then sterilised in an autoclave.

Ferric citrate solution

0.1g ferric citrate was dissolved in boiling deionised water and made up to 100mls

Trace element solution

Per 1 litre of solution

EDTA di-sodium salt	0.5 g
Ferrous sulphate.$7H_2O$	10 mg
Manganous chloride.$4H_2O$	3 mg
Boric acid (H_3BO_3)	30 mg
Cobalt chloride.$2H_2O$	1 mg
Nickel chloride.$6H_2O$	2 mg
Sodium molybdate.$2H_2O$	3 mg

Succinate media for growth of *Rsp. sphaeroides*

Per 1 litre of media

Concentration base (see below)	20 ml
1M dipotassium hydrogen orthophaosphate	10 ml
1M Potassium dihydrogen orthophosphate	10 ml
10% (w/v) ammonium sulphate solution	5 ml
1M sodium succinate	10 ml
Growth factors (see below)	1 ml
Casamino acids	1 g

The pH of the media was adjusted to 6.8 using HCl and then sterilised in an autoclave.

Concentration Base

Per 1 litre of solution

Nitrilotriacetic acid	10 g
Magnesium sulphate	14.45 g
Calcium chloride.$2H_2O$	3.4 g
Ammonium molybdate	9.25 mg
Ferrous sulphate.$7H_2O$	99 mg
Nicotinic acid	50 mg

Aneurine hydrochloride	25 mg
Biotin	0.5 mg
Metos 44 (see below)	50 ml

Add to 500 ml deionised water and adjust to pH 6.8 using 5M KOH. Make up to 1 l.

Growth Factors

Per 1 litre solution

Biotin	0.02 g
Sodium hydrogen carbonate	0.5 g

Make up to 1 litre with deionised water to dissolve, then add

Nicotinic acid	1 g
Aneurine hydrochloride	0.5 g
4-aminobenzoic acid	1 g

Boil to dissolve

METOS 44

Per 100 ml of solution

Disodium EDTA	0.25 g
Zinc sulphate	1.095 g
Manganous sulpate.$4H_2O$	0.154 g
Copper sulphate.$5H_2O$	39.2 mg
Cobaltous nitrate.$6H_2O$	24.8 mg
Ferrous sulpate.$7H_2O$	0.55 g
Di-sodium tetraborate.$10H_2O$	17.7 mg

Make up to 100ml with deionised water and add 2 drops concentrated sulphuric acid

Appendix 2- Crystallisation screens conditions

Cryo I screen (Emerald Biosystems)

No.	Precipitant	Buffer (0.1M)	Additives
4	40% (v/v) PEG-300	HEPES pH 7.5	0.2M NaCl
7	40% (v/v) ethanol	Tris pH 8.5	0.05M $MgCl_2$
10	45% (v/v) glycerol	imidazole pH 8.0	none
11	35% (v/v) 2-methyl-2,4-pentanediol	Tris pH 8.5	0.2M $(NH_4)_2SO_4$
15	50% (v/v) PEG-400	CHES pH 9.5	0.2M NaCl
17	40% (v/v) 1,2-propanediol	HEPES pH 7.5	none
18	35% (v/v) 2-ethoxyethanol	imidazol pH 8.0	0.05M $Ca(OAc)_2$
19	35% (v/v) 2-propanol	Tris pH 8.5	none
23	40% (v/v) 2-methyl-2,4-pentanediol	Tris pH 7.0	0.2M $(NH_4)_2SO_4$
25	30% (v/v) PEG-300	Tris pH 8.5	0.2M $(NH_4)_2HPO_4$
26	40% (v/v) PEG-300	CHES pH 9.5	0.2M NaCl
27	30% (v/v) PEG-400	CAPS pH 10.5	0.2M$(NH_4)_2SO_4$, 10% (v/v) glycerol
28	40% (v/v) PEG-600	HEPES pH 7.5	0.05M Li_2SO_4, 10% (v/v) glycerol
29	40% (v/v) PEG-300	CHES pH 9.5	0.2M sodium citrate
32	40% (v/v) 1,2-propanediol	CHES pH 9.5	0.2M sodium citrate
33	25% (v/v) 1,2-propanediol	imidazole pH 8.0	0.2M $Zn(OAc)_2$, 10% (v/v) glycerol
34	40% (v/v) 2-methyl-2,4-pentanediol	imidazole pH 8.0	0.2M $MgCl_2$
35	40% (v/v) ethylene glycol	HEPES pH 7.5	5% (w/v) PEG-3000
36	50% (v/v) PEG-200	Tris pH 7.0	0.05M Li_2SO_4
38	30% (v/v) PEG-400	Tris pH 8.5	0.2M Li_2SO_4
43	50% (v/v) ethylene glycol	Tris pH 8.5	0.2M $MgCl_2$
45	30% (v/v) PEG-300	Tris pH 8.5	5% (w/v) PEG-3000, 10%(v/v)glycerol
47	40% (v/v) PEG-600	imidazole pH 8.0	0.2M $Zn(OAc)_2$

Cryo II screen (Emerald Biosystems)

No.	Precipitant	Buffer (0.1M)	Additives
2	50% (v/v) PEG-200	CHES pH 9.5	none
4	30% (v/v) PEG-400	HEPES pH 7.5	0.2M $Ca(OAc)_2$
5	40% (v/v) PEG-300	Tris pH 7.0	5% (w/v) PEG-1000
7	40% (v/v) ethanol	Tris pH 7.0	none
9	35% (v/v) 2-propanol	imidazole pH 8.0	0.05M $Zn(OAc)_2$
14	40% (v/v) ethylene glycol	imidazole pH 8.0	0.2M $Ca(OAc)_2$
16	20% (v/v) PEG-300	imidazole pH 8.0	1M $(NH_4)_2SO_4$, 10% (v/v) glycerol
20	50% (v/v) ethylene glycol	CHES pH 9.5	0.5M K/Na tartrate
21	35% (v/v) 2-ethoxyethanol	Tris pH 8.5	0.2M Li_2SO_4
23	30% (v/v) 1,2-propanediol	HEPES pH 7.5	20% (w/v) PEG-400
24	25% (v/v) 1,2-propanediol	Tris pH 8.5	0.2M $MgCl_2$, 10% (v/v) glycerol
25	40% (v/v) 2-methyl-2,4-pentanediol	CAPS pH 10.5	none

Appendix 3- Abbreviations and Masses of common amino acids

Name	3 letter abbreviation	1 letter abbreviation	Average Mass
Alanine	Ala	A	71.1
Arginine	Arg	R	156.2
Asparagine	Asn	N	114.1
Aspartic Acid	Asp	D	115.1
Cysteine	Cys	C	103.1
Glutamic Acid	Glu	E	129.1
Glutanime	Gln	Q	128.1
Glycine	Gly	G	57.1
Histidine	His	H	137.1
Isoleucine	Ile	I	113.2
Leucine	Leu	L	113.2
Lysine	Lys	K	128.2
Methionine	Met	M	131.2
Phenylalanine	Phe	F	147.2
Proline	Pro	P	97.1
Serine	Ser	S	87.1
Threonine	Thr	T	101.1
Tryptophan	Trp	W	186.2
Tyrosine	Tyr	Y	163.2
Valine	Val	V	99.1

References

Aargaard, J. and W. Sistrom (1972). Control of Synthesis of Reaction Center Bacteriochlorophylls in Photosynthetic Bacteria Photochemistry and Photobiology **15**: 209-225.

Adir, N., Axelrod, H., Beroza, P., Isaacson, R., Rongey, S., Okamura, M. Y., and Feher, G. (1996). "Co-crystallisation and characterization of the photosynthetic reaction centre cytochrome *c*-2 complex from *Rhodobacter sphaeroides*." Biochemistry **35**(8): 2535-2547.

Allen, J. P., Feher, G., Yeates, T. O., Rees, D. C., Deisenhofer, J., Michel, H., and Huber, R. (1986). Structural Homology of Reaction Centers from Rhodopseudomonas- Sphaeroides and Rhodopseudomonas-Viridis as Determined by X- Ray-Diffraction. Proceedings of the National Academy of Sciences of the United States of America **83**, 8589-8593

Angerhofer, A., Cogdell, R., and Hipkins, M. F. (1986). "A Spectral Characterization of the Light-Harvesting Pigment- Protein Complexes from Rhodopseudomonas-Acidophila." Biochimica Et Biophysica Acta **848**(3): 333-341.

Bailey, S. (1994) The CCP4 Suite - Programs for Protein Crystallography*Acta Crystallographica Section D-Biological Crystallography* **50**, 760-763
Barkigia, K., and Fajer, J. (1993) in *The Photosynthetic Reaction Centre* (Deisenhofer, J., and Norris, J., eds) Vol. ll, pp. 513-539, Academic Press, London

Beavis, R. C., Chaudhary, T., and Chait, B. T. (1992). Alpha-Cyano-4-Hydroxycinnamic Acid as a Matrix for Matrix- Assisted Laser Desorption Mass-Spectrometry Organic Mass Spectrometry **27**: 156-158

Bergstrom, H., V. Sundstrom, R. van Grondelle, E. Akesson, T. Gillbro (1986). "Energy transfer within the isolated light-harvesting B800-850 pigment-protein complex of *Rhodobacter sphaeroides*." Biochimica et Biophysica Acta **852**: 279-287.

Bergstrom, H., V. Sundstrom, R. van Grondelle, T. Gillbro, R. Cogdell (1988). "Energy transfer dynamics of isolated B800-850 and B800-820 pigment-protein complexes of *Rhodobacter sphaeroides* and *Rhodopseudomonas acidophila*." Biochimica et Biophysica Acta **936**: 90-98.

Bissig, I., Wagner-Huber, R., Brunisholz, R., and Zuber, H. (1990). Multiple Antenna Complexes in Various Purple Photosynthetic Bacteria. Molecular Biology of Membrane-Bound Complexes in Phototrophic Bacteria. G. Drews and E. Dawes. New York, Plenum Press. **53:** 199-210.

Brandt, M. and G. Drews (1997). "The role of pigments in the assembly of photosynthetic compleces in *Rhodobacter capsulatus*." Journal of Basic Microbiology **37**: 235-244.

Brown, R. and J. Lennon (1995). Mass resolution improvement byincorporation of pulsed ion extraction in a matrix-assisted laser-desorption ionization linear time-of-flight mass-spectrometer. Analytical Chemistry **67**(13): 1988.

Carson, M. (1997). "Ribbons." Methods in Enzymology **277**: 493-505.

Chang, C., D. Tiede, et al. (1986). "Structure of *Rhodopseudomonas sphaeroides* R-26 reaction centre." FEBS Letters **205**(2): 82-86.

Chirino, A., E. Lous, M. Huber, J.P. Allen, C.C. Schenck, M.L. Paddock, G. Feher, D.C. Rees (1994). Crystallographic analyses of site directed mutants of the photosynthetic reaction-center from Rhodobacter sphaeroides. Biochemistry **33**: 4584-4593.

Chory, J., T.J. Donohue, A.R. Varga, L.A. Staehelin, S. Kaplan (1984). "Induction of the photosynthetic membranes of *Rhodopseudomonas sphaeroides*: Biochemical and morphological studies." Journal of Bacteriology **159**(2): 540-554.

Cogdell, R., P. Fyfe, S. Barrett, S. Prince, A. Freer, N. Isaacs, P. McGlynn, and C. Hunter,(1996). "The Purple Bacterial Photosynthetic Unit." Photosynthesis Research **48**: 55-63.

Cogdell, R., M. F. Hipkins, W. MacDonald, and T. Truscott, (1981). "Energy transfer between the carotenoid and bacteriochlorophyll within the B800-850 light-harvesting pigment-protein complex of *Rps. sphaeroides*." Biochimica et Biophysica Acta **634**: 191-202.

Cogdell, R., Howard TD, Isaacs NW, McLuskey K, Gardiner AT (2002). "Structural factors which control the position of the Q_y absorption band of bacteriochlorophyll*a* in purple bacterial antenna complexes." Photosynthesis Research **74** (2): 135-141 2002

Cogdell, R., T. Monger, W. Parson (1975). "Carotenoid Triplet States in Reaction Centres from *Rhodopsuedomonas sphaeroides* and *Rhodospirillum rubrum*." Biochimica et Biophysica Acta **408**: 189-199.

Collins, M. and C. Rensen (1991). The purple phototrophic bacteria. Structure of Phototrophic Prokaryotes. J. Stolz. Boco Ranton, CRC Press: 49-77.

Debus, R. J., G. Feher, and M.Y. Okamura, (1986). "Iron-Depleted Reaction Centers from Rhodopseudomonas- Sphaeroides R-26.1 - Characterization and Reconstitution with Fe-2+, Mn-2+, Co-2+, Ni-2+, Cu-2+, and Zn-2+." Biochemistry **25**(8): 2276-2287.

Deinum, G., Otte, Gardiner, A., Aartsma, T., Cogdell, R., and Amesz, J. (1991). "Antenna organisation of *Rhodopseudomonas acidophila*: a study of photosynthetic light reactions in bacteria." Biochimica et Biophysica Acta **1060**: 125-131.

Deisenhofer, J., Epp, O., Miki, R., Huber, R., and Michel, H. (1985). "Structure of the protein subunits in the photosynthetic reaction centre of *Rhodopseudomonas viridis* at 3Å resolution." Nature **318**: 618-624.

Deisenhofer, J., Michel, H., Epp, O., Miki, K., Lottspeich, F., and Weyer, K. A. (1985). "The Crystal-Structure at 3Å Resolution of the Photosynthetic Reaction Center from Rhodopseudomonas Viridis." Biological Chemistry Hoppe-Seyler **366**(9): 778-778.

Dexter (1953). Journal of Chemical Physics **21**: 836-860.

Drews, G. and J. Imhoff (1991). Phototrophic Purple Bacteria. Variations in Autotrophic Life. J. Shively and L. Barton. London, Accademic Press: 51-97.

Eccles, J. and B. Honig (1982). "Spectral Shifts in Chlorophyll and Bacteriochlorophyll Systems Induced by Point Charges." Biophysical Journal **37**(2): A228-A228.

Fleming, G. R. and R. van Grondelle (1994). "The primary steps of photosynthesis." Physics Today **47**: 48-55.

Foote (1968). "Mechanisms of photosensitized oxidation." Science **162**: 963-970.

Frank, H. (1999). Incorporation of Carotenoids into Reaction Centre and Light-Harvesting Pigment-protein Complexes. The Photochemistry of Carotenoids. H. Frank, A. Young, G. Britton and R. Cogdell. The Netherlands, Kluwer Academic Publishers. **8**.

Frank, H. and R. Christensen (1995). Singlet Transfer from Carotenoid to Bacteriochlorophylls. Anoxygenic Photosynthetic Bacteria. R. Blankenship, M. Madigan and C. Bauer. Netherlands, Kluwer Academic Publishers: 373-384.

Frank, H., Taremi S., Knox, J., and Mantele, W. (1988). Single Crystals of the Photochemical Reaction Centre from *Rb. sphaeroides* wild type strain 2.4.1 analyzed by polarised light. The Photosynthetic Bacterial Reaction Centre. J. Breton and A. Vermeglio. New York, Plenum Press: 27-32.

Freer, A., Prince, S., Sauer, K., Papiz, M., Hawthornwaite-Lawless, A., McDermott, G., Cogdell, R., and Isaacs, N. (1996). "Pigment-Pigment Interactions and Energy Transfer in the Antenna Complex of the Photosynthetic Bacterium *Rps. acidophila*." Structure **4**: 449-462.

Freiberg, A. (1995). Coupling of Antennas to Reaction Centers. Anoxygenic Photosynthetic Bacteria. R. Blankenship, M. Madigan and C. Bauer. Netherlands, Kluwer Academic Publishers: 385-398.

Frese, R., Olsen, J., Branvall, R., Westerhuis, W., Hunter, C., and van Grondelle, R.(2000). "The long range supraorganisation of the bacterial photosynthetic unit: A key role for PufX." Proceedings of the National Academy of Science USA **97**: 5197-5202.

Fyfe, P. (1997). Biophysical Investigations of Photosynthetic Reaction Centres From *Rhodobacter sphaeroides*. Biochemistry and Molecular Biology. Glasgow, Scotland, Univesity of Glasgow: 273.

Fyfe, P. and M. R. Jones (2000). "Re-emerging structures: continuing crystallography of the bacterial reaction centre." Biochimica et Biophysica Acta **1459**: 413-421.

Fyfe, P.K., McAuley, K., Roszak, A., Isaacs, N., Cogdell, R., and Jones, M. R. (2001). "Probing the interface between membrane proteins and membrane lipids by X-ray crystallography." Trends in Biochemical Sciences **26**(2): 106-112.

Gabellini, N., Bowyer, J. R., Hurt, E., Melandri, B. A., and Hauska, G.(1982). "A cytochrome b/c_1 complex with ubiquinol-cytochrome c_2 oxidoreductase activity from *Rhodopseudomonas sphaeroides* GA." European Journal of Biochemistry **126**: 105-111.

Gardiner, A. (1992). Peripheral Antenna Complexes From *Rhosopseudomonas acidophila*: Structure, Function and Genetic Manipulation. Department of Botany. Glasgow, University of Glasgow, Scotland.

Garman, E. and T. Schneider (1997). "Macromolecular Cryocrystallography." Journal of Applied Crystallography **30**: 211-237.

Gentemann, S., Nelson, N. Y., Jaquinod, L., Nurco, D. J., Leung, S. H., Medforth, C. J., Smith, K. M., Fajer, J., and Holten, D.(1997). "Variations and temperature dependence of the excited state properties of conformationally and electronically perturbed zinc and free base porphyrins." Journal of Physical Chemistry B **101**(7): 1247-1254.

Griffiths, M., Sistrom, W., Cohen-Bazire, G., and Stanier, R. (1955). "Function of carotenoids in photosynthesis." Nature **176**: 1211-1214.

Guthrie, N., McDermott, G., Cogdell, R., Freer, A., Isaacs, N., Hawthornwaite-Lawless, A., Halloren, E., and Lindsay, J. (1992). "Crystallisation of the B800-820 Light-harvesting Complex from *Rhodopseudomonas acidophila* Strain 7750." Journal of Molecular Biology **224**: 527-528.

Haas, C. and J. Drenth (2000). "The interface between a protein crystal and an aqueous solution and its effects on nucleation and crystal growth." Journal of Physical Chemistry B **104**(2): 368-377.

Hartigan, N., Tharia, H. A., Sweeney, F., Lawless, A. M., and Papiz, M. Z. (2002). "The 7.5A electron density and spectroscopic properties of a novel low-light B800 LH2 from *Rhodopseudomonas palustris*." Biophysical Journal **82**: 963-977.

Hawthornwaite, A. and R. Cogdell (1991). Bacteriochlorophyll-Binding Proteins. Chlorophylls. H. Scheer. Boca Raton, CRC Press: 493-528.

Heller, B., Holten, D., and Kirmaier, C. (1995). "Control of electron transfer between the L- and M-Sides of Photosynthetic Reaction Centres." Science **269**: 940-945.

Hess, S., Chachisvilis, M., Timpmann, K., Jones, M., Fowler, G., Hunter, C., and Sundstrom, V. (1995). "Temporally and spectrally resolved subpicosecond energy transfer within peripheral antenna complex (LH2) and from LH2 to the core antenna complex in photosynthetic purple bacteria." Proceedings of the National Academy of Science USA **92**: 12333-12337.

Hoff, A. J. (1988). Nomen est omen. The Photosynthetic Reaction Centre: Structure and dynamics. J. Breton and A. Vermeglio. New York, Plenum Press: 98-99.

Hoff, A. J. and J. Deisenhofer (1997). "Photophysics of photosynthesis. Structure and spectroscopy of reaction centres of purple bacteria." Physics Reports **287**: 1-247.

Holzapfel, W., Finkele, U., Kaiser, W., Oesterhelt, D., Scheer, H., Stilz, H. U., and Zinth, W. (1989). Observation of a Bacteriochlorophyll Anion Radical During the Primary Charge Separation in a Reaction Center. Chemical Physics Letters **160**: 1-7.

Hu, X., T. Ritz, et al. (1997). "Pigment organization and transfer of electronic excitation in the photosynthetic unit of purple bacteria." Journal of Physical Chemistry **101**: 3854-3871.

Hu, X. and K. Schulten (1998). "Model for the light-harvesting complex I (B875) of Rhodobacter sphaeroides." Biophysical Journal **75**(2): 683-694.

Imhoff, J. F. (1984a). "Reassignment of the genus *Ectothiorhodospira* Pelsh 1936 to a new family Ectothiorhodospiraceae fam. nov.,and emended desciption of the Chromatiaceae Bavendamm 1924." International Journal of Systematic Bacteriology **34**: 338-339.

Imhoff, J. F. (1984b). "Quinones of Phototrophic Purple Bacteria." Fems Microbiology Letters **25**(1): 85-89.

Imhoff, J. F. (1995). Taxonomy and Physiology of Phototrophic Purple Bacteria and Green Sulfur Bacteria. Anoxygenic Photosynthetic Bacteria. R. Blankenship, M. Madigan and C. Bauer. Netherlands, Kluwer Academic Publishers: 1-15.

Imhoff, J. F. and H. G. Truper (1989). The purple non-sulphur bacteria. Bergey's Manual of Systematic Bacteriology. J. Stanley, M. Bryant, N. Pfennig and J. Holt. Baltimore, Williams and Wilkins. **3:** 1658-1661.

Johnson, R. S. and K. Biemann (1989).Computer-Program (Seqpep) to Aid in the Interpretation of High- Energy Collision Tandem Mass-Spectra of Peptides. Biomedical Environmental Mass Spectrometry **18**: 945.

Jungas, C., Ranck, J.-L., Rigaud, J.-L., Joliot, P., and Vermeglio, A. (1999). "Supramolecular organisation of the photosynthetic apparatus of *Rhodobacter sphaeroides*." EMBO Journal **18**: 534-542.

Karas, M., Bachmann, D., Bahr, U., and Hillenkamp, F. (1987). Matrix-Assisted Ultraviolet-Laser Desorption of Nonvolatile Compounds. International Journal of Mass Spectrometry and Ion Processes **78**: 53-68.

Karrasch, S., Bullough, P., and Ghosh, R. (1995). "The 8.5A projection map of the light-harvesting complex I from *Rhodospirillium rubrum*." The EMBO Journal **14**: 631-638.

Katilius, E., Turanchik, T., Lin, S., Taguchi, A. K. W., and Woodbury, N. W. (1999). "B-Side Electron Transfer in a *Rhodobacter sphaeroides* Reaction Centre Mutant in Which the B-Side Monomer bacteriochlorophyll Is Replaced with Bacteriopheophytin." Journal of Physical Chemistry B **103**: 7386-7389.

Kendrew, J., G. Bodo, et al. (1958). "A three-dimensional model of the myoglobin molecule obtained by x-ray analysis." Nature **181**(4610): 662-666.

Kiley, P. and S. Kaplan (1988). "Molecular Genetics of Photosynthetic Membrane Biosynthesis in *Rhodobacter sphaeroides*." Microbiological Reviews **52**: 50-69.

Kirmaier, C., He, C., and Holten, D. (2001). "Manipulating the Direction of Electron Transfer in the Bacterial Reaction Centre by Swapping Phe for Tyr Near $Bchl_M$ (L181) and Tyr for Phe Near $Bchl_L$ (M208)." Biochemistry **40**: 12132-12139.

Kirmaier, C., Weems, D., and Holten, D. (1999). "M-Side electron transfer in Reaction Centre mutants with a lysine near the nonphotoactive Bacteriochlorophyll." Biochemistry **38**: 11516-11530.

Koepke, J., Hu, X., Muenke, C., Schulten, K., and Michel, H. (1996). "The Crystal Structure of the Light-Harvesting Complex II (B800-850) from *Rhodospirillium molischianum*." Structure **4**: 581-597.

Lancaster, C., U. Ermler, and Michel, H. (1995). The structures of Photosynthetic Reaction Centres from purple bacteria as revealed by x-ray crystallography. Anoxygenic Photosynthetic Bacteria. R. Blankenship, M. Madigan and C. Bauer. Netherlands, Kluwer Academic Publishers: 503-526.

Lang, H. and C. Hunter (1994). "The relationship between carotenoid biosynthesis and the assembly of the light-harvesting LH2 complex in *Rhodobacter sphaeroides*." Biochemical Journal **298**: 197-205.

Lendzian, F., Huber, M., Isaacson, R. A., Endeward, B., Plato, M., Bonigk, B., Mobius, K., Lubitz, W., and Feher, G. (1993). "The electronic structure of the primary donor cation radical in *Rhodobacter sphaeroides* R-26: ENDOR and TRIPLE resonance studies in single crystyals of reaction centers." Biochimica et Biophysica Acta **1183**: 139-160.

Leupold, D., Voigt, B., Beenken, W., and Stiel, H. (2000). "Pigment-protein architecture in the light-harvesting antenna complexes of purple bacteria: does the crystal structure reflect the native pigment-protein arrangement?" Febs Letters **480**(2-3): 73-78.

Macpherson, A. N., Arellano, J., Fraser, N., Cogdell, R., and Gillbro, T. (1999). Photosynthesis: Mechanisms and Effects. G. Garab, Kluwer. **1:** 9-14.

McAuley, K., Fyfe, P. K., Ridge, J., Isaacs, N., Cogdell, R., and Jones, M. R. (1999). "Structural details of an interaction between cardiolipin and an integral membrane protein." Proceedings of the National Academy of Sciences of the United States of America **96**(26): 14706-14711.

McAuley, K. E., Fyfe, P. K., Ridge, J. P., Cogdell, R. J., Isaacs, N. W., and Jones, M. R. (2000). "Ubiquinone binding, ubiquinone exclusion, and detailed cofactor conformation in a mutant bacterial reaction center." Biochemistry **39**: 15032-15043.

McDermott, G. (1997). Structural Studies on an Integral Membrane Light-Harvesting Complex. Department of Chemistry. Glasgow, University of Glasgow, Scotland.

McDermott, G., Prince, S., Freer, A., Hawthornwaite-Lawless, A., Papiz, M., Cogdell, R., and Isaacs, N. (1995). "Crystal structure of an integral membrane light-harvesting complex from photosynthetic bacteria." Nature **374**: 517-521.

McGlynn, P., Hunter, C., and Jones, M. (1994). "The *Rhodobacter sphaeroides* PufX protein is not required for photosynthetic competence in the absence of the light harvesting system." FEBS Letters **349**: 349-353.

McGlynn, P., Westerhuis, W., Jones, M., and Hunter, C. (1996). "Consequences for the Organisation of Reaction Center-Light Harvesting Antenna 1 (LH1) Core Complexes of *Rhodobacter sphaeroides* Arising from Deletion of Amino Acid Residues from the C Terminus of the LH1 α Polypeptide." Journal of Biological Chemistry **271**: 3285-3292.

McLuskey, K. (1999). Crystallographic studies on integral membrane light harvesting complexes from photosynthetic bacteria. Department of Chemistry. Glasgow, University of Glasgow, Scotland.

McLuskey, K., Prince, S., Cogdell, R., and Isaacs, N. (1999). "Crystallization and preliminary X-ray crystallographic analysis of the B800-820 light-harvesting complex from Rhodopseudomonas acidophila strain 7050." Acta Crystallographica Section D-Biological Crystallography **55**: 885-887.

McLuskey, K., Prince, S., Cogdell, R., and Isaacs, N. (2001). "The crystallographic structure of the B800-820 LH3 light- harvesting complex from the purple bacteria Rhodopseudomonas acidophila strain 7050." Biochemistry **40**(30): 8783-8789.

McPherson, P. H., Okamura, M. Y., and Feher, G. (1990). "Electron transfer from the reaction center of *Rb. sphaeroides* to the quinone pool: doubly reduced Q_B leaves the reaction center." Biochimica et Biophysica Acta **1016**: 289-292.

Michel, H. (1990). Crystallisation of membrane proteins. Crystallisation of membrane proteins. H. Michel. Boca Raton, CRC Press: 73-88.

Michel, H., Weyer, K. A., Gruenberg, H., Dunger, I., Oesterhelt, D., and Lottspeich, F. (1986). "The "light" and "medium" subunits of the photosynthetic reaction centre from *Rhodopseudomonas viridis*. Isolation of the genes, nucleotide and amino acid sequence." EMBO Journal **J5**: 1149-1158.

Mitchell, E. and E. Garman (1994). "Flash freezing of protein crystals: Investigation of mosaic spread and diffraction limit with variation of cryoprotectant solution." Journal of Applied Crystallography **27**: 1070-1074.

Murshudov, G. N., Vagin, A. A., and Dodson, E. J. (1997). "Refinement of macromolecular structures by the maximum-liklihood method." Acta Crystallographica **D53**: 240-255.

Navaza, J. and P. Saludjian (1997). AMoRe: An automated molecular replacement program package. Macromolecular Crystallography, Pt A. **276:** 581-594.

Oberle, B., H. Tichy, et al. (1990). Regulation of formation of photosynthetic light-harvesting complexes in *Rhodobacter capsulatus*. Molecular biology of membrane-bound complexes in phototrophic bacteria. G. Drews and E. Dawes. New York, Plenum Press: 77-84.

Oelze, J. and G. Drews (1972). "Membranes of photosynthetic bacteria." Biochimica et Biophysica Acta **265**: 209-239.

Otwinowski, Z. and W. Minor (1997). "Processing of x-ray diffraction data collected in oscillation mode." Methods in Enzymology **276**: 307-326.

Papiz, M., Prince, S., Hawthornwaite-Lawless, A., McDermott, G., Freer, A., Isaacs, N., and Cogdell, R. (1996). "A model for the photosynthetic apparatus of purple bacteria." Trends in Plant Science **1**(6): 198-206.

Parson, W., R. Clayton, et al. (1975). "Excited states of photosynthetic reaction centers at low redox potentials." Biochimica et Biophysica Acta **387**: 265-278.

Pfennig, N. (1969). "*Rhodopseudomonas acidophila* sp. n., a new species of the budding purple non-sulphur bacteria." Journal of Bacteriology **99**: 597-602.

Phillips-Jones, M. (1998). Light Regulation of Pigment-Protein Gene Expression in Rhodobacter species. Microbial Responses to Light and Time. SGM Symposium 56. M. Caddick, S. Baumberg, D. Hodgson and M. Phillips-Jones. UK, Cambridge University Press: 159-183.

Qi, J. and N. Wakayama (2000). "Solute convection during the whole process of protein crystal growth." Journal of Crystal Growth **219**: 465-476.

Ricci, M., Bradforth, S., Jimenez, R., and Fleming, G. (1996). "Internal conversion and energy transfer dynamics of spheroidene in solution and in the LH-1 and LH-2 light harvesting complexes." Physical Chemistry **259**: 381-390.

Ridge, J., Fyfe, P. K., McAuley, K. E., van Brederode, M., Robert, B., van Grondelle, R., Isaacs, N., Cogdell, R., and Jones, M. R. (2000). "An examination of how structural changes can affect the rate of electron transfer in a mutated bacteril photoreaction centre." Biochemical Journal **351**: 567-578.

Roberts, J. A., Holten, D., and Kirmaier, C. (2001). "Primary events in photosynthetic Reaction Centres with multiple mutations near the photoactive electron carriers." Journal of physical Chemistry B **105**: 5575-5584.

Rodgers, D. (1994). "Cryocrystallography." Structure **2**: 1135-1140.

Savage, H., Cyrklaff, M., Montoya, G., Kuhlbrandt, W., and Sinning, I. (1996). "Two-dimensional structure of light harvesting II (LHII) from the purple bacterium *Rhodovulum sulfidophilum* and comparison with LHII from *Rhodopseudomonas acidophila*." Structure **4**: 243-252.

Shreve, A. P., Trautman, J. K., Owens, T. G., and Albrecht, A. C. (1991).Determination of the S2 Lifetime of Beta-Carotene Chemical Physics Letters **178**: 86.

Sistrom, W. (1978). Purple Bacteria The photosynthetic bacteria. R. Clayton and W. Sistrom. New York, Plenum Press: 899-906.

Sporlein, S., Zinth, W., Meyer, M., Scheer, H., and Wachtveitl, J. (2000).Primary electron transfer in modified bacterial reaction centers: optimization of the first events in photosynthesis Chemical Physics Letters **322**: 454-464.

Stowell, M., McPhillips, T., Rees, D., Soltis, S., Abresch, E., and Feher, G. (1997) Light-Induced Structural Changes in Photosynthetic Reaction Centre: Implications for Mechanism of Electron-Proton Transfer. Science **276**, 812-816

Subir, K. (1963). Media for anaerobic growth of photosynthetic bacteria. Bacterial Photosynthesis. H. Gest, A. Pietro and L. Vernon. Yellow Springs, Ohio, Antioch Press.

Sundstrom, V., Pullerits, T., and van Grondelle, R. (1999) Photosynthetic light-harvesting: Reconciling dynamics and structure of purple bacterial LH2 reveals function of photosynthetic unit. Journal of Physical Chemistry B **103**, 2327-2346

Sundstrom, V. and R. van Grondelle. (1995). Kinetics of Excitation Transfer and Trapping in Purple Bacteria. Anoxygenic Photosynthetic Bacteria. R. Blankenship, M. Madigan and C. Bauer. Netherlands, Kluwer Academic Publishers: 349-372.

Takaichi, S. (1999). Carotenoids and Carotenogenesis in Anoxygenic Photosynthetic Bacteria. The Photochemistry of Carotenoids. H. Frank, A. Young, G. Britton and R. Cogdell. The Netherlands, Kluwer Academic Press. **8:** 39-69.

Thornber, J. P., Cogdell, R. J., Seftor, R. E. B., and Webster, G. D. (1980). Further studies on the composition and spectral properties of the photochemical reaction centers of bacteriochlorophyll b-containing bacteria Biochimica et Biophysica Acta **593**: 60-75.

Timmins, P., Hauk, J., Wacker, T., and Welte, W. (1991). "The influence of hepane-1,2,3-triol on the size and shape of LDAO micelles. Implications for the crystallisation of membrane proteins." FEBS Letters **280**: 115-120.

van Grondelle, R., Dekker, J., Gillbro, T., and Sundstrom, V. (1994). "Energy Transfer and Trapping in Photosynthesis." Biochimica et Biophysica Acta **1187**: 1-65.

van Neil, C. (1941). "The bacterial photosyntheses and their importance for the general problem of photosynthesis." Advances in Enzymology **1**: 263-328.

Visschers, R. W., Germeroth, L., Michel, H., Monshouwer, R., and Vangrondelle, R. (1995). "Spectroscopic Properties of the Light-Harvesting Complexes from Rhodospirillum-Molischianum." Biochimica Et Biophysica Acta-Bioenergetics **1230**(3): 147-154.

Walz, T., Jamieson, S., Bowers, C., Bullough, P., and Hunter, C. (1998). "Projection structures of Three Photosynthetic Complexes from *Rhodobacter sphaeroides* : LH2 at 6A, LH1 and RC-LH1 at 25A." Journal of Molecular Biology **282**: 833-845.

Weyer, K. A., Schafer, W., Lottspeich, F., and Michel, H. (1987). "The cytochrome subunit of the photosynthetic reaction centre from *Rhodopseudomonas viridis* is a lipoprotein." Biochemistry **26**: 2909-2914.

Willems, A., Gillis, M., and de Ley, J.(1991). "Transfer of *Rhodocyclus gelatinosis* to *Rubrivivax gelatinosis* gen. nov., comb nov., and phylogenetic relationships with *Leptothrix, Sphaerotilus natans, Pseudomonas saccharophila,* and *Alcaligenes latus*." International Journal of Systematic Bacteriology **41**: 65-73.

Williams, J. C., L.A. Steiner, G. Feher, M.I. Simon (1984). "Primary structure of the L-subunit of the Reaction Centre from *Rhodopseudomonas-sphaeroides*." Proceedings of the National Academy of Science USA **81**(23): 7303-7307.

Williams, J. C., Paddock, M., Feher, G., and Allen, J. (1991). "Effects of iron ligand substitutions in Reaction Centres from *Rhodobacter sphaeroides*." Biophysical Journal **59**: 142a.

Youvan, D. C., Bylina, E. J., Alberti, M., Begusch, H., and Hearst, J. E. (1984). "Nucleotide and deduced polypeptide sequences of the photosynthetic reaction centre, B870 antenna, and flanking polypeptides from *Rb. capsulatis*." Cell **37**: 949-957

Zuber, H. and R. Brunisholz (1991). Structure and Function of Antenna Polypeptides and Chlorophyll- protein Complexes: Principles and Variability. Chlorophylls. H. Scheer. Boca Raton, CRC Press: 627-704.